INVESTIGATION OF ADVANCED CONTROL FOR THE UNIFIED POWER FLOW CONTROLLER (UPFC)

MOHAMED EMAD ELDIN ABDELHADY FARRAG

BSc MSc MIEE MIEEE

A thesis submitted in partial fulfilment of the requirement of Northumbria University at Newcastle for the degree of Doctor of Philosophy (PhD)

August 2002

UNIVERSITY OF NORTHUMBRIA AT NEWCASTLE

Thesis Declaration

TITLE OF THE THESIS **INVESTIGATION OF ADVANCED CONTROL FOR THE UNIFIED POWER FLOW CONTROLLER (UPFC)**

AUTHOR **MOHAMED EMAD ELDIN ABDELHADY FARRAG**

Date.....3.1/10/05.....

Dedication

To my Father's Spirit

To my Mother, Brothers and Sisters

To Hady, Mostafa and Noha

Abstract

The Unified Power Flow Controller (UPFC) is the versatile FACTS controller that can control up to three transmission system parameters individually or simultaneously in appropriate combinations.

The work presented in this thesis is concentrated on the modelling and control of the UPFC. The overall aim is to provide effective tools for optimising the impact of the UPFC in the reinforcement of a transmission system.

Existing modelling techniques for the UPFC together with the associated control strategies have been systematically reviewed. An exact power injection model is proposed which is based on the polar representation of the UPFC parameters and includes the reactive power capability of the shunt inverter. In addition, a steady-state model based on an ideal controlled voltage source has been developed using MATLAB/SIMULINK which provides a useful tool to analyse and develop the UPFC control system.

The UPFC internal limits have been identified and accordingly, the feasible operating area of a transmission system incorporating a UPFC has been determined based on the UPFC maximum limits. The influence of both the series and shunt inverters on this controlled area has been analysed. The impact of a change in the system short circuit level on the UPFC operation and the size of the feasible area has also been investigated.

Three modern controllers have been designed and tested for controlling the UPFC in a power flow mode for the series part and a voltage control mode for the shunt part. These controllers are: a fuzzy knowledge based controller, an artificial neural network based controller and a neuro-fuzzy based controller. For the former, the fuzzy rules are deduced from the relationship between the controlled power system parameters and the UPFC control variables. The second is a simple RBFNN controller which is constructed from a single neuron and trained on-line by a gradient descent algorithm. The third controller is designed using the adaptive capabilities of neural networks to estimate and tune the fuzzy rules.

Computer simulation and experimental implementation of a UPFC using DS1103 data acquisition board have been used to verify the proposed control strategies. In the experimental lab model, two 6-pulse inverters implementing the SPWM technique have been used to realise the UPFC system.

Acknowledgement

All thanks to my Lord in whom I believe

I would like to express my sincere gratitude to my supervisor Dr. Ghanim Putrus for his invaluable guidance, advice and encouragement throughout my study. His support was always there when I needed it. I appreciate his idea for allowing me to create my own academic interest.

I wish to express my profound thanks to Dr. Li Ran and Dr. Seán Danaher for their advice and help during the course of this work.

Extensive appreciation is also expressed to each member of the power and control research group, as the discussion in the weekly meeting was very valuable for me. Also, I would like to thank all technical, administrative and staff at the school of Engineering for their continuous support.

I also wish to acknowledge the Egyptian government represented by the Ministry of Higher Education for providing the grants to do my study.

My sincere appreciation to my beloved wife Eman for giving me strength, moral support, encouragement and patience throughout my study. Finally, I can not forget my loving kids Hady, Mostafa, Noha and their simple smiles.

Table of Contents

Glossary of Abbreviations

ANFIC	Adaptive Neuro Fuzzy Inference Controller
ADC	Analogue to Digital Converter
ANFIS	Adaptive Neuro Fuzzy Inference System
ANN	Artificial Neural Network
ASVC	Advanced Static VAr Compensator
AVR	Automatic Voltage Regulator
COG	Centre Of Gravity
CVS	Controlled Voltage Source
DAC	Digital to Analogue Converter
DPLL	Digital Phase Locked Loop
DSP	Digital Signal Processing
EMTDC	Electromagnetic Transient D.C.
EMTP	Electromagnetic Transient Programme
EPRI	Electrical Power Research Institute
FACTS	Flexible A.C. Transmission Systems
FFM	Fundamental Frequency Modulation
FLC	Fuzzy Logic Control
GTO	Gate Turn Off
HCF	Hysteresis Current Forcing
IEEE	Institute of Electrical and Electronics Engineers
IGBT	Insulated Gate Bipolar Transistor
IGCT	Insulated Gate Controlled Thyristor
IPFC	Interline Power Flow Control
LMS	Least Mean Squares
LQ	Linear Quadratic
MCT	MOS Controlled Thyristor
MIMO	Multi Input Multi Output
MLP	Multi Layer Perceptron
MLPBP	Multi Layer Perceptron Backpropagation
MSE	Mean Square Error
PI	Proportional Integral

PLL	Phase Locked Loop
PPC	Power PC
PSS	Power System Stabiliser
PWM	Pulse Width Modulation
RB	Radial Basis
RBFNN	Radial Basis Function Neural Network
RTI	Real Time Interface
RTW	Real Time Workshop
SCL	Short Circuit Level
SHEM	Selective Harmonic Elimination Modulation
SISO	Single Input Single Output
SMIB	Synchronous Machine Infinite Bus
SPWM	Sinusoidal Pulse Width Modulation
SSSC	Static Synchronous Series Compensator
STATCOM	STATic COMpensator
SVC	Static VAr Compensator
TCPS	Thyristor Controlled Phase Shifter
TCR	Thyristor Controlled Reactor
TCSC	Thyristor Controlled Series Compensator
TSC	Thyristor Switched Capacitor
UPFC	Unified Power Flow Controller
VA	Volt-Ampere
VAr	Volt-Ampere reactive
VSI	Voltage Source Inverter

List of Figures

List of Tables

INTRODUCTION

1.1 POWER SYSTEM OVERVIEW

Electric power systems, including generation, transmission and distribution are considered to be the largest and most expensive man-made systems in the world. Electrical power plays an essential role in the daily lives in modern societies. The demand for electric power is continuing to grow worldwide. In most developed countries, a major population shift to urban areas has led to geographically uneven growth of power demand around main cities. This motivated building new power plants where power generation resources e.g. water falls, mine's coal or natural gases are located normally far away from the high power consumption areas. In order to meet the continually increasing power demand, power transfer capabilities must be increased by using interconnected transmission systems via long transmission lines or grid topology. In practice, power networks are organised at various voltage levels linked by transformers. Depending on the voltage level, a power transmission system may be classified into distribution systems, sub-transmission systems and transmission systems, the latter are the subject of this study.

Building new power system facilities, in particular transmission systems can be difficult due to:

- Environmental constraints.
- Right of way difficulties.
- High cost of building new elements.
- Competitions due to privatisation of the electric supply industry.

These factors, provided the momentum for exploring new ways of maximising the power transfer capability of the existing transmission facilities. This has increased the focus on transmission constraints and means by which such constraints can be alleviated. Power

transfer should ensure that limits due to thermal, voltage or electromechanical stability are not violated. For long overhead transmission systems, stability limits are much lower than thermal limits.

The stability of a power system can be preserved and enhanced by proper design and operation of the system. This is normally achieved through a compromise between operating the system near its stability limit and operating a system with excessive reserve of generation and transmission. At the design stage, allowance is normally made for sufficient transmission capacity. The risk of losing stability can be reduced by using additional elements installed into the system. There are two different levels of power system enhancement elements. The first is placed at the machine level, e.g. Automatic Voltage Regulator (AVR) and Power System Stabiliser (PSS). The second is placed at the transmission level, e.g. reactive power (VAr) compensators and phase angle regulators. The latter comprises conventional compensators, normally mechanically switched elements, and advanced power electronic-based controllers which are collectively known as FACTS devices (introduced by Electrical Power Research Institute EPRI). Due to their slow response, high cost and sensitivity to voltage changes, conventional compensators have limited effects on the power system dynamics and are progressively replaced by the FACTS devices. Detailed overview of FACTS devices is given in Chapter 2.

FACTS technology provides a great operating flexibility for power systems and hence better utilisation of existing systems. FACTS devices are used to regulate one or more of the three main parameters which determine the transmitted power over a line namely: voltage magnitude, transmission impedance and angle. This would permit the maximum power capacity of a transmission system to be increased to or near its thermal limit which has been seldom reached without the aid of FACTS technology.

The UPFC is the most versatile FACTS device that can influence the three transmission parameters individually or simultaneously. It controls the power transfer through a transmission system which can be adjusted to suit the overall system loading conditions. The fast dynamic response of the UPFC makes it adequate for enhancing system stability.

1.2 STUDIES OF THE UPFC CONTROL SCHEMES

The practical realisation of the UPFC requires an a.c. to a.c. converter in which the real power can freely flow between its two ends while the reactive power can be exchanged locally between the converter and the a.c. system. This can be implemented using two voltage source inverters operated from a common d.c. link, as shown in Figure 1.1. Having multiple functions, the UPFC plays a vital role in optimising the transmission system operation. Inverter 2 controls the power flow by inserting a controlled series voltage with the transmission system. Inverter 1 may help in supporting the bus voltage by

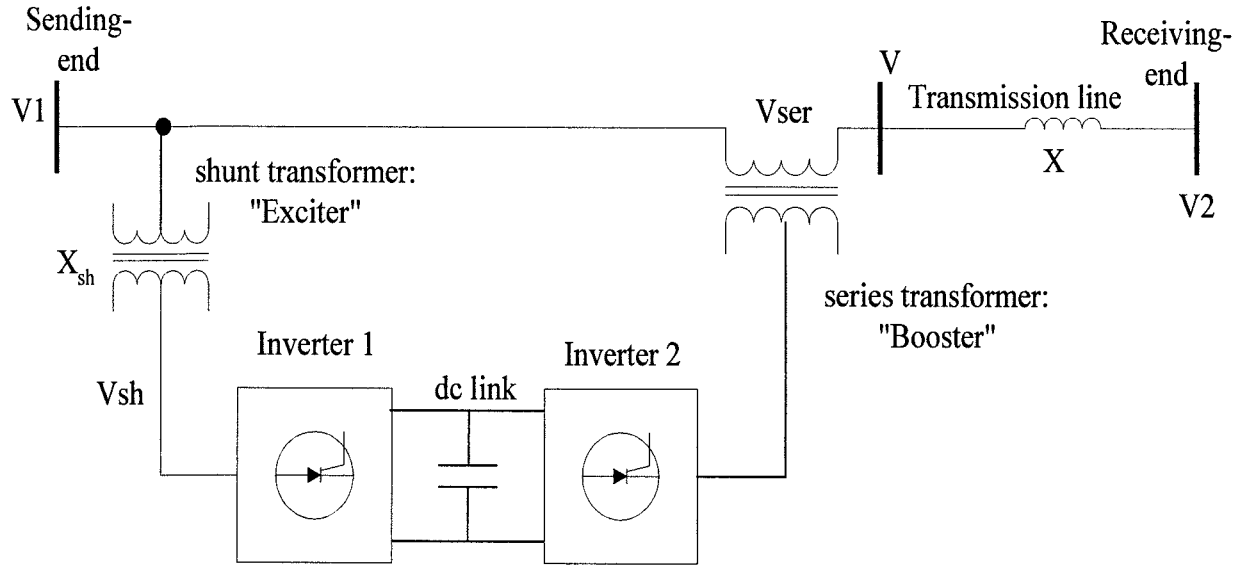

Figure 1.1 Schematic diagram of a UPFC system.

generating/absorbing shunt reactive power. The UPFC can be used for enhancing system damping and improving transient stability margins. The study of the UPFC includes two major parts; modelling the device in different power system states and designing control strategies based on the model used and the system objectives.

The main concern in this study is to design a new control algorithm for the UPFC and investigate its capability in controlling the power flow and supporting the bus voltage at which the shunt inverter is connected. The UPFC has two levels of control: Internal controller, which specifies the switching pattern of the solid-state devices within each inverter. External controller, which uses the references and system output signals to determine the control variables for each inverter.

Internal controller

The Pulse Width Modulation (PWM) scheme is normally used to control the UPFC inverter outputs. In this work, the SPWM is implemented.

External controller

Significant research efforts have been put into developing appropriate methods for controlling the UPFC operation in order to improve the overall system performance. A conventional PI controller has been proposed to control the UPFC which is modelled in d-q reference frame [1-5]. PI de-coupled and PI cross-coupled controllers were introduced to minimise the interaction between the active and reactive power flow [2,3]. Papič [4] proposed a PI controller associated with predictive control loop to compensate for the delay in system current measurements. A hybrid PI controller (de-coupled and cross-coupled) was investigated by Fujita [5] to reduce the power fluctuations in transient state and in the same time to minimise the interaction between the d- and q- axis quantities. Lombard [6] proposed a Linear-Quadratic (LQ) controller by solving Liapunov and Ricatti equations to determine the controller parameters. This method needs intensive computation and precise UPFC model. Robust controller based on H_∞ was suggested by Vilathgamuwa [7,8] to

ensure robust performance and internal stability of the UPFC against disturbances and unstructured parameter variations.

With rapid development of modern control theory, new control schemes for the UPFC have been studied. Fuzzy logic control theory has been applied to develop a new controller for the UPFC [9-12]. Kannan [9] proposed a fuzzy controller to control the UPFC series inverter, the UPFC shunt reactive capability was ignored in this study. In another study [10], the same author suggested an intelligent fuzzy controller to control the d.c. link voltage and the real power flow in the transmission system with some sort of co-ordination between them, reactive power control through the series inverter was not included. Yixin [11] proposed a non-linear PI type fuzzy supplementary controller to damp power oscillation on a tie line of interconnected power systems incorporating a UPFC while the UPFC main variables are controlled using conventional PI controllers.

Takagi-Sugeno fuzzy controller was proposed by Mishra [12] to control the operation of the UPFC series part. This controller provides a wide range of control gain variations by including both linear and non-linear terms in the consequent part of the rules. A PI controller is used to regulate the d.c. capacitor voltage. In his study, the capability of the shunt inverter to support the system busbar voltage is ignored.

Artificial Neural Network (ANN) based controllers for the UPFC have also been proposed [13,14]. Ma [13] investigated the use of an ANN to memorise the damping control strategy of a well-tuned PI controller. This required different tuning parameters of the PI controller for each operating point and many operating points to be included to achieve good performance. The radial basis function neural network was used by Dash [14] to regulate the UPFC control variables. Extended Kalman filter was used to adjust the network parameters which is a time consuming process that limits the real time applicability of the algorithm.

In this thesis, three types of controllers have been investigated to control the UPFC main variables. Fuzzy knowledge based controller has been investigated for controlling the

real and reactive power flow using the UPFC series inverter capabilities. The fuzzy rules are derived from the relationship between the UPFC control variables and the desired power flow. The adaptive capability of ANNs has been used to design two ANN based controllers using Multi-Layer Perceptron Back Propagation (MLPBP) and Radial Basis Function Neural Network (RBFNN). Also, a simple neural network controller containing one RBF neuron, which is suitable for real time control has been investigated. Finally, an adaptive neuro-fuzzy controller is proposed to increase the accuracy of the fuzzy based rules controller.

1.3 SCOPE OF THE RESEARCH

In order to design an appropriate controller, different operating modes of the UPFC have been first investigated, together with advanced control schemes, they are used to control the real and reactive power flow in a transmission system and to regulate the system bus voltage. Power system constraints have been identified and system operating feasible area when using the UPFC has been defined. The effects of system short-circuit level on the operating area is also analysed and presented.

Three types of advanced controllers for the UPFC are proposed and analysed. These are; fuzzy-knowledge-based controller, neural network based controller and adaptive neuro-fuzzy controller.

Two tools have been used to verify the validity of the new controllers' design. The first is a simulation model of the system in MATLAB/SIMULINK environment. The second is an experimental lab model comprising two 6-pulse inverters to realise the UPFC. The controllers are implemented using the power and flexibility provided by the dSPACE DS1103 data acquisition board. The experimental work has led to the observation of the physical interactions between different parts of the system. Comparative analysis between simulation-based and hardware-based results is performed.

1.4 OVERVIEW OF THE THESIS

The thesis is structured as follows;

Chapter 2 gives an overview of FACTS devices, their operating principles, classifications and applications.

Chapter 3 introduces the UPFC structure, principles and modes of operation. The effects of the system reference signal on the modes of operation and performance of the UPFC are also presented in details.

Chapter 4 discusses the effects of the UPFC on the power flow and the operational constraints of a power system when incorporating a UPFC device. The system feasible operating region as a function of the UPFC inserted voltage parameters is defined. The effects of changes in the system fault level on the system feasible region and the UPFC speed of response are also investigated.

Chapter 5 presents a review of different modelling techniques of the UPFC that are used to analyse the UPFC controller performance. A complete UPFC power injection model based on polar representation is proposed in this chapter.

Chapter 6 presents the design of a fuzzy-knowledge-based controller for the UPFC. The fuzzy rules are derived from the mathematical relationship between the UPFC control variables and the power system parameters.

Chapter 7 introduces the design aspects of learning based controllers. Two neural network topologies (MLPBP and RBFNN) are used to design pre-learned controllers. To overcome

the network structure complexity, the RBFNN with a simple structure trained by gradient descent is proposed. Also, an adaptive neuro-fuzzy controller is proposed to increase the robustness of the fuzzy controller described in Chapter 6.

Chapter 8 gives details of the construction and performance of the UPFC laboratory model employing DS1103 data acquisition board. Development of the power circuit together with the associated drivers and controllers are presented.

Chapter 9 summarises and discusses the conclusions drawn from the theoretical analysis, simulation and experimental work. In addition, suggestions for further research in this area are given.

1.5 CONTRIBUTIONS OF THE THESIS

The work reported in this thesis has resulted in the following contributions:

1. The development of FACTS controllers has been systematically reviewed. The operation of the UPFC has been analysed and different modes of operation have been defined. Modelling techniques of the UPFC have been investigated. A complete power injection model (based on polar representation of the UPFC parameters and including the effect of the shunt inverter reactive compensation capability) is proposed.
2. The operational constraints of the UPFC and their effects on the overall system performance have been analysed. The system feasible operating area in terms of the desired active and reactive power flow has been defined. In addition, the effects of system operating conditions, in particular the system fault level, on the available controlled area and UPFC speed of response have been analysed.

3. Different control algorithms for the UPFC have been investigated and a conventional Fuzzy-like-PI controller has been applied and its performance evaluated.
4. Fuzzy rules-based controller is proposed and its performance analysed. The rules are stimulated from the relationship between the system parameters and the UPFC control variables which cover all the predefined feasible control area. To increase the sensitivity of the fuzzy rules-based controller, an intelligent Adaptive Neuron-Fuzzy Inference Controller (ANFIC) has been applied to tune the membership functions. The results obtained show some improvement in the system performance.
5. An artificial neural network based controller for the UPFC has also been investigated. A comparison between the backpropagation and radial basis function neural network is made to demonstrate the accuracy of each technique in determining the UPFC control variables.
6. An adaptive single neuron radial basis neural network suitable for the real time implementation (including adaptability to changes of system conditions) has also been designed and analysed. The controller has been trained on-line using the gradient descent learning algorithm in order to continually update the controller parameters.
7. An experimental model has been developed and implemented to verify in real time the performance of the UPFC and the proposed controllers. The effects of changes in system short circuit level have also been investigated and experimentally verified.

These contributions are supported by the following publications:

1. M. E. A. Farrag, G. A. Putrus," Advanced control of the unified power flow controller," UPEC'99, Vol. 1, Leicester, U.K., Sep. 1999, PP. 74-77.
2. M. E. A. Farrag, G. A. Putrus, L. Ran," Analysis of a transmission system incorporating a UPFC for optimum power flow control," UPEC'00, Belfast, U.K., Sep. 2000.
3. M. E. A. Farrag, G. A. Putrus, L. Ran," Using PWM control to improve the speed of response of the advanced static VAr compensator (ASVC)," UPEC'01, Swansea, U.K., Sep. 2001.
4. M. E. A. Farrag, G. A. Putrus, L. Ran," Real time hybrid control system for the advanced static VAr compensator," accepted for presentation in UPEC'02, Staffordshire, U.K., Sep. 2002.
5. M. E. A. Farrag, G. A. Putrus, L. Ran," Design of fuzzy based-rules control system for the unified power flow controller," accepted for presentation in IECON'02, Sevilla, Spain, Nov. 2002.
6. M. E. A. Farrag, G. A. Putrus, L. Ran," Design of an adaptive neuro-fuzzy inference controller for a transmission system incorporating a UPFC, " prepared for publication.
7. M. E. A. Farrag, G. A. Putrus, L. Ran," Investigation of a real time radial basis function neural network trained by gradient descent for the unified power flow controller," prepared for publication.

FACTS OVERVIEW

2.1 INTRODUCTION

Many transmission systems are of the radial type, where one side of the system is predominantly generation and the other side is predominantly load. The concept of using series/shunt capacitors/inductors to control the line power flow and to support the load bus voltage derived from the fundamental equations of power transfer have been used for long now. Since then, many attempts have been made to solve problems arising from supplying cheap, reliable and high quality power to continually growing customers. To control and optimize power flow in transmission systems, mechanically switched devices (phase shifters, series and shunt VAr compensators) have been implemented. These devices have been successfully used, but proved to be very slow in responding to transient changes in the system. Another problem with the mechanically switched devices is that control can not be initiated frequently, because switches tend to wear out quickly. Therefore, power system engineers have learned to live with these limitations by using a variety of ingenious techniques to make the system work effectively, but at a price of providing greater operating margins and redundancies.

2.2 FACTS TECHNOLOGY

In addition to problems of acquiring new rights of way, increasing demands on transmission power and nature of today's grid topology, all together have created tendencies toward a new technology called Flexible A.C. Transmission Systems (FACTS). FACTS technology was introduced to overcome the operational difficulties with the conventional methods of power compensation. This technology is capable to alleviate some of the difficulties by enabling utilities to get the most service from existing transmission facilities

and enhance the grid reliability. Due to the use of semiconductor switches, FACTS controllers are faster and more accurate as compared to their mechanical counter parts.

The Institute of Electrical and Electronics Engineers (IEEE) defines FACTS as "Alternating Current transmission systems incorporating power electronic based and other static controllers to enhance controllability and increase power transfer capability" [15].

The primary goal in many applications of FACTS controllers is to increase the use of existing transmission facilities, without compromising the system adequacy (the ability of the system to meet energy demands within components rating and system limits) and security (the ability of the system to withstand incidents without uncontrolled loss of customer loads).

2.3 CLASSIFICATION OF FACTS CONTROLLERS

There are two main ways of categorising the FACTS controllers. These are:

- Classification according to the connection of the device within a transmission system
    1. Series devices.
    2. Shunt devices.
    3. Hybrid devices.
- Classification according to the concept of operation, i.e. the function and operating principles of the power electronics implemented in FACTS controllers.

There are two distinctly different approaches to the realisation of power electronics based FACTS controllers, each resulting in a comprehensive group of controllers able to address specific transmission problems [16].

a) Thyristor controlled FACTS devices.

This group employs reactive impedances or tap-changing transformer with thyristor switches working as the control elements.

b) Voltage source inverter based FACTS devices.

This group uses self-commutated static converters as controlled voltage sources.

In this chapter, the second classification of identifying the FACTS controllers (concept of operation) will be reviewed.

2.3.1 Thyristor Controlled FACTS Devices

This group of controllers, shown in Figure 2.1, includes the Static VAr Compensator (SVC), Thyristor Controlled Series Compensator-Switched Capacitor- (TCSC) and Thyristor Controlled Phase Shifter (TCPS). They employ conventional thyristors in circuit arrangements which allow fast control response compared to the corresponding mechanical system. Each device is capable of controlling only one of the three power transmission control variables (bus voltage, transmission impedance and phase angle).

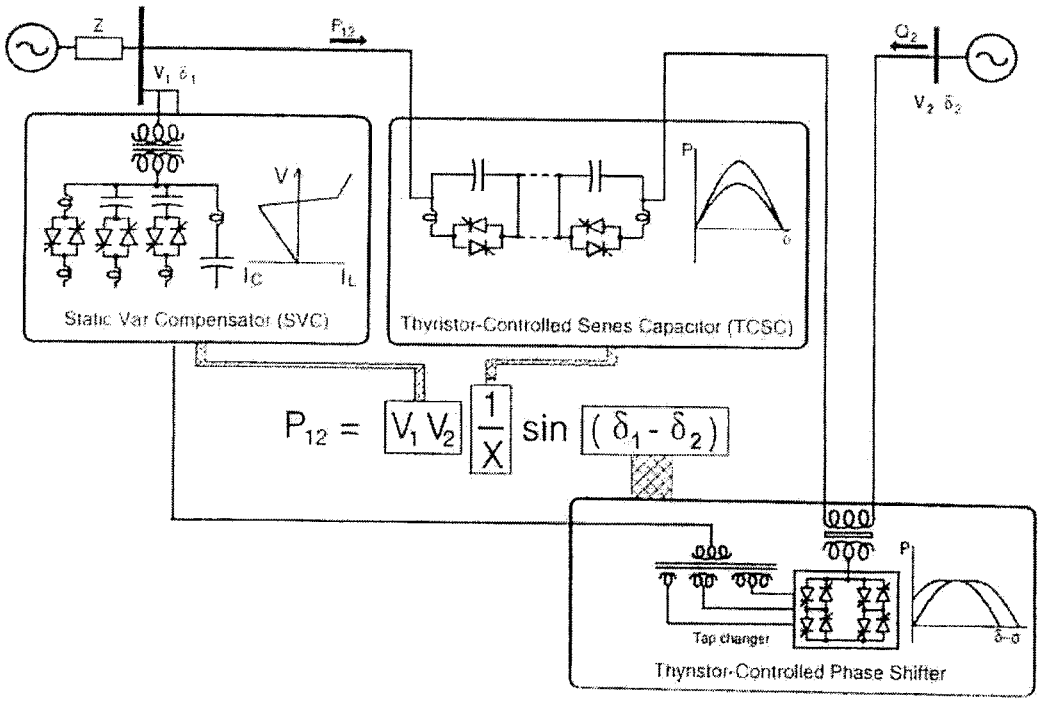

Figure 2.1 Thyristor controlled FACTS devices [16].

2.3.1.1 Static VAr compensator (SVC)

The SVC is effectively a variable shunt reactance which is able to produce a compensating reactive current. It comprises a Thyristor Switched Capacitor (TSC) and a Thyristor Controlled Reactor (TCR), as shown in Figure 2.2. The device is operated to regulate the voltage at a selected terminal of the transmission system by a proper co-ordination of the capacitor switching and reactor phase angle control. It may be controlled to improve the transient and dynamic stability of the transmission system [17]. The V-I characteristics of the SVC shown in Figure 2.3 indicates that voltage regulation (with a given slope around the uncompensated nominal voltage) can be achieved in the normal operating range defined by the maximum capacitive and inductive current. This current is generated or absorbed by the passive elements of the SVC. Moreover, the SVC may be controlled to damp power oscillation by adjusting its output between appropriate capacitive and inductive values to oppose the angular acceleration and deceleration of the involved synchronous machines.

2.3.1.2 Thyristor controlled series compensator (TCSC)

The TCSC is used to control the voltage across the series impedance of a given transmission line that ultimately determines the line current and transmitted power. The TCSC is connected in series with the transmission line and hence the compensating voltage is inherently a function of the line current. The power-angle curves shown in Figure 2.4 illustrate different degree of transmission compensation. From those curves it is obvious that the variable series capacitive compensation can be effective in improving both transient and steady-state stability limits [18].

There are two schemes of the TCSC as shown in Figure 2.5.

a) Thyristor Switched Capacitor (TSC).

b) Fixed capacitor in parallel with a Thyristor Controlled Reactor (TCR).

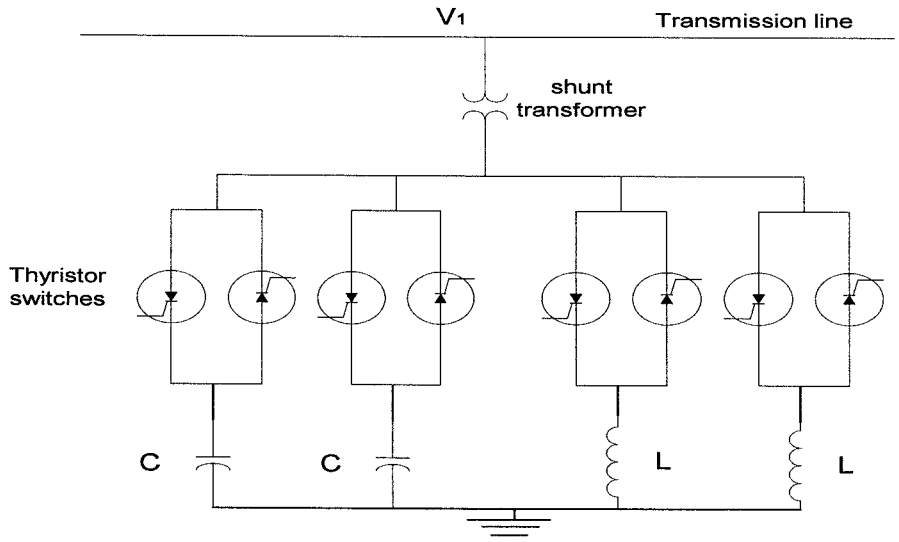

Figure 2.2 Static VAr compensator.

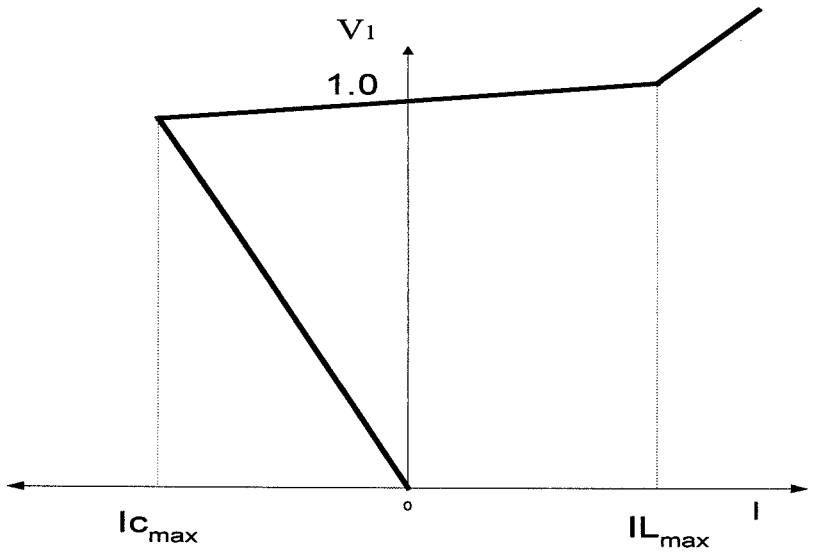

Figure 2.3 V-I characteristics of the SVC.

In the first topology, the degree of series compensation is determined by increasing or decreasing the number of capacitor banks in series. By controlling the firing angle of the corresponding thyristors pair, the bank is switched in service or bypassed.

In the second topology, the variable compensation is achieved by controlling the thyristor conduction period within the TCR. Maximum series compensation is reached when the TCR is off.

One of the difficulties of using TCSC is that the interaction can occur between the series capacitor-compensated transmission line and the mechanical system of a turbo-generator set resulting in torsional mechanical oscillation with negative damping effect. Another limitation of the TCSC is its operation depends on the amplitude of the transmission system line current.

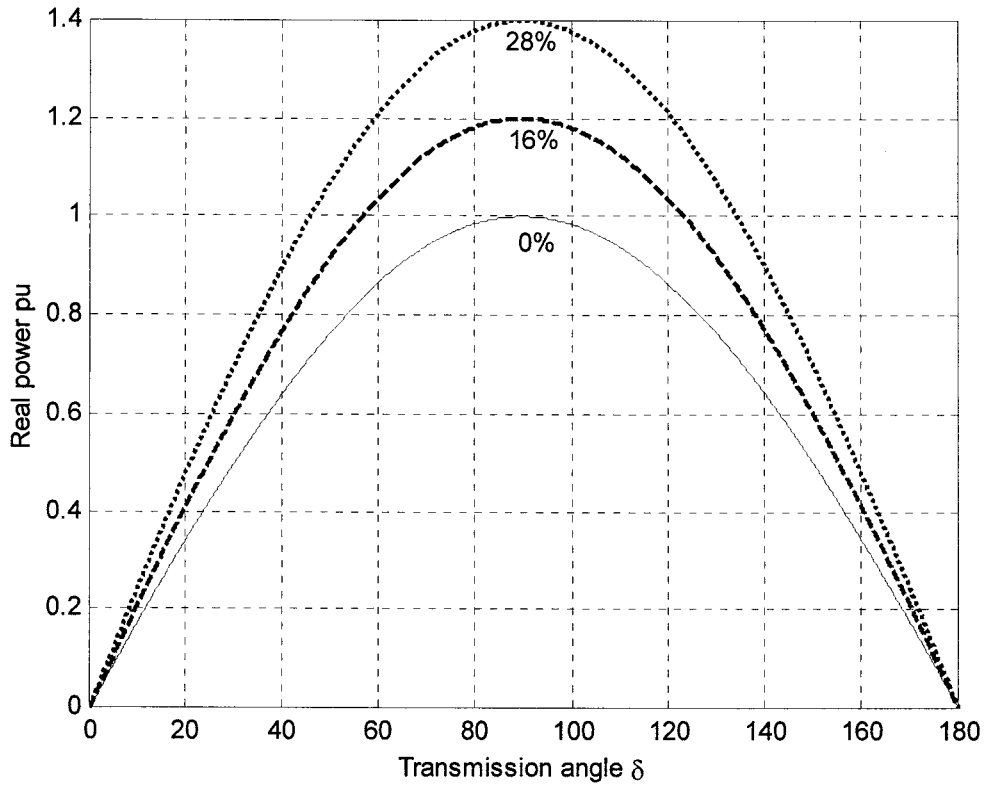

Figure 2.4 Power-angle curves for a transmission system with TCSC.

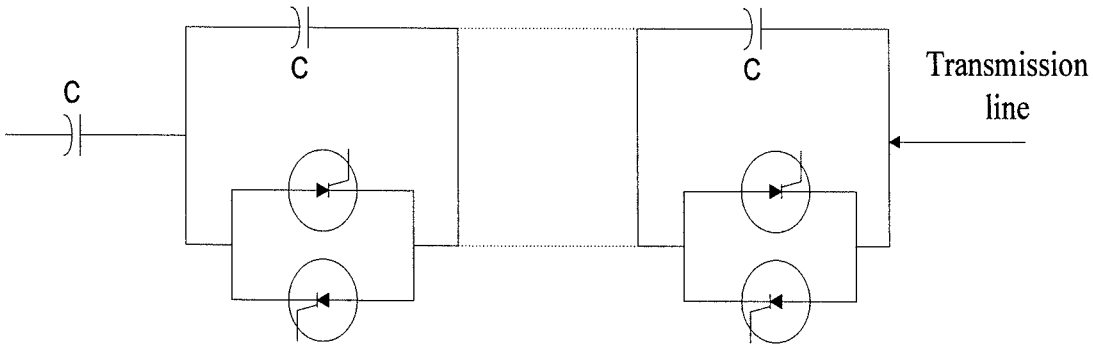

(a) TSC

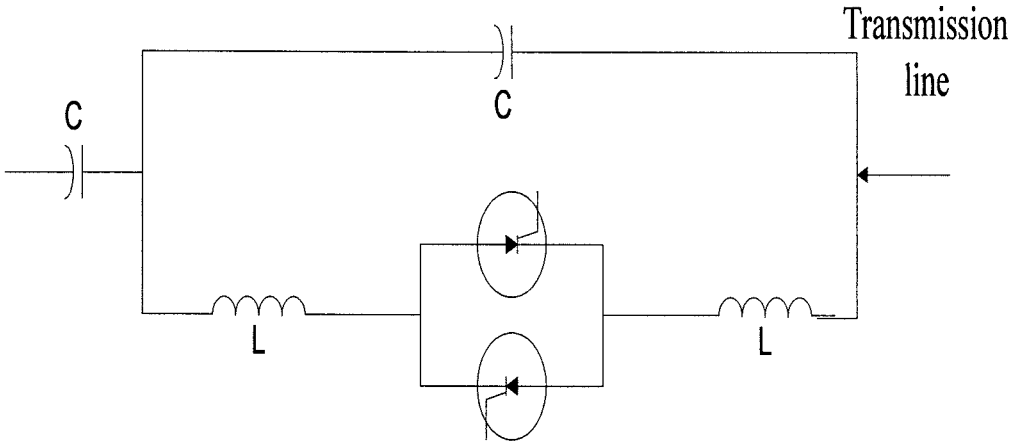

(b) TCR

Figure 2.5 Thyristor controlled series compensator.

2.3.1.3 Thyristor controlled phase shifter (TCPS)

The thyristor controlled phase shifter is used to regulate the system transmission angle by injecting a quadrature voltage in series with the transmission line. This is done in order to maintain balanced power flow in multiple transmission corridors, or to control it so as to increase the transient and dynamic stability of a transmission system [19]. As shown in Figure 2.6, the TCPS consists of a multiple tap-changing shunt transformer, a booster series transformer and a thyristor switch arrangement used to connect a selected combination of tap-voltages to the series transformer. If the injected voltage angle is stipulated to be $\pm 90^0$, the phase shifter is called a quadrature booster and the phase angle between the injected voltage and the line current is arbitrary determined by the relevant parameters of the power system. The significant drawback of the thyristor controlled phase shifter is that it is not capable to locally generate or absorb either real or reactive power. Therefore, any exchange of real or reactive power with the a.c. system should come from the system itself. Consequently, if the exchanged reactive power has to flow through the line, a corresponding voltage drop will be caused. Hence, the installation of the TCPS must be located close to strong power generation node or be complemented by a shunt compensator to provide the required reactive power.

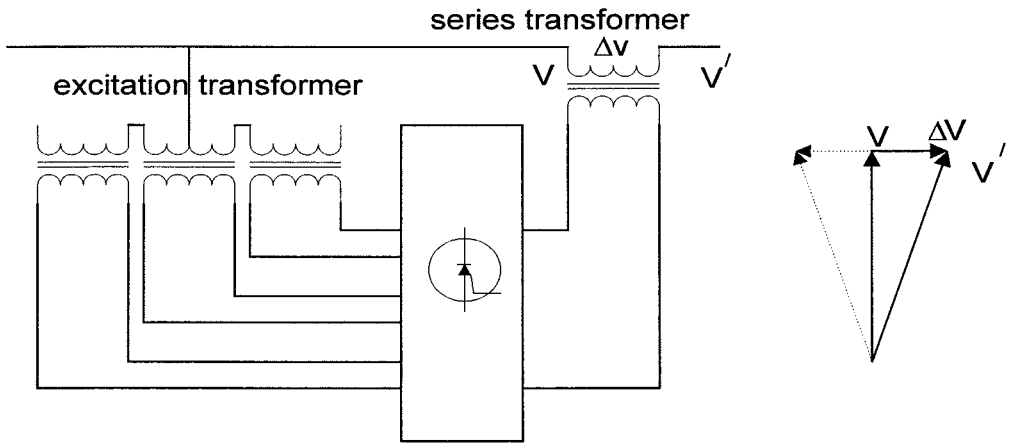

(a) schematic diagram (b) vector diagram

Figure 2.6 Thyristor controlled phase shifter.

2.3.2 Voltage Source Inverter Based FACTS Devices

This group of FACTS controllers, shown in Figure 2.7, employs a synchronous Voltage Source Inverter (VSI) to realise controllers that have superior performance characteristic and uniform applicability for the three transmission system parameters. The VSI can have a d.c. storage or supply, so it is capable of creating a bi-directional real power flow between it's a.c. and d.c. sides, in addition to generate and absorb reactive power at the a.c. side. Connecting the d.c. terminals of two or more VSIs adds new dimension of controlling the power flow.

The VSI FACTS controllers can be used to control independently the real and reactive power flow in individual power transmission lines or balance real and reactive power flow among different lines. Besides, it can also support the system voltage at selected terminals. This group includes the Advanced Static VAr Compensator (ASVC) or STATic COMpensator (STATCOM) as often known in the USA, Static Synchronous Series Compensator (SSSC), Unified Power Flow Controller (UPFC) and the latest device Interline Power Flow Controller (IPFC).

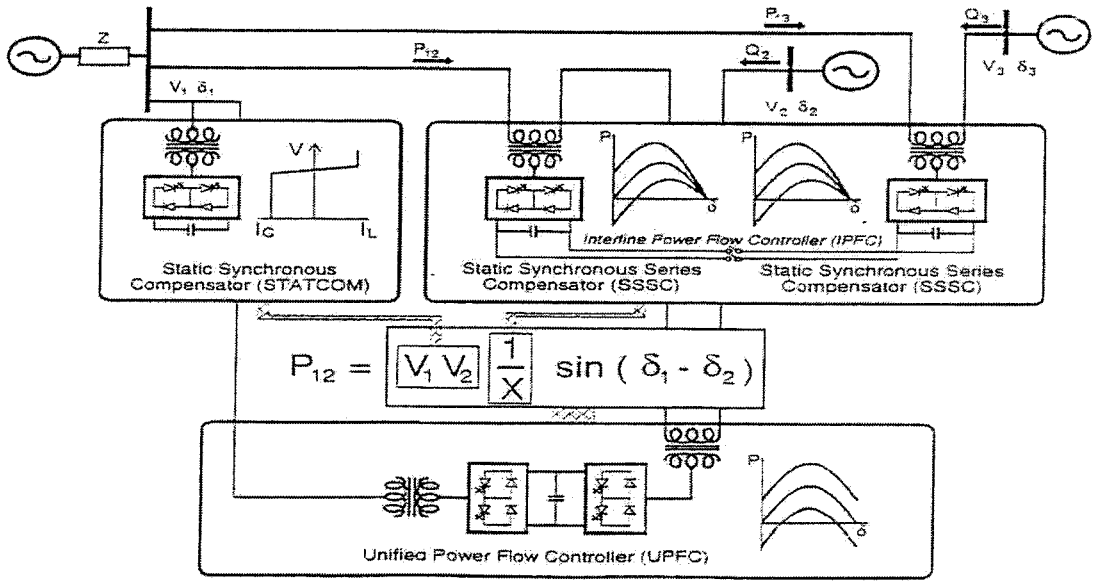

Figure 2.7 VSI based FACTS devices [16].

2.3.2.1 The advanced static VAr compensator (ASVC)

The ASVC is used strictly for shunt reactive power compensation by controlling the converter to generate output voltages that have the same frequency and almost in-phase with the a.c. system voltages. By controlling the magnitude of the converter voltage, it is possible to exchange reactive power with the a.c. system [20]. The ASVC basic system is shown schematically in Figure 2.8-a. That is, if the magnitude of the converter output voltage is increased above that of the a.c. system voltage, then the current flows through the tie reactance from the converter to the a.c. system and leads the voltage by 90^0. Thus, the converter generates capacitive reactive power when viewed from the a.c. system perspective, as shown in Figure 2.8-b. If the amplitude of the converter output voltage is decreased below that of the a.c. system, then the reactive current flows from a.c. system to the converter and lags the voltage by 90^0. Therefore, the converter absorbs inductive reactive power from the a.c. system as shown in Figure 2.8 c. If the amplitude of the output voltage is equal to that of the a.c. system voltage, the reactive power exchange is zero.

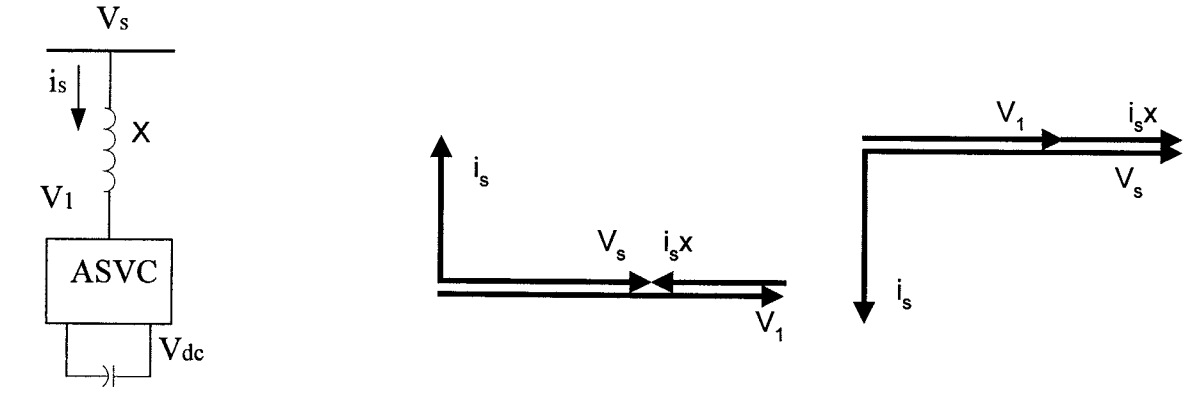

(a) schematic diagram

(b) supplying reactive power

(c) absorbing reactive power

Figure 2.8 The ASVC basic system.

For a lossless converter switches, the net instantaneous power at the a.c. side must always be equal to the net instantaneous power at the d.c. terminal. If the converter supplies only reactive power, the real power provided by the d.c. side must be zero and the d.c. source may be replaced by a d.c. capacitor. Furthermore, since the d.c. reactive power is zero, then the d.c. capacitor plays no role in the reactive power generation. This means that the converter interconnects the three a.c. terminals (for a 3-phase system) in such a way that the reactive output currents can flow freely between them.

There are two main methods of controlling the ASVC reactive power and hence the switching strategy of the inverter [21].

1. Indirect control

The amplitude of the inverter output voltage is varied by changing the d.c. capacitor voltage while maintaining the gate signal pattern fixed. The d.c. voltage is controlled by changing the phase difference between the inverter output voltage and a.c. system bus voltage. Therefore, the reactive power is indirectly controlled by this phase angle difference. As illustrated in the vector diagram in Figure 2.9, by making the ASVC output voltage lead or lag the system voltage, a real power is exchanged between the inverter and the a.c. system which allows for discharging or charging the d.c. capacitor.

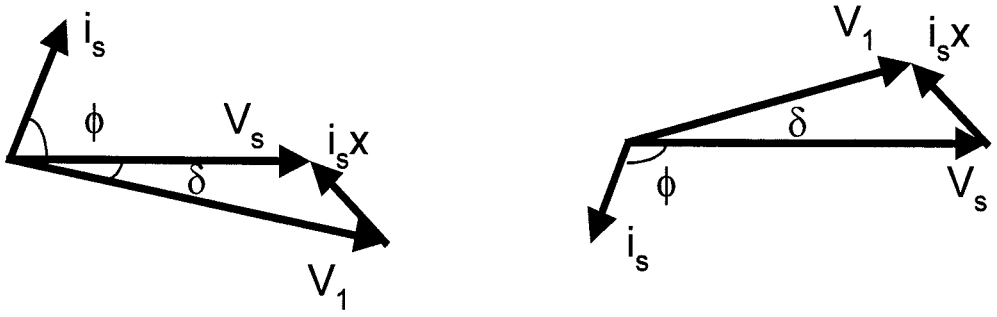

(a) leading mode (b) lagging mode

Figure 2.9 Phasor diagram of a practical ASVC.

2. Direct control

In this method the d.c. voltage is kept constant and the output voltage is directly controlled by the switching strategy (e.g. PWM).

The ASVC V-I characteristics shown in Figure 2.10 imply that the ASVC can provide both capacitive and inductive VAr compensation and is able to control its output current over the rated maximum capacitive or inductive range irrespective of the a.c. system voltage. This is very important when the ASVC is employed to improve the transient stability and damp power oscillations, as it can maintain full compensating current at depressed line voltage occurring during abnormal conditions. The ASVC effectiveness in damping power oscillations is due to its capability to quickly switch between generating and absorbing reactive power.

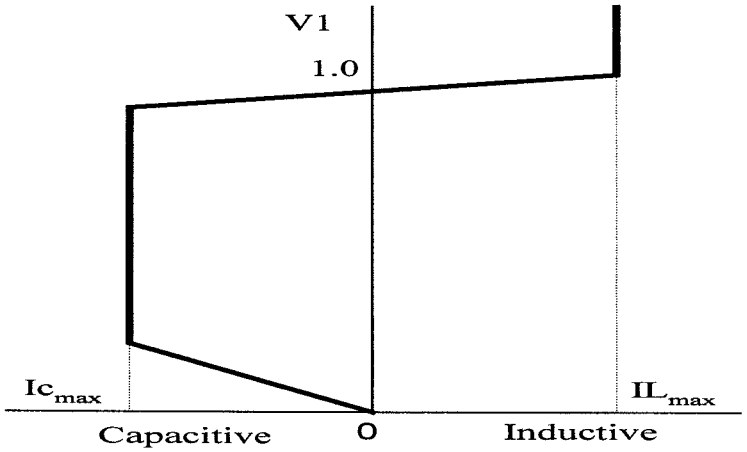

Figure 2.10 V-I characteristic of the ASVC.

2.3.2.2 The static synchronous series compensator (SSSC)

The structure of the SSSC was proposed by Gyugyi in 1989 [22] within the concept of using voltage-source inverter based FACTS for series compensation. The SSSC is similar to the ASVC in construction with the exception that it is connected in series with the transmission line through a booster transformer, as shown in Figure 2.11a. The main idea of

the SSSC is to inject a controlled voltage in series with the transmission line. The magnitude of the inserted voltage is fully controlled while the phase angle is maintained in quadrature with the line current. Unlike the TCSC, the SSSC is able to maintain a constant compensating voltage in face of variable line current or control the amplitude of the injected compensating voltage independent of the amplitude of the line current. However, the angle of the injected voltage can lead or lag the line current which corresponds to adding a series capacitance or inductance with the transmission line, as indicated by the vector diagram shown in Figure 2.11-b. Note that V_q is the injected voltage and V_X is the line impedance voltage drop [23].

As the SSSC is based on the principle of voltage source inverter, it is self sufficient in generating or absorbing reactive power. The power angle curves for a transmission system with and without the SSSC are shown in Figure 2.11-c. The P-δ relationship for a two-machine system can be expressed as follows;

$$P = \frac{V^2}{X}\sin\delta + \frac{V}{X}V_q \cos\delta/2 \qquad (2.1)$$

As explained earlier, the TCSC can only increase the transmitted power by a fixed percentage of the uncompensated power at a given transmission angle. However, the SSSC can increase or decrease the transmitted power by a fixed fraction of the maximum power transmitted by the uncompensated line.

The SSSC can exchange both reactive and active power with the a.c. system, simply by controlling the phase angle of the injected voltage with respect to the line current. The exchange of real power requires that the d.c. terminal of the SSSC to be connected to an energy source / sink.

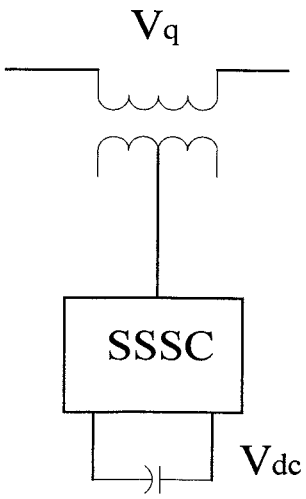

(a) schematic diagram

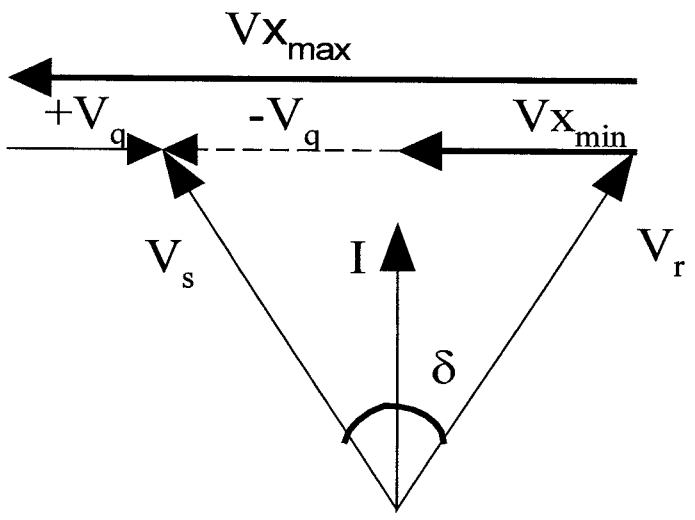

(b) phasor diagram

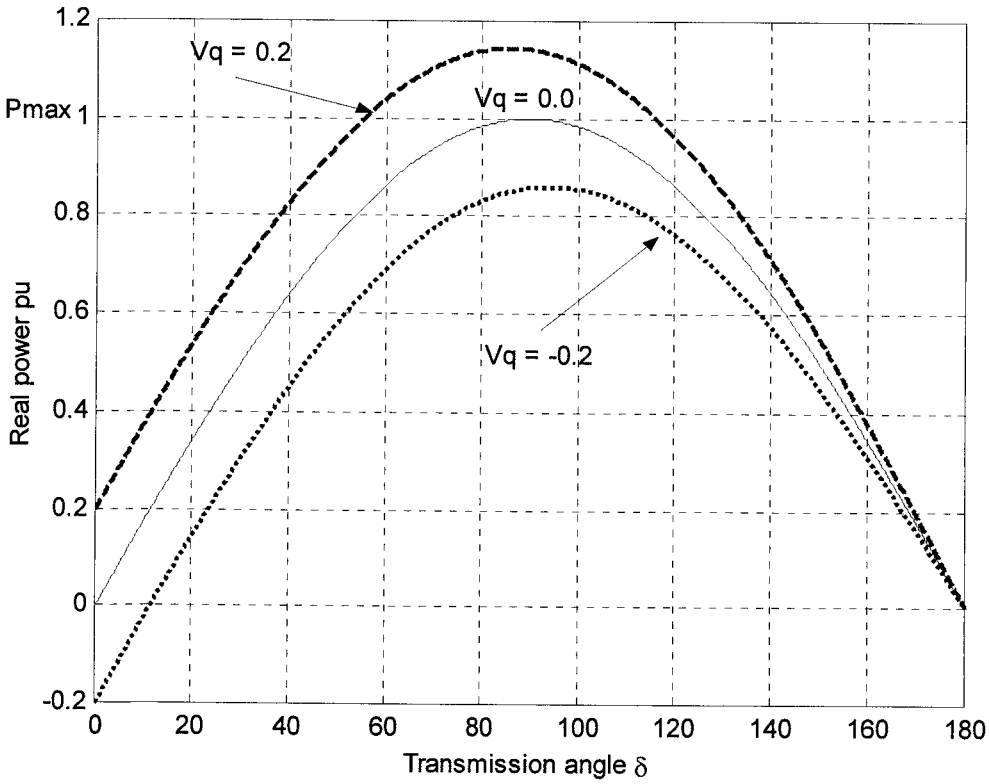

(c) power-angle curves

Figure 2.11 The SSSC basic system.

2.3.2.3 The interline power flow controller (IPFC)

As discussed in the previous sections, the TCSC and SSSC are used to control the real power flow in a given transmission line, they are unable to control the reactive power flow. When using these controllers, the real power flow is increased by reducing the transmission line effective impedance which in turn changes the X/R ratio and thereby changes the reactive power flow and losses in the line.

The Interline Power Flow Controller (IPFC) was proposed by Gyugyi in 1998 [24]. The IPFC consists of two voltage source inverters connected back-to-back through the d.c. link, as shown in Figure 2.12. Each converter works as a SSSC to produce a controllable a.c. output voltage. The magnitude and phase angle of each SSSC output voltage is controlled with respect to a selected bus voltage and the current of the controlled line. Generally, the injected voltage may be split into two components, one in quadrature and one in phase with the relevant line current. The quadrature components provide series reactive compensation for the line while the in-phase components influence the real power transferred between the two lines. The quadrature component of each inverter output can be independently controlled (within the converter VA rating) according to the level of compensation required. As the converters are coupled through the d.c. link, the in-phase components must be controlled so as to ensure a real power balance at their d.c. sides. In other words, the real power taken from one line must be given to the other line. Therefore, the IPFC is capable to control both real and reactive power flow between the lines; thus transfer power from the over-loaded line to the under-loaded line. The voltage components may also be controlled in such a way to compensate against resistive line voltage drops or to increase the effectiveness of the compensating system for dynamic disturbances.

The IPFC concept applied for two lines can be generalised for multiple lines. Thus, under-loaded lines can share the power from over-loaded lines in order to optimize the transmission system utilisation. The net real power exchanged by all the converters must be zero.

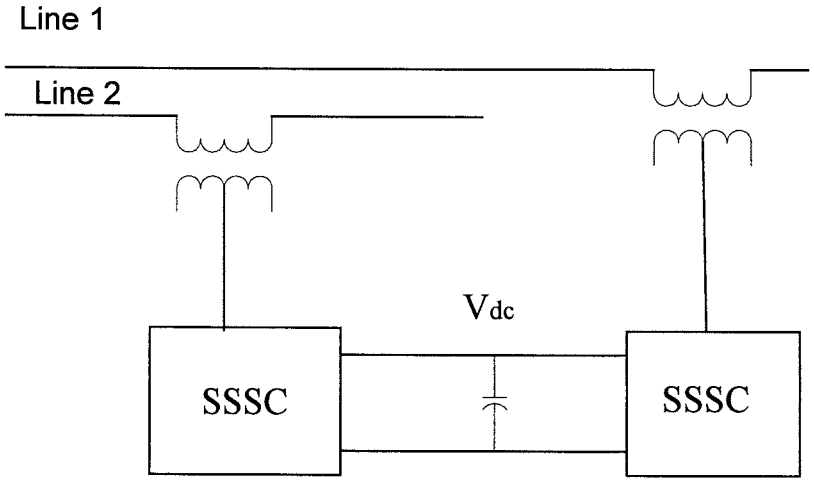

Figure 2.12 The IPFC schematic diagram.

2.3.2.4 The unified power flow controller (UPFC)

The UPFC is the versatile voltage source FACTS device that is capable of controlling any or all of the transmission system parameters (voltage, impedance and angle) [25]. As the UPFC represents the objective in this study, more details of this device are given in the next chapters.

2.4 ADVANTAGES OF THE VOLTAGE SOURCE CONVERTER BASED FACTS

The voltage source inverter provides a set of three-phase output voltages, each of which can be controlled in magnitude and phase angle. FACTS controllers based on voltage source inverters have the following advantages over the thyristor controlled devices.

- They normally employ turn-off power electronic devices like GTO, IGCT, MCT or IGBT which can be more expensive and have higher losses as compared to the thyristor without turn-off capability, however they have significant overall system cost and performance advantages.
- Passive components required for the converter based FACTS controllers are considerably smaller than the corresponding thyristor type.

- Converter-based controllers are able to control their output voltage over the whole VA rating independent of the a.c. system parameters.
- They are able to exchange controllable real power with the a.c. system.
- There is no risk of shunt or series resonant with the inductive line impedance that may initiate sub-synchronous oscillation.

2.5 ADVANTAGES OF THE UPFC OVER CONVERTER BASED FACTS DEVICES

The UPFC is basically a SSSC and an ASVC operated from a common d.c. link. It is capable of generating an a.c. voltage of variable magnitude and phase angle in series with the phase voltage. The SSSC can not independently control the reactive power flow in the line and thus the reactive power remains proportional to the real power. Unlike the SSSC, the magnitude and phase angle of the compensating voltage for the UPFC are independent of the line current and the transmission angle. Therefore, the maximum change in power flow achievable by the UPFC is independent of the transmission angle and is determined only by the maximum inserted voltage. The ASVC part is responsible for supplying the real power demand of the SSSC. Hence, the UPFC allows precise control of both real and reactive power flow. In addition, the ASVC part can operate independently within its VA rating to support the bus voltage or compensate for the load and/or line reactive power. The co-ordination between the UPFC two parts is much depending on the kind of the bus at which the UPFC is connected. It could be a PQ or a PV bus. The total VA exchanged between the UPFC and the a.c. system is not supplied or absorbed by the a.c. system. The UPFC generates the reactive power part of the total exchanged VA by its own capability while exchanges only the real power with the a.c. system.

UPFC PRINCIPLES AND MODES OF OPERATION

3.1 INTRODUCTION

The Unified Power Flow Controller (UPFC) is a sort of multi-function (multi-arm) controller which can play an important role in solving various transmission system problems. The objective of this chapter is to describe the construction, principles and different modes of operation of the UPFC. For clarity a simple single-phase circuit is considered in this chapter to describe the different modes of the UPFC operation.

3.2 CONSTRUCTION OF THE UPFC

The UPFC concept was proposed by Gyugyi [26] in 1992 within the concept of using converter based FACTS technology. It consists of two voltage source inverters connected back-to-back through a common d.c. link, as illustrated in Figure 1.1 which is redrawn in Figure 3.1. This arrangement functions as an ideal a.c. to a.c. power converter in which the real power can freely flow in either direction between the a.c. sides of the two inverters. Due to the different functions of the two inverters in the system, inverter 1 is referred to as the exciter and inverter 2 as the booster. The reactive power on the two a.c. sides of the inverters can be controlled independently.

The series inverter (inverter 2) is connected to the transmission line through a booster transformer in a manner similar to the SSSC. The shunt inverter is connected to the system bus through an excitation transformer in the same way as an ASVC. Therefore, the UPFC can be considered as a multi-function controller which is capable of providing the performance of one or two FACTS devices. Because of its structure, the UPFC provides

new dimensions of controllability, which have not been achieved with other FACTS controllers.

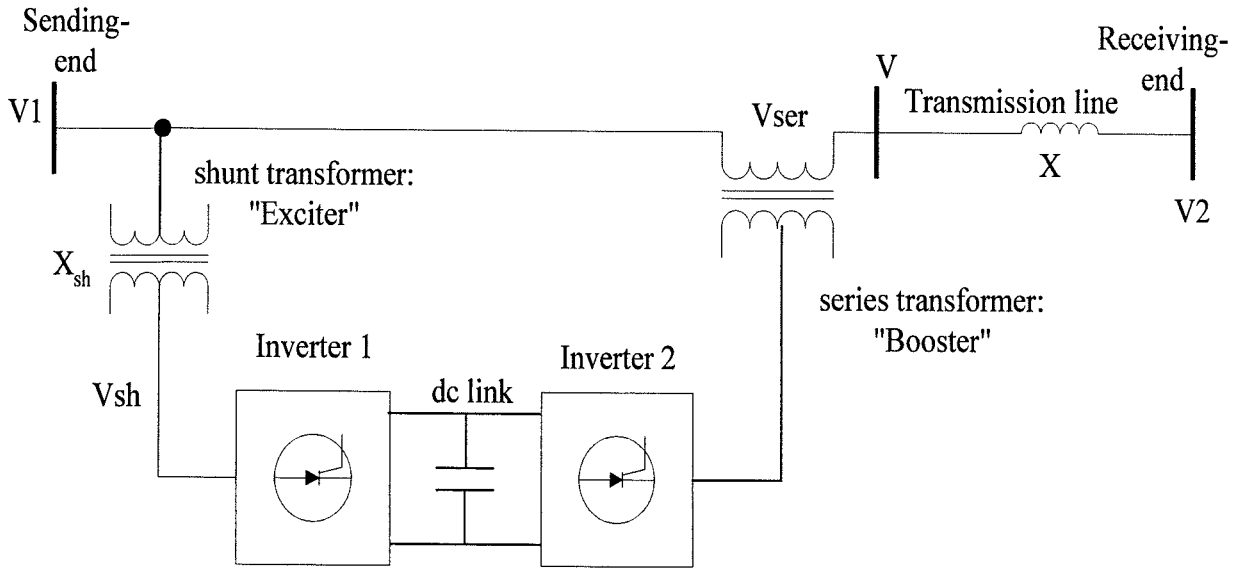

Figure 3.1 Schematic diagram of a UPFC system.

3.3 PRINCIPLES OF OPERATION

The SSSC part of the UPFC performs the main function of the UPFC by injecting a voltage V_{ser} in series with the transmission line. The injected voltage can be controlled with theoretically little restrictions. That is, the phase angle of V_{ser} can be controlled independently of the line current between 0 and 2π, and the magnitude is ranging from zero to a predefined maximum value. This maximum value is determined by the VA rating of the UPFC series inverter [27].

The transmission line current flows through the injected voltage resulting in active and reactive power exchange between the series inverter and the a.c. system. The real power

measured at the inverter output is supplied or absorbed by the d.c. link side. The reactive power is generated or absorbed internally between phases connected by the inverter switches. As the magnitude and phase angle of the series inverter injected voltage is fully controllable, it can be used to achieve different conventional compensation e.g. voltage regulation, series compensation or phase angle regulation.

Inverter 1 (the exciter) which is connected in shunt with the a.c. system is used essentially to provide the active power demand of the series inverter at the common d.c. link. As inverter 1 is a voltage source (viewed from the system), it can generate or absorb reactive power at its connection point. Such reactive power is independent of both the reactive power generated by the series inverter and the active power through the d.c. link. Therefore, the shunt inverter can fulfil the function of the ASVC in providing reactive power compensation at the system busbar and at the same time performing an indirect d.c. voltage regulation within the UPFC.

3.4 MODES OF OPERATION

Conventional power transmission systems employ shunt compensation, series compensation and phase angle regulation. The UPFC can fulfil all these functions and thereby meet multiple control objectives by an appropriate choice of the injected voltage magnitude and angle, as illustrated in the diagram given in Figure 3.2. Therefore, there are different modes of operation for each of the inverters comprising the UPFC depending on the available local reference signals. The UPFC global controller needs to be able to switch between these modes according to the system requirements [28,29].

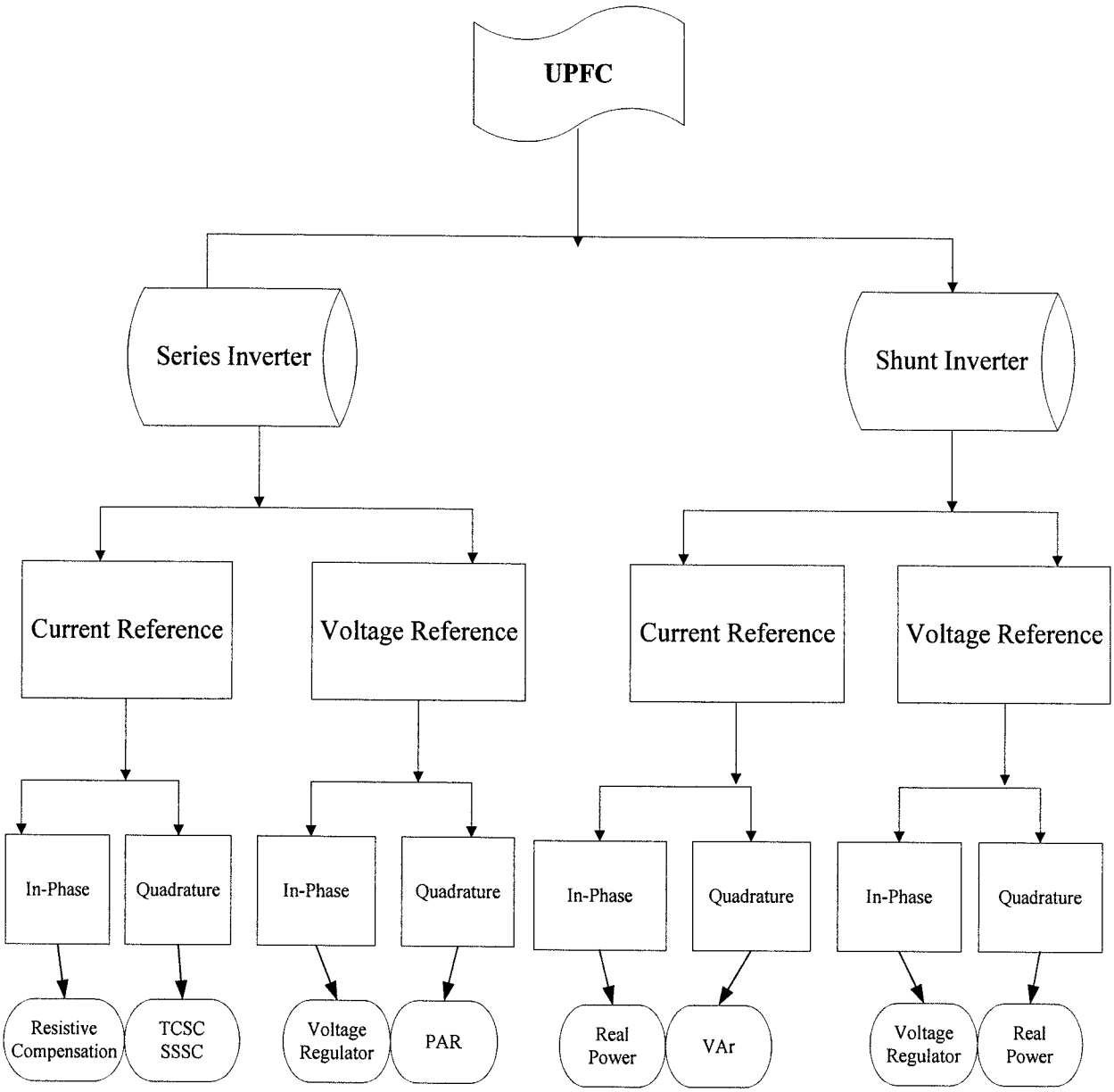

Figure 3.2 UPFC modes of operation.

3.4.1 Series Inverter Modes of Operation

The operation of the series inverter is divided into different modes with distinctive characteristics. These modes are dependent on the reference signal used to derive the magnitude and phase angle of the injected voltage. In power systems the local reference signals normally available are the line current and the system bus voltage. Therefore, these two signals are recommended by many power system researchers to be the reference signals for the UPFC control variables.

3.4.1.1 System voltage as a reference

In these modes, the series inverter generates a voltage vector, which is controlled in both magnitude and phase-angle with reference to the voltage of the system bus at which the UPFC is connected.

Voltage regulation mode

The injected voltage V_{ser} is adjusted to be always in-phase or anti-phase with the bus voltage, as shown in Figure 3.3, while its magnitude is determined by the required percentage voltage regulation. The effective line voltage V (see Figure 3.1) is given as:

$$V = V_1 \pm V_{ser} \tag{3.1}$$

$$V_{ser} = \psi V_1 \tag{3.2}$$

The real power transfer in the transmission line is governed by the following equation:

$$P = \frac{(1 \pm \psi) V_1 V_2}{X} \sin \delta \tag{3.3}$$

Phase angle regulation mode

The UPFC can be operated in this mode to regulate the angle between the two ends of the transmission line. This is achieved by inserting a quadrature voltage of controllable

magnitude with respect to the terminal voltage, as illustrated by the vector diagram shown in Figure 3.4-a. In this case,

$$V_{ser} = \psi V_1 \angle \frac{\pm\pi}{2} \tag{3.4}$$

The effective sending-end voltage V and the real power transfer are described as:

$$V = V_1\sqrt{1+\psi^2} \tag{3.5}$$

$$P = \frac{VV_2}{X}\sin(\delta \pm \theta) \tag{3.6}$$

where $\theta = \tan^{-1}\psi$

Alternatively, the UPFC may play the role of a phase shifting device, if the angle of the injected voltage is controlled such that the magnitude of the voltages at the two transmission ends are kept equal, as shown in Figure 3.4-b.

The effective sending-end voltage and the real power transfer are given as,

$$\overline{V} = \overline{V_1} + \overline{V_{ser}} \tag{3.7}$$

$$P = \frac{V^2}{X}\sin(\delta \pm \theta) \tag{3.8}$$

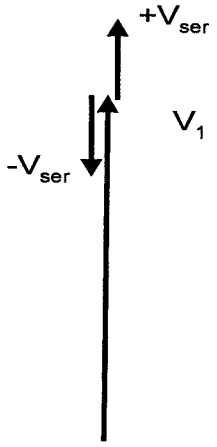

Figure 3.3 UPFC working as a voltage regulator.

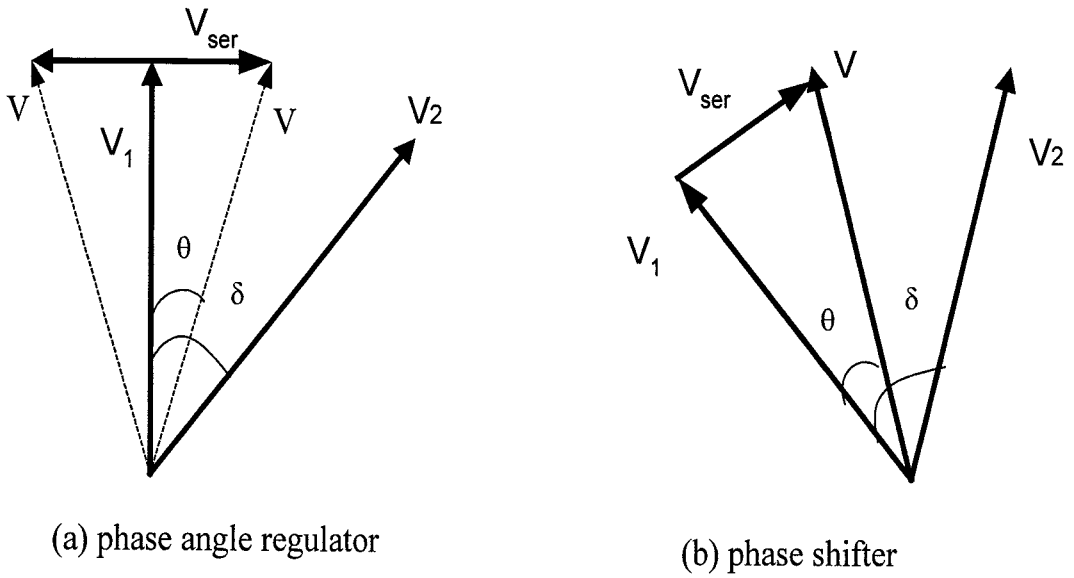

(a) phase angle regulator (b) phase shifter

Figure 3.4 UPFC working as a phase angle regulator or shifter.

3.4.1.2 Line current as a reference

In these modes the injected voltage generated by the series inverter is determined by the transmission line current, as depicted in Figure 3.5.

Line resistive compensation

In this mode, the injected voltage is maintained to be in-phase with the line current in order to compensate the transmission line resistive voltage drop. The key point of such a compensation scheme is to keep the transmission system X/R ratio within an acceptable range based on the line voltage rating.

Line reactive compensation

The injected voltage compensates for the reactive part of the transmission system impedance when it is perpendicular to the line current and its magnitude is proportional to

the current magnitude. If the injected voltage is always made to lag the line current by 90^0, the UPFC operates similar to the TCSC and the injected voltage is given as:

$$V_{ser} = -jkI \tag{3.9}$$

where I is the line current and k is the required compensation ratio.

The series inverter can be controlled to behave similar to the SSSC if the injected voltage is in quadrature with the transmission line current and its magnitude is controlled between zero and maximum value. In this case, the inserted voltage magnitude is dependent on the system requirements and independent of the line current magnitude (with the assumption that the inverter has an energy storage source at its d.c. side). The injected voltage equation in this case is:

$$V_{ser} = \pm j|V_{ser}|\frac{\bar{I}}{I} \tag{3.10}$$

Therefore, the series inverter is able to maintain a constant compensating voltage against the variable line current.

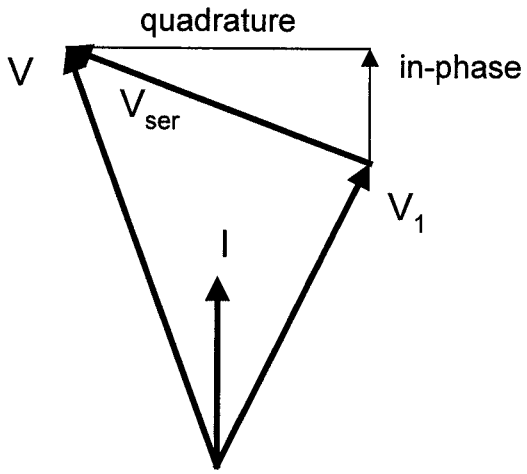

Figure 3.5 UPFC with current reference.

3.4.1.3 Power flow mode

The unified power flow control approach (series inverter) can be broadening the basic power transmission concepts. It is not only possible to implement the individual compensation scheme discussed above but also a combination or real time transition from one mode of operation to another one in order to handle particular system contingencies more effectively than the other single function FACTS controllers.

In theory, the UPFC may be used to maintain a prescribed and independently controllable real and reactive power flow in a certain transmission corridor. In this case, the injected voltage V_{ser} is stipulated to have no phase angle restrictions and its magnitude is variable between zero and a maximum permissible value. In practice, the UPFC may be used to maintain or vary the active and reactive power flow in a transmission system within a specific margin. The operating point can be anywhere inside a circle with a radius $\left|V_{ser_{\max}}\right|$, as shown in Figure 3.6.

This particular, but more general, mode of operation has been chosen in this work to analyse the capabilities of the UPFC to control the system power flow.

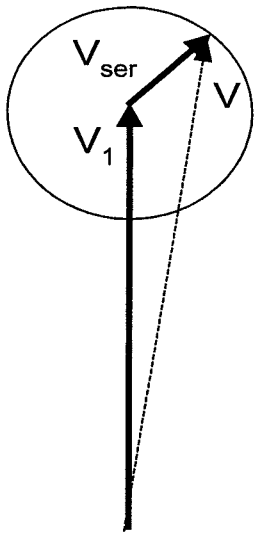

Figure 3.6 UPFC in the power flow mode.

3.4.2 Shunt Inverter Modes of Operation

The shunt inverter is operated to absorb or generate certain amount of reactive power from/to the a.c. system. In addition, it provides the real power demand of the series inverter and power losses. Similar to the series inverter, the shunt inverter modes of operation are dependent on the reference signal used to derive the magnitude and angle of the inverter output voltage.

3.4.2.1 System bus voltage as a reference

The inverter output voltage (V_{sh}) may be split into two components (V_p and V_q) with respect to the a.c. system bus voltage (V_1) at which the UPFC is connected, as shown in Figure 3.7. The in-phase component may be used to control the system bus voltage in order to immune the controlled transmission line from the changes within the rest of the network. The quadrature component allows the shunt inverter to exchange real power with the a.c. system which is required for the series inverter. This mode of operation is quoted as "Bus Voltage Control Mode", and is chosen to be the principle mode of operation of the shunt inverter throughout the thesis.

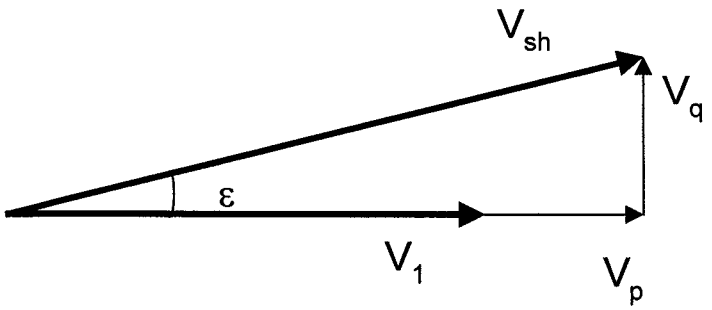

Figure 3.7 Shunt inverter in "voltage control mode".

3.4.2.2 Shunt inverter current as a reference

When the current is used as a reference signal, the inverter output voltage may be divided into two perpendicular components. The in-phase component will allow the shunt inverter to exchange real power with the d.c. link and provide for the power losses. The quadrature component is responsible for the exchange of reactive power with the a.c. system. This in turn support the reactive power in the transmission system irrespective of the variation of the bus voltage. This case is called "Reactive Power Mode".

3.5 VA RATING OF THE UPFC

The UPFC composes of two inverters, each inverter has its own VA rating which could be identical or different. For the series inverter, the VA rating is determined by the series injected voltage and the system line current which is a function of the transferred power and the impedance of the transmission line. The maximum VA rating of the series inverter is calculated from the product of the maximum injected voltage and the maximum line current at which the power flow is provided. This rating is split into two components. The first is the maximum active power exchanged between the series inverter and the a.c. system which is determined by the maximum line current and the component of the maximum injected voltage in-phase with the current. As discussed earlier, this active power must be provided to the series inverter at its d.c. side. The second component is the maximum reactive power that the inverter can internally generate or absorb at it's a.c. side. This rating can be calculated from the maximum line current and the component of the maximum injected voltage in quadrature with the current.

For the shunt inverter, the maximum VA rating is composed from two main components. The first is realized by the maximum real power to be exchanged with the series inverter through the common d.c. link. The second component is determined by the

maximum reactive power required to support the transmission system (a.c. bus voltage in the "bus voltage mode", or reactive power demand in the "reactive power mode"). For the shunt inverter operation, the series inverter real power demand should have a higher priority over the reactive power support.

POWER FLOW CONTROL AND UPFC OPERATING LIMITS

4.1 INTRODUCTION

FACTS devices are used for the reinforcement of power transmission networks. UPFC as the most comprehensive FACTS device has been under intensive investigations since it was introduced. To analyse the impact of the UPFC on a transmission system, two types of constraints need to be considered. One is the system constraint which relates to the feasible operating region to ensure voltage and power stability (defining the optimum boundaries of this region is not the purpose of this study). The other constraint relates to the UPFC control parameters which are determined by the VA rating of the UPFC inverters. These parameters specify how the UPFC should be controlled to operate within its feasible region and enhance the a.c. system. In this chapter, the impact of the UPFC series and shunt inverters on the power flow is analysed. The system constraints and their effects on the UPFC control are investigated. The operation range of the UPFC control variables is defined and the effects of the system short circuit level on the UPFC operating area are analysed.

4.2 POWER FLOW CONTROL USING THE UPFC

As discussed earlier, the UPFC has two main parts which can work independently or together to perform its multiple function. The series inverter injects a controlled synchronous voltage in series with the transmission system and the shunt inverter produces a voltage which is used to support the bus voltage at which the UPFC is connected. In this

section, the effects of the UPFC control variables on the power-angle curve of the power system are analysed and the system control strategy is defined.

4.2.1 Analysis of the Series Part

The system shown in Figure 4.1 is used to analyse the effectiveness of the injected series voltage on the power transfer. Assuming V_i is fixed and the series injected voltage is split into two orthogonal components, as shown by the phasor diagram in Figure 4.2. The voltage of bus *i* (at which the shunt inverter is connected) is taken as the phase reference. The two components of the injected voltage are in-phase (reactive component ΔV_Q) and quadrature (active component ΔV_P) with the reference. The two components are normalised by introducing new parameters β and γ which represent the injected voltage in per unit (pu) as follows:

$$\beta = \frac{\Delta V_Q}{V_i} \tag{4.1}$$

$$\gamma = \frac{\Delta V_P}{V_i} \tag{4.2}$$

4.2.1.1 Control of real power flow

Ignoring the resistance in the transmission system, the real power transfer through the transmission system prior to installing the UPFC is approximately given as:

$$P_{prior} = \frac{V_i V_j}{X_s} \sin\theta_{ij} \tag{4.3}$$

The inserted voltage modifies the magnitude and relative phase angle of the transmission line sending-end voltage with respect to the receiving-end. Therefore, the real power flow

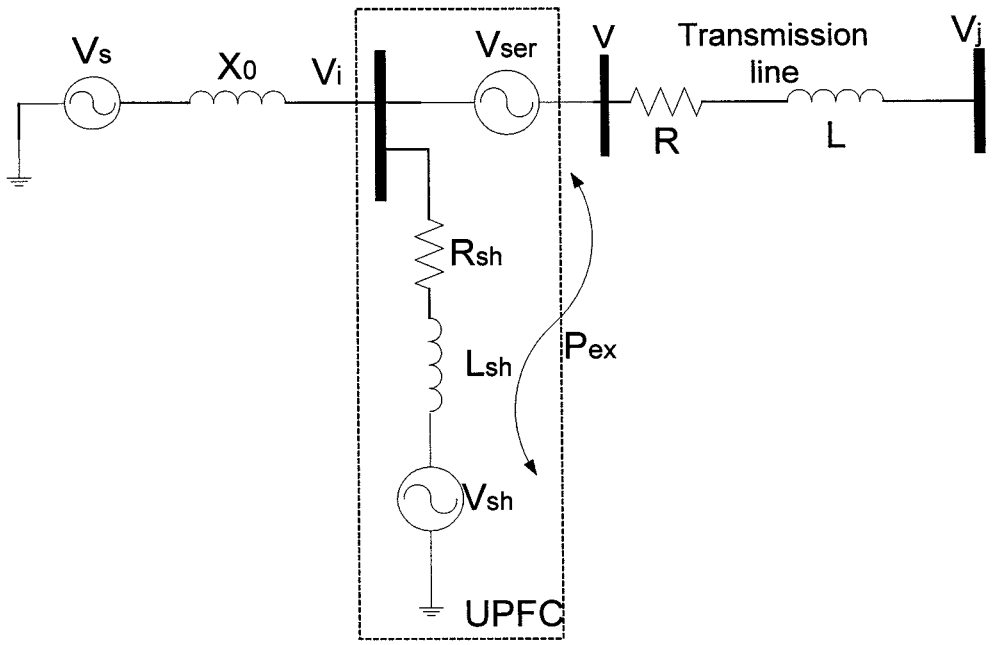

Figure 4.1 A simple transmission system model including the UPFC.

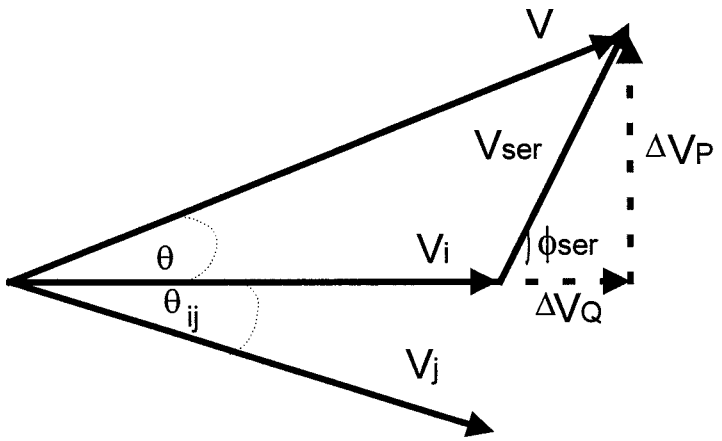

Figure 4.2 UPFC vector diagram "series part".

through the line may be controlled by the two components of the injected voltage as shown below;

$$P = \frac{VV_j}{X_s}\sin(\theta_{ij} + \theta) \tag{4.4}$$

$$P = \frac{VV_j}{X_s}(\sin\theta_{ij}\cos\theta + \cos\theta_{ij}\sin\theta) \tag{4.5}$$

From the phasor diagram illustrated in Figure 4.2

$$\sin\theta = \frac{\Delta V_P}{V} = \frac{\gamma V_i}{V} \tag{4.6}$$

$$\cos\theta = \frac{V_i + \Delta V_Q}{V} = \frac{V_i + \beta V_i}{V} \tag{4.7}$$

Therefore, $P = \frac{V_i V_j}{X_s}(\sin\theta_{ij} + \beta\sin\theta_{ij} + \gamma\cos\theta_{ij})$ (4.8)

It can be noted from Equation 4.8 that the combination of both the in-phase and quadrature components of the inserted voltage determines the rating of the series part of the UPFC.

The power-angle curves are shown in Figure 4.3. The calculation regarding each curve has been determined for one controlled variable while the other one is set to zero. The real power is monotonically increasing with the increase in the in-phase component level β. As can be noticed, the effect of the in-phase injected voltage (β) on real power flow is considerable at large values of the transmission angle where it influences the maximum power transferable in the steady-state. The quadrature-injected voltage (γ) has a significant effect at small transmission angle while the maximum power is not affected. At transmission angle less than 45°, the real power is dominantly affected by γ and hence this component is normally used to control the real power flow in a transmission system.

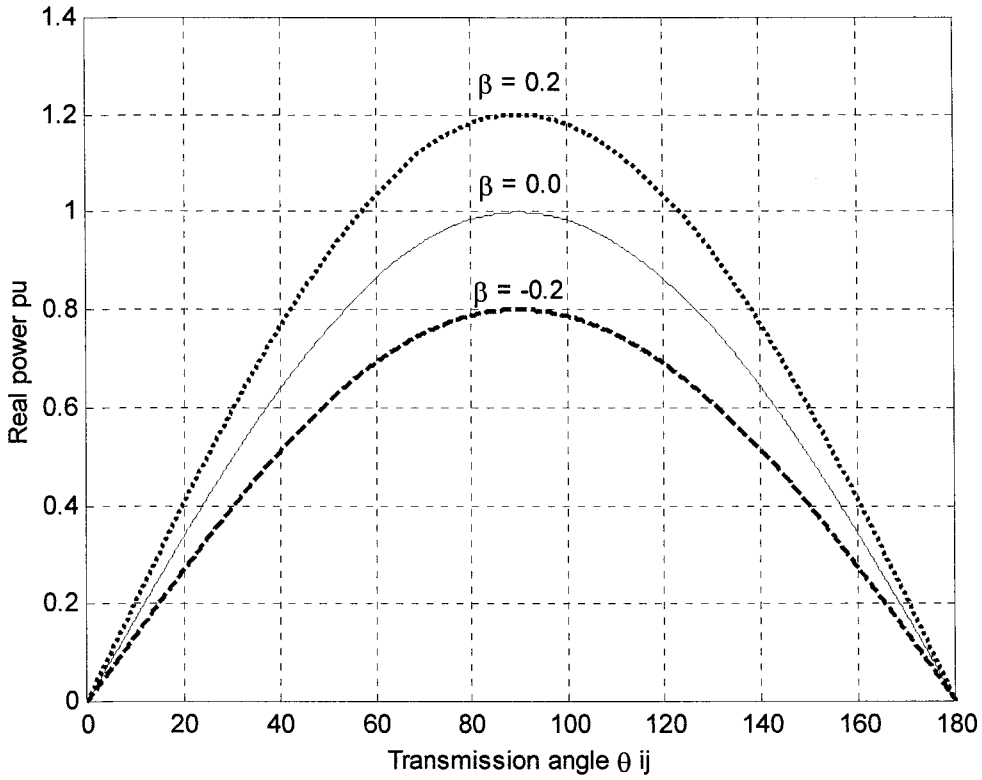

(a) $\beta = 0.2, 0.0, -0.2, \gamma = 0.0$

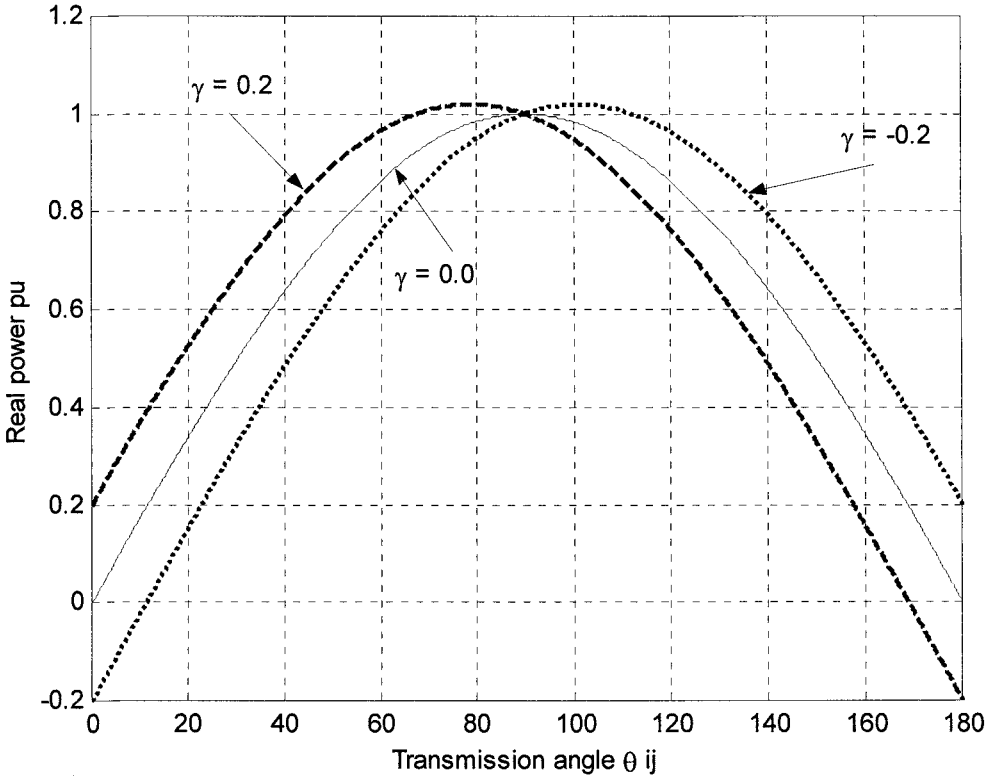

(b) $\beta = 0.0, \gamma = 0.2, 0.0, -0.2$

Figure 4.3 Real power-angle curves for different series injected voltages.

4.2.1.2 Control of reactive power flow

Ignoring the effects of the transmission system resistance, the reactive power transferred through the transmission system prior to installing the UPFC is approximately equal to:

$$Q_{prior} = \frac{V_i^2}{X_S} - \frac{V_i V_j}{X_S}\cos\theta_{ij} \tag{4.9}$$

Adding a series voltage will modify the reactive power flow in the transmission line as follows:

$$Q = \frac{V^2}{X_s} - \frac{V V_j}{X_s}\left(\cos\theta_{ij}\cos\theta - \sin\theta_{ij}\sin\theta\right) \tag{4.10}$$

Substituting Equations 4.6 and 4.7 into Equation 4.10 yields:

$$Q = \frac{\left(1+\gamma^2+2\beta+\beta^2\right)V_i^2}{X_S} - \frac{V_i V_j}{X_S}\left(\cos\theta_{ij} + \beta\cos\theta_{ij} - \gamma\sin\theta_{ij}\right) \tag{4.11}$$

The reactive power-angle curves are shown in Figure 4.4. As for the real power case, each curve was determined for one control parameter with the other assumed to be zero. It is obvious from the graphs that both voltage components β and γ have significant effect on the reactive power flow. The in-phase component influence is uniformly distributed over the controlled range of the transmission angle. However, the quadrature component major effect occurs in the interval 45°-90°. Therefore, the in-phase component of the injected voltage may be used to control the reactive power flow.

4.2.2 Analysis of the Shunt Part

The bus voltage V_i or the shunt current may be taken as a reference for the shunt inverter. In order to reduce the reference signals used for the whole UPFC, the bus voltage is chosen as a reference for the shunt inverter output voltage. The inverter output voltage is

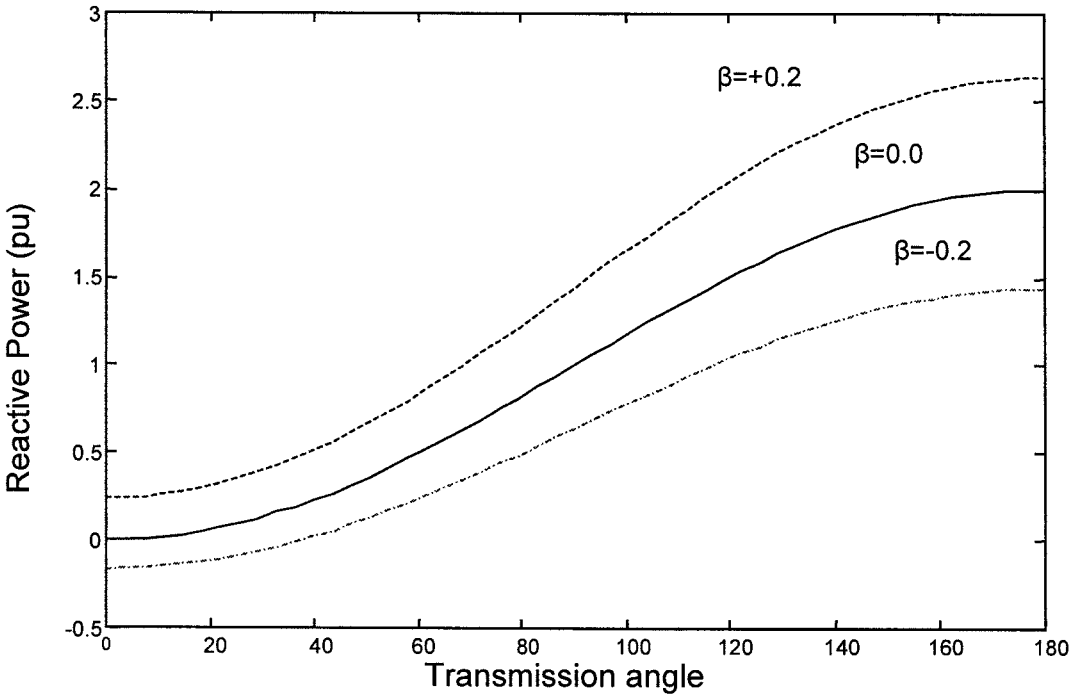

(a) $\beta = 0.2, 0.0, -0.2, \ \gamma = 0.0$

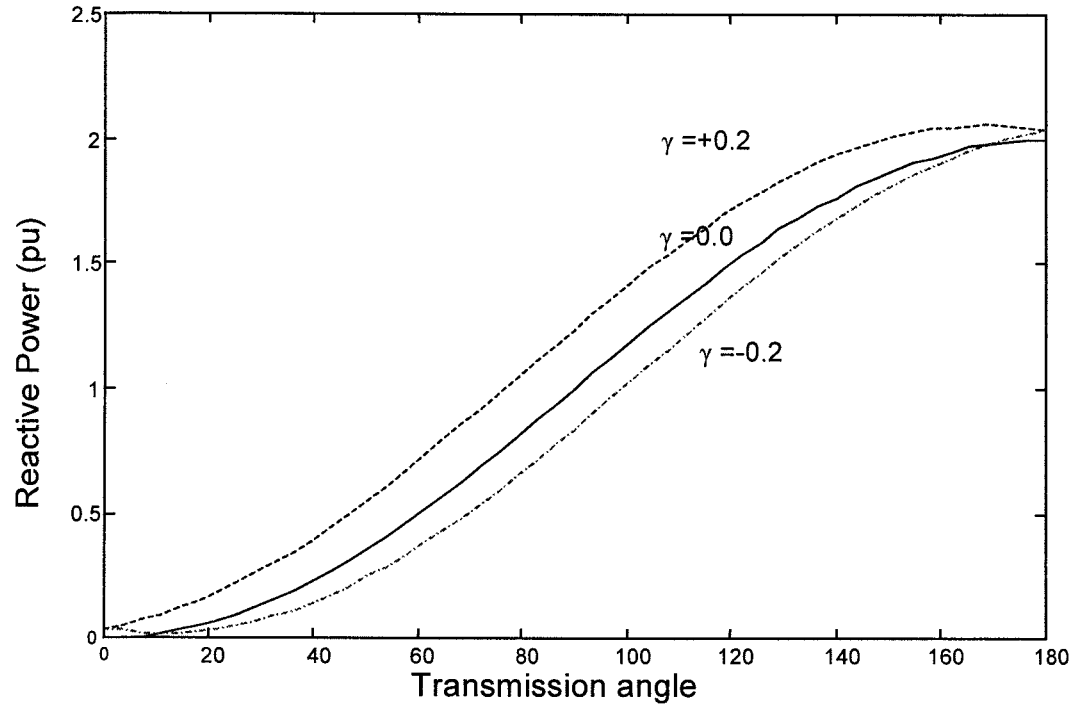

(b) $\beta = 0.0, \gamma = 0.2, 0.0, -0.2$

Figure 4.4 Reactive power-angle curves for different series injected voltages.

split into two orthogonal components, as shown in Figure 4.5. The real and reactive power flow in the shunt branch may be expressed as:

$$P_{sh} = \frac{V_i V_{sh}}{X_{sh}} \sin \varepsilon \tag{4.12}$$

$$Q_{sh} = \frac{V_i^2}{X_{sh}} - \frac{V_i V_{sh}}{X_{sh}} \cos \varepsilon \tag{4.13}$$

From the phasor diagram illustrated in Figure 4.5

$$\sin \varepsilon = \frac{\xi V_i}{V_{sh}} \tag{4.14}$$

$$\cos \varepsilon = \frac{V_i + \eta V_i}{V_{sh}} \tag{4.15}$$

Substituting Equations 4.14 and 4.15 into Equations 4.12 and 4.13, yields:

$$P_{sh} = \frac{V_i^2}{X_{sh}} \xi \tag{4.16}$$

$$Q_{sh} = -\frac{V_i^2}{X_{sh}} \eta \tag{4.17}$$

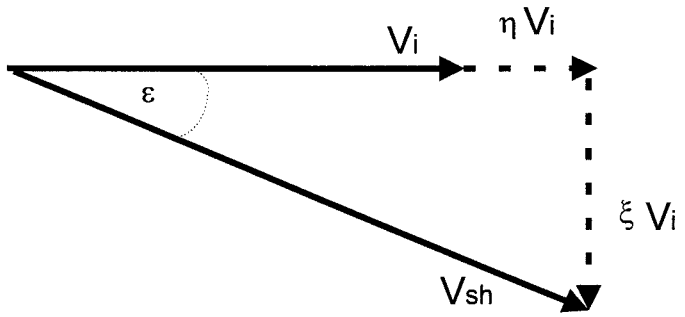

Figure 4.5 UPFC vector diagram "shunt part".

It is obvious that the real power exchanged between the shunt inverter and the a.c. system is determined by the level of the quadrature component of the inverter output voltage (ξ). This power must be balanced by the real power demand of the series inverter, in addition to supply the inverter losses. The reactive power generated or absorbed by the shunt inverter is controlled by the in-phase component of the inverter output voltage (η). The maximum value of the reactive power exchanged with the a.c. system is determined by the VA rating of the inverter and the real power transferred across the d.c. link to support the series inverter.

The effects of the shunt part of the UPFC on the power flow are similar to those for the ASVC and are well addressed in the literatures. The ASVC is normally used to support the mid-point voltage which in turn allows for controlling the active and reactive power flow in the transmission line. In the UPFC operation, the shunt part is used to support the sending-end voltage. Therefore, the shunt part has no role in increasing or decreasing the active power flow in the transmission line. However, it will affect the reactive power flow as will be shown later in this chapter.

4.3 THE UPFC INTERNAL LIMITS

The power system feasible operating region is determined by the system topology and the physical limits of its components. The aim of this study is to determine the UPFC control variables which allow the best use of the existing a.c. system. The most common constraints that should be taken into account when dealing with the UPFC control capabilities are [30,31]:

- The maximum injected current by the shunt inverter.
- The maximum injected voltage by the series inverter.
- The maximum current in the series inverter.
- The maximum power transfer between inverters.
- The line voltage limits for the transmission line.

These limits can be summarized as the VA rating of the UPFC inverters. This VA rating is determined at the planning phase where its value depends on the characteristic parameters and the control requirement of the system network under study. From these limits, the feasible region of the UPFC control variables is identified which should ensure that collapse of the system voltage or violation of the system security limits will never occur. Also, the UPFC feasible operating area is affected by the system short circuit level. In this study, the feasible region is defined as the allowable combination of the active and reactive power flow in a transmission system operating under the influence of a UPFC.

There are two ways of determining the UPFC feasible region, each way depends on the modelling technique used to represent the UPFC. The first is the power injection-based method and the second depends on the dynamic operation of the device.

Since the UPFC has more than one control variable to be determined, its global feasible region is a hyper space and is not straightforward to be defined. Therefore, only one

control variable is varied while the other control variables are fixed until the system reaches the yield point on the boundary of the feasible region. This process is repeated for all control variables and at the end, a complete vision of the UPFC feasible region can be obtained. The yield point at which the system starts collapsing is defined as the point at which the Jacobian matrix of the power flow injection model becomes singular [32].

For the dynamic UPFC model, all the system limits are continuously monitored and the UPFC control variables are re-adjusted upon violation of the limits. When one of the constraints is violated, the range of ϕ_{ser} (which makes the violated variable stay within the feasible range) are recalculated while the amplitude of the series injected voltage is kept constant at its maximum value [33]. The optimal value of ϕ_{ser} is chosen from this range which maximises the real power flow in the transmission line. The drawback of this method is that the role of the shunt inverter is ignored and the series inverter has to operate under its maximum rating.

In this work, the dynamic model of the UPFC is considered. The system limits are determined during the design stage, which are mainly reflected in the inserted voltages. Therefore, the effects of the maximum inserted voltage on the UPFC feasible region are investigated. The feasible operating area of the power system incorporating an unrestricted UPFC is first identified. Then, the UPFC operating area in terms of active and reactive power transfer capability is derived. Based on this analysis the UPFC control variables are defined. If a limit is exceeded, a power flow optimiser is designed to identify the best operating point.

4.4 THE UPFC FEASIBLE OPERATING AREA

The operating characteristic of a transmission network expressed in the P_Q plane shown in Figure 4.6 can be characterised by the system transmission angle. An increase of

real power flow in certain corridor requires an increase of the system transmission angle which will also increase the reactive power.

When using the UPFC, the active and reactive power flow in the transmission line can be controlled. The real power flow prior to installing the UPFC and after installation are described by Equations 4.3 and 4.8, respectively:

The per unit change in real power is given as follows,

$$\Delta P = \beta \sin\theta_{ij} + \gamma \cos\theta_{ij} \tag{4.18}$$

The reactive power flow prior to installing the UPFC and after installation are described by Equations 4.9 and 4.11, respectively:

The per unit change in reactive power is given as follows,

$$\Delta Q = \gamma^2 + \gamma \sin\theta_{ij} + \left(2 - \cos\theta_{ij}\right)\beta + \beta^2 \tag{4.19}$$

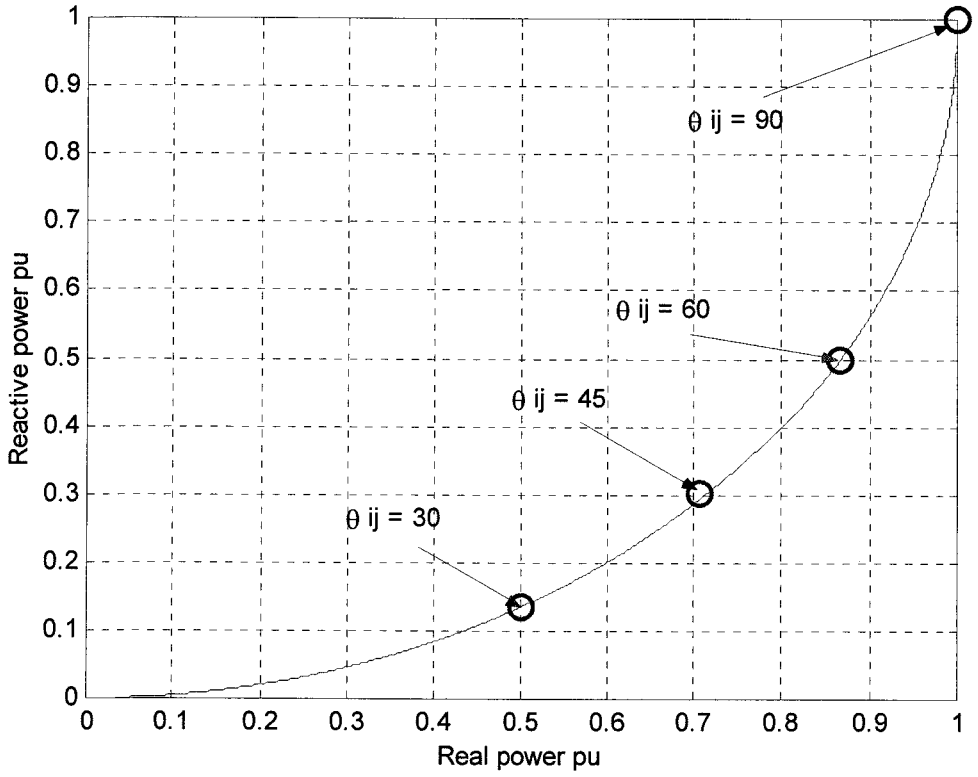

Figure 4.6 P-Q curve for an uncompensated system.

The quadrature phase voltage γ can be derived from Equation 4.18 as:

$$\gamma = \frac{\left(\Delta P - \beta \sin\theta_{ij}\right)}{\cos\theta_{ij}} \tag{4.20}$$

Substituting for γ from Equation 4.20 into Equation 4.19 yields:

$$\Delta Q = \frac{\left(\Delta P - \beta \sin\theta_{ij}\right)^2}{\cos^2\theta_{ij}} + \frac{\left(\Delta P - \beta \sin\theta_{ij}\right)}{\cos\theta_{ij}} \sin\theta_{ij} + \left(2 - \cos\theta_{ij}\right)\beta + \beta^2 \tag{4.21}$$

Rearrange Equation 4.21

$$a\beta^2 + b\beta + c = 0 \tag{4.22}$$

where $a = 1$, $b = 2\cos^2\theta_{ij} - \cos\theta_{ij} - 2\Delta P \sin\theta_{ij}$, and

$$c = \Delta P^2 + \Delta P \sin\theta_{ij} \cos\theta_{ij} - \Delta Q \cos^2\theta_{ij}$$

$$\therefore \beta = \min\left(\left|\frac{-b \pm \sqrt{b^2 - 4ac}}{2a}\right|\right) \tag{4.23}$$

β is the minimum value of the in-phase injected voltage component. To find a real solution for Equation 4.23, the inequality condition of the following general quadratic equation should be satisfied.

$$b^2 - 4ac \geq 0$$

which leads to:

$$\Delta P^2 + 2\Delta P \sin\theta_{ij} - \Delta Q \leq 0.25 - \cos\theta_{ij} + \cos^2\theta_{ij} \tag{4.24}$$

This means that the desired change in the active and reactive power flow in the transmission line must satisfy this condition so that the required series compensation voltage can be provided.

The Inequality 4.24 represents the feasible operating area assuming an ideal UPFC without control restrictions. This feasible region is characterised by the initial transmission

angle θ_{ij}. The feasible area is shown in Figure 4.7 as the inside region of the curve. Two feasible areas are given in the figure for transmission angles $\theta_{ij} = 20^0$ and $\theta_{ij} = 30^0$.

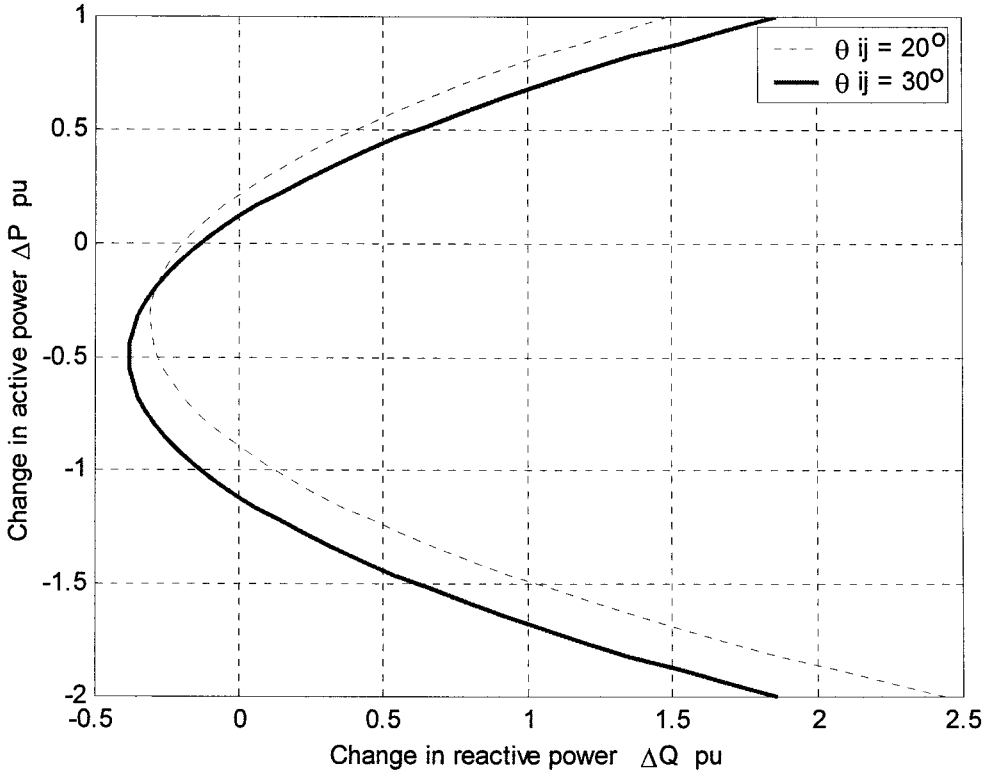

Figure 4.7 Operating area of a transmission system with an ideal UPFC.

4.4.1 Impact of the Series Inverter on the Feasible Operating Area

The whole area defined by Inequality 4.24 is only available for the system designers if there is no limits on the UPFC rating. In practice, the UPFC VA rating limits this area. The changes in active and reactive power flow resulting from the injection of the series voltage are expressed by Equation 4.18 and 4.19 where,

$$\beta = V_{ser} \cos\phi_{ser}$$
$$\gamma = V_{ser} \sin\phi_{ser}$$

Therefore, ΔP and ΔQ may be given as,

$$\Delta P = V_{ser}\cos\phi_{ser}\sin\theta_{ij} + V_{ser}\sin\phi_{ser}\cos\theta_{ij} \tag{4.25}$$

$$\Delta Q = V_{ser}^2 - \left(\cos\theta_{ij} - 2\right)V_{ser}\cos\phi_{ser} + V_{ser}\sin\phi_{ser}\sin\theta_{ij} \tag{4.26}$$

In order to eliminate ϕ_{ser} from Equations 4.25 and 4.26, the relationship between the real power deviation ΔP and the reactive deviation power ΔQ in terms of the injected voltage can be obtained as:

$$\sin\theta_{ij}\cos\phi_{ser} + \cos\theta_{ij}\sin\phi_{ser} = \frac{\Delta P}{V_{ser}} \tag{4.27}$$

$$\left(2 - \cos\theta_{ij}\right)\cos\phi_{ser} + \sin\theta_{ij}\sin\phi_{ser} = \frac{\Delta Q}{V_{ser}} - V_{ser} \tag{4.28}$$

Arranging Equations 4.25 and 4.26 in matrix notation gives:

$$\begin{bmatrix} \sin\theta_{ij} & \cos\theta_{ij} \\ 2-\cos\theta_{ij} & \sin\theta_{ij} \end{bmatrix}\begin{bmatrix} \cos\phi_{ser} \\ \sin\phi_{ser} \end{bmatrix} = \begin{bmatrix} \dfrac{\Delta P}{V_{ser}} \\ \dfrac{\Delta Q}{V_{ser}} - V_{ser} \end{bmatrix} \tag{4.29}$$

The solution for the injected angle is given by,

$$\begin{bmatrix} \cos\phi_{ser} \\ \sin\phi_{ser} \end{bmatrix} = \frac{1}{1-2\cos\theta_{ij}}\begin{bmatrix} \sin\theta_{ij} & -\cos\theta_{ij} \\ -2+\cos\theta_{ij} & \sin\theta_{ij} \end{bmatrix}\begin{bmatrix} \dfrac{\Delta P}{V_{ser}} \\ \dfrac{\Delta Q}{V_{ser}} - V_{ser} \end{bmatrix} \tag{4.30}$$

As $$\cos^2\phi_{ser} + \sin^2\phi_{ser} = 1 \tag{4.31}$$

Equation 4.30 gives:

$$\frac{\Delta P^2}{V_{ser}^2}\left(5 - 4\cos\theta_{ij}\right) - 4\frac{\Delta P}{V_{ser}}\left(\frac{\Delta Q}{V_{ser}} - V_{ser}\right)\sin\theta_{ij} + \left(\frac{\Delta Q}{V_{ser}} - V_{ser}\right)^2 = \left(1 - 2\cos\theta_{ij}\right)^2 \tag{4.32}$$

This can be simplified to give the following ellipse equation (a detail derivation is given in Appendix A).

$$\left(\Delta P+\frac{B}{A}\right)^2-C\Delta P\Delta Q+\left(\frac{\Delta Q-V_{ser}}{A}\right)^2=\frac{AD^2-B^2}{A^2} \tag{4.33}$$

where

$$A=5-4\cos\theta_{ij}$$

$$B=2V_{ser}^2\sin\theta_{ij}$$

$$C=-4\sin\theta_{ij}$$

$$D=V_{ser}^2\left(1-2\cos\theta_{ij}\right)^2$$

The change in the line power flow (ΔP and ΔQ) is illustrated in Figure 4.8 for $V_{ser}=0.35pu$ and $V_{ser}=0.25pu$. The transmission angle θ_{ij} is assumed to be initially equal to 30°.

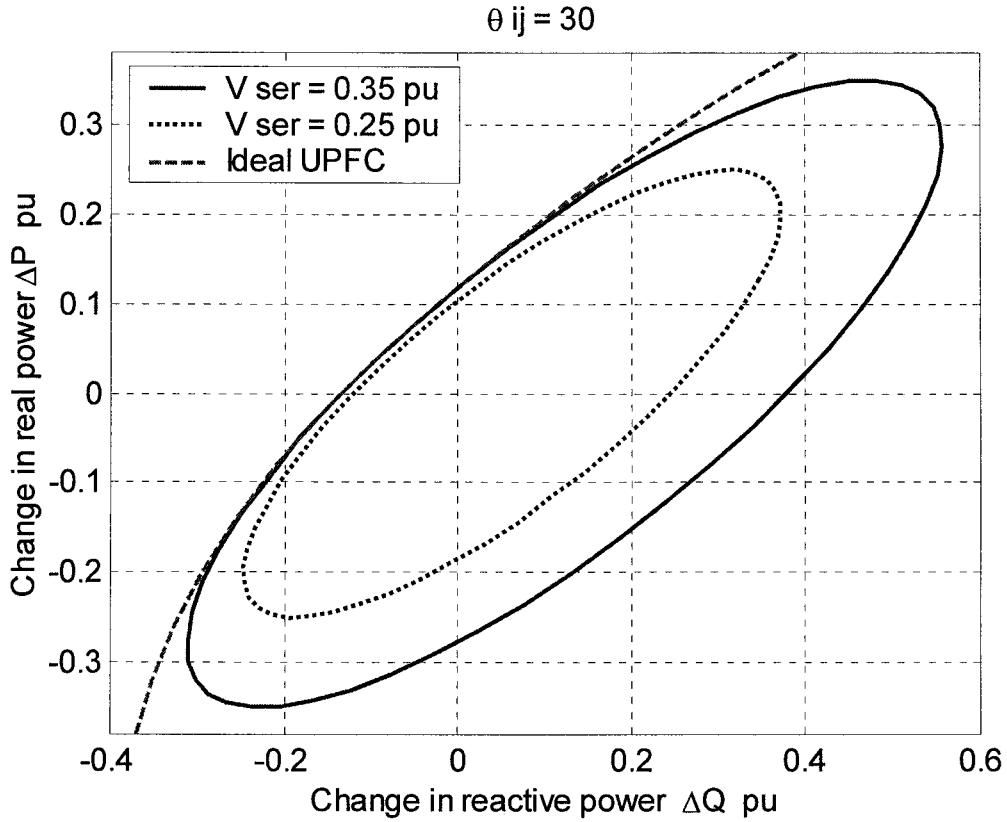

Figure 4.8 Series part feasible area.

This graph represents the UPFC feasible region under the effect of the maximum series injected voltage. It is obvious that any operating point (e.g. $\theta_{ij} = 30°$) of the uncompensated system shown in Figure 4.6 can be mapped onto an operating area, as shown in Figure 4.8, by installing a UPFC into the system. The maximum injected voltage limits this area, also the maximum per unit change of the real power is defined by the same limit. Inside this region, it is possible to find a suitable combination of the in-phase and quadrature components of the injected voltage that satisfies the system requirements.

Before investigating the effects of the shunt inverter on the UPFC feasible region, the effects of the system short circuit level are first considered.

4.4.2 Impact of the System Fault Level on the Feasible Operating Area

The effectiveness of any FACTS device depends on the network configuration beyond the bus bar at which the device is connected, i.e. the Short Circuit Level (SCL). A power system may be represented by using the Thevenin's equivalent circuit of the system viewed from the UPFC side, as shown in Figure 4.9. Ignoring the resistive part of the equivalent circuit impedance, the system short circuit level is given as,

$$SCL = \frac{V_s^2}{X_{th}} \tag{4.34}$$

The effects of the SCL are analysed by using the system shown in Figure 4.10, where the impact of the UPFC series part only is considered. It is clear that the SCL is inversely proportional to the reactance behind the bus bar (KX). The system's fault level decreases as the factor K increases (i.e. the system becomes weaker) while a strong system corresponds to a small value of K. Referring to the vector diagram given in Figure 4.2, introducing the system reactance KX into the active and reactive power flow equations

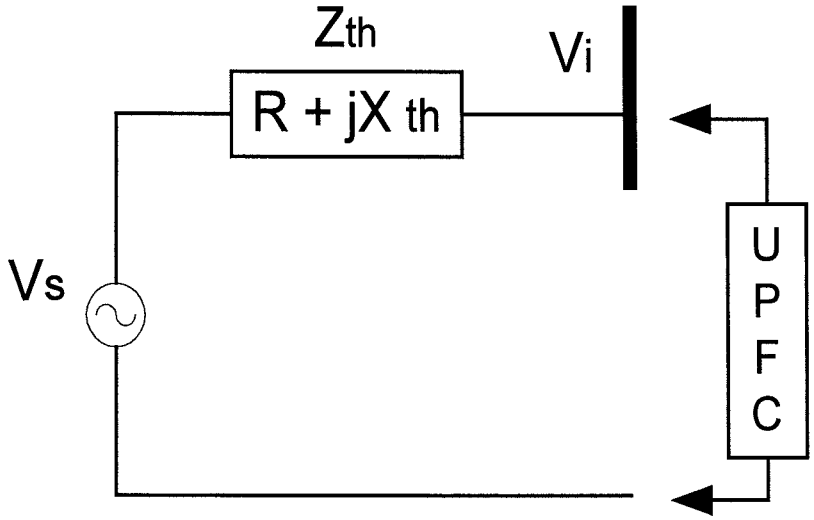

Figure 4.9 Thevenin's equivalent circuit.

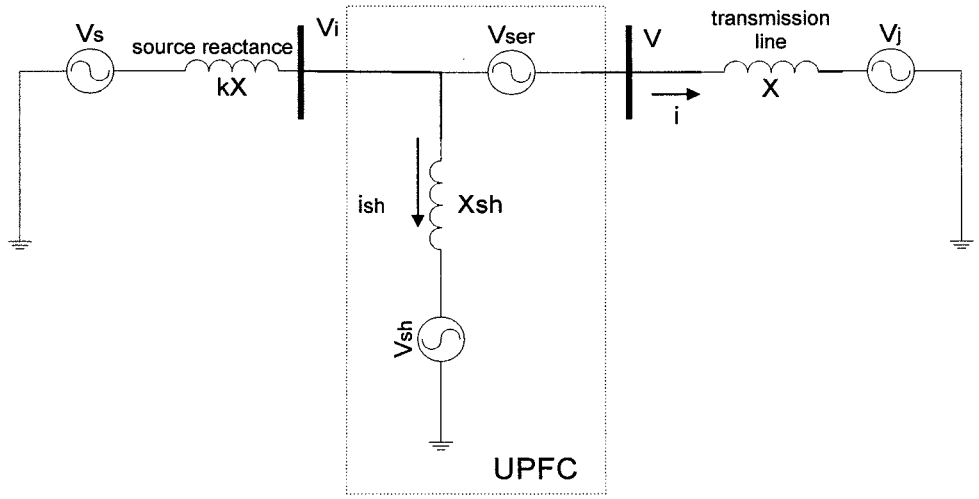

Figure 4.10 System model.

described by Equations 4.5 and 4.10, (with the assumption that the UPFC shunt part is supporting the system bus voltage, so that $|V_s| = |V_i|$) yields,

$$P = \frac{VV_j}{(1+K)X}\sin(\theta_{ij} + \theta) \tag{4.35}$$

$$Q = \frac{1}{(1+K)^2 X}\{V^2 - VV_j\cos(\theta_{ij} + \theta)\} - \frac{K}{(1+K)^2 X}\{V_j^2 - VV_j\cos(\theta_{ij} + \theta)\} \tag{4.36}$$

where $V^2 = V_i^2 + V_{ser}^2 + 2V_iV_{ser}\cos\phi_{ser}$

and $\theta = \tan^{-1}\dfrac{V_{ser}\sin\phi_{ser}}{V_i + V_{ser}\cos\phi_{ser}}$

The effect of the system short circuit level is shown in Figure 4.11 for K = 0, 0.1, and 0.5. It is clear that a weak system (low SCL) results in a reduced feasible area.

To validate the accuracy of the approximation given by Equations 4.35 and 4.36, the system described in Figure 4.10 is simulated using SIMULINK with $\dfrac{V_iV_j}{X} = 1pu$.

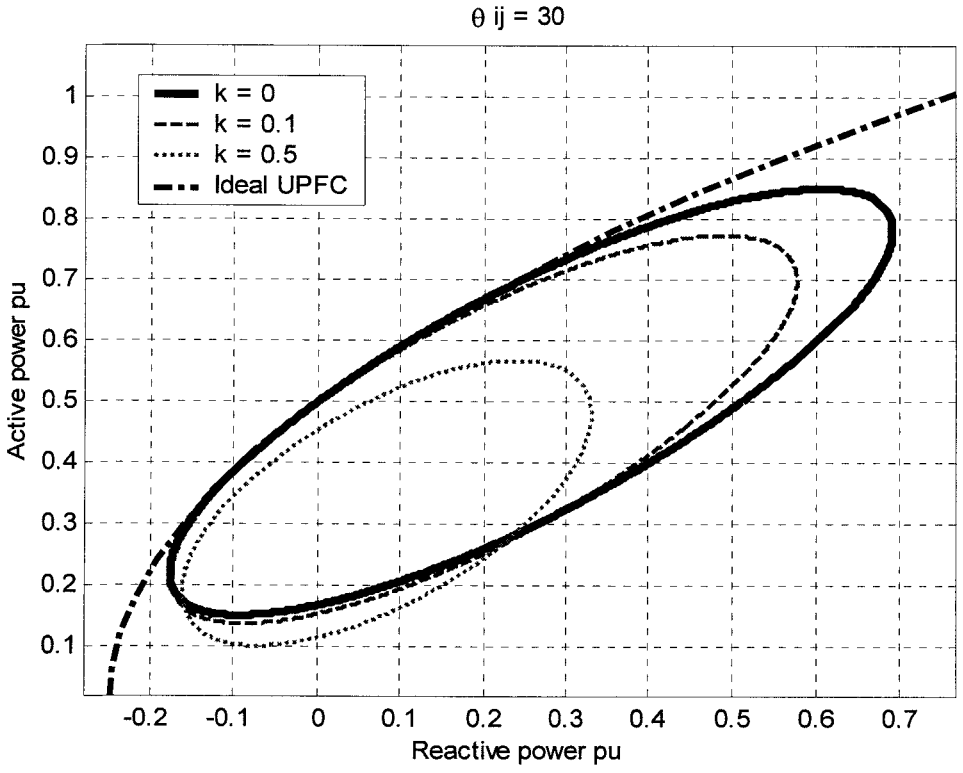

Figure 4.11 System feasible region under series part effect.

The simulated and calculated changes in power flow as a function of the inserted voltage parameters are shown in Figure 4.12 for different system fault levels. It is clear from the figure that Equations 4.35 and 4.36 well describe the real and reactive power flow in the power system for changing system short circuit level conditions.

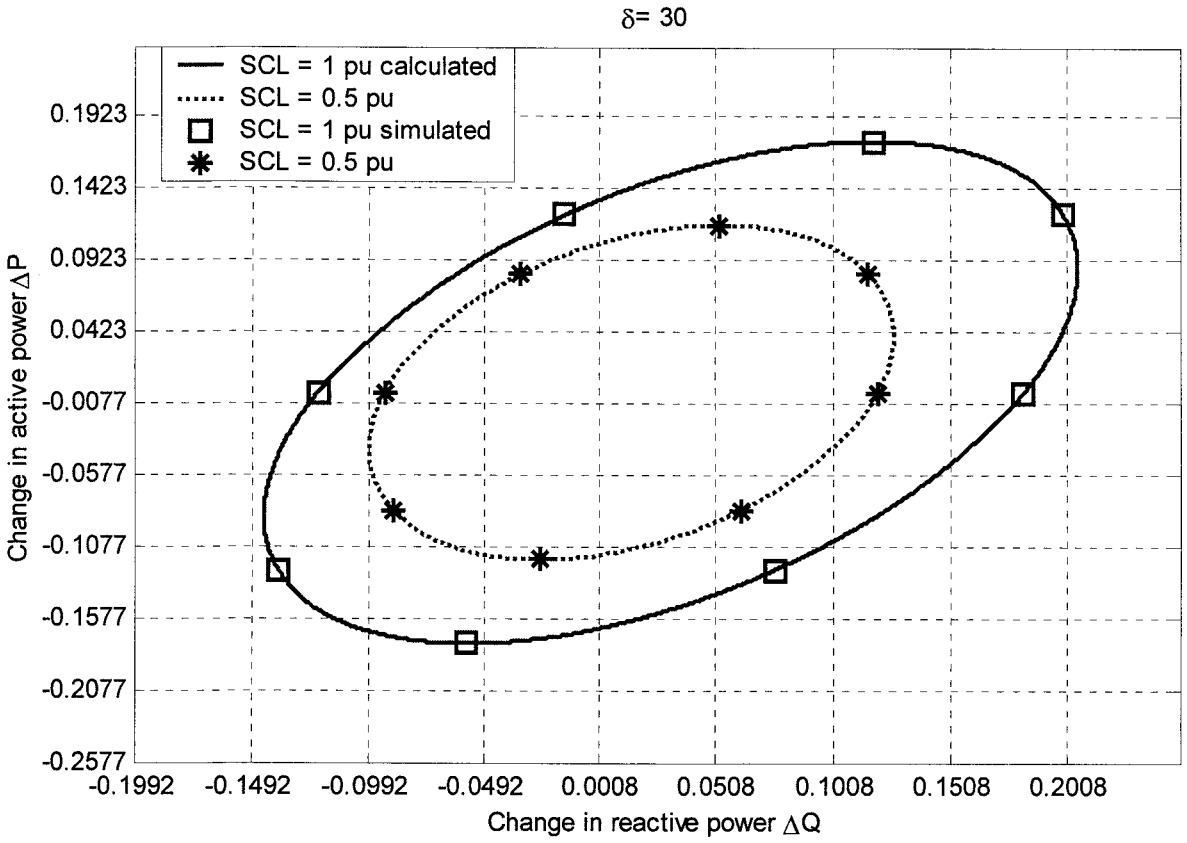

Figure 4.12 Simulated and calculated feasible region.

4.4.3 Impact of the Shunt Inverter

In the previous sections, the influence of the series inverter and the system impedance on the power system feasible region has been investigated. The shunt inverter was assumed to be ideal (i.e. has the right VA rating to supply the active power demand of the series inverter and keep the system bus voltage constant).

As a result of the fact that the UPFC does not supply or absorb real power to or from the system, the shunt inverter has no effect on the maximum value of the real power in the feasible region. However, it does affect the reactive power flow at a level depending on its VA rating.

During the design stage of the UPFC it is desirable to have a large VA rating for the shunt inverter. The active power demand of the series inverter should be within the rating of the shunt inverter. The difference between the VA rating of the shunt inverter and the real power demand of the series inverter may be used for reactive power control to enhance the UPFC voltage control capability. Therefore, the shunt inverter VA rating must be sufficient to provide the active power transfer between the two inverters and for voltage support. If this is satisfied, the feasible region of the system will be determined by the series inverter capability only.

To analyse the effects of the shunt inverter VA rating on the feasible region, the system given in Figure 4.10 was set up for operation with high short circuit level and $V_i = V_s$. This results in the operating region shown by the dashed line ellipse in Figure 4.13. When the system short circuit level is reduced, the system feasible region is also reduced (as discussed in Section 4.4.2), which results in the area shown by the solid line ellipse in Figure 4.13. This reduction is due to the increased voltage drop across the source impedance which affects the magnitude and phase angle of the system bus voltage. The function of the shunt inverter now is to generate sufficient reactive power to maintain the bus voltage at its nominal value. If the shunt inverter has enough VA rating to provide the series inverter real power demand and the required reactive power to bring back $V_i = V_s$, the feasible region may be enlarged as shown by the dotted lines in Figure 4.13. Therefore, the size of the new feasible operating area is determined by three elements, the maximum inserted series voltage, VA rating of the shunt inverter and the system short circuit level.

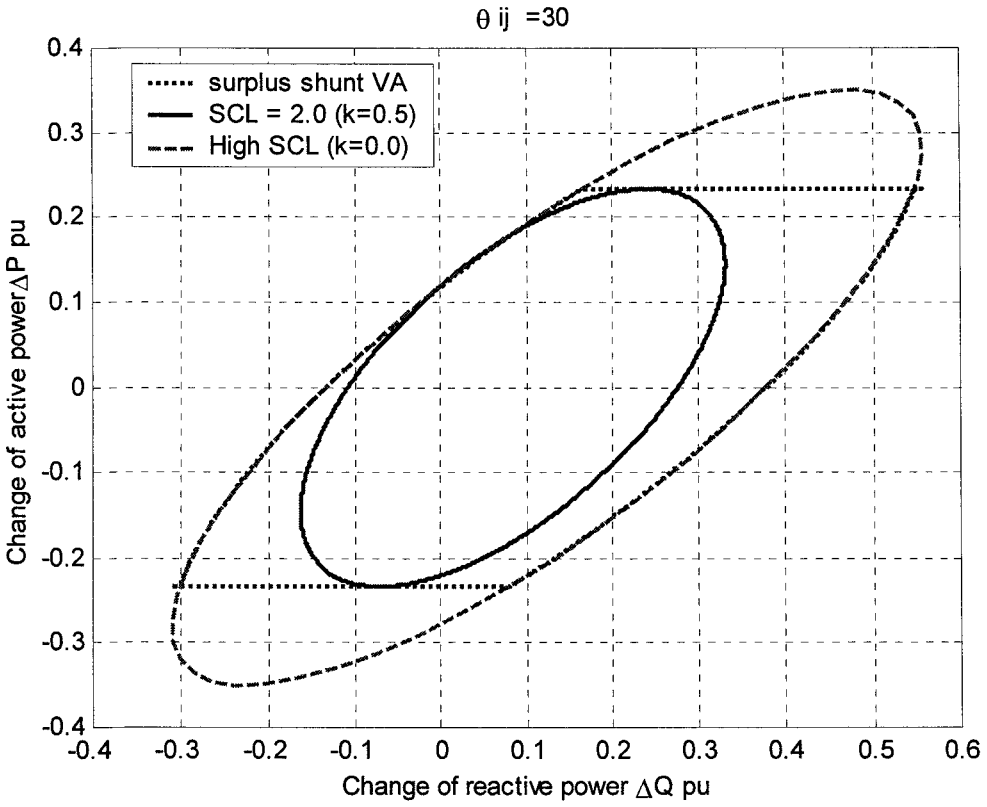

Figure 4.13 System feasible region with effect of both UPFC parts.

4.5 EFFECTS OF SCL ON THE SPEED OF RESPONSE

It has been shown that as a result of changing system fault level, the busbar voltage also changes and consequently the speed of response of the UPFC shunt branch is affected [34]. The system response becomes faster if the system short circuit level is reduced and vice versa. In this section, a mathematical analysis is performed to define the effect of the SCL on the UPFC shunt branch performance [35,36].

Considering the UPFC shunt part model shown in Figure 4.14, the voltage drop across the source reactance is given by,

$$V = V_s - V_1 \tag{4.37}$$

If the system fault level changes, the corresponding change in the voltage drop is given as (V_s is assumed to be constant),

$$\Delta V = -\Delta V_1 \tag{4.38}$$

From Figure 4.14,

$$\frac{V_s - V_1}{sL_s} = \frac{V_1}{sL_l + R_l} + \frac{V_1 - V_{sh}}{sL + R} \tag{4.39}$$

$$V_1 \frac{(sL+R)(sL_l+R_l) + sL_s(sL+R) + sL_s(sL_l+R_l)}{sL_s(sL+R)(sL_l+R_l)} = \frac{V_s}{sL_s} + \frac{V_{sh}}{(sL+R)} \tag{4.40}$$

By considering small perturbation of variables in Equation 4.40:

$$\frac{\Delta V_1}{\Delta V_{sh}} = \frac{sL_s(sL_l+R_l)}{s^2(L_s(L+L_l)+LL_l)+s(L_s(R+R_l)+L_lR+LR_l)+RR_l} \tag{4.41}$$

Substituting for ΔV_1 from Equation 4.38 into Equation 4.41,

$$\frac{\Delta V}{\Delta V_{sh}} = -\frac{sL_s(sL_l+R_l)}{s^2(L_s(L+L_l)+LL_l)+s(L_s(R+R_l)+L_lR+LR_l)+RR_l} \tag{4.42}$$

For a 6-pulse PWM inverter, the peak output voltage can be expressed as,

$$V_{sh} = m_a \frac{V_{dc}}{2} \tag{4.43}$$

where, V_{dc} is the average voltage across the d.c. capacitor and m_a is the modulation index.

Substituting Equation 4.43 into Equation 4.42 gives:

$$\frac{\Delta V}{\Delta m_a} = -\frac{sL_s(sL_l+R_l)\frac{V_{dc}}{2}}{s^2(L_s(L+L_l)+LL_l)+s(L_s(R+R_l)+L_lR+LR_l)+RR_l} \tag{4.44}$$

Equation 4.44 defines the effect of the system fault level on the ASVC speed of response. The inductance value L_s affects both the steady-state gain and the time constant. Figure 4.15 shows the system response to step change in the bus voltage under the effect of simple PI controller for three different short circuit levels. It is clear that when the system fault level increases, the system response becomes slower and the steady-state gain is lowered which requires high controller gain.

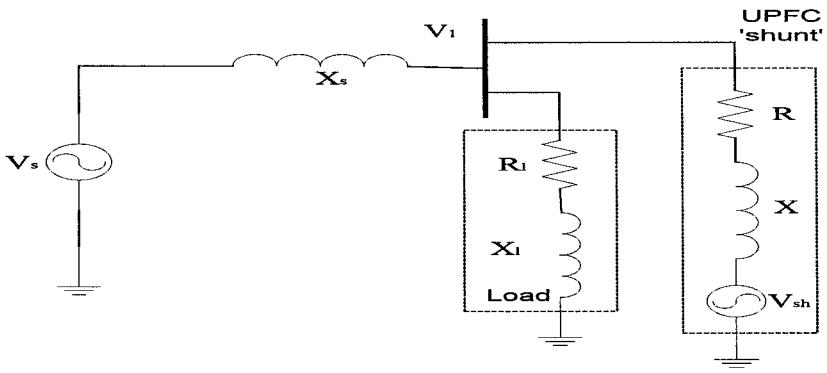

Figure 4.14 UPFC shunt part and a.c system equivalent circuit.

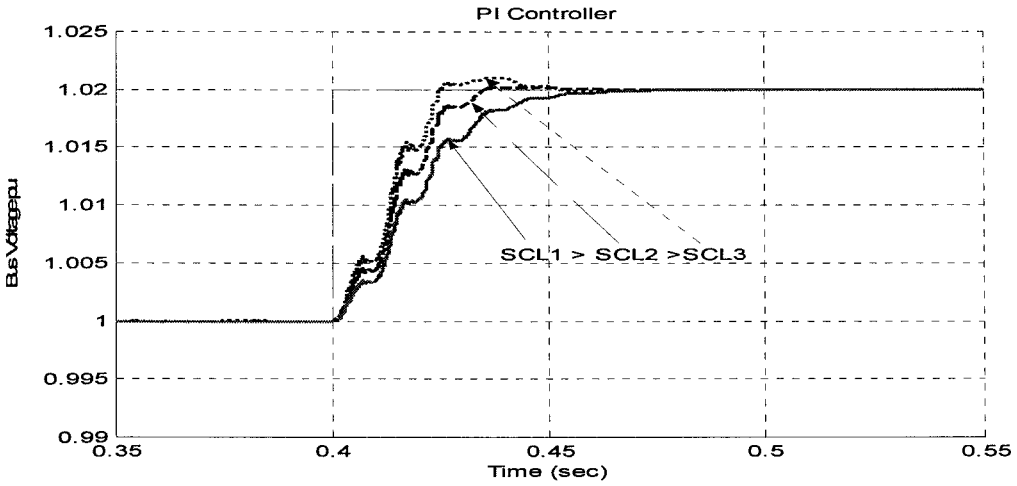

Figure 4.15 Effect of SCL on the system speed of response.

4.6 POWER FLOW OPTIMISATION

Under normal operating conditions the power system operating point falls within the space of the defined feasible region. During certain abnormal operating conditions, the system desired operating point might be located outside the ellipse defining the achievable real and reactive power limits of the UPFC (see Figure 4.8). In this case, the required inserted voltage of the series inverter would exceed its limit and hence a new operating point should be selected. As shown in Figure 4.16, the new operating point must be on the feasible region circumference, which corresponds to the maximum injected voltage. The exact operating point can be chosen according to real or reactive power priority. For the former, the angle of the injected voltage which gives the desired real power (or the closest

possible value) is selected regardless of the reactive power value. This is preferred as the UPFC shunt inverter provides the reactive power for the system. The second function of the optimiser is to check for the SCL changes and adjust the system settings accordingly. The maximum real power and effective sending-end voltage may be expressed as:

$$\hat{P} = \frac{\hat{V}V_j}{(K+1)X}\sin\left(\theta_{ij} + \hat{\theta}\right) \tag{4.45}$$

$$\hat{V}^2 = V_i^2 + V_{ser_{\max}}^2 + 2V_iV_{ser}\cos\hat{\phi}_{ser} \tag{4.46}$$

where $\hat{V}$ corresponds to the maximum inserted voltage V_{ser}.

By equating the real power in Equation 4.45 and Equation 4.35, the required angle can be found as,

$$\hat{\theta} = -\theta_{ij} + \sin^{-1}\left\{\frac{V}{\hat{V}}\sin\left(\theta_{ij} + \theta\right)\right\} \tag{4.47}$$

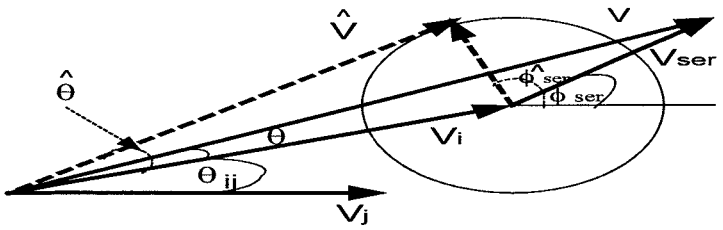

Figure 4.16 Injected voltage under real power priority.

The idea of power flow optimiser will be used to design the UPFC control rules as will be seen in Section 6.5.

In this chapter, the impacts of the UPFC control variables on the transmitted power have been analysed and the system feasible operating area is defined. The in-phase component of the series injected voltage mainly dominates the reactive power while the quadrature component affect the real power. The reduction in the SCL minimises the system feasible operating area. To develop a suitable computer model for the UPFC, different modelling techniques will be analysed in the next chapter.

UPFC MODELLING

5.1 INTRODUCTION

Modelling of the UPFC is a fundamental step for any UPFC related studies. It is also necessary to establish a model that is suitable for the present study. There are three main states of a power system that are of interest: electromagnetic transient state, steady-state and electromechanical transient state. Different UPFC models are used to investigate its behaviour in these three states. Each model should emphasise the basic features of the UPFC and take into consideration its ability to be implemented using the available software package and tools. In this chapter, existing modelling techniques are reviewed and an exact power injection model of the UPFC (based on the polar representation of the injected voltages) is developed. The electromagnetic transient model is considered in this work especially in the experimental phase, as a PWM technique is used to generate the switching patterns of the series and shunt inverter switches. The present study is concerned with the power flow control in the steady-state and electromechanical transient conditions. Ideal voltage sources are used to model the UPFC in steady-state, where the active and reactive power flow through the transmission line are directly related to the injected voltage components of the UPFC.

5.2 ELECTROMAGNETIC TRANSIENT STATE MODELLING

The concept of the UPFC is based on Voltage Source Inverters (VSI) using self-commutated power electronic devices, e.g. GTOs or IGBTs [37]. Figure 5.1 shows two six-pulse three-phase inverters tied through a common d.c. link (the power electronic devices are replaced by ideal switches for simplicity). Since it was proposed by Gyugyi in 1992, the

UPFC has received intensive consideration. Many researches have been published which covered different aspects of the UPFC modelling and operation. Ooi [38] has introduced the use of a matrix converter to provide the UPFC specifications, where it can operate as an asynchronous link joining power systems at different frequency standards. An electromagnetic transient state UPFC model was suggested and simulated using Electromagnetic Transient Programme (EMTP) simulator [39,40]. Toufan [41] describes the UPFC model at the component level using EMTDC programme, where the Hysteresis Current Forcing (HCF) and PWM switching schemes are used to generate the switching patterns for the shunt and series inverters, respectively. Fujita [42] has modelled the UPFC in a reverse connection to work as a power quality conditioner.

The principle of operation of the VSI is to convert the d.c. voltage into a three-phase a.c. voltage which is synchronised and connected to the a.c. system through a reactor or the leakage reactance of the associated transformer.

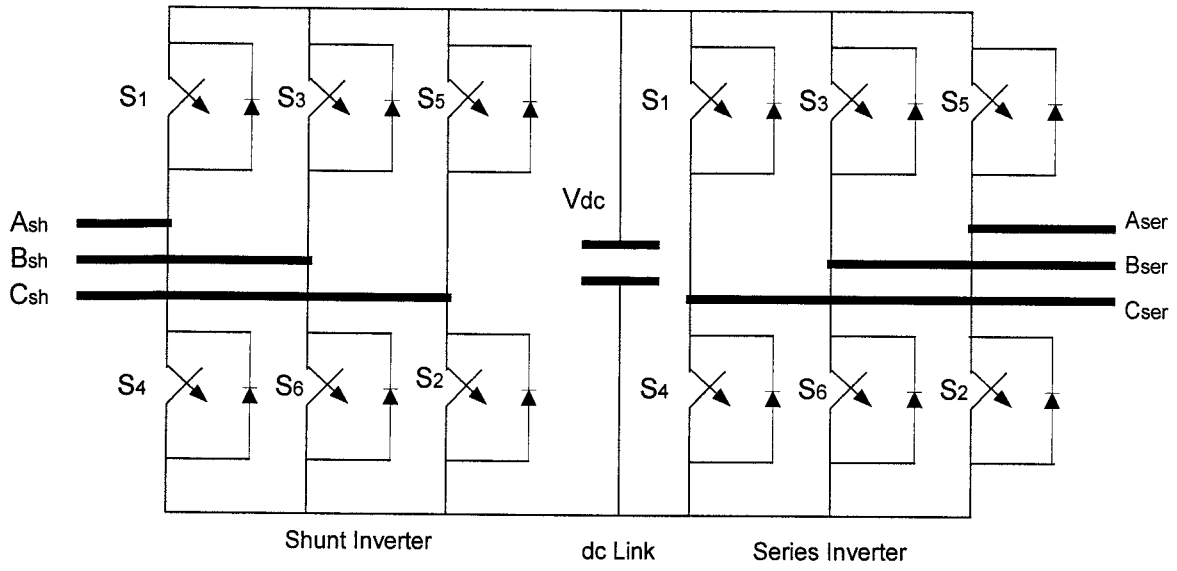

Figure 5.1 UPFC schematic diagram.

Amplitude of the inverter a.c. output voltage can be controlled by three ways [43]:

- Control of the inverter d.c. input voltage.
- Control of the inverter a.c. output voltage.
- Control of the inverter-switching patterns.

As continuous and fast control of the UPFC output voltage is normally required to achieve the control objectives of the device, controlling the d.c. link to change the inverter output voltage can be inappropriate. This is because charging and discharging the d.c. capacitor can be a slow process, in addition to requiring co-ordination between the two inverters. Controlling the inverter output voltage through regulators might lead to a complex control circuit of the UPFC. Therefore, controlling the switching pattern is the most common way to control the VSI output voltage in FACTS devices, in particular the UPFC [44-47]. Generally, two techniques are used to control the inverter output voltage. These are:

- Fundamental Frequency Modulation FFM.
- Pulse Width Modulation PWM.

5.2.1 Fundamental Frequency Modulation

The Fundamental Frequency Modulation (FFM) strategy is characterised by using a switching frequency equal to the a.c. system frequency. The inverter can operate in the following two switching patterns.

180^o conduction

In this mode, each switch is conducting for 180^o, so each output terminal is always connected to either the positive or negative terminal of the d.c. side. At any given instant only three switches are conducting. Two situations should be avoided in this process. The first is having two switches in the same inverter arm to be on at the same time. The second is having three upper or three lower switches to be on at the same time. Six distinct intervals are defined for one output cycle. The inverter output frequency can be controlled by the rate

of repeating these intervals. The six switching patterns are $S_1S_2S_3$, $S_2S_3S_4$, $S_3S_4S_5$, $S_4S_5S_6$, $S_5S_6S_1$ and $S_6S_1S_2$.

The r.m.s values of the phase and line-line voltages at the inverter output are given as:

$$V_{ph}(rms) = \frac{\sqrt{2}}{3} V_{dc} \tag{5.1}$$

$$V_{LL}(rms) = \frac{\sqrt{2}}{\sqrt{3}} V_{dc} \tag{5.2}$$

120^o conduction

The six-pulse inverter can also be controlled such that each switch conducts only for 120^o. Therefore, two switches are in the on-state at any given time; one switch belongs to the upper group and another from the lower group. The switching sequence is S_1S_2, S_2S_3, S_3S_4, S_4S_5, S_5S_6 and S_6S_1.

The r.m.s. values of the phase and line-line voltages at the inverter output are expressed as follows;

$$V_{ph}(rms) = \frac{\sqrt{2}}{\sqrt{3}} \frac{V_{dc}}{2} \tag{5.3}$$

$$V_{LL}(rms) = \frac{V_{dc}}{\sqrt{2}} \tag{5.4}$$

The FFM results in low losses in the switching devices, which makes it attractive for high power applications. However, it produces low order harmonics in the inverter output voltage and current. Therefore, means are required to minimise the harmonic distortion e.g. filters. Also, using FFM leads to a fixed inverter output voltage. In this respect FFM is not preferred in controlling the UPFC, where independent inverters outputs are required.

5.2.2 Pulse Width Modulation (PWM)

Instead of controlling the width of the pulse during which the corresponding switch is on (120^o or 180^o), the output of the inverter can be switched on and off several times during each half cycle to produce a train of pulses with constant magnitude and different widths. This is achieved by PWM control of the inverter switches in order to eliminate or reduce some of the harmonics in the output voltage. There are many schemes for PWM, two of which are discussed here; the Selective Harmonic Elimination Modulation (SHEM) scheme and the Sinusoidal Pulse Width Modulation (SPWM) scheme.

Selective harmonic elimination modulation (SHEM)

In this case, the inverter output is controlled to eliminate some of the harmonics contained in the output waveforms, in particular the low order harmonics which are more difficult to be filtered out [48,49]. Figure 5.2 shows the voltage waveform with three notches in each half cycle characterised by the switching angles β_1, β_2 and β_3. Each notch adds one degree of freedom to the scheme. Therefore, it is able to control the fundamental component of the output voltage in addition to eliminating the fifth and seventh harmonics. In this case the magnitude of the fundamental component is given as;

$$V_a \cong 1.188\frac{V_{dc}}{2} \tag{5.5}$$

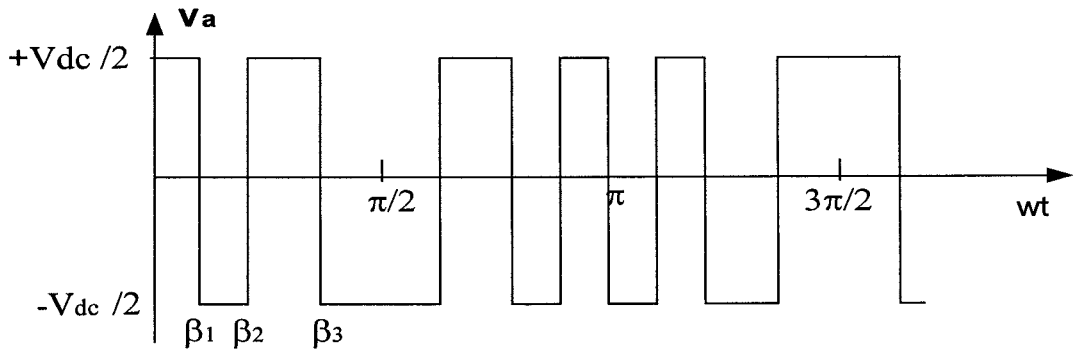

Figure 5.2 Output voltage with harmonic elimination.

Sinusoidal pulse width modulation (SPWM)

In this scheme, the switching instants are determined by the intersection between a sinusoidal reference modulating signal (having an amplitude V_m and a frequency f_m) and a high frequency triangular carrier signal of amplitude V_c and frequency f_c [39]. The pulse width is determined by the time during which the magnitude of the carrier signal is less than that of the modulating signal. Figure 5.3 shows the SPWM waveform where a triangular carrier wave is compared with three-phase modulating signals which have a 120^o phase displacement between each other. The frequency of the modulating signal specifies the inverter output voltage frequency. In FACTS applications this frequency should be the same as the a.c. system frequency.

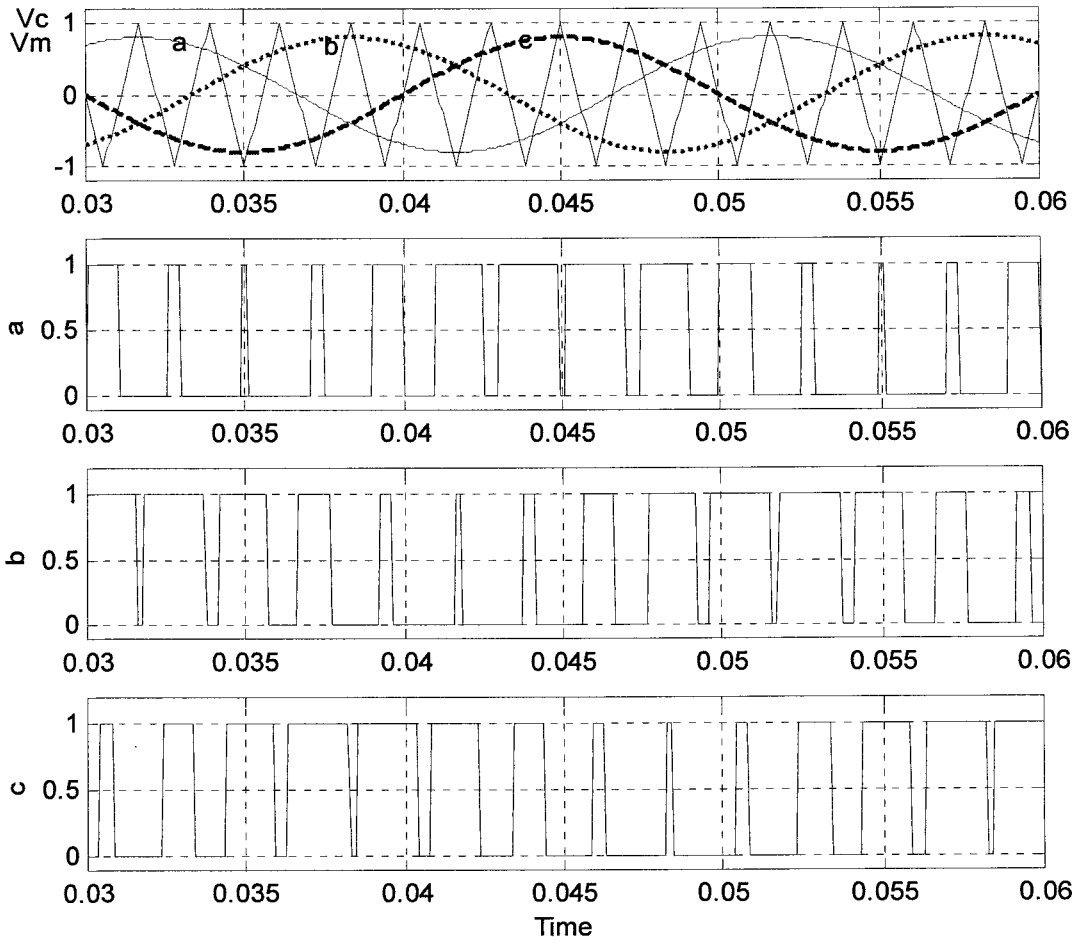

Figure 5.3 Three-phase SPWM.

The carrier frequency specifies the switching frequency of the inverter, which is normally chosen according to the inverter switches type, switching losses produced and the regulation relevant to the electromagnetic compatibility for the power electronic conversion equipment.

There are two control parameters that adjust the SPWM inverter output voltage, amplitude modulation index m_a and frequency ratio m_f, they are given as:

$$\left.\begin{aligned} m_a &= \frac{V_m}{V_c} \\ m_f &= \frac{f_c}{f_m} \end{aligned}\right\} \tag{5.6}$$

where V_m,V_c, f_c, and f_m, are as defined earlier.

m_a determines the width of the on-state pulses and therefore the r.m.s. value of the inverter output voltage. Generally, m_a is adjusted by varying the amplitude of the modulating signal while keeping the carrier wave amplitude fixed. The phase angle of the inverter output voltage can be adjusted by phase shifting the modulating signal with respect to the carrier signal. The operation of the inverter is normally in the linear range when $m_a \leq 1$. The amplitude of the inverter fundamental frequency varies linearly with the modulation index and the inverter output voltage is given by:

$$V_1 = m_a \frac{V_{dc}}{2} \tag{5.7}$$

An overmodulation results from increasing the modulation index beyond unity. This will increase the amplitude of the output voltage in a non-linear relationship with the modulation index and causes the output voltage to contain more harmonics in the side bands than in the linear range. Normally overmodulation is avoided in the applications which require small distortion in the inverter output voltage (e.g. uninterruptible power supplies).

The frequency modulation index m_f determines the harmonics contribution in the output voltage. In order to get a good performance, m_f should satisfy the following requirements:

- it should be an integer, to avoid sub-harmonics,
- it should be an odd number, to eliminate even order harmonics, and
- it should be multiple of three, to eliminate the triplen harmonics.

From the previous discussion, it is clear that using SPWM will provide linear control of the inverter output voltage. In addition, it is able to eliminate or reduce the low order harmonics and some higher harmonics depending on the switching frequency. The use of SPWM may results in high switching losses which may not be acceptable for high power applications. For such applications, the SHEM technique is normally used. For the UPFC, as the inverters output voltages are continuously controlled based on a fixed d.c. link voltage, the SHEM technique is not appropriate. Hence, the SPWM based UPFC apparently provides more flexible control ability which in turn matches the concept of multiple functions of the UPFC than other techniques. Therefore, the SPWM is used in this study to generate the gate patterns for the UPFC inverters.

5.3 STEADY-STATE MODELLING

In this case, a simple model of the UPFC is used where details of the switching patterns of the inverters are not required. A steady-state model of UPFC in terms of two voltage source representations has been suggested [50-52]. Mihalič [53] proposed a UPFC model based on a controlled voltage source to represent the series inverter and a current source to represent the shunt inverter. A power injection model of the UPFC, which is more appropriate for load flow analysis, has also been suggested [54-56].

The UPFC model (considered in this thesis for power flow control studies) consists of two controllable voltage sources, as shown in Figure 5.4. V_{ser} represents the series inverter voltage while V_{sh} represents the shunt inverter voltage. R_{sh} and L_{sh} represent the resistance and inductance of the shunt transformer. R and L represent the transmission line impedance including the series transformer leakage reactance. In steady-state, the UPFC neither absorbs nor injects real power with respect to the a.c. system. Physical interpretation of this state is that, in steady-state, the voltage of the d.c. link capacitor remains constant at a pre-specified value.

5.3.1 Power Injection Model

The main function of the UPFC in steady-state is investigated using power flow analysis. The two-voltage source model of the UPFC is converted into a form compatible with power flow algorithms. Then, the results obtained from the power flow analysis are used to compute the required inverter control variables, which in terms of the PWM strategy are the modulation index and the phase angle [57-61]. The power injection model in a rectangular form given in references [57,58] has some numerical advantages based on the quadratic form of the power flow equations. In the work suggested by Kim [59] a de-coupled UPFC model is proposed where an approximation was made that the UPFC shunt

inverter has no reactive power contributions to its busbar. Noroozian [60] used the UPFC parameters in a polar form which is intuitive because the state variables are voltage magnitudes and angles having a physical meaning. Also, the author assumed that the UPFC is lossless and the shunt inverter rating is used only for supplying the active power required by the series inverter.

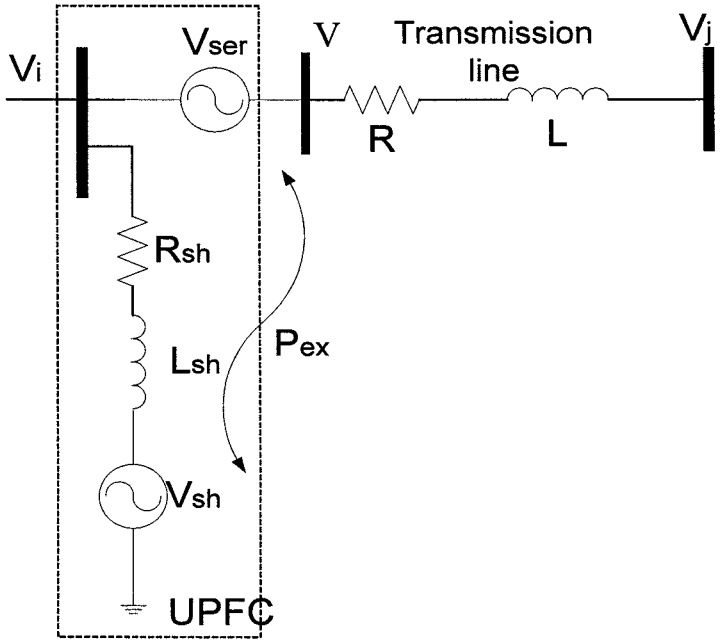

Figure 5.4 UPFC model employing ideal voltage sources.

In this study, an exact polar representation is developed to describe the UPFC in a power injection model, which takes into account the reactive power injection of the shunt inverter. The power injection model is shown in Figure 5.5. The impedance in front of each voltage source is assumed to be reactive dominant.

The series and shunt voltage sources are expressed in a polar form as:

$$\overline{V}_{ser} = r_{ser}\overline{V}_i e^{-j\phi_{ser}} \tag{5.8}$$

$$\overline{V}_{sh} = r_{sh}\overline{V}_i e^{-j\phi_{sh}} \tag{5.9}$$

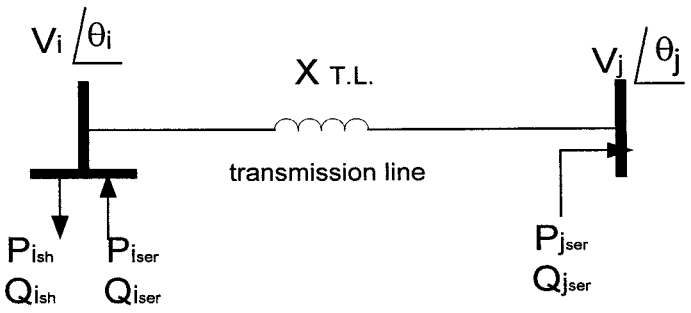

Figure 5.5 UPFC injection model.

where;

$$0 \le r_i \le r_{\max}$$
$$0 \le \phi_i \le 2\pi$$

The first step is to transform the shunt part of the UPFC into a power injection at busbar *i* where the UPFC is connected.

$$S_{i_{sh}} = P_{i_{sh}} + jQ_{i_{sh}} = \overline{V_i}\left[\frac{\overline{V_i} - \overline{V_{sh}}}{jX_{sh}}\right]^* \tag{5.10}$$

Substitute for V_{sh} from Equation 5.9 into Equation 5.10

$$P_{i_{sh}} = r_{sh}\frac{V_i^2}{X_{sh}}\sin\phi_{sh} \tag{5.11}$$

$$Q_{i_{sh}} = \frac{V_i^2}{X_{sh}}[1 - r_{sh}\cos\phi_{sh}] \tag{5.12}$$

where, $P_{i_{sh}}$ is the real power exchange between the shunt inverter and the a.c. system. Note that, the exact real power is determined by the series inverter requirements, as will be shown later in this section.

The second step is to relate the series part of the UPFC to the power injection at busbars i and j. The power injection at busbar i is:

$$S_{i_{ser}} = P_{i_{ser}} + jQ_{i_{ser}} = \overline{V}_i \left[\frac{r_{ser}\overline{V}_i e^{-j\phi_{ser}}}{jX_S} \right]^* \tag{5.13}$$

$$P_{i_{ser}} = \frac{r_{ser}}{X_S} V_i^2 \sin\phi_{ser} \tag{5.14}$$

$$Q_{i_{ser}} = \frac{r_{ser}}{X_S} V_i^2 \cos\phi_{ser} \tag{5.15}$$

In the same way, the power injection at busbar j is:

$$S_{j_{ser}} = P_{j_{ser}} + Q_{j_{ser}} = \overline{V}_j \left[\frac{r_{ser}}{jX_S} \overline{V}_i e^{-j\phi_{ser}} \right]^* \tag{5.16}$$

which gives

$$P_{j_{ser}} = \frac{r_{ser}}{X_S} V_i V_j \sin\left(\theta_{ij} + \phi_{ser}\right) \tag{5.17}$$

$$Q_{j_{ser}} = \frac{r_{ser}}{X} V_i V_j \cos\left(\theta_{ij} + \phi_{ser}\right) \tag{5.18}$$

where,

$$\theta_{ij} = \theta_i - \theta_j$$

The apparent power exchanged between the UPFC series part and the a.c. system is given as;

$$S = P + jQ = \overline{V}_{ser} \left[\frac{\overline{V}_i + \overline{V}_{ser} - \overline{V}_j}{jX_S} \right]^* \tag{5.19}$$

$$P = \frac{r_{ser}}{X_S} V_i V_j \sin\left(\theta_{ij} + \phi_{ser}\right) - \frac{r_{ser}}{X_S} V_i^2 \sin\phi_{ser} \tag{5.20}$$

$$Q = -\frac{r_{ser}}{X_S} V_i V_j \cos\left(\theta_{ij} + \phi_{ser}\right) + \frac{r_{ser}}{X_S} V_i^2 \cos\phi_{ser} + \frac{r_{ser}^2}{X_S} V_i^2 \tag{5.21}$$

According to the requirement that no real power is generated or absorbed by the UPFC, Equation 5.20 will replace Equation 5.11 in the final model.

Based on the above analysis, the net power injections of the UPFC at busbars *i* and *j* are summarized as;

$$P_{i_{net}} = P_{i_{ser}} - P_{i_{sh}} = P_{i_{ser}} + P$$

$$P_{i_{net}} = \frac{r_{ser}}{X_S} V_i V_j \sin(\theta_{ij} + \phi_{ser}) \tag{5.22}$$

$$Q_{i_{net}} = Q_{i_{ser}} - Q_{i_{sh}}$$

$$Q_{i_{net}} = \frac{r_{ser}}{X_S} V_i^2 \cos\phi_{ser} - \frac{V_i^2}{X_{sh}}[1 - r_{sh}\cos\phi_{sh}] \tag{5.23}$$

However,

$$P_{j_{net}} = -P_{i_{net}} \quad \text{and} \quad Q_{j_{net}} = -Q_{j_{ser}}$$

$$P_{j_{net}} = -\frac{r_{ser}}{X_S} V_i V_j \sin(\theta_{ij} + \phi_{ser}) \tag{5.24}$$

$$Q_{j_{net}} = -\frac{r_{ser}}{X_S} V_i V_j \cos(\theta_{ij} + \phi_{ser}) \tag{5.25}$$

The UPFC injection model can now be incorporated in a load flow programme. The admittance matrix is modified by adding a reactance equivalent to X_S between busbar *i* and busbar *j*. The Jacobian matrix is modified by addition of appropriate injection powers. For the linearized load flow model as;

$$\begin{bmatrix} \Delta P \\ \Delta Q \end{bmatrix} = \begin{bmatrix} H & N \\ M & L \end{bmatrix} \begin{bmatrix} \Delta\theta \\ \Delta V/V \end{bmatrix} \tag{5.26}$$

The Jacobian matrix is modified as given in Table 5.1, where superscript 0 denotes the Jacobian elements without UPFC (More details are given in appendix B).

Table 5.1 Modified Jacobian Matrix

$H_{ii} = H_{ii}^0 - Q_{j_{net}}$	$N_{ii} = N_{ii}^0 - P_{j_{net}}$
$H_{ij} = H_{ij}^0 + Q_{j_{net}}$	$N_{ij} = N_{ij}^0 - P_{j_{net}}$
$H_{ji} = H_{ji}^0 + Q_{j_{net}}$	$N_{ji} = N_{ji}^0 + P_{j_{net}}$
$H_{jj} = H_{jj}^0 - Q_{j_{net}}$	$N_{jj} = N_{jj}^0 + P_{j_{net}}$
$M_{ii} = M_{ii}^0$	$L_{ii} = L_{ii}^0 + 2Q_{i_{net}}$
$M_{ij} = M_{ij}^0$	$L_{ij} = L_{ij}^0$
$M_{ji} = M_{ji}^0 - P_{j_{net}}$	$L_{ji} = L_{ji}^0 + Q_{j_{net}}$
$M_{jj} = M_{jj}^0 + P_{j_{net}}$	$L_{jj} = L_{jj}^0 + Q_{j_{net}}$

5.3.2 Control of the UPFC in Steady-State

There are two types of control methods when analysing the UPFC in steady-state. The first is an *open loop* control, where the control variables of the UPFC (e.g. $r_{ser}, \phi_{ser}, r_{sh}$ and ϕ_{sh}) are given and the power flow programme is used to evaluate the effect of the UPFC on the a.c. network under different operating conditions.

The second is a *closed loop* control in which the UPFC power injections ($P_{i_{net}}, Q_{i_{net}}, P_{j_{net}}$ and $Q_{j_{net}}$) are iteratively adjusted until the system reaches the required set point. At each step, after modifying the injection parameters, the UPFC control variables are determined based on Equations 5.22-5.25. The process continues until the difference

between the actual and desired operating points falls within an acceptable margin. The system set points could be specified as the desired bus voltages or the real and reactive power flow in a certain transmission line. Different methods have been investigated in the literature to regulate the UPFC control variables in a steady-state based on the power flow injection model [62,63]. This is out of the scope of this thesis.

In chapters 6 and 7, different types of advanced controllers to adjust the UPFC control parameters are investigated. The controller parameters are extracted from the relationship between the UPFC control variables and the desired set points.

5.4 ELECTROMECHANICAL TRANSIENT STATE MODELLING

The electromechanical transient model is often deduced from the steady-state model. It may be represented in three-phase form for unbalanced system, two-frame (d-q) or as a power injection model for a balanced system. The main function of the UPFC represented in a dynamic model is to investigate its ability to damp power oscillation and improve the transient stability of a power system. Literature survey shows that some work have been conducted to model the UPFC for dynamic studies and to define the damping control strategy. Lo [64] describes a time domain analysis of power system transient energy function to damp low frequency electromechanical oscillations.

The analysis proposed by Ma [65] is based on the power injection model and the controller input/output signals are chosen in order to minimise the transient energy of the a.c. system incorporating the UPFC. The UPFC model proposed by Noroozian [66] to damp power oscillation operates to keep the series injected voltage at the maximum value while controlling its phase angle.

Wang [67,68] studied the effect of the UPFC d.c. voltage regulator on the power system transient stability in order to select an appropriate input signal for the UPFC damping

controller. This analysis is suitable for a Single Machine Infinite Bus (SMIB) power system model. In a real system, this may not be the case where the UPFC is installed away from the generation station [69].

The most appropriate dynamic model of the UPFC is based on a d-q reference frame which is reviewed in the next section. This is because it simplifies the three-phase system to two-phase, hence, the system control loops are significantly reduced.

5.4.1 D-Q Model of the UPFC

The three-phase dynamic differential equations of the UPFC represented in Figure 5.6 are described as follows.

For the series part

$$\frac{d}{dt}\begin{bmatrix} i_{ser_a} \\ i_{ser_b} \\ i_{ser_c} \end{bmatrix} = \begin{bmatrix} \frac{-R}{L} & 0 & 0 \\ 0 & \frac{-R}{L} & 0 \\ 0 & 0 & \frac{-R}{L} \end{bmatrix} \begin{bmatrix} i_{ser_a} \\ i_{ser_b} \\ i_{ser_c} \end{bmatrix} + \frac{1}{L}\begin{bmatrix} V_{i_a} + V_{ser_a} - V_{j_a} \\ V_{i_b} + V_{ser_a} - V_{j_a} \\ V_{i_c} + V_{ser_a} - V_{j_a} \end{bmatrix} \tag{5.27}$$

For the shunt part

$$\frac{d}{dt}\begin{bmatrix} i_{sh_a} \\ i_{sh_b} \\ i_{sh_c} \end{bmatrix} = \begin{bmatrix} \frac{-R_{sh}}{L_{sh}} & 0 & 0 \\ 0 & \frac{-R_{sh}}{L_{sh}} & 0 \\ 0 & 0 & \frac{-R_{sh}}{L_{sh}} \end{bmatrix} \begin{bmatrix} i_{sh_a} \\ i_{sh_b} \\ i_{sh_c} \end{bmatrix} + \frac{1}{L}\begin{bmatrix} V_{sh_a} - V_{i_a} \\ V_{sh_a} - V_{i_a} \\ V_{sh_a} - V_{i_a} \end{bmatrix} \tag{5.28}$$

By applying Park's transformation, a three-phase system can be transformed into an equivalent d-q system [70]. The transformation matrix for a symmetrical system, is given as:

$$\begin{bmatrix} f_d \\ f_q \end{bmatrix} = \frac{2}{3}\begin{bmatrix} \cos(\omega t) & \cos(\omega t - 120) & \cos(\omega t + 120) \\ \sin(\omega t) & \sin(\omega t - 120) & \sin(\omega t + 120) \end{bmatrix}\begin{bmatrix} f_a \\ f_b \\ f_c \end{bmatrix} \tag{5.29}$$

Therefore, the instantaneous two-phase d-q representation of the UPFC may be derived as follows;

d-q representation of the series inverter

$$\frac{d}{dt}\begin{bmatrix} i_{ser_d} \\ i_{ser_q} \end{bmatrix} = \begin{bmatrix} \frac{-R}{L} & \omega \\ -\omega & \frac{-R}{L} \end{bmatrix}\begin{bmatrix} i_{ser_d} \\ i_{ser_q} \end{bmatrix} + \frac{1}{L}\begin{bmatrix} V_{i_d} + V_{ser_d} - V_{j_d} \\ V_{i_q} + V_{ser_q} - V_{j_q} \end{bmatrix} \tag{5.30}$$

d-q representation of the shunt inverter

$$\frac{d}{dt}\begin{bmatrix} i_{sh_d} \\ i_{sh_q} \end{bmatrix} = \begin{bmatrix} \frac{-R_{sh}}{L_{sh}} & \omega \\ -\omega & \frac{-R_{sh}}{L_{sh}} \end{bmatrix}\begin{bmatrix} i_{sh_d} \\ i_{sh_q} \end{bmatrix} + \frac{1}{L}\begin{bmatrix} V_{ser_d} - V_{i_d} \\ V_{ser_q} - V_{i_q} \end{bmatrix} \tag{5.31}$$

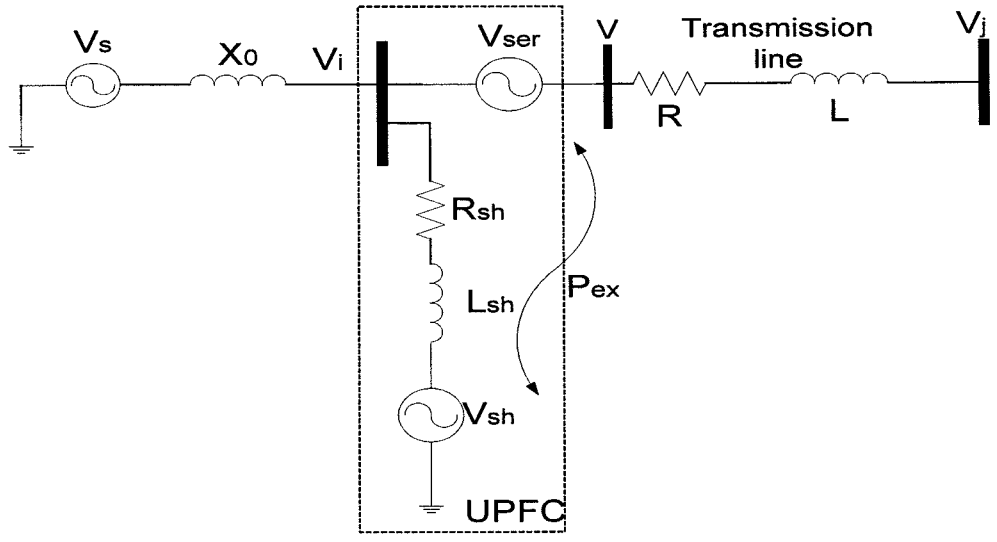

Figure 5.6 A simple transmission system model including the UPFC.

For the d.c. link

The d.c. link state is determined by the fact that the UPFC can not generate real power into the a.c. system by its own. The UPFC must work under a balanced condition. Therefore, the real power generated or absorbed by the series inverter, in addition to the inverters losses, should be supplied from the shunt inverter. The power balance of the d.c. link gives;

$$\frac{dV_{dc}}{dt} = \frac{1}{CV_{dc}}(P_{sh} - P) \tag{5.32}$$

where P_{sh} and P are defined by Equations 5.11 and 5.20, respectively.

The four parameters (V_{ser_d}, V_{ser_q}, V_{sh_d} and V_{sh_q}) are then controlled to satisfy the system requirements.

Designing a control strategy for the UPFC should include the control objectives (local-global), the input signals to the controller and the co-ordination between the UPFC and other FACTS devices installed in the power network. Based on these considerations, various conventional or modern control theory can be used to design the UPFC control algorithm (e.g. robust control, optimisation, fuzzy logic control or ANN) [8,12,13,71].

5.5 COMPUTER SIMULATION OF THE UPFC

In order for the impact of the UPFC to be effectively investigated, its model and implementation in available software packages are essential. In this work, the MATLAB software is used for performing the computer simulation of the power system incorporating the UPFC where two voltage sources are employed to represent both of the UPFC inverters. MATLAB is a wide spread commercial software package that has several supporting toolboxes. The SIMULINK and POWER SYSTEM BLOCKSET of the MATLAB can be used to simulate different power system configurations and power electronic devices. The corresponding control systems can be simulated with the aid of appropriate toolboxes (e.g. control, fuzzy, neural network, etc). Therefore, various analysis tasks of power system operation can be conducted and the appropriate control system can be designed.

UPFC controlled system model

Figure 5.7 shows the UPFC controlled system as constructed using SIMULINK. As presented earlier, ideal voltage sources are used to model the UPFC inverters. Each inverter voltage is constructed using two controlled voltage sources; one produces the in-phase voltage component with reference to the sending-end bus voltage while the other produces the quadrature voltage component. Note that leakage inductance of the series (booster) transformer is included in the transmission line inductance while the leakage inductance of the shunt (excitation) transformer reactance is exclusively represented by X_{sh}.

The a.c. system at the sending-end is modelled as a balanced three-phase voltage source with the Thevenin's reactance determined according to the system short circuit level. The receiving-end system is represented by a balanced three-phase voltage source with an initial phase shift of 30^0 lag with respect to the sending-end voltage.

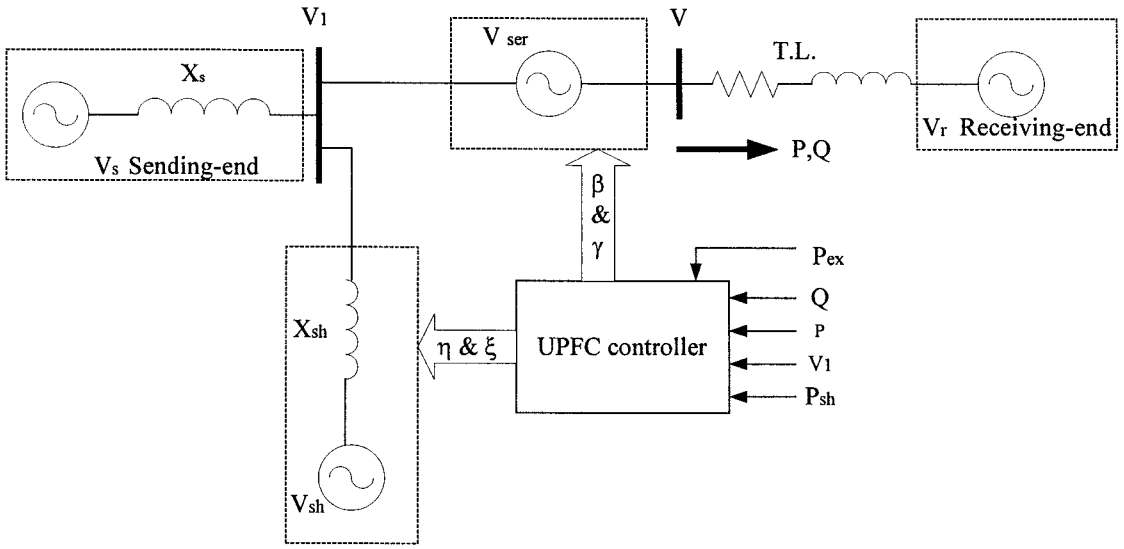

Figure 5.7 UPFC controlled system.

Controlled voltage source subsystem

The series and shunt-injected voltages are represented by Controlled Voltage Sources (CVS) in the SIMULINK model. The CVS generates an a.c. voltage signal in the time domain controlled by its driving signal and initial conditions. Each injected voltage is split into two perpendicular components, the first is used to add an in-phase voltage while the second adds the quadrature component, as shown in Figure 5.8. The sending-end bus voltage is taken as the reference signal for both the series and shunt voltages. This has the advantage of reducing the number of control system input measurements in particular in real time implementation of the UPFC control system.

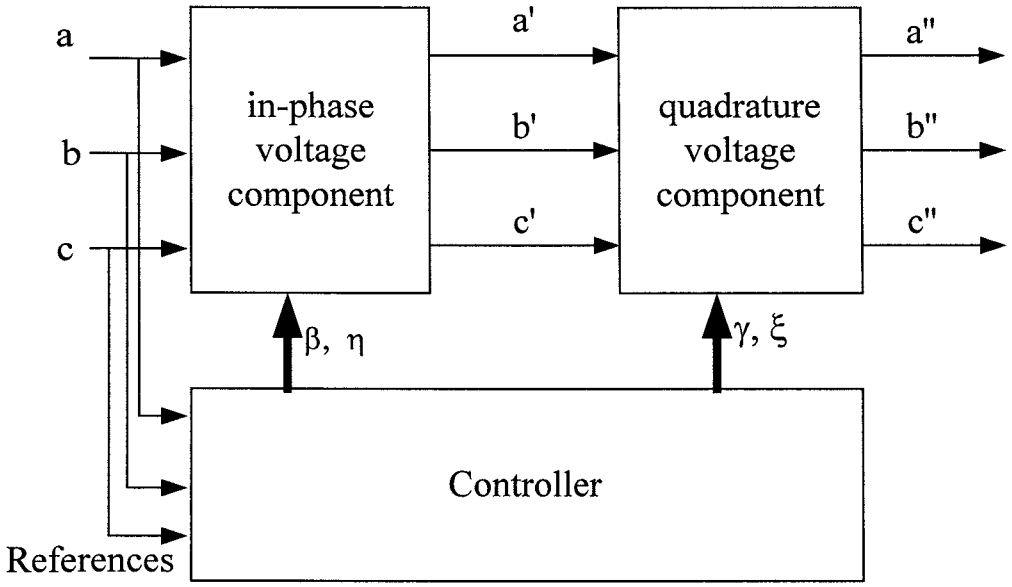

(a) schematic diagram.

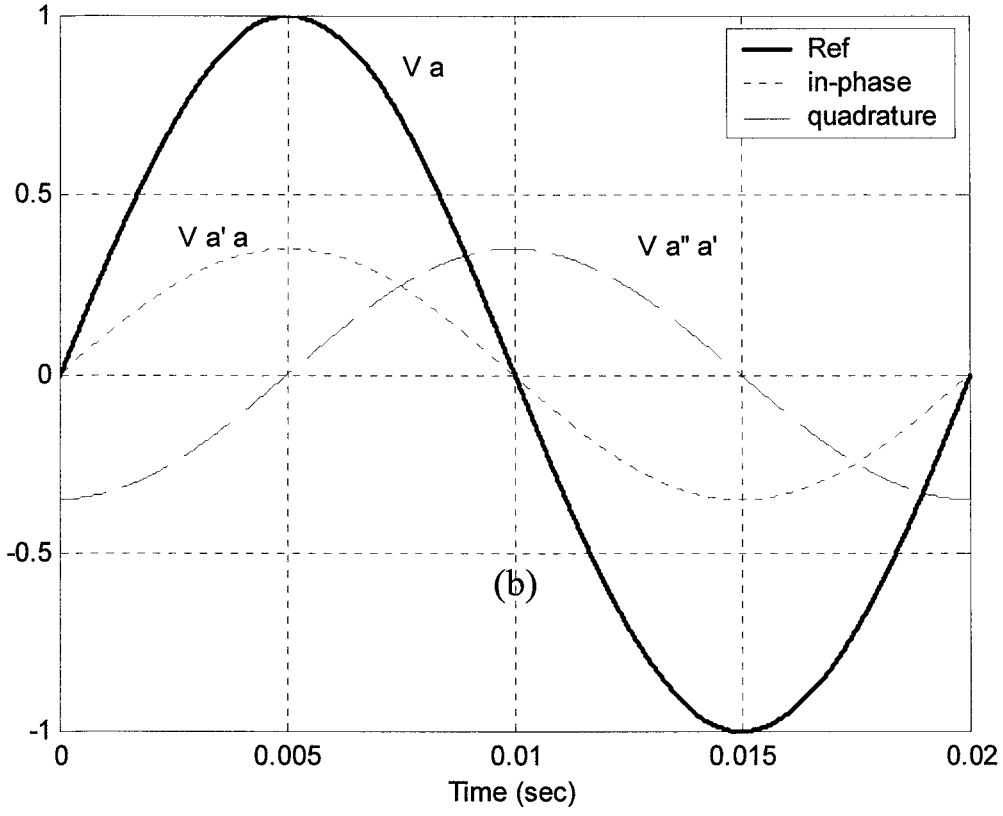

(b) voltage waveforms.

Figure 5.8 Inserted voltage components.

The system is simulated in the continuous-time domain, hence special precautions should be taken into account for the driving signals of the voltage sources. Arbitrary changes of the injected voltage level might lead to a d.c. offset in the current waveforms. Therefore, each change in the quadrature voltage component (series & shunt) should start only at its peak value, which corresponds to the zero-value of the reference signal (assuming a lossless circuit). Also, the effect of the control signal on the in-phase voltage should occur at the peak value of the reference signal, as shown in Figure 5.9. This will take place on the expense of up to a half cycle dead time of the control signal. The SIMULINK subsystem for both the quadrature and in-phase voltage components is shown in Figure 5.10. The actual injected voltage is obtained as a result of multiplying the reference signal by the control variables (β & γ) for the series part and (η & ζ) for the shunt part.

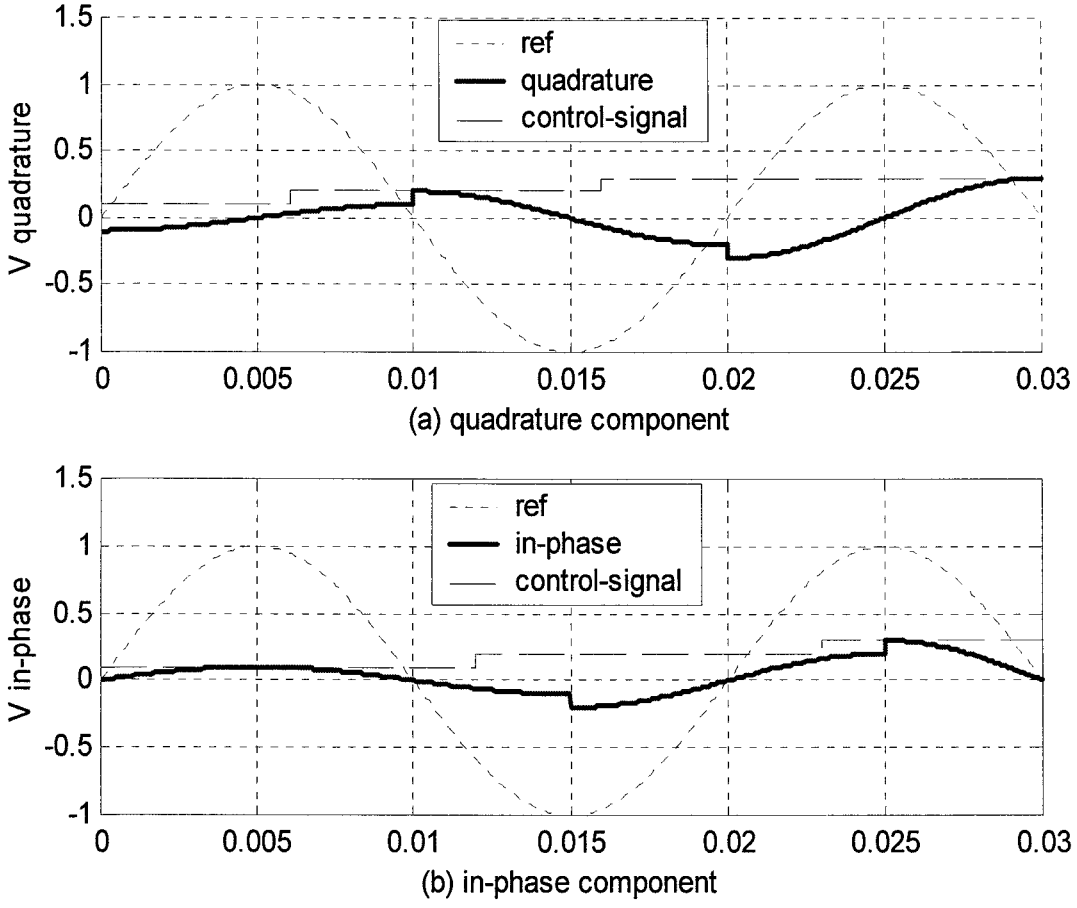

Figure 5.9 Inserted voltage components.

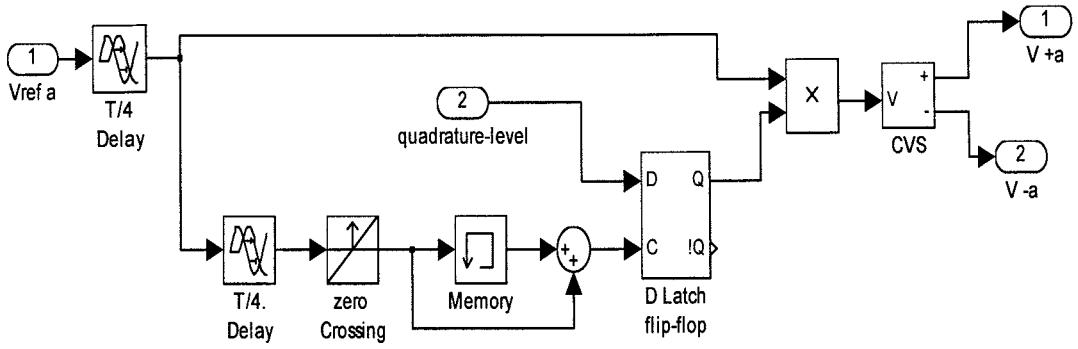

(a) quadrature subsystem.

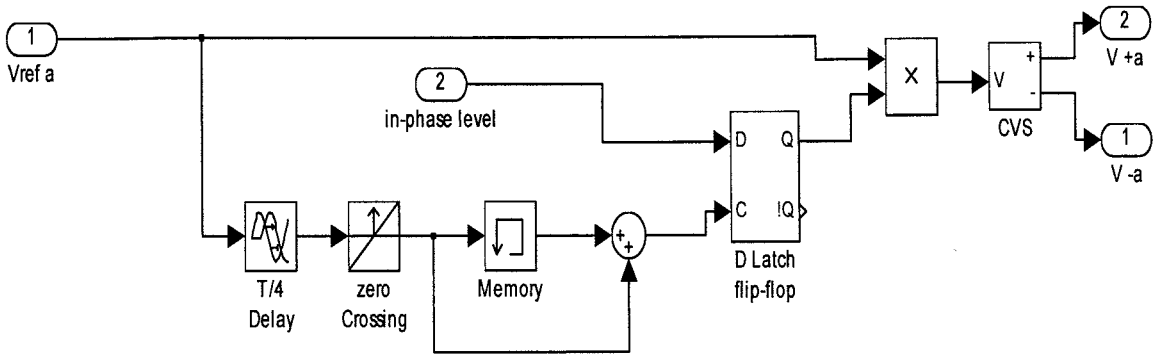

b) in-phase subsystem.

Figure 5.10 Simulink subsystems of the inserted voltages.

Measurements subsystem

The POWER SYSTEM BLOCKSET has a wide range of measurement tools for the instantaneous electric quantities (e.g. voltage and current), the real and reactive power and the signal magnitude and phase angle calculated at any specific signal frequency. The available measuring devices are summarised in Figure 5.11, where each block is used to measure a single-phase quantity. Therefore, three-phase system measurements require combined blocks for monitoring the system parameters. In this work, a symmetrical power system is considered; hence, single-phase parameters and measurements are enough to obtain the required feedback signals.

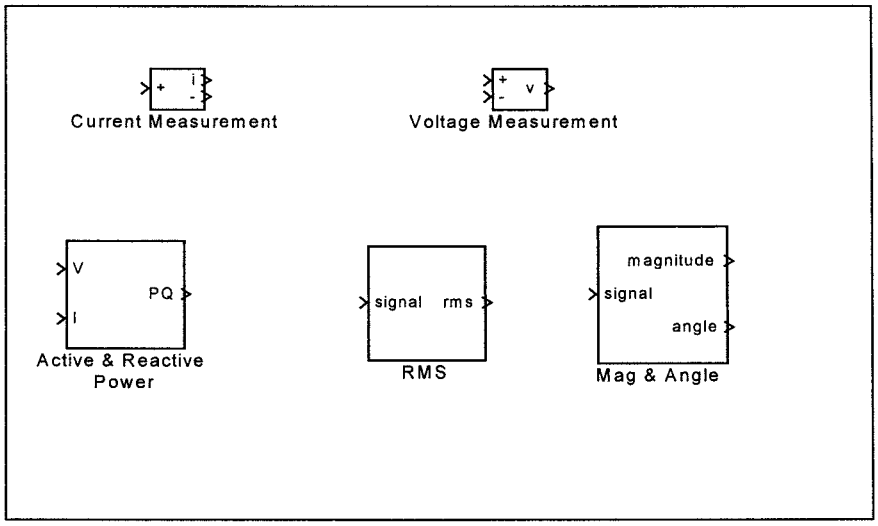

Figure 5.11 Simulink measurements devices.

In this chapter, the UPFC models in the three power system states (electromagnetic transient state, steady-state and electromechanical transient state) have been analysed. The SPWM technique was proved to be more appropriate to generate the UPFC inverters switching patterns. An exact power injection model is proposed which is suitable for load flow analysis. The controlled voltage sources model has been used to represent the UPFC in the steady-state analysis. Different control schemes will be investigated in the next two chapters.

UPFC FUZZY KNOWLEDGE BASED CONTROL SYSTEM

6.1 INTRODUCTION

The UPFC offers new horizons in terms of power system control, with the potential to independently control up to three power system parameters (bus voltage, active power and reactive power). Two aspects of the UPFC control have been considered. When the UPFC control variables are given, the control duty is to evaluate the impact of the UPFC on the power system; this is known as the open-loop control. When the control technique is used to derive the UPFC control variables; this is known as the closed loop control, which is the subject of this chapter. Two fuzzy knowledge based controllers are designed to control the UPFC operation in order to achieve the desired power flow. The Fuzzy-like-PI controller and the fuzzy based-rules controller.

6.2 THE UPFC CONTROL SYSTEM

The UPFC control system has two main parts, the series inverter controller and the shunt inverter controller. The operation of each control block is mainly dependent on the UPFC mode of operation. In this investigation, the series inverter is controlled to operate in an automatic power flow mode. At the same time, the shunt inverter is operated in an automatic voltage control mode. The controller subsystem receives the feedback quantities from the measuring devices and/or the set points as designed according to the system requirements. The output of the control subsystem is a set of control variables which defines the level of the inverters output voltages of the UPFC as follows:

- β, the in-phase series injected voltage level.
- γ, the quadrature series injected voltage level.
- η, the in-phase shunt inverter output voltage level.
- ξ, the quadrature shunt inverter output voltage level.

6.2.1 Open-Loop Control

Generally, the open-loop simulation of the UPFC model can help planners to determine the device operating range and justify its impact on the power system. It is often used to validate control strategies for the UPFC. A block diagram to illustrate the UPFC open-loop control system is shown in Figure 6.1. The series inserted voltage components β and γ are calculated using Equations 4.20 and 4.23. For the shunt inverter, the quadrature component is calculated by re-arranging Equation 4.16 in order to balance the active power exchanged between the two inverters. The in-phase component is used to adjust the inverter output voltage to generate or absorb reactive power, as described by Equation 4.17.

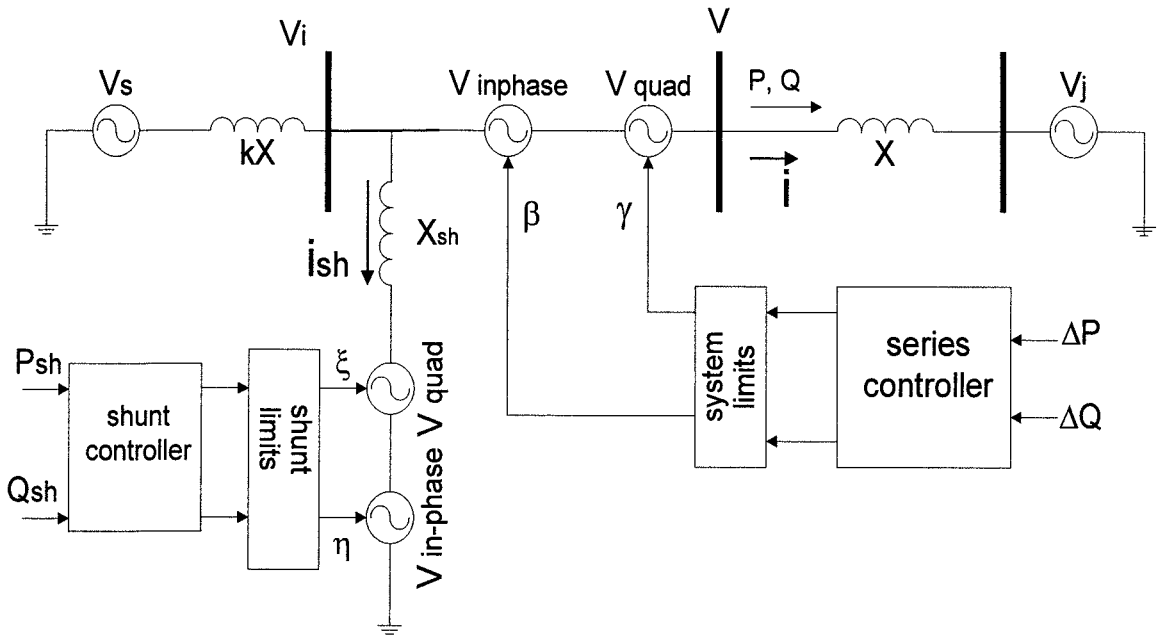

Figure 6.1 Block diagram for the UPFC open-loop control system.

Practically, the series inverter may be operated in the open-loop control scheme to provide the required power change. However, the shunt inverter must be operated in a closed loop mode in order to perform its function to support the voltage and provide the series inverter real power demand.

Figure 6.2 illustrates the performance of the UPFC series part in open-loop control mode. The real and reactive power flow are subjected to step changes by varying the inserted voltage levels β and γ, as shown in the same figure. Note that the bus voltage is taken as a reference signal. Therefore, any change in the real and/or reactive power flow requires changes in both control variables β and γ at the same time. The open-loop control performance depends on the power system variables which may be subjected to violations. Therefore, a closed loop control scheme is essential.

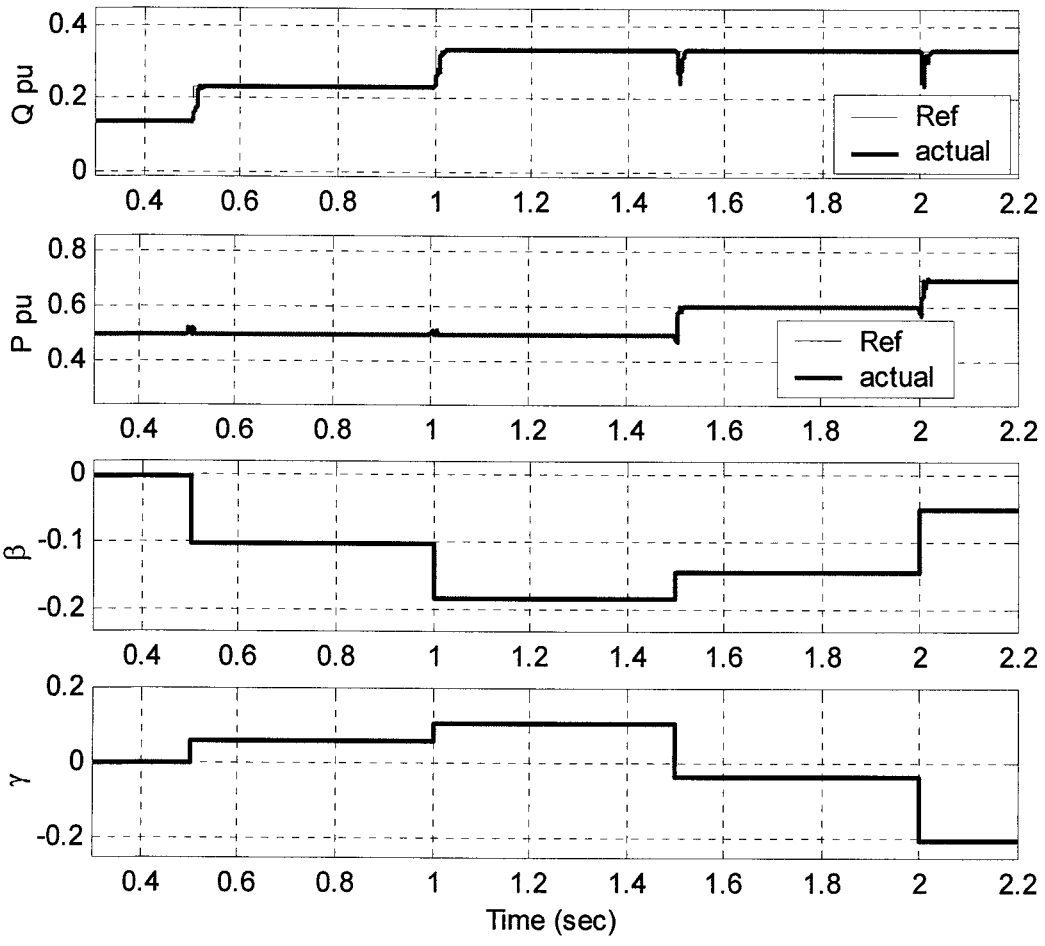

Figure 6.2 System response when UPFC is in open-loop control mode.

6.2.2 Closed Loop Control

To analyse the performance of the UPFC control system investigated in this study, the following specific modes of operation were selected:

6.2.2.1 The series inverter controller

The injected voltage components are controlled so as to maintain or vary the active and reactive power flow in the transmission system within a pre-determined margin. This is referred to as the automatic power flow control mode. In this case, the magnitude and phase angle of the injected voltage, which is synthesised from the in-phase and quadrature components, are continuously updated by the series controller to achieve the required change in the power flow. As described by Equations 4.8 and 4.11, the quadrature component of the inserted voltage mainly affects the real power flow while the in-phase voltage level dominates the reactive power flow.

The series controller is therefore driven by the change in power flow. The real power change is used to deduce the control signal γ while the reactive power change is used to obtain the control signal β, as shown in Figure 6.3. For a standard PI controller, the control signals are obtained as follow:

$$\gamma = \left(P_{ref} - P\right)\left(K_{PP} + \frac{K_{IP}}{S}\right) \tag{6.1}$$

$$\beta = \left(Q_{ref} - Q\right)\left(K_{PQ} + \frac{K_{IQ}}{S}\right) \tag{6.2}$$

where, K_{PP}, K_{IP}, K_{PQ} and K_{IQ} are the corresponding gains of the controller.

6.2.2.2 The shunt inverter controller

The shunt inverter output voltage components are controlled in order to generate or absorb certain amount of reactive power required to maintain the shunt bus voltage at a pre-specified set point. In addition, the inverter should supply or absorb the real power demand of the series inverter, given by Equations 4.16 and 4.17.

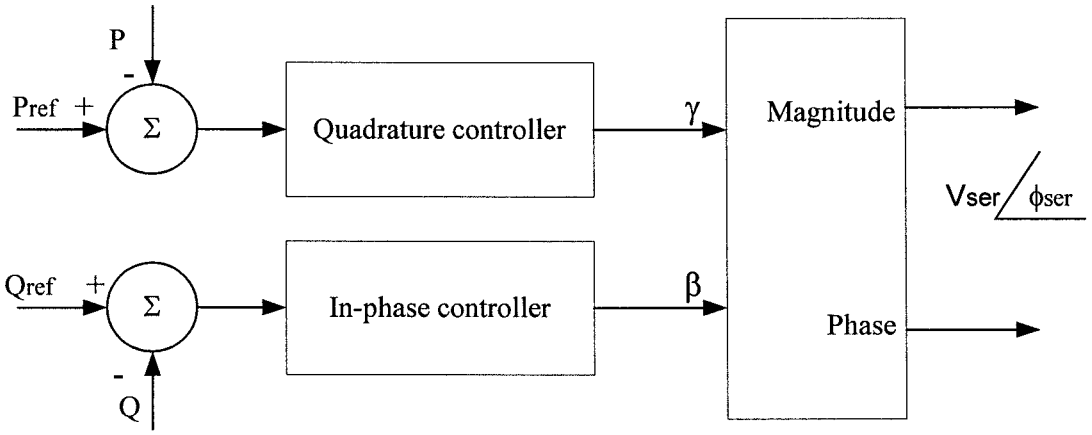

Figure 6.3 Block diagram of the series inverter controller.

In this case, the mode of operation is referred to as the automatic voltage control mode. The quadrature component of the shunt voltage may be determined from the deviation of the d.c. bus voltage from its reference value. Therefore, the controller function is to keep the d.c. voltage smoothly constant. The control signal is obtained for the PI controller as illustrated in Figure 6.4, as follows:

$$\xi = \left(V_{dcref} - V_{dc}\right)\left(K_{Pdc} + \frac{K_{Idc}}{S}\right) \tag{6.3}$$

This method is more suitable for a practical application (therefore it has been used during the experimental phase of this study) as the voltage reference signal is already available, hence, it reduces the number of measured input signal.

Alternatively, the quadrature controller may be driven by the difference between the series inverter real power exchanged with the a.c. system and the real power generated/absorbed by shunt inverter. In this case, the control signal is defined as:

$$\xi = (P_{ex} - P_{sh})\left(K_{Pdc} + \frac{K_{Idc}}{S}\right) \tag{6.4}$$

In the simulation phase of this study, the second method is used to control the quadrature level of the shunt inverter output voltage. Although this method needs four parameters to be measured (voltage & current of the series inverter and voltage & current of the shunt inverter), it is more convenient for the voltage source model of the UPFC where the d.c. link is not available.

The driving signal for the in-phase controller is obtained from the deviation of the bus voltage from its reference value, as shown in Figure 6.4. The control signal is given as:

$$\eta = (V_{iref} - V_i)\left(K_{Pvi} + \frac{K_{Ivi}}{S}\right) \tag{6.5}$$

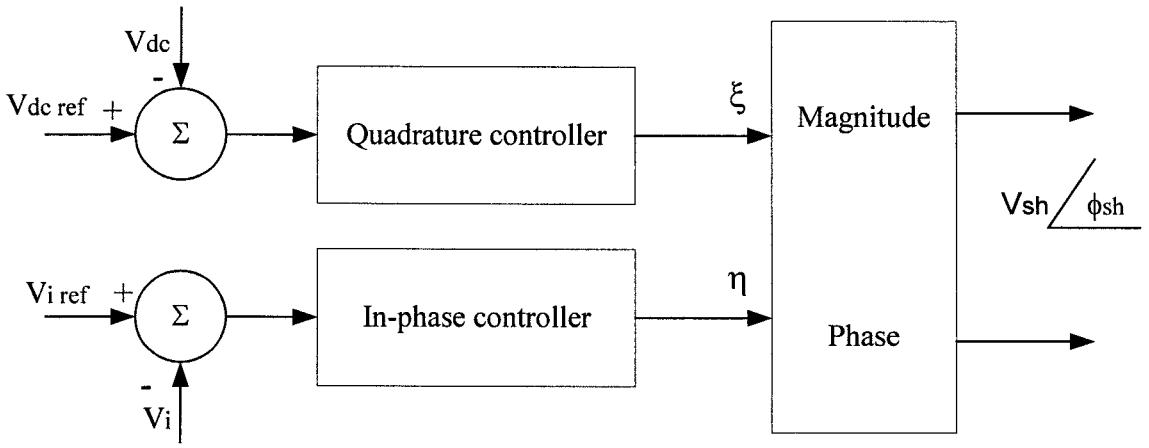

Figure 6.4 Block diagram of the shunt inverter controller.

6.3 FUZZY KNOWLEDGE BASED CONTROL SYSTEM

Fuzzy sets were introduced by Zadeh [72] as a mean of representing and manipulating data that are not precise, but rather fuzzy. Fuzzy logic provides an inference morphology that enables approximate human reasoning capabilities to be applied to knowledge-based systems. The theory of fuzzy logic provides a mathematical strength to capture the uncertainties associated with human cognitive processes, such as thinking and reasoning. There are two main characteristics of fuzzy systems that give them better performance for many practical applications [73].

- Fuzzy systems are suitable for uncertain or approximate reasoning, especially for the system with a mathematical model that is difficult to be derived.
- Fuzzy logic allows decision making with estimated values under incomplete or uncertain information.

Fuzzy controllers are being used in various control schemes [74]. The most obvious one is *direct control*, where the fuzzy controller is in the forward path in a feedback control system, as shown in Figure 6.5. The process output is compared with a reference and if there is a deviation, the fuzzy controller takes action according to the control strategy. A fuzzy controller in a *feed forward control* scheme is shown in Figure 6.6 where a measurable disturbance is being compensated by the fuzzy controller. The controller block may be a linear conventional controller. The third typical fuzzy control scheme is shown in Figure 6.7, where the fuzzy rules are used to correct the tuning parameters of a conventional controller in a *parameter adaptive control* scheme. The control parameters are tuned to compensate for any change in the plant operating point.

Human supervision of the fuzzy control system slows down the correction of the system performance. Hence, a self-organising controller was introduced to adjust the control strategy in a fuzzy controller without human intervention [75-78].

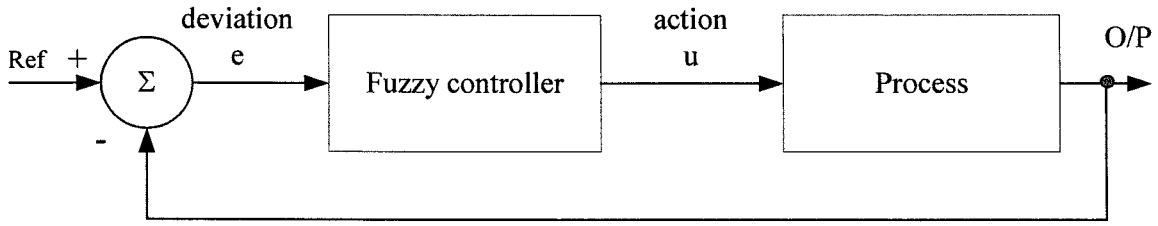

Figure 6.5 Fuzzy direct controller.

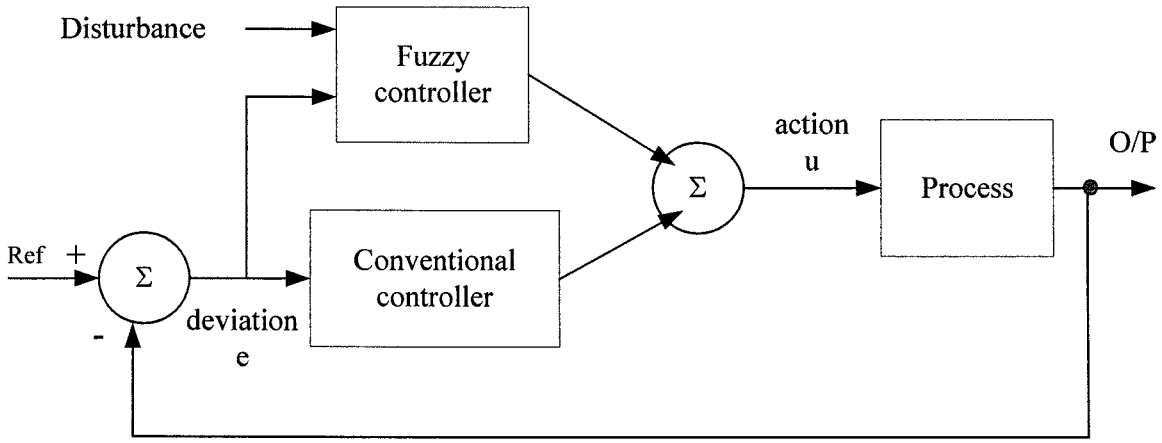

Figure 6.6 Fuzzy feed forward controller.

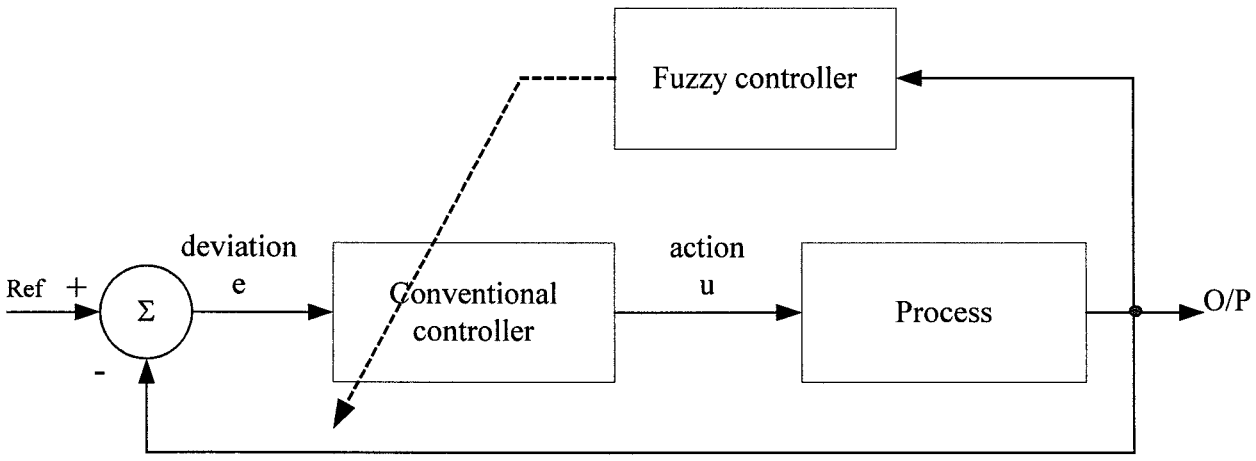

Figure 6.7 Fuzzy parameter adaptive controller.

Based on the current performance of the controller, if the performance is poor, the responsible rule is modified in order to improve the control signal.

6.3.1 Structure of a Fuzzy Control System

There are specific main components of a fuzzy controller to support a design procedure. In the block diagram of Figure 6.8, the controller main function lies between pre-processing and post processing blocks. The following explains the components of the fuzzy control system:

Pre-processing

The inputs are most often hard or crisp measurements from measuring equipment, rather linguistic. A pre-processor conditions the measurements before they enter the controller. Examples of pre-processing are:

- Quantisation in connection with sampling or rounding to integers.
- Normalisation or scaling onto a particular range.
- Filtering, in order to remove noise.
- Averaging to obtain long-term or short-term tendencies.
- A combination of several measurements to obtain key indicators.

Fuzzification

Fuzzification converts each piece of input data to degrees of membership in one or more membership functions. The fuzzification process matches the input data with the conditions of the rules to determine how well the condition of each rule matches that particular input instance. There is a degree of membership for each linguistic term that applies to that input variable. The choice of membership functions depends on the problem to be dealt with and the number of fuzzy sets. There is no standard design scheme that can be followed to obtain the most effective number and type of the membership functions. In this study the triangular membership functions with 50% overlapping have been chosen to

represent the equivalent fuzzy input of the physical measured quantities. This is shown in Figure 6.9 defined over the fuzzy set (NB, NM, NS, ZE, PS, PM, PB), standing for negative big, negative medium, negative small, zero, positive small, positive medium and positive big, respectively.

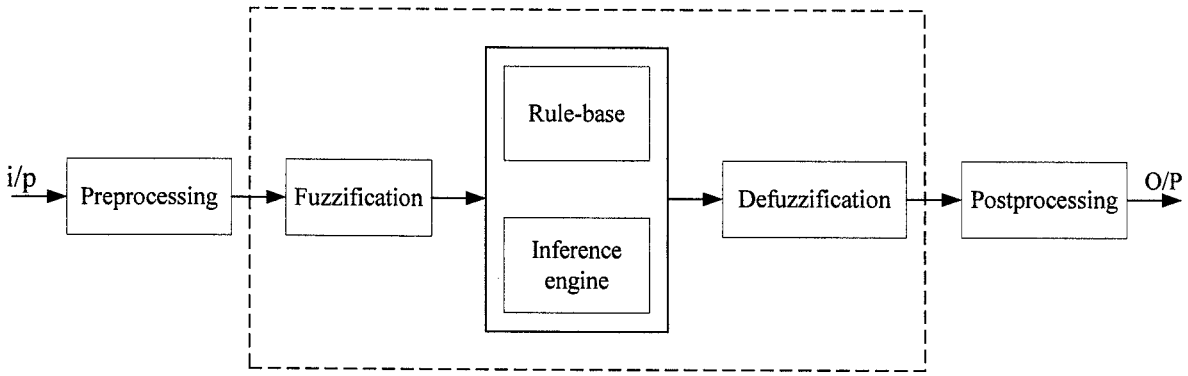

Figure 6.8 Block diagram of a Fuzzy controller.

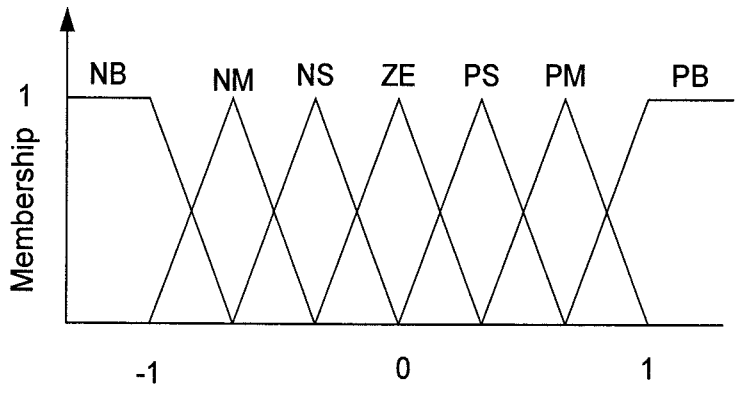

Figure 6.9 Triangular membership functions

Rule-base

The rules may use one or several variables in the condition and the conclusion of each rule. Fuzzy controllers can therefore be applied to both multi-input multi-output (MIMO) problems and single-input single-output (SISO) problems. Generally, a linguistic controller contains a set of rules described as:

if condition then conclusion

These rules can be presented in different format; *relational format* is a more compact representation, which is better suited for an experienced user who wants to get an overview of the rule base. The *tabular* linguistic format may be used to express the rules routine. In this format the input variables are sorted out along the axes and the output variable is inside the table. This format is useful for checking completeness.

Generating the control rules is the main step in designing fuzzy based-rules controllers. Many methods are reported in the literature for deriving suitable rules for the system under study [79,80]. These are based on:

- knowledge from experienced human operators,
- a fuzzy model of the plant,
- mathematical analysis of the system, and
- learning mechanisms.

Inference engine

The basic function of the inference engine is to compute the overall value of the current process states based on the contribution of each rule in the rule base.

Defuzzification

The defuzzifier converts the resulting output fuzzy set to a crisp value that can be sent to the process as a control signal. There are several defuzzification methods among them the Centre Of Gravity (COG) is the common defuzzification method [81]. In this method the centre of the area below the combined membership functions is determined.

Post-processing

The output of the defuzzification process is usually defined on a standard universe. This must be scaled by the post-processing block to the engineering units suitable for the system under study.

6.4 FUZZY-LIKE-PI CONTROLLER

The conventional PI controller described by Equations 6.1-6.5 can be generalised as:

$$u = K_P e + K_I \int e dt \tag{6.6}$$

where u is the control variable (β, γ, ξ *or* η),

e is the error signal for the corresponding controlled variable,

K_P and K_I are the proportional and integral gains.

The derivative of Equation 6.6 is given as:

$$\dot{u} = K_P \dot{e} + K_I e \tag{6.7}$$

To drive a fuzzy logic that behaves like a PI controller, the algorithm defined by Equation 6.7 is then transferred into a set of fuzzy rules [82].

The conventional approach to the Fuzzy Logic Controller (FLC) design is to generate a fuzzy rule set based on the system quantities to be controlled. In this study, such quantities are defined as the real and reactive power flow in the transmission system for the series inverter controller (P and Q). For the shunt inverter controller, the bus voltage and the difference in power flow between the shunt and series inverters are chosen to be the controlled variables (V_i and $(P_{ex} - P_{sh})$). From Equation 6.7 the error (e) and change of error (cer) are used to produce a two-input single-output controller rule-base, as described in Table 6.1.

The crisp inputs of the error and change of error are fuzzified using a term set of seven linguistic variables. Each variable is characterised by a triangular membership function as shown in Figure 6.9. The size of the term set determines the granularity of the control action of the FLC. To obtain a high control quality around the set point, a large number of linguistic variables is recommended. However, a large number of term set parameters leads to an increase of rules and hence more computation time.

Table 6.1 Rule-base for Fuzzy-like-PI

e \ cer	NB	NM	NS	ZE	PS	PM	PB
NB	NB	NB	NB	NB	NM	NS	ZE
NM	NB	NB	NB	NM	NS	ZE	PS
NS	NB	NB	NM	NS	ZE	PS	PM
ZE	NB	NM	NS	ZE	PS	PM	PB
PS	NM	NS	ZE	PS	PM	PB	PB
PM	NS	ZE	PS	PM	PB	PB	PB
PB	ZE	PS	PM	PB	PB	PB	PB

6.4.1 Simulation Study

The system shown in Figure 6.10 is used to investigate the performance of the designed controllers to regulate the UPFC operation under different system conditions. The system short circuit level is assumed to be 10.0 p.u. (k=0.1) with $\left(\frac{V_i V_j}{X}\right)$ as the power base. The system is controlled such that it operates at different points inside the defined controlled area. Three cases have been conducted to analyse the capability of the UPFC incorporating PI and Fuzzy like-PI controllers.

Case 1

This case is to demonstrate that the UPFC can independently control the flow of reactive power in the transmission system. In this case, the series inverter is controlled to create a step change in the reactive power while keeping the active power constant. The

shunt inverter is controlled to regulate the system bus voltage at its set point. The system response is shown in Figure 6.11 for both PI and FLC.

Case 2

In this case, the active power is subjected to a step change while the reactive power is left unchanged. The shunt inverter is also controlled to regulate the bus voltage. The system response is shown in Figure 6.12 for both PI and FLC. It is clear from the results that the UPFC can also control the real power flow in a transmission system while maintaining the reactive power fairly constant.

Case 3

The objective of this case is to show the system response for a step change in the system bus voltage. The voltage set point is changed by 3%. Figure 6.13 shows the system response in which the UPFC regulates the real and reactive power while controlling the bus voltage.

The results obtained from these simulation studies show that the Fuzzy-like-PI controller performs slightly better than the standard PI controller. This is particularly true in reducing the interaction between the real and reactive power flow.

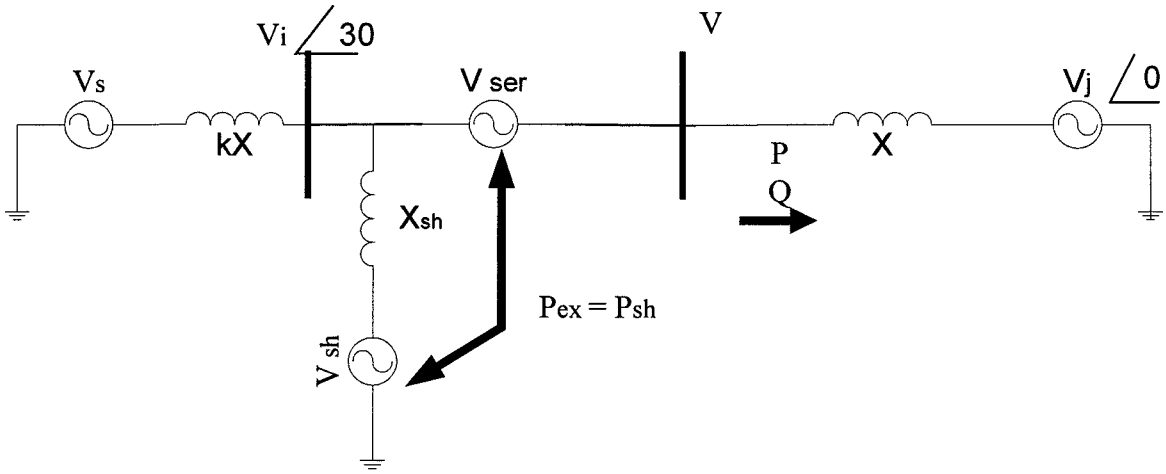

Figure 6.10 Transmission system simulation model

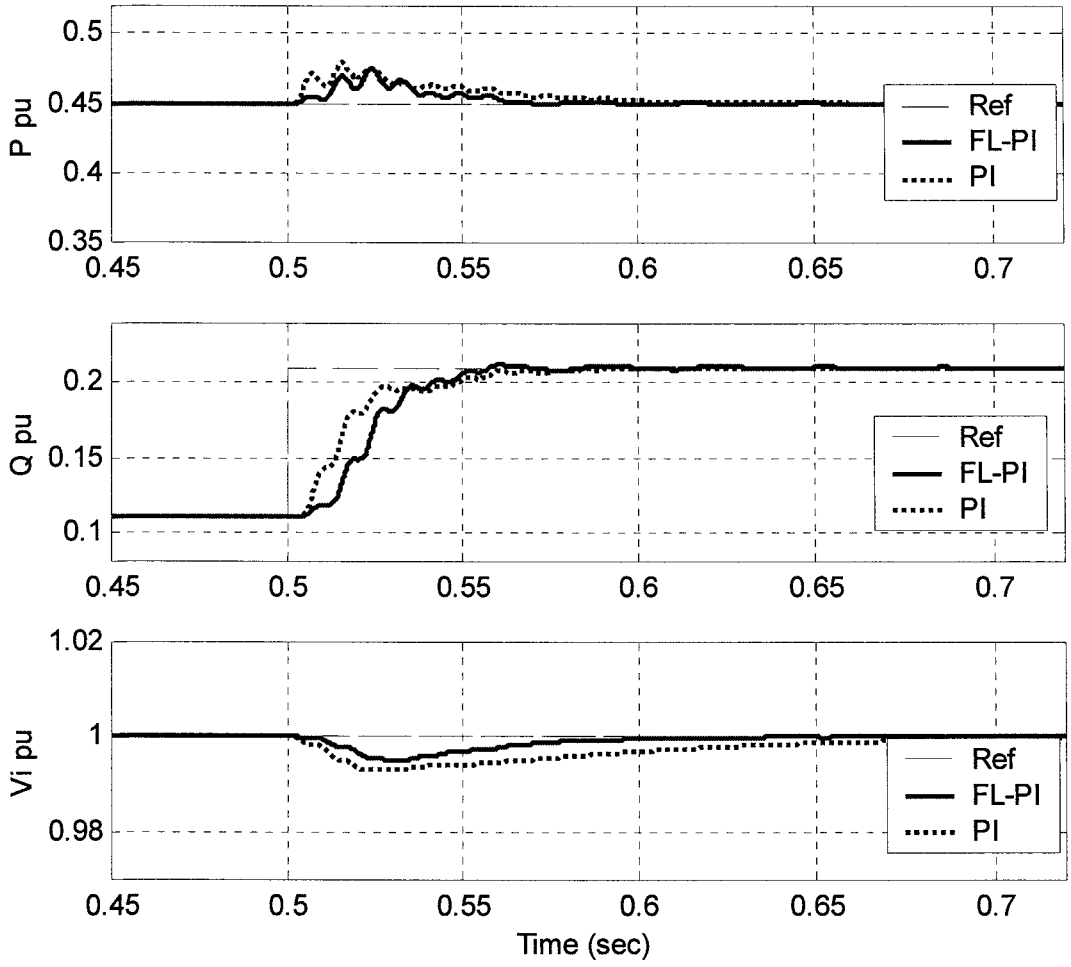

Figure 6.11 System response for a change in reactive power flow.

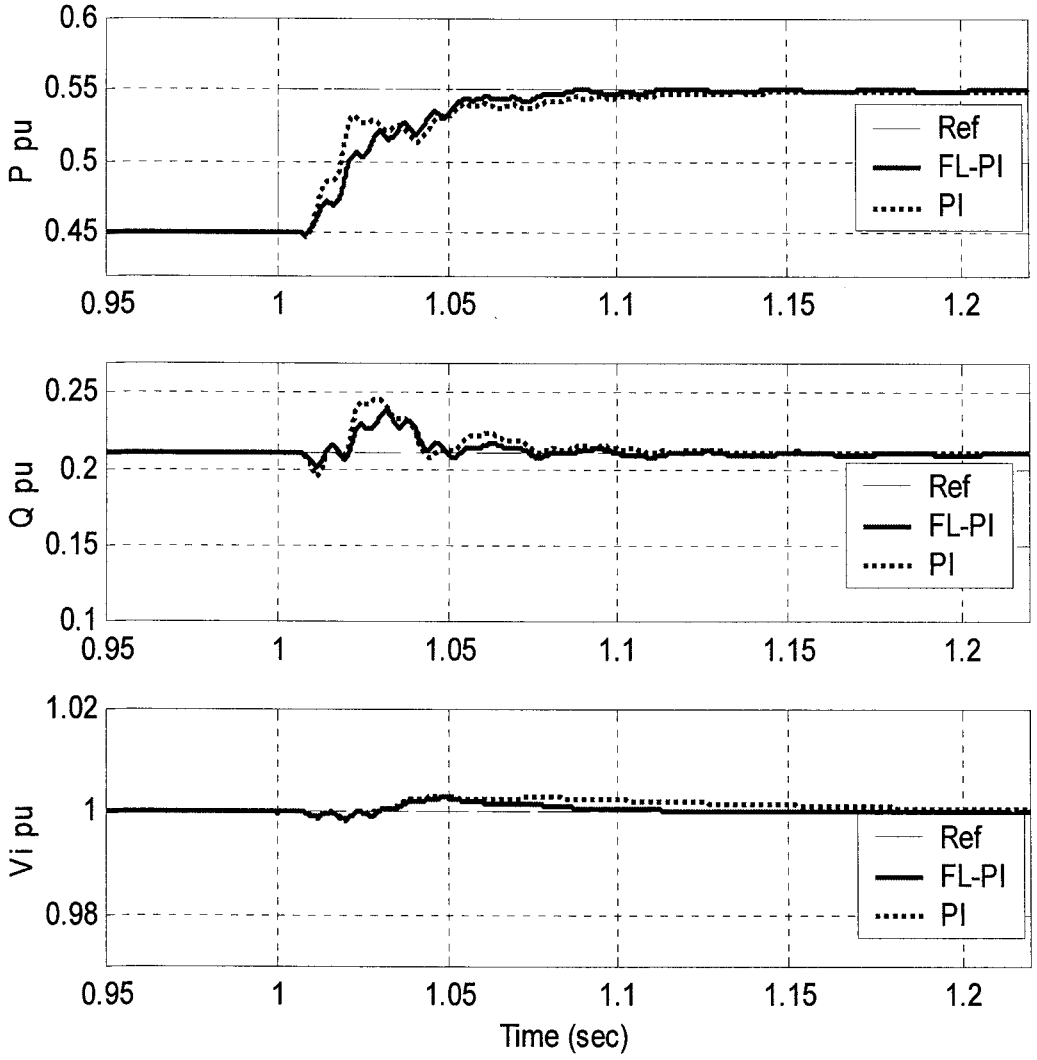

Figure 6.12 System response for a change in active power flow.

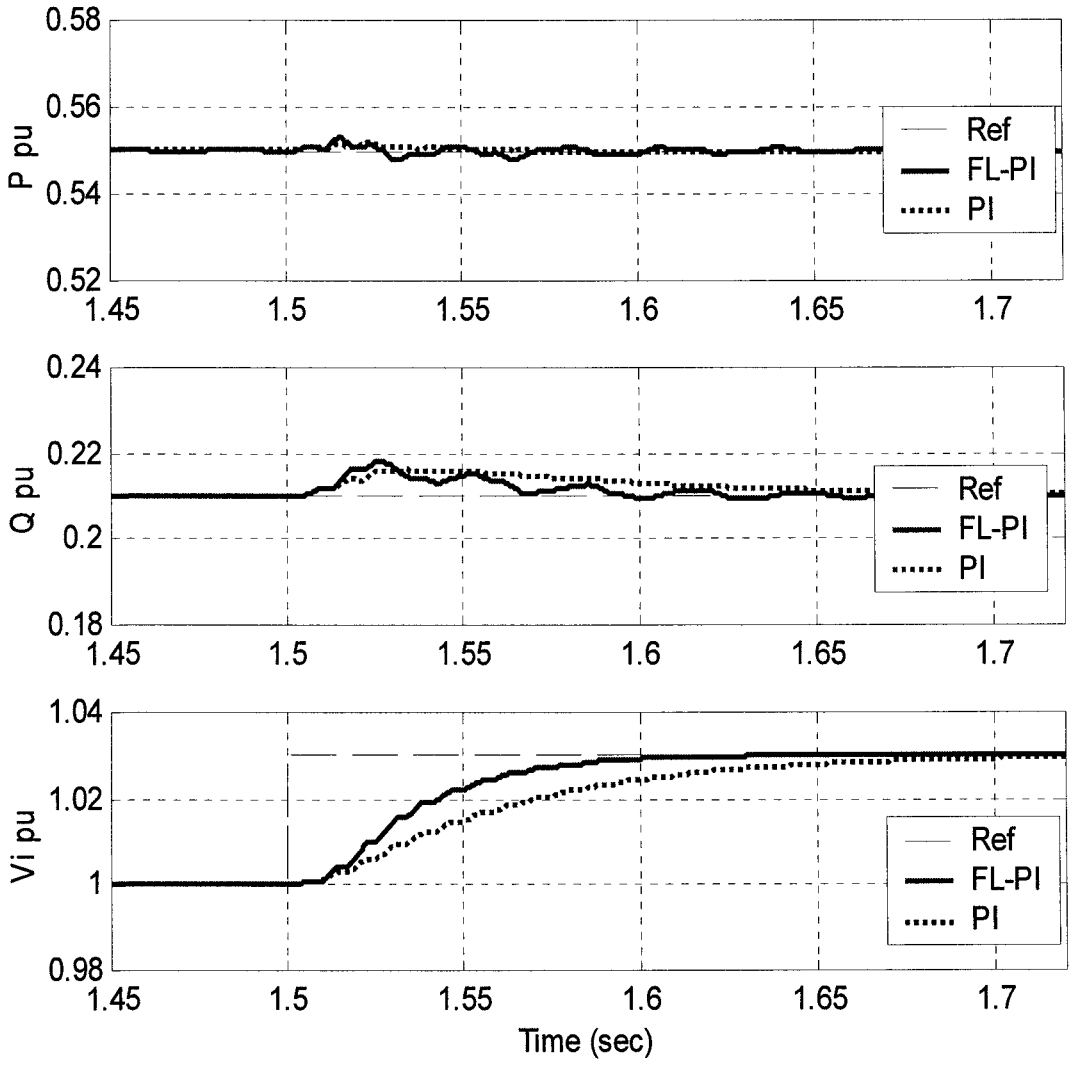

Figure 6.13 System response for a change in bus voltage.

6.5 FUZZY BASED-RULES CONTROLLER (FBRC)

Generating the control rules represents the corner stone in designing fuzzy based-rules controllers. Many methods are reported in the literature for deriving suitable rules for the power system incorporating FACTS devices. The relationships among variables (rules) are deduced from the system response to a test signal [83]. In this case, an open-loop test is performed by applying a pulse input to the plant, the rules are extracted from the output response. The power of the test signal is a critical issue where the signal should be strong enough to cause a sufficient variation in the signal observed. Also, it should not be too strong to cause a controller saturation or to make the system unstable. The phase-plane analysis of the system under study is used to define the fuzzy rules from the plane transition points [84]. Therefore, a switching line should be defined to help in finding the transition points, which requires intensive mathematical analysis of the system.

In this work, generating the controller rules is based on the mathematical analysis of the UPFC. Therefore, the controller behaviour is extracted from the relationship between the series/shunt inserted voltage components and real/reactive power flow in the transmission line and the shunt branch.

6.5.1 Series Controller-Rules

The change of real and reactive power flow in the transmission system, shown in Figure 6.10, have been derived and expressed by Equations 4.18 and 4.19 (see page 51). The inserted voltage control parameters β and γ may be obtained as a function of the changes in real and reactive power as given by Equation 4.20 and 4.23.

The variables' relationships for β and γ with maximum inserted voltage $V_{ser} = 0.35pu$ are shown in Tables 6.2 and 6.3, respectively. The blank cells represent the uncontrolled region where it is beyond the system capability to follow the required changes in active and reactive power. The **bold red** (highlighted) cells represent the values of β and

γ which are practically available under the system constraints. The *italic blue* cells represent the operating points where β and/or γ exceed the limit. To implement Tables 6.2 and 6.3 in the fuzzy logic controller design, they are transformed into linguistic values which are the symbolic description of the control parameters (ΔP, ΔQ, β and γ), as shown in Tables 6.4 and 6.5. The universe of discourse of each controller variable is assumed to contain 11 triangular membership functions with 50% overlapping, as shown in Figure 6.14.

Table 6.2 β values.

ΔP \ ΔQ	-0.5	-0.45	-0.339	-0.2260	-0.1130	0.0	0.1130	0.2260	0.3390	0.4520	0.5650
-0.3510			*-0.3618*	-0.1734	*-0.0605*	*0.0284*	*0.1042*	*0.1715*	*0.2325*	*0.2887*	*0.3412*
-0.2808				-0.1703	-0.0485	*0.0446*	*0.1229*	*0.1918*	*0.2541*	*0.3113*	*0.3646*
-0.2106				-0.1863	-0.0476	0.0522	0.1344	*0.2059*	*0.2701*	*0.3288*	*0.3833*
-0.1404				-0.2406	-0.0612	0.0498	0.1379	0.2132	0.2801	*0.3408*	*0.3969*
-0.0702					-0.0978	0.0345	0.1318	0.2127	0.2833	0.3468	*0.4050*
0.0					-0.1916	0.0	0.1134	0.2026	0.2786	0.3459	*0.4071*
0.0702						-0.0718	0.0771	0.1803	0.2644	0.3371	*0.4021*
0.1404							0.0085	0.1404	0.2376	0.3184	*0.3889*
0.2106								0.0690	0.1927	0.2866	*0.3654*
0.2808								*-0.1610*	0.1150	0.2354	0.3279
0.3510										0.1480	0.2691

Table 6.3 γ values.

ΔP \ ΔQ	-0.5	-0.45	-0.339	-0.2260	-0.1130	0.0	0.1130	0.2260	0.3390	0.4520	0.5650
-0.3510			*-0.1964*	-0.3052	*-0.3703*	*-0.4217*	*-0.4655*	*-0.5043*	*-0.5395*	*-0.5720*	*-0.6023*
-0.2808				-0.2259	-0.2962	*-0.3500*	*-0.3952*	*-0.4350*	*-0.4709*	*-0.5040*	*-0.5348*
-0.2106				-0.1356	-0.2157	-0.2733	-0.3208	*-0.3621*	*-0.3991*	*-0.4330*	*-0.4645*
-0.1404				-0.0232	-0.1268	-0.1909	-0.2418	-0.2852	-0.3238	*-0.3589*	*-0.3913*
-0.0702					-0.0246	-0.1010	-0.1572	-0.2038	-0.2446	-0.2813	*-0.3149*
0.0					0.1106	0.0	-0.0655	-0.1170	-0.1609	-0.1997	*-0.2350*
0.0702						0.1225	0.0365	-0.0230	-0.0716	-0.1136	*-0.1511*
0.1404							0.1572	0.0811	0.0249	-0.0217	*-0.0624*
0.2106								0.2034	0.1319	0.0777	*0.0322*
0.2808								*0.4172*	0.2579	0.1883	0.1349
0.3510										0.3198	0.2499

Table 6.4 β linguistic.

ΔP \ ΔQ	NVB	NB	NM	NS	NVS	ZE	PVS	PS	PM	PB	PVB
NVB			*NVB*	**NS**	*NVS*	*ZE*	*PVS*	*PS*	*PM*	*PB*	*PVB*
NB				**NS**	**NVS**	*PVS*	*PS*	*PM*	*PB*	*PB*	*PVB*
NM				**NM**	**NVS**	**PVS**	**PS**	*PM*	*PB*	*PVB*	*PVB*
NS				**NM**	**NVS**	**PVS**	**PS**	**PM**	**PB**	*PVB*	*PVB*
NVS					**NVS**	**ZE**	**PS**	**PM**	**PB**	**PVB**	*PVB*
ZE					**NM**	**ZE**	**PS**	**PM**	**PB**	**PVB**	*PVB*
PVS						**NVS**	**PVS**	**PM**	**PB**	**PVB**	*PVB*
PS							**ZE**	**PS**	**PM**	**PVB**	*PVB*
PM								**PVS**	**PM**	**PB**	*PVB*
PB								*NS*	**PS**	**PM**	**PVB**
PVB										**PS**	**PB**

Table 6.5 γ linguistic.

ΔP \ ΔQ	NVB	NB	NM	NS	NVS	ZE	PVS	PS	PM	PB	PVB
NVB			*NM*	**NB**	*NVB*	*NVB*	*NVB*	*NVB*	*NVB*	*NVB*	*NVB*
NB				**NM**	**NB**	*NVB*	*NVB*	*NVB*	*NVB*	*NVB*	*NVB*
NM				**NS**	**NM**	**NB**	**NVB**	*NVB*	*NVB*	*NVB*	*NVB*
NS				**ZE**	**NS**	**NM**	**NM**	**NB**	**NVB**	*NVB*	*NVB*
NVS					**ZE**	**NVS**	**NS**	**NM**	**NM**	**NB**	*NB*
ZE					**PS**	**ZE**	**NVS**	**NS**	**NS**	**NM**	*NM*
PVS						**PS**	**PVS**	**ZE**	**NVS**	**NS**	*NS*
PS							**PS**	**PVS**	**ZE**	**ZE**	*NVS*
PM								**PM**	**PS**	**PVS**	*ZE*
PB								*PVB*	**PB**	**PM**	**PS**
PVB										**PVB**	**PB**

Referring to the real power priority defined in section 4.6, if the required operating point is located outside the controlled area, a new operating point must be decided on the feasible region circumference which satisfies the maximum inserted voltage. Hence, the series inverter control rules are modified to keep the active power at the desired value within the limit regardless of the reactive power. Therefore, the rules describing the inserted voltage components outside the feasible region are completed to include the real power priority criteria. This is reflected into the linguistic variables as shown in Tables 6.6 and 6.7 for β and γ, respectively.

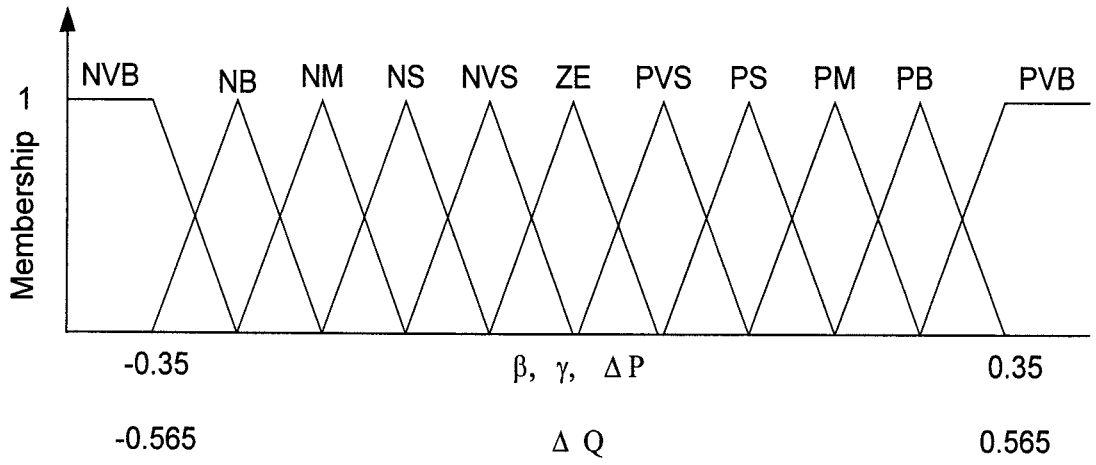

Figure 6.14 Triangular membership functions.

Table 6.6 β extended linguistic.

ΔP \ ΔQ	NVB	NB	NM	NS	NVS	ZE	PVS	PS	PM	PB	PVB
NVB	PM	PM	*PS*	**ZE**	*NS*	*NS*	*NS*	*NS*	*NS*	*NS*	*NS*
NB	PB	PB	PB	**NS**	**NVS**	*NS*	*NS*	*NS*	*NS*	*NS*	*NS*
NM	PB	PB	PB	**NM**	**NVS**	**PVS**	**PS**	*NS*	*NS*	*NS*	*NS*
NS	PVB	PVB	PVB	**NM**	**NVS**	**PVS**	**PS**	**PM**	**NVS**	*NS*	*NS*
NVS	PVB	PVB	PVB	PVB	**NVS**	**ZE**	**PS**	**PM**	**PVS**	**PVS**	*ZE*
ZE	PVB	PVB	PVB	PVB	**NM**	**ZE**	**PS**	**PM**	**PB**	**PS**	*PS*
PVS	PVB	PVB	PVB	PVB	PVB	**NVS**	**PVS**	**PM**	**PB**	**PM**	*PM*
PS	PB	PB	PB	PB	PB	PB	**ZE**	**PS**	**PM**	**PVB**	*PB*
PM	PM	PM	PM	PM	PM	PM	PM	**PVS**	**PM**	**PB**	*PVB*
PB	PM	PM	PM	PM	PM	PM	PM	*PM*	**PS**	**PM**	**PVB**
PVB	PM	PM	PM	PM	PM	PM	PM	PM	PM	**PB**	**PVB**

Table 6.7 γ extended linguistic.

ΔP \ ΔQ	NVB	NB	NM	NS	NVS	ZE	PVS	PS	PM	PB	PVB
NVB	NB	NB	*NB*	**NVB**	*NB*	*NB*	*NB*	*NB*	*NB*	*NB*	*NB*
NB	NM	NM	NM	**NM**	**NB**	*NB*	*NB*	*NB*	*NB*	*NB*	*NB*
NM	NM	NM	NM	**NS**	**NM**	**NB**	**NVB**	*NB*	*NB*	*NB*	*NB*
NS	NS	NS	NS	**ZE**	**NS**	**NM**	**NM**	**NVB**	**NVB**	*NB*	*NB*
NVS	NVS	NVS	NVS	NVS	**ZE**	**NVS**	**NS**	**NM**	**NVB**	**NVB**	*NVB*
ZE	ZE	ZE	ZE	ZE	**PS**	**ZE**	**NVS**	**NS**	**NS**	**NVB**	*NVB*
PVS	PVS	PVS	PVS	PVS	PVS	**PS**	**PVS**	**ZE**	**NVS**	**NB**	*NB*
PS	PS	PS	PS	PS	PS	PS	**PS**	**PVS**	**ZE**	**ZE**	*NM*
PM	PB	PB	PB	PB	PB	PB	PB	**PM**	**PS**	**PVS**	*NS*
PB	PB	PB	PB	PB	PB	PB	PB	*PB*	**PB**	**PM**	**NVS**
PVB	PB	PB	PB	PB	PB	PB	PB	PB	PB	**PM**	**PVS**

6.5.2 Shunt Controller-Rules

By rearranging Equations 4.16 and 4.17, the control parameters of the shunt inverter (ξ and η) may be expressed as,

$$\xi = \frac{X_{sh}}{V_i^2} P_{ex} \tag{6.8}$$

$$\eta = -\frac{X_{sh}}{V_i^2} Q_{sh} \tag{6.9}$$

where, P_{ex} is the real power exchanged between the series inverter and the a.c. system. The variables' relationships are shown in Tables 6.8 and 6.9 for ξ and η, respectively. The VA rating of the shunt inverter is assumed to be $S_{sh} = 0.25pu$.

where,

$$S_{sh} = \sqrt{P_{ex}^2 + Q_{sh}^2} \tag{6.10}$$

It can be deduced from Tables 6.8 and 6.9 that the main part of the shunt inverter VA rating is used to supply the real power demand of the series inverter. The rest is used to generate or absorb the reactive power necessary to support the bus voltage at which the UPFC is connected. To explain the values given in Tables 6.8 and 6.9, a numerical example is given. Assuming that 0.15 p.u. real power is to be transferred across the d.c. link, the quadrature controller parameter should be $\xi = 0.15\ pu$ regardless of the required shunt reactive power (see Table 6.8). Therefore, the corresponding in-phase controller parameter η must not exceed $\pm\sqrt{(0.25)^2 - (0.15)^2}$ p.u. The actual value within the limit is determined by the reactive power demand in p.u. The linguistic values of ξ and η are given in Tables 6.10 and 6.11.

It can be noted from Tables 6.8 and 6.9 that the relationship between the shunt inverter voltage components ξ or η and their driving signals P_{ex} or Q_{sh} is nearly one to one.

As explained earlier, the main function of the shunt inverter is to support the bus voltage and to maintain the d.c. link voltage constant. Hence, and in order to increase its controller sensitivity, the error signal produced from (P_{ex} - P_{sh}) is used to find the quadrature component control signal while the bus voltage deviation from its set point is used to find the in-phase component signal (taking into consideration the shunt inverter limits).

Table 6.8 ξ values.

Q_{sh} \ p_{ex}	-0.25	-0.20	-0.15	-0.10	-0.05	0.0	0.05	0.10	0.15	0.20	0.25
-0.25	-0.25	-0.20	-0.15	-0.10	-0.05	0.0	0.05	0.10	0.15	0.20	0.25
-0.20	-0.25	-0.20	-0.15	-0.10	-0.05	0.0	0.05	0.10	0.15	0.20	0.25
-0.15	-0.25	-0.20	-0.15	-0.10	-0.05	0.0	0.05	0.10	0.15	0.20	0.25
-0.10	-0.25	-0.20	-0.15	-0.10	-0.05	0.0	0.05	0.10	0.15	0.20	0.25
-0.05	-0.25	-0.20	-0.15	-0.10	-0.05	0.0	0.05	0.10	0.15	0.20	0.25
0.0	-0.25	-0.20	-0.15	-0.10	-0.05	0.0	0.05	0.10	0.15	0.20	0.25
0.05	-0.25	-0.20	-0.15	-0.10	-0.05	0.0	0.05	0.10	0.15	0.20	0.25
0.10	-0.25	-0.20	-0.15	-0.10	-0.05	0.0	0.05	0.10	0.15	0.20	0.25
0.15	-0.25	-0.20	-0.15	-0.10	-0.05	0.0	0.05	0.10	0.15	0.20	0.25
0.20	-0.25	-0.20	-0.15	-0.10	-0.05	0.0	0.05	0.10	0.15	0.20	0.25
0.25	-0.25	-0.20	-0.15	-0.10	-0.05	0.0	0.05	0.10	0.15	0.20	0.25

Table 6.9 η values.

Q_{sh} \ p_{ex}	-0.25	-0.20	-0.15	-0.10	-0.05	0.0	0.05	0.10	0.15	0.20	0.25
-0.25	0.0	0.0	0.0	0.0	0.0	0.0	0.0	0.0	0.0	0.0	0.0
-0.20	0.0	0.0	0.0	0.20	0.20	0.20	0.20	0.20	0.0	0.0	0.0
-0.15	0.0	0.0	0.15	0.15	0.15	0.15	0.15	0.15	0.15	0.0	0.0
-0.10	0.0	0.10	0.10	0.10	0.10	0.10	0.10	0.10	0.10	0.10	0.0
-0.05	0.0	0.05	0.05	0.05	0.05	0.05	0.05	0.05	0.05	0.05	0.0
0.0	0.0	0.0	0.0	0.0	0.0	0.0	0.0	0.0	0.0	0.0	0.0
0.05	0.0	-0.05	-0.05	-0.05	-0.05	-0.05	-0.05	-0.05	-0.05	-0.05	0.0
0.10	0.0	-0.10	-0.10	-0.10	-0.10	-0.10	-0.10	-0.10	-0.10	-0.10	0.0
0.15	0.0	0.0	-0.15	-0.15	-0.15	-0.15	-0.15	-0.15	-0.15	0.0	0.0
0.20	0.0	0.0	0.0	-0.20	-0.20	-0.20	-0.20	0.20	0.0	0.0	0.0
0.25	0.0	0.0	0.0	0.0	0.0	0.0	0.0	0.0	0.0	0.0	0.0

Table 6.10 ξ linguistic.

Q_{sh} \ p_{ex}	NVB	NB	NM	NS	NVS	ZE	PVS	PS	PM	PB	PVB
NVB	NVB	NB	NM	NS	NVS	ZE	PVS	PS	PM	PB	PVB
NB	NVB	NB	NM	NS	NVS	ZE	PVS	PS	PM	PB	PVB
NM	NVB	NB	NM	NS	NVS	ZE	PVS	PS	PM	PB	PVB
NS	NVB	NB	NM	NS	NVS	ZE	PVS	PS	PM	PB	PVB
NVS	NVB	NB	NM	NS	NVS	ZE	PVS	PS	PM	PB	PVB
ZE	NVB	NB	NM	NS	NVS	ZE	PVS	PS	PM	PB	PVB
PVS	NVB	NB	NM	NS	NVS	ZE	PVS	PS	PM	PB	PVB
PS	NVB	NB	NM	NS	NVS	ZE	PVS	PS	PM	PB	PVB
PM	NVB	NB	NM	NS	NVS	ZE	PVS	PS	PM	PB	PVB
PB	NVB	NB	NM	NS	NVS	ZE	PVS	PS	PM	PB	PVB
PVB	NVB	NB	NM	NS	NVS	ZE	PVS	PS	PM	PB	PVB

Table 6.11 η linguistic.

Q_{sh} \ p_{ex}	NVB	NB	NM	NS	NVS	ZE	PVS	PS	PM	PB	PVB
NVB	ZE	ZE	ZE	ZE	ZE	ZE	ZE	ZE	ZE	ZE	ZE
NB	ZE	ZE	ZE	PB	PB	PB	PB	PB	ZE	ZE	ZE
NM	ZE	ZE	PM	PM	PM	PM	PM	PM	PM	ZE	ZE
NS	ZE	PS	PS	PS	PS	PS	PS	PS	PS	PS	ZE
NVS	ZE	PVS	PVS	PVS	PVS	PVS	PVS	PVS	PVS	PVS	ZE
ZE	ZE	ZE	ZE	ZE	ZE	ZE	ZE	ZE	ZE	ZE	ZE
PVS	ZE	NVS	NVS	NVS	NVS	NVS	NVS	NVS	NVS	NVS	ZE
PS	ZE	NS	NS	NS	NS	NS	NS	NS	NS	NS	ZE
PM	ZE	ZE	NM	NM	NM	NM	NM	NM	ZE	ZE	ZE
PB	ZE	ZE	ZE	NB	NB	NB	NB	NB	ZE	ZE	ZE
PVB	ZE	ZE	ZE	ZE	ZE	ZE	ZE	ZE	ZE	ZE	ZE

6.5.3 Simulation Study Using Fuzzy Based-Rules Controller

The system model shown in Figure 6.10 is used to test the fuzzy based-rules controller. The same cases studied for the conventional and Fuzzy-like-PI controllers are followed in this simulation test. The series inverter is controlled using the proposed FBRC while the shunt inverter is controlled using the classical Fuzzy-like-PI controller. The system response is shown in Figures 6.15-6.17. It is clear from the results that the proposed

fuzzy rules controller is capable of independently controlling the real and reactive power flow in the transmission system, in addition to supporting the bus voltage. Also, it is noticeable from the graphs that the FBRC is able to reduce the interaction between the active and reactive power flow, especially for the real power control loop. Improvement of the FBRC speed of response may be achieved if an adaptive technique is used to estimate the fuzzy rules.

A second test is performed where the operating points are located outside the feasible region but within the VA limits of the UPFC. The desired system operating points considered in this case are marked in Figure 6.18 where points 0, 1 and 3 are located inside the controlled region while points 2 and 4 are outside. Ideally, the system should follow the operating points, hence the sequence 0, 1, 2, 3, and 4. For the points outside the controlled region (2 or 4) the FBRC is designed to select an appropriate operating point on the circumference of the feasible operating area based on the real power priority criterion discussed earlier. As shown in Figure 6.19, the FBRC modifies the reactive power while keeping the real power at the desired level, at the same time, it maintains the bus voltage constant. Due to the nature of the Fuzzy-like-PI controller (lack of intelligence), it could not define a suitable operating point. As the controller output is limited by the maximum inserted voltage components, it can not produce the required real power flow as shown in Figure 6.19. Moreover, the Fuzzy-like-PI controller takes longer time to transfer from point 2 (outside) to point 3 which is located inside the controlled area.

To overcome the drawback of the classical fuzzy controller, a power flow optimiser is designed to define the best operating point. This optimiser works to provide real power priority. The system is simulated under the effect of the power flow optimiser and the results are shown in Figure 6.20.

It is obvious that the proposed fuzzy based-rules controller has the capability to define the best operating point of the UPFC under different system conditions and at the same time reduce the interaction between the real and reactive power flow.

In this chapter, a fuzzy based knowledge controller has been investigated. The controller rules are deduced from the relationship between the UPFC control variables and the power flow in the transmission system. The real power priority discussed in Section 4.6 has been used to define the best operating point for the system. From the simulation analysis, it is recognised that this controller requires large computation time, therefore, other control schemes are sought and will be proposed in the next chapter.

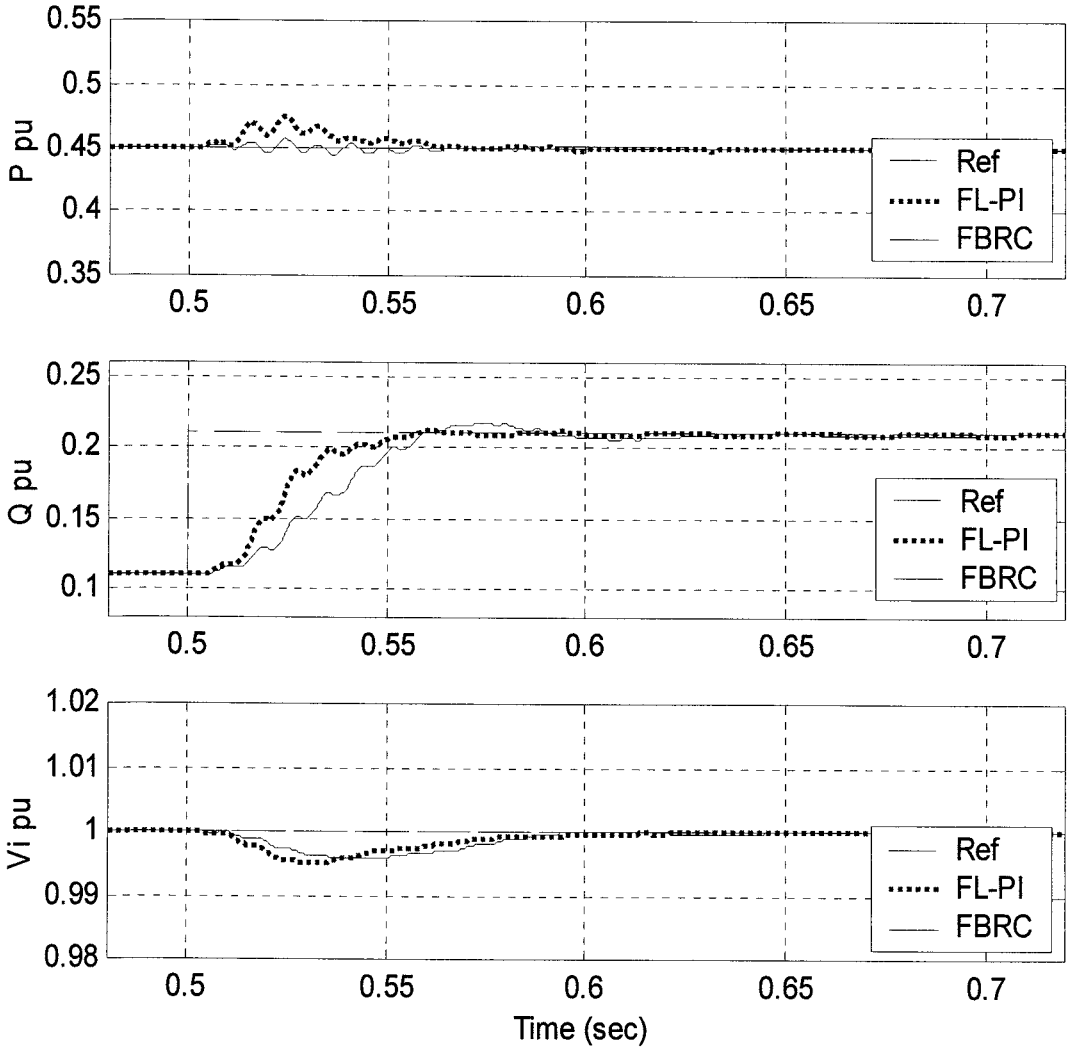

Figure 6.15 System response to a step change in reactive power.

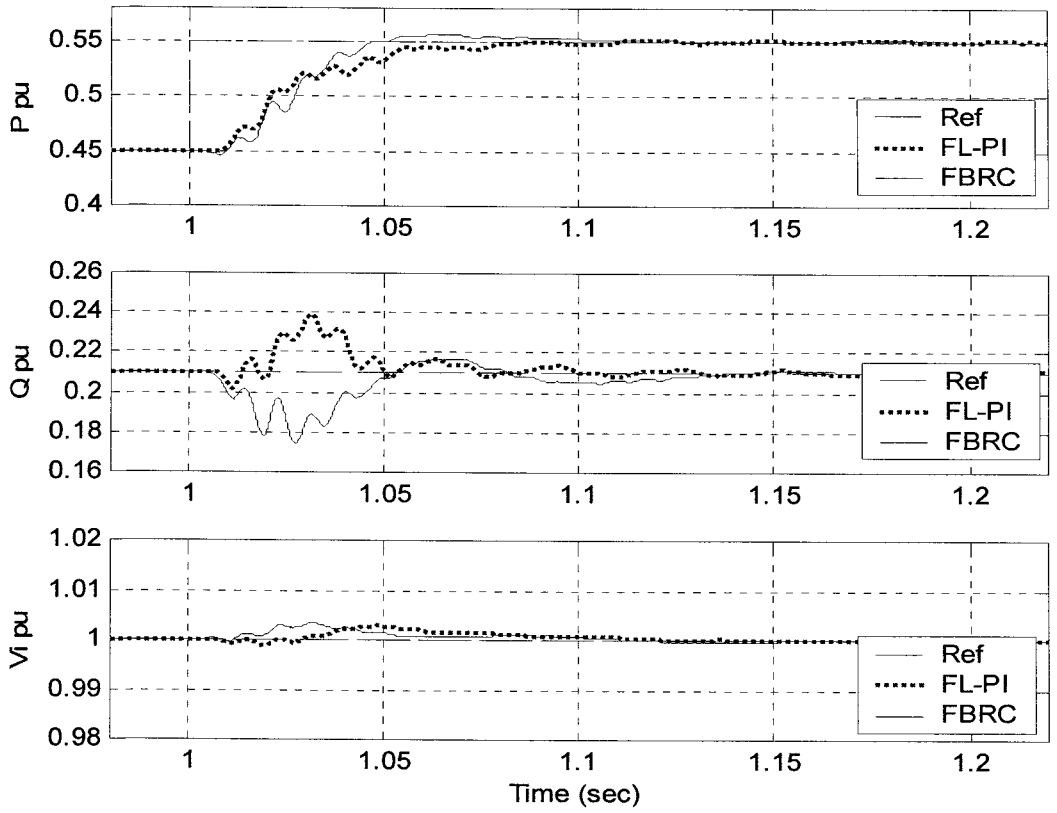

Figure 6.16 System response to a step change in active power.

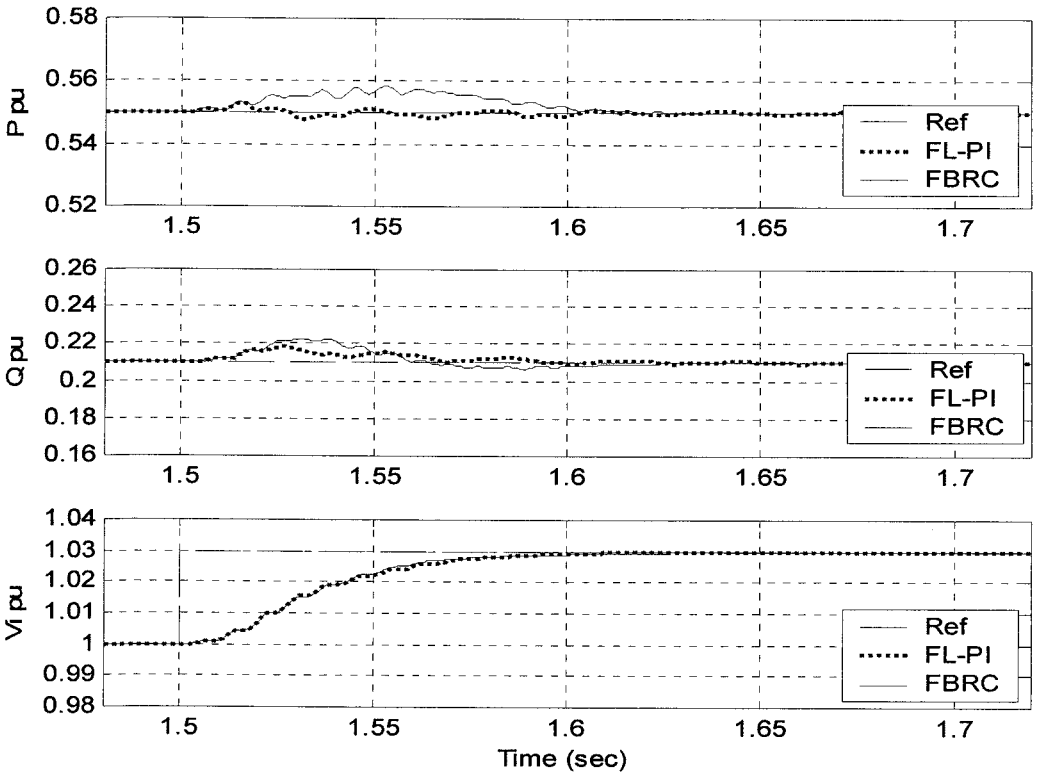

Figure 6.17 System response to a 3% step change in the bus voltage.

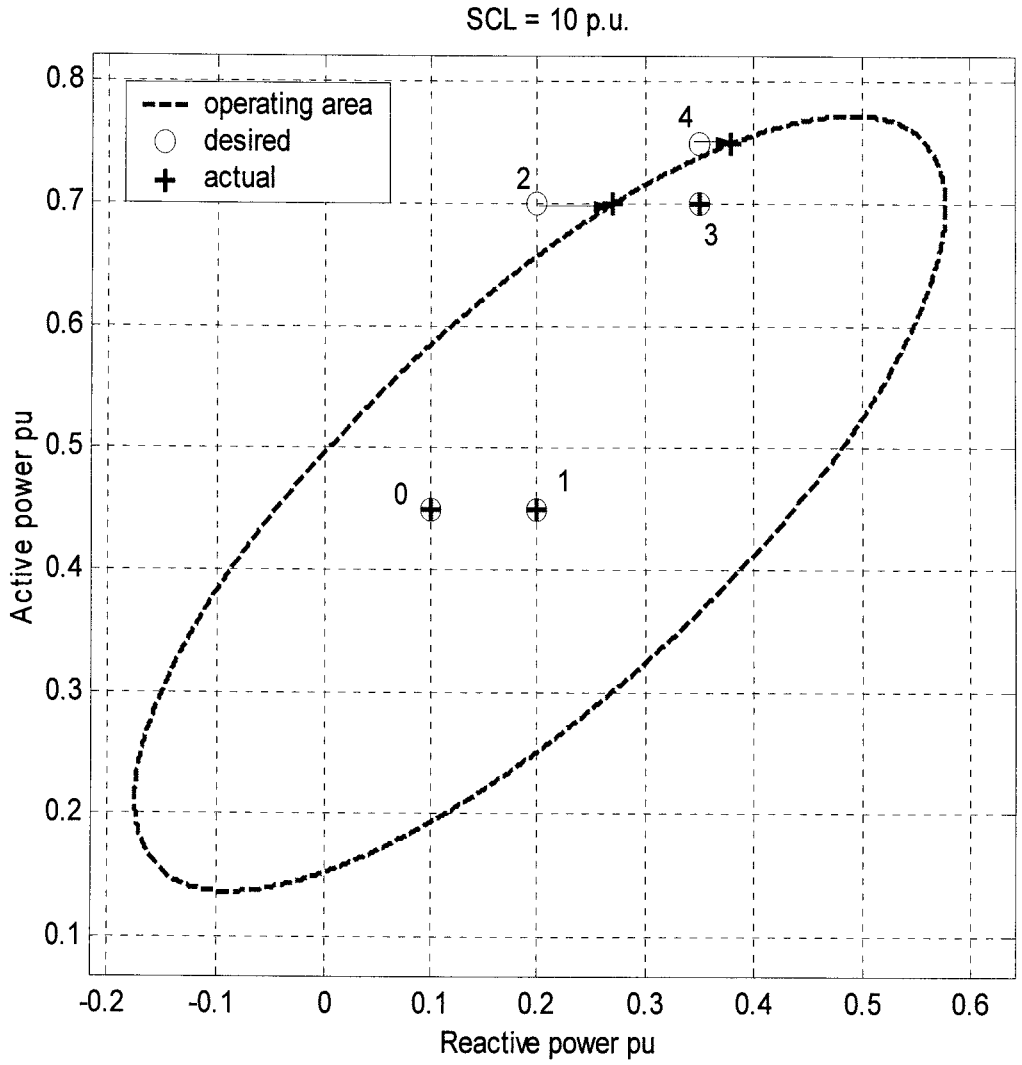

Figure 6.18 System desired set points and actual operating points.

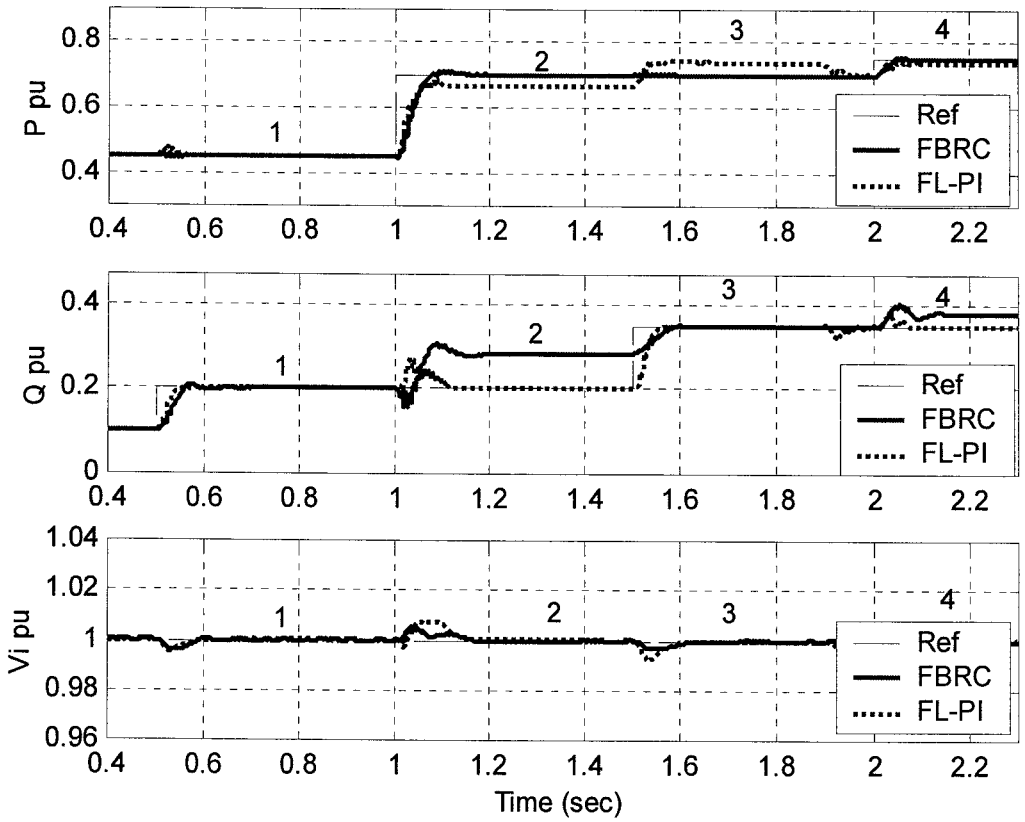

Figure 6.19 System response when the UPFC driven outside the operating area.

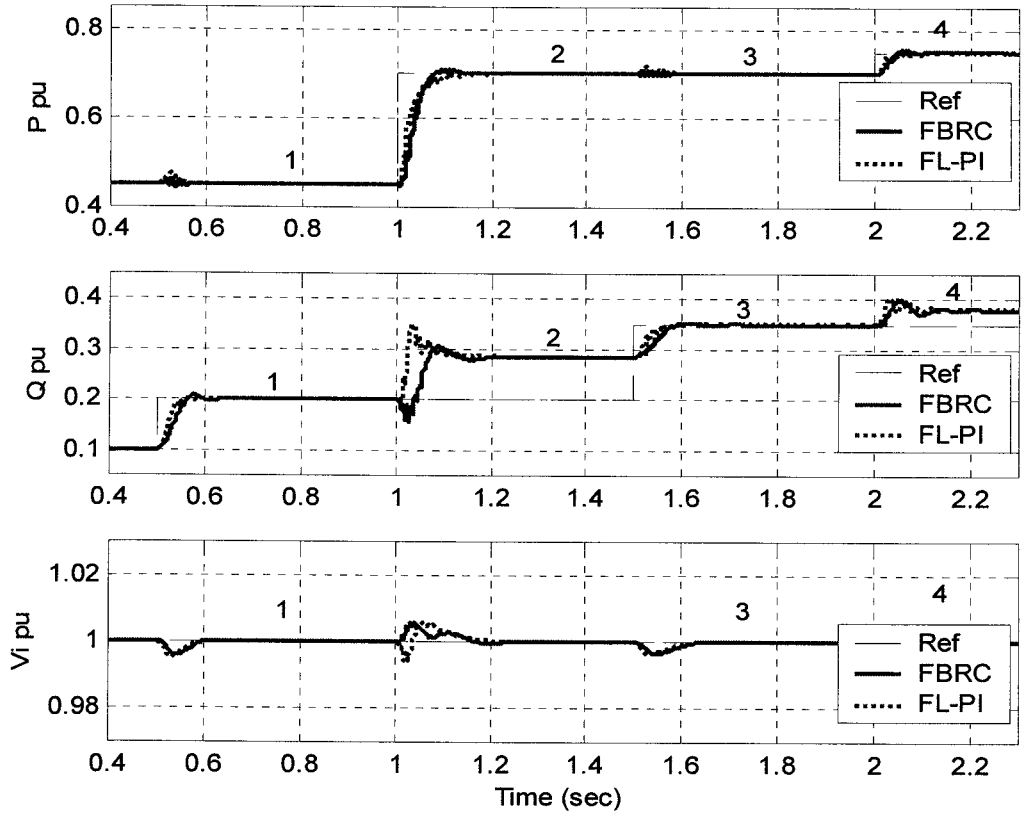

Figure 6.20 System response with power flow optimiser.

DESIGN OF LEARNING BASED CONTROL SYSTEM

7.1 INTRODUCTION

Artificial Neural Networks (ANNs) and their learning capabilities have been examined for many decades. They enjoyed a strong popularity in 1960's with the development of perceptrons. However, after the limitations of perceptrons became known, interest in neural networks research suffered a setback. But interest revived when more powerful learning algorithms were discovered in 1980's. Since then neural networks have formed a large active research area and have been used in many applications. The most prominent feature of the neural networks is their ability to learn from examples, using so called learning algorithms, they solve problems by processing a set of training data.

ANNs have shown to be useful in solving some power system control problems (e.g. non-linear, large scale, time variant parameters). It can solve algorithmic type problems and deals well with problems for which algorithms are not available but significant data is already at hand or can be obtained during operation [85,86]. There are many applications of ANNs in power systems including load forecasting, fault classification, voltage stability and harmonics detection [87-90]. ANNs are also used to enhance the power system stability through controlling the compensators installed in the system [91].

The use of ANNs in controlling the operation of FACTS devices is still in its early stage. ANN is used to memorise and emulate the damping control strategy of a well-tuned (over a set of desired operating conditions) PI controller proposed by Ma [92]. Therefore, the trained controller acts like a tuned PI controller and has the same control performance on the trained operating conditions with better-interpolated output for the untrained operating

conditions within the training range. This scheme has three drawbacks. Firstly, it requires intensive simulation analysis to tune the PI controller parameters for every operating point. Secondly, too many operating points need to be identified to obtain a good interpolation. Lastly, it may have poor performance for operating points located outside the trained space rather than between the trained points.

A Radial Basis Function Neural Network (RBFNN) has been proposed by Dash [93] to regulate the UPFC series inverter control variables. In this method, no training data a priori is required for generating the UPFC control signals. An extended Kalman filter has been used to adjust the network parameters, which is a time consuming process leading to restrictions in applying the algorithm in real time.

There are several constructions of neural networks, among them, the Multi-Layer Perceptron (MLP) trained by back propagation learning algorithm and the RBFNN are considered in the present study in order to train the UPFC control variables. Each network has a feedforward-supervised configuration. They exhibit a universal function approximator, as they can approximate any continuous function to a desired degree of accuracy. Therefore, the UPFC control variables can be trained to achieve the required system performance. Also, a simple RBFNN based on on-line training is investigated which is suitable for real-time implementation of the control system.

As discussed in Chapter 6, the fuzzy logic control theory is used to build a control expert system whose rules are deduced from the relationship between the UPFC control variables and the a.c. system parameters. The combination of neural networks and fuzzy controllers into neuro-fuzzy controllers helps to enhance the performance of the controller by using special learning algorithms. There are several approaches to neuro-fuzzy systems from which Adaptive Neuro-Fuzzy Inference System (ANFIS) is used in this work. In this technique, Takagi-Sugeno first order fuzzy system is used to generate the UPFC controller

output signal, in conjunction with a neural network which is used to tune the size of the membership functions in every fuzzy rule.

7.2 ARTIFICIAL NEURAL NETWORKS (ANNs) CLASSIFICATIONS

Neural networks have the potential of accurately describing the behaviour of an extremely complex system through their parallel-distributed structure and their ability to learn [94]. Neural networks may be classified according to their architecture, learning algorithm used to train the network or the applications.

7.2.1 ANNs Architecture-based Classification

In general, there are two different classes of neural network architectures.

Static neural network (non-recurrent)

The structure of this network is shown in Figure 7.1. It consists of one input layer, one or more hidden layers and an output layer. The input data is presented to the input layer and then are fed as weighted inputs to the first hidden layer, and subsequently the outputs from the first hidden layer are fed as weighted inputs to the second hidden layer. This process continues until the output layer is reached. This network is termed a *static network* as the input signals are fed directly from the network input to the network output with no feedback signal [95,96].

Dynamic neural network (recurrent)

The structure of this network is shown in Figure 7.2. It can be distinguished from the static network by that it has at least one feedback loop. Therefore, the current output of the network depends not only on the current input, but also on the previous outputs or states of the network. The presence of feedback loops has profound impact on the learning capability of the network and on its performance [97-99].

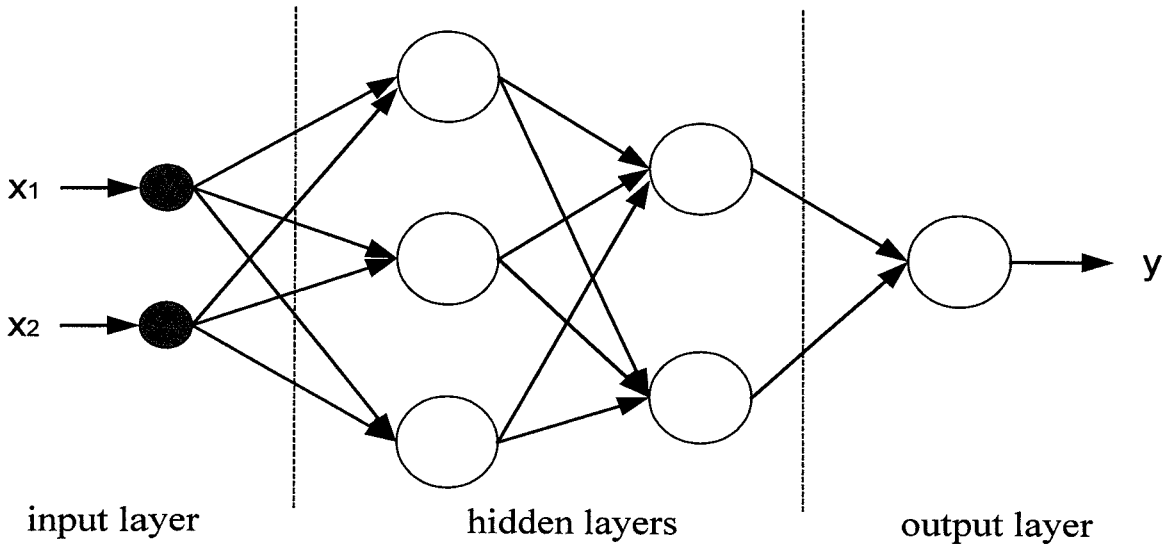

Figure 7.1 Static neural network.

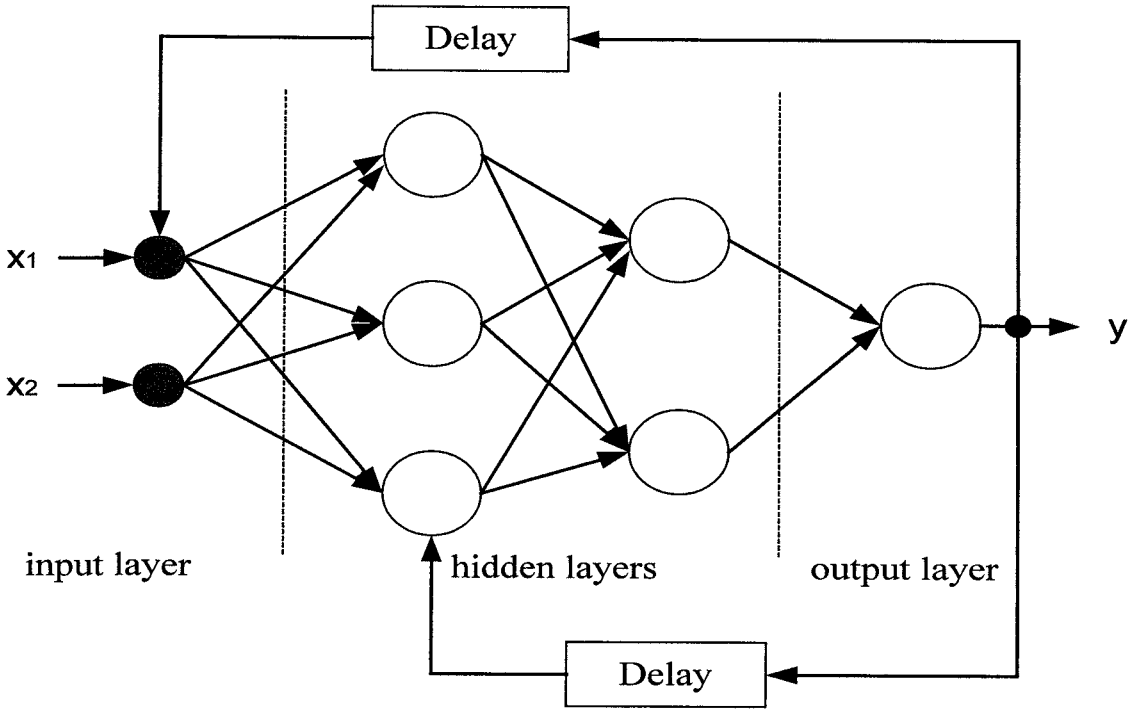

Figure 7.2 Dynamic neural network

7.2.2 ANNs Learning-based Classification

The second network classification is based on the learning strategy. There are three major learning algorithms for the neural network, supervised, unsupervised and reinforcement network.

Supervised learning network

In this network, a supervisor is assumed to be present during the learning process to teach the network the correct answer for each input pattern. A comparison can be made between the computed network output and the correct (desired) output to determine the error. The error can then be used through some form of computations and feedback to change the network parameters. This results in an improvement in the performance [100-103].

Unsupervised learning network

In this learning algorithm, the network has no information regarding the desired or correct output. Therefore, the system must learn by discovering and adapting to structured features in the input patterns. The most popular learning algorithms in this class are the competitive learning and Kohonen's self organising learning [104,105].

Reinforcement learning network

In this network, there is no supervisor to provide the exact answer. Instead, the network is only presented with an indication of whether the output answer it computes is right or wrong. The network must then use this information to improve its performance. Typically, the network is rewarded by reinforcing weights on units which give the right answer and punished by reducing the weights on units giving the wrong answer. Therefore, these networks are used to control physical systems. Neural controllers are applied to do the same tasks as the conventional controllers.

7.2.3 ANNs Application-based Classification

The third classification of neural network is based on the type of application. There are several applications of neural networks in every day life e.g.; Associative memory, Classification, Pattern recognition, Prediction, Optimisation and General mapping.

7.3 MLP NETWORK FOR THE UPFC

MLP network is the most widely used ANN. It has been used mainly for pattern recognition, control and classification. The structure of an ANN MLP trained by the back propagation algorithm for the UPFC series inverter is shown in Figure 7.3. The network has been presented with the system training data given in Tables 7.1 and 7.2. These tables are only extended version of Tables 6.2 and 6.3, the difference results from applying the real power priority discussed earlier. The input represents the changes in real and reactive power flow while the output represent the required level of the inserted voltage components β and γ.

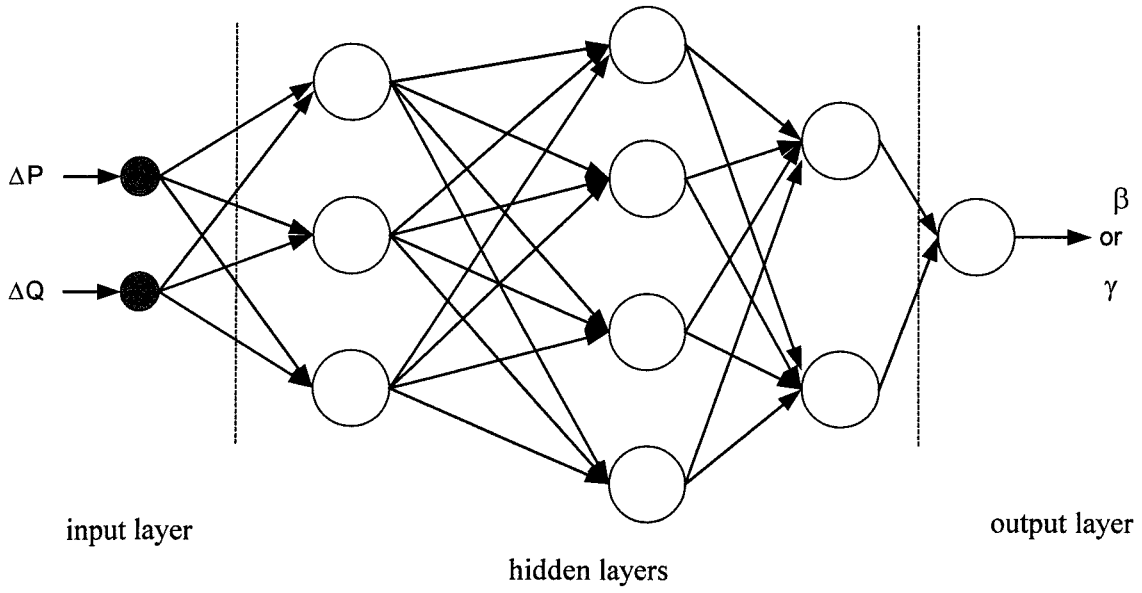

Figure 7.3 MLP neural network for the UPFC

Table 7.1 Extended β values.

ΔP \ ΔQ	-0.565	-0.452	-0.339	-0.226	-0.113	0.0	0.113	0.226	0.339	0.452	0.565
-0.351	-0.175	-0.175	*-0.175*	-0.175	*-0.175*	*-0.175*	*-0.175*	*-0.175*	*-0.175*	*-0.175*	-0.175
-0.280	-0.321	-0.321	-0.321	**-0.170**	**-0.048**	0.040	0.040	0.040	0.040	0.040	0.040
-0.210	-0.347	-0.347	-0.347	**-0.186**	**-0.047**	**0.052**	**0.134**	0.136	0.136	0.136	0.136
-0.140	-0.347	-0.347	-0.347	**-0.240**	**-0.061**	**0.049**	**0.137**	0.207	0.207	0.207	0.207
-0.070	-0.332	-0.332	-0.332	-0.332	**-0.097**	**0.034**	**0.131**	**0.212**	0.261	0.261	0.261
0.0	-0.303	-0.303	-0.303	-0.303	**-0.191**	**0.0**	**0.113**	**0.202**	**0.278**	**0.303**	0.303
0.070	-0.261	-0.261	-0.261	-0.261	-0.261	**-0.071**	**0.077**	**0.180**	**0.264**	**0.332**	0.332
0.140	-0.207	-0.207	-0.207	-0.207	-0.207	-0.207	**0.008**	**0.140**	**0.237**	**0.318**	0.347
0.210	-0.136	-0.136	-0.136	-0.136	-0.136	-0.136	-0.136	**0.069**	**0.192**	**0.286**	0.347
0.280	-0.040	-0.040	-0.040	-0.040	-0.040	-0.040	-0.040	-0.040	**0.115**	**0.235**	**0.321**
0.351	0.175	0.175	0.175	0.175	0.175	0.175	0.175	0.175	0.175	0.175	0.175

Table 7.2 Extended γ values.

ΔP \ ΔQ	-0.565	-0.452	-0.339	-0.226	-0.113	0.0	0.113	0.226	0.339	0.452	0.565
-0.351	-0.304	-0.304	*-0.30*	-0.304	*-0.304*	*-0.304*	*-0.304*	*-0.304*	*-0.304*	*-0.304*	*-0.304*
-0.280	-0.138	-0.138	-0.138	**-0.225**	**-0.296**	-0.347	-0.347	-0.347	-0.347	-0.347	-0.347
-0.210	-0.042	-0.042	-0.042	**-0.135**	**-0.215**	**-0.273**	**-0.320**	-0.322	-0.322	-0.322	-0.322
-0.140	0.038	0.038	0.038	**-0.023**	**-0.126**	**-0.190**	**-0.241**	**-0.281**	**-0.281**	-0.281	-0.281
-0.070	0.110	0.110	0.110	0.110	**-0.024**	**-0.101**	**-0.157**	**-0.203**	**-0.232**	**-0.232**	-0.232
0.0	0.175	0.175	0.175	0.175	**0.110**	**0.0**	**-0.065**	**-0.117**	**-0.160**	**-0.175**	-0.175
0.070	0.232	0.232	0.232	0.232	0.232	**0.122**	**0.036**	**-0.023**	**-0.071**	**-0.110**	-0.110
0.140	0.281	0.281	0.281	0.281	0.281	0.281	**0.157**	**0.081**	**0.024**	**-0.021**	-0.038
0.210	0.322	0.322	0.322	0.322	0.322	0.322	0.322	**0.203**	**0.131**	**0.077**	0.042
0.280	0.347	0.347	0.347	0.347	0.347	0.347	0.347	0.347	**0.257**	**0.188**	**0.138**
0.351	0.304	0.304	0.304	0.304	0.304	0.304	0.304	0.304	0.304	0.304	0.304

The parameters of this network, like any other neural network have two major steps to be considered, the construction of the network and the learning mechanism. The architecture of the network includes determining the following parameters:

- *The number of hidden layers.*
- *The number of neurons in each layer.*
- *The activation function of each layer.*

The learning mechanism includes the adaptation technique by which the weights of every connection are adjusted to achieve the desired performance.

For MLP in the UPFC application, the number of hidden layers and the number of neurons in each layer are adjusted by measuring the Mean Square Error (MSE) of the network output in order to achieve the minimum acceptable network size. The training procedure starts with a small number of hidden layers and neurons in each layer. The MSE is calculated for each training step of the input pattern. If the goal error is met, the training stops. Otherwise, the number of neurons is increased until a maximum pre-set number is reached. If the error goal is not achieved the number of hidden layers is increased. The error is checked again, the process continues until the goal error is obtained and the network structure is saved. The flow-chart for training the MLP is shown in Figure 7.4. The activation function of each hidden layer is chosen to be the most common sigmoidal function while the linear function is used for the output layer. The two functions are shown in Figure 7.5.

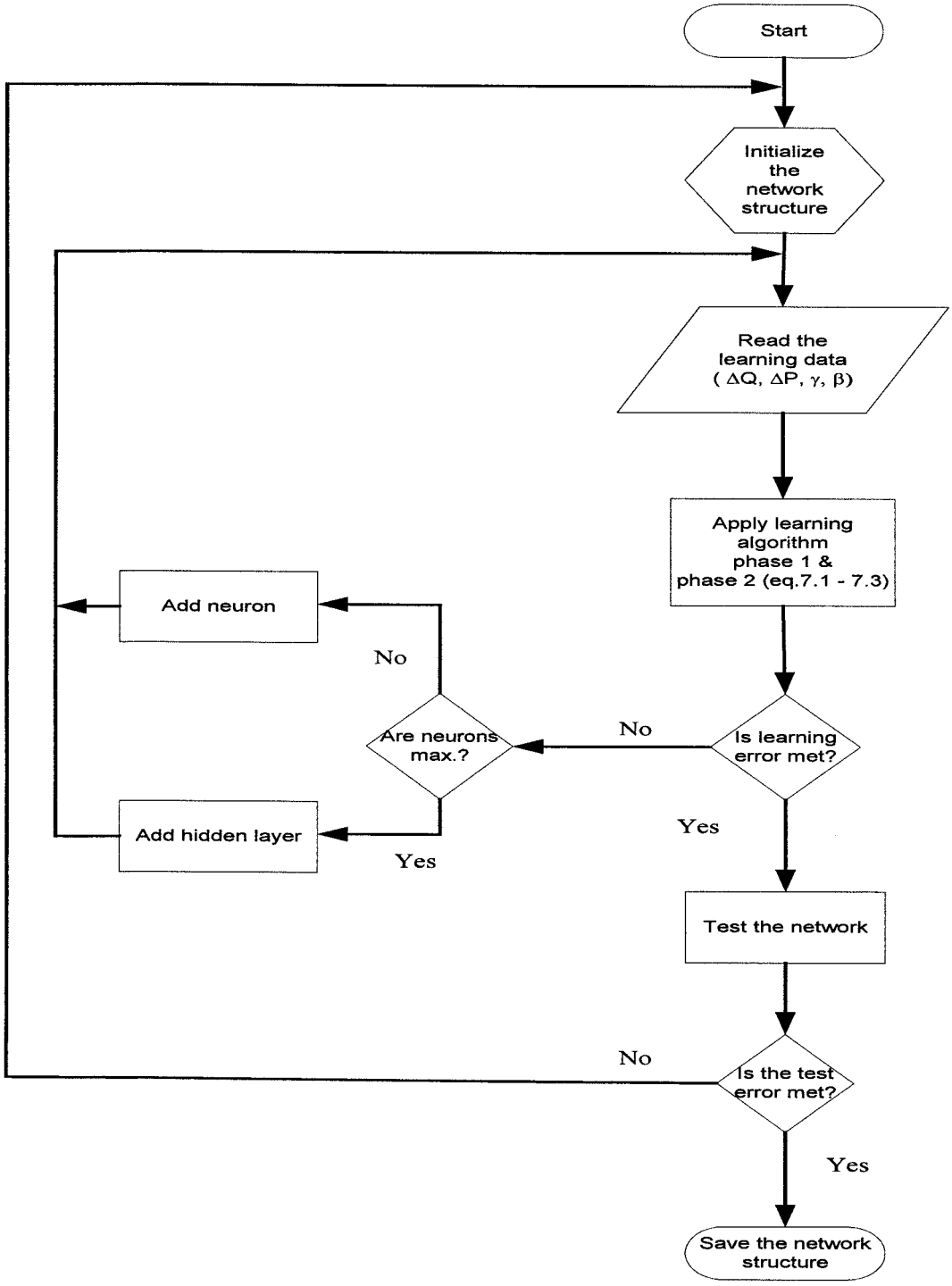

Figure 7.4 MLP learning flow chart.

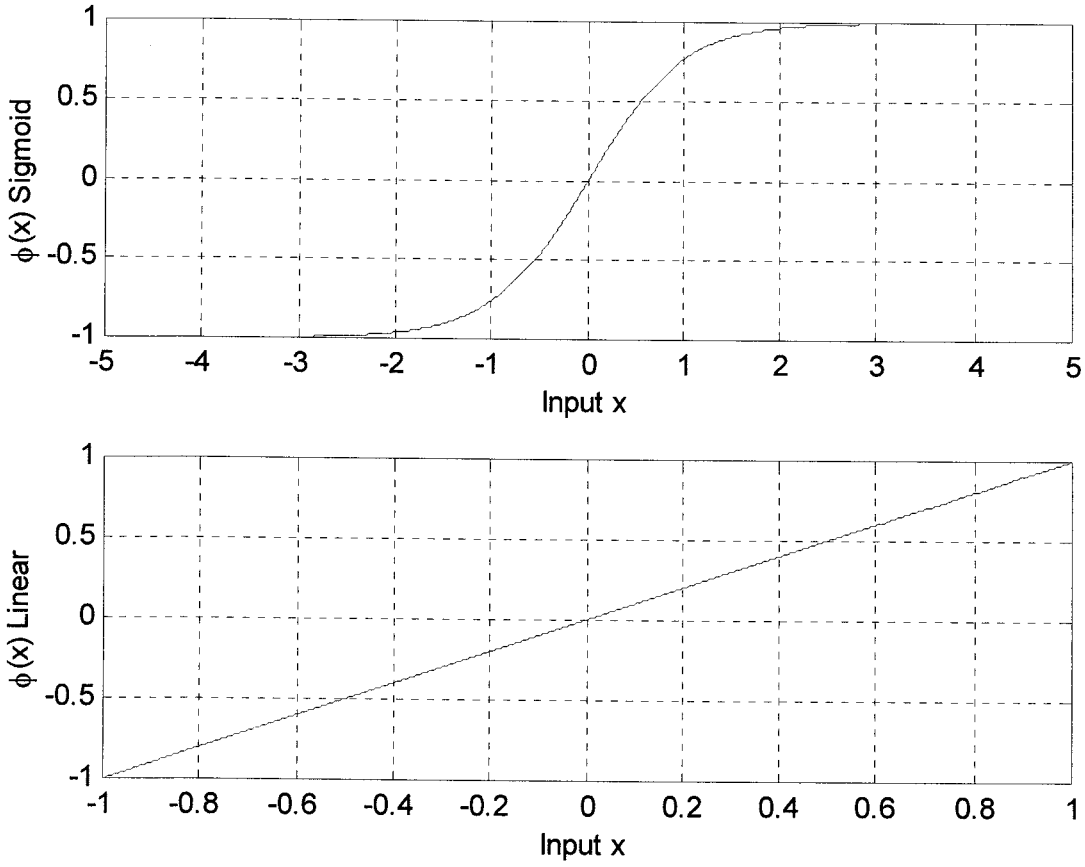

Figure 7.5 Sigmoidal and linear activation functions.

7.3.1 Backpropagation Learning Algorithm

The back propagation learning algorithm implements a gradient descent procedure. The goal of the learning procedure is to minimise the sum of squared differences between the actual output and the target by adjusting the weights of the connections [106,107]. The sum of squared error of the UPFC series inverter control variables (β and γ) are given as:

$$E_{\beta} = \sum_{\forall i} \left(\beta_{d_i} - \beta_{o_i}\right)^2$$
$$E_{\gamma} = \sum_{\forall i} \left(\gamma_{d_i} - \gamma_{o_i}\right)^2 \qquad (7.1)$$

where $\beta_{d_i}, \gamma_{d_i}$ are the desired inserted voltage components, $\beta_{o_i}, \gamma_{o_i}$ are the network outputs. The change of the network weights may be expressed as;

$$\Delta W = -\lambda \frac{\partial E_{\beta,\gamma}}{\partial W} \tag{7.2}$$

where W is the weight on the connection between neurons and λ is the learning rate. Using the chain rule, the derivative in Equation (7.2) can be written as;

$$\left.\begin{aligned} \frac{\partial E_\beta}{\partial W} &= \frac{\partial E_\beta}{\partial \beta}\frac{\partial \beta}{\partial h_{o_\beta}}\frac{\partial h_{o_\beta}}{\partial W} \\ \frac{\partial E_\gamma}{\partial W} &= \frac{\partial E_\gamma}{\partial \gamma}\frac{\partial \gamma}{\partial h_{o_\gamma}}\frac{\partial h_{o_\gamma}}{\partial W} \end{aligned}\right\} \tag{7.3}$$

The first term in Equation (7.3) reflects the change in the error depending on the change of the network output. The second term represents the change of the network output based on the change of the previous hidden layer. The chain can be extended to include all the hidden layers.

The application of the back propagation algorithm is organised in two phases:

Phase 1

The input is presented to the network and propagated forward through the network to determine the output of each layer till the final network layer.

Phase 2

The error signal in the network output is determined by comparing the network output with the target value. The weights of the connections between the last hidden layer and the output are changed to minimise this error. Then the process of backward error propagation starts. The error of the network output (modified) is back propagated to the preceding hidden layer and the weights are changed accordingly to reduce the error. The error propagation continues until there are no hidden layer left.

Table 7.3 summarises the MLPBP network architecture for the UPFC parameters β and γ. The quadrature-phase component data set is more consistent than the in-phase data

set, where γ-trained error is always less than the β-trained error for the same network structure. This is because the parameter γ has a high correlation with one of the inputs, which is the change in real power. However, the parameter β has almost the same correlation with both network inputs. The trained error is reduced as a result of increasing the network complexity with larger number of hidden layers and more neurons in each layer. It is clear from the table that the training time significantly increases with the size of data set and the architecture.

Table 7.3 MLPBP network parameters

Network parameters		β	γ
Training data set		961	961
Test data set		441	441
Hidden layers / Neurons			
4 (10 10 5 5)	Training time (sec)	2064	2078
	Training error	8.30e-7	9.38e-8
	Test error	5.19e-5	2.23e-5
3 (5 5 5)	Training time (sec)	358	352
	Training error	5.81e-5	2.08e-5
	Test error	7.30e-4	4.31e-5
2 (10 5)	Training time (sec)	430	416
	Training error	7.47e-5	2.39e-5
	Test error	9.47e-5	3.24e-5
2 (5 2)	Training time (sec)	99	98
	Training error	5.22e-4	1.78e-4
	Test error	4.74e-4	1.86e-4

7.4 Radial Basis Function Neural Network

The design of a supervised neural network may be pursued in a variety of ways. The back propagation algorithm for the design of the MLP described in the previous section has some drawbacks which makes the training process more tedious and time consuming. In this section, a different approach is used by viewing the design of a neural network as an approximation problem in a multi-dimensional space. In this approach, the learning process is equivalent to defining a surface in a hyper space that provides a best fit to the training data set and well interpolate the test data. This is the motivation behind the method of the Radial Basis Function Neural Network (RBFNN).

The structure of the RBFNN involves three layers with entirely different rules as shown in Figure 7.6. The input layer connects the network to its environment. The second layer, the only hidden layer in the network, applies a non-linear transformation from the input space to the hidden space. The output layer is linear, providing the response of the network to the active input. The network output is described as:

$$a_2 = B_2 + W * \phi(x, \mu, B_1) \tag{7.4}$$

where B_2 is the bias, W is weight, μ is the centre and B_1 is the spread.

Each neuron in the radial basis layer calculates the Euclidean distance between the centre vector (μ) and the network input vector (X); the result is passed through a non-linear function. Different schemes of non-linear activation functions are shown in Figure 7.7, among them the Gaussian function is used in this study. This function is normalised, radially symmetrical around its centre and can approximate well any power integrable function.

The output of the radial basis layer is determined according to how close is the input vector to each neuron centre. Thus, a radial basis network with centres quite different from

the input vector will have an output near zero. In contrast, a radial basis neuron with a centre close to the input vector will produce a value near one. The output of the hidden layer is then scaled and biased through W and B_2, respectively to produce the network output.

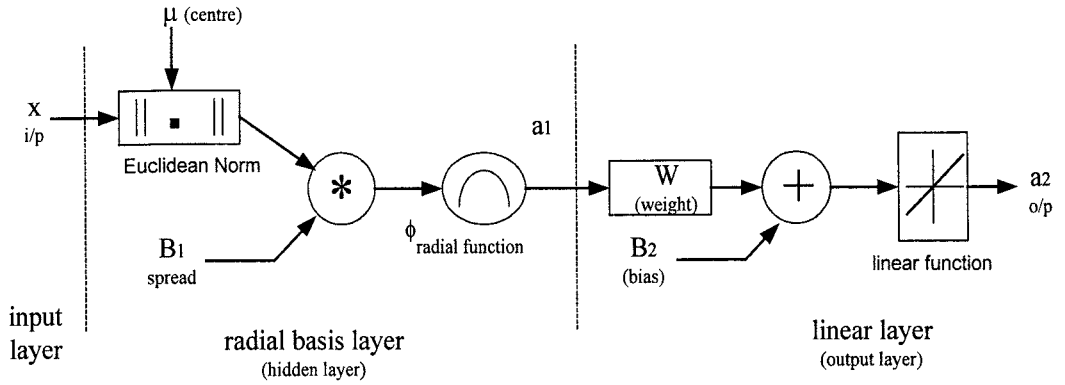

Figure 7.6 The radial basis function neural network (RBFNN) structure.

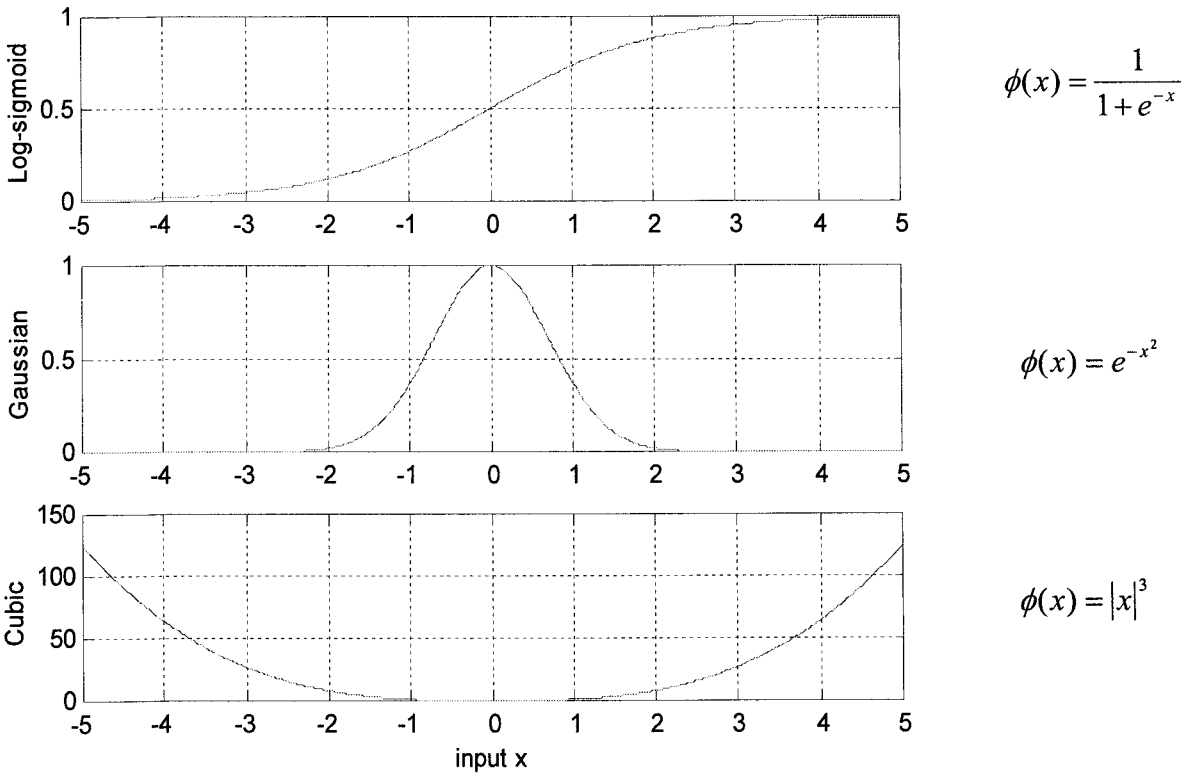

Figure 7.7 RBFNN activation nonlinear functions.

7.4.1 Learning Strategies

The RBFNN has the following parameters which need to be tuned during the learning process:

The hidden layer parameters

- The centres (weights) of each neuron.
- The spread (bias).

The output layer parameters

- The weights of the radial basis layer output (W).
- The biases of the linear layer (B_2).

The important point is that the different layers of an RBFNN perform different tasks, and so it is reasonable to separate the optimisation of the hidden and output layers of the network by using different learning techniques. There are two learning paradigms for any neural network. The first is the *batch learning* (off-line learning) where the training data is available from analysis or previous operation. The update action of the network parameters take place only after the whole training data set has been presented. The second paradigm is the *pattern learning* (on-line learning) where the network parameters are updated after each new input pattern has been presented.

For the RBFNN batch learning, there are two learning schemes depending on how the centres of the neurons are specified:

Fixed centres:

The centres of the neurons in the hidden layer may be chosen randomly from the data set which cover the input space with a fixed spread. The Gaussian activation function in this case is expressed as;

$$\phi(x) = \exp\left(-\frac{m}{d_{\max}}\|x-\mu_i\|^2\right) \qquad i = 1,2.....m \tag{7.5}$$

where m is the number of centres and $d_{\max}$ is the maximum distance between the chosen centres. The spread σ is then fixed and expressed as;

$$\sigma = \frac{d_{\max}}{\sqrt{m}} \tag{7.6}$$

The only parameters that would need to be learned in this approach are the weights and biases of the network linear layer. A straightforward procedure for doing this is to make sure the network output is identical to the target value.

Self-organised selections of centres:

The main problem with the method of fixed centres, described above, is that it may require a large training data set for a satisfactory level of performance and also for determining the best centres locations. One way to overcome this limitation is to use a hybrid learning process, consisting of two different stages [108].

Self-organised learning stage: The purpose of this stage is to estimate appropriate locations for the centres of the radial basis functions in the hidden layer. This is achieved by partitioning the given data set into sub-groups, each of which should be homogenous. The centre point of each sub-group is then assigned as centre for the corresponding neuron [109].

Supervised learning stage: This completes the design of the network by estimating the weights and biases of the output layer. A simple method of this estimation is the Least Mean Squares (LMS).

For the RBFNN pattern learning, the network free parameters are updated as a result of minimising a certain cost function $(\Im)$, e.g. the error function given below;

$$\Im = \frac{1}{2}\sum_{j=1}^{N} e_j^2 \tag{7.7}$$

where N is the size of the training sample and

$$e_j = T_j - a_{2_j} \tag{7.8}$$

is the error signal defined as the difference between the system target and the network output for pattern j.

7.4.2 Design of RBFNN for the UPFC

The network structure described in Figure 7.6 (static and supervised) is used as a basis for obtaining the UPFC control variables. Batch learning strategy with modified fixed centres is introduced to train the network. Training data similar to the data given in Tables 7.1 and 7.2 are used in the form of vectors notation. The data presented to the network input layer comprises two main vectors representing the possible change in reactive power and possible change in active power. The target of the network output is represented by the desired inserted voltage components β and γ. Therefore, two neural networks are trained in a similar way.

The algorithm implemented is shown in Figure 7.8, where the network iteratively creates one neuron at a time. The input pair (ΔQ_j , ΔP_j) which result in reducing the network error, is used to create a neuron. Neurons are added to the network until the mean squared error falls within an error goal margin or the maximum number of neurons has been reached (which is determined by the size of the input data set).

The centres (weights) of the radial basis layer are assigned to be the transpose of the input vector which results in a small error.

$$\mu_j = \begin{bmatrix} \Delta Q_j & \Delta P_j \end{bmatrix}^T \tag{7.9}$$

The spread (σ) determines the width of an area in the input space to which the neuron responds. σ is chosen to be fixed in this training algorithm in order to reduce the number of tuning parameters and the network complexity. The Gaussian radial basis function is chosen as the activation function in this algorithm as it exhibits good approximation to any continuos function [110]. The biases are set to be

$$B_1 = 0.8326 / \sigma \tag{7.10}$$

Therefore, the Gaussian function output crosses 0.5 at weighted inputs of $\pm\sigma$ which reflect the closeness between the input data and the centres. The output of the radial layer for each network is described as:

$$a_{1_\beta} = \phi_\beta(B_1 * \mu) \tag{7.11}$$

$$a_{1_\gamma} = \phi_\gamma(B_1 * \mu) \tag{7.12}$$

The weights (W) and biases (B_2) of the output linear layer are determined in such a way to minimise the sum-squared error ($\sum_{\forall j}\left(T_{\beta,\gamma} - a_2\right)^2$) between the target values of β or γ and the network output. The following equation is solved every time to define these parameters;

$$\begin{bmatrix} W & B_2 \end{bmatrix} * a_1 = T \tag{7.13}$$

where a_1 is the output of the radial basis layer and T is the target.

A summary of RBFNN design parameters for the UPFC application is given in Table 7.4. It is obvious that the training time for the RBFNN is much less than the MLPBP for the same data set. The RBFNN produces a good approximation of the given test data and the Mean Squared Error (MSE) of the training data is close to the MSE of the test data. In order to get a small-trained error as the one obtained with the complex MLPBP network described earlier, there is a need to increase the size of the training data set. This may increase the complexity of the network, which means more neurons to be added in the hidden layer.

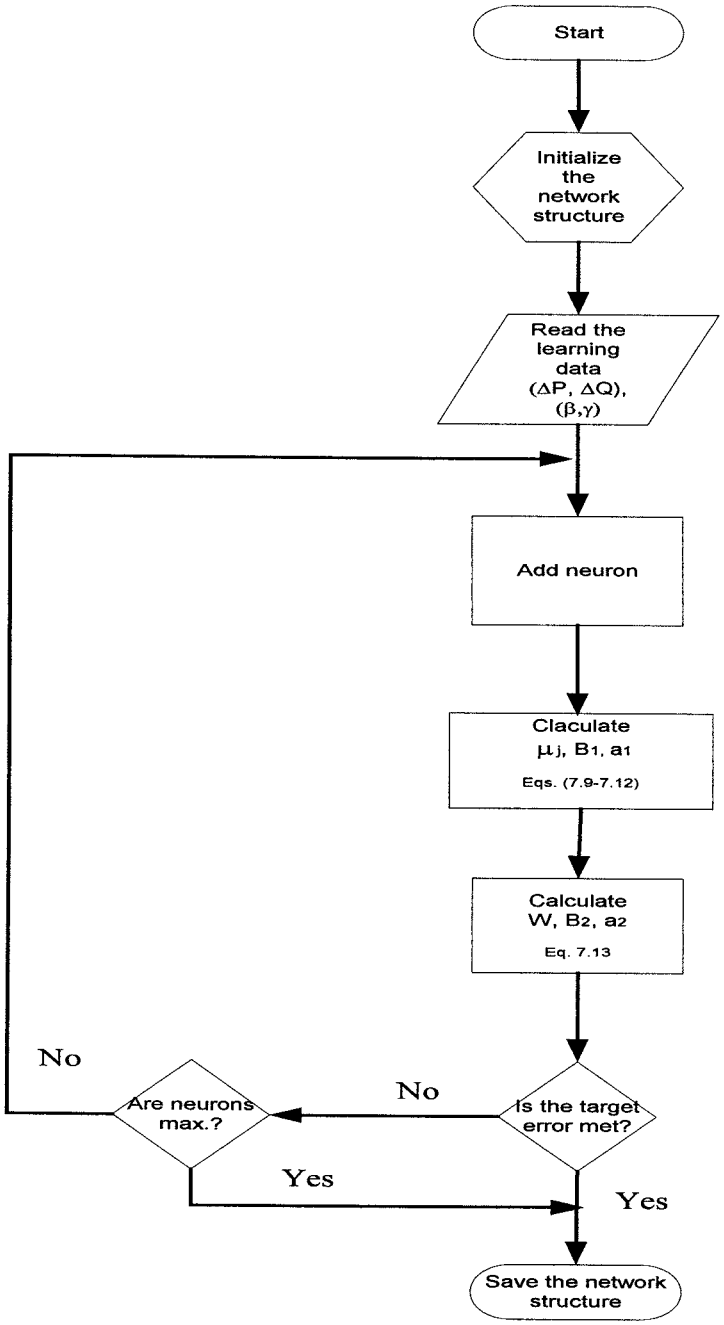

Figure 7.8 RBFNN learning algorithm flow chart.

Table 7.4 RBFNN parameters

Network parameters	β	γ
Training data set	961	961
Test data set	441	441
Training time (sec)	6.12	5.50
Training error	2.2140e-4	2.4456e-4
Test error	2.2138e-4	2.4454e-4

7.4.3 Comparison Between MLPBP and RBFNN

From the above analysis, the advantages and drawbacks of the MLPBP and the RBFNN are summarised in Table 7.5.

Table 7.5 Comparison between MLPBP and RBFNN

	MLPBP	***RBFNN***
Advantages	• It has a straightforward structure, which lead to its wide use. • It has a long training time. • It has a good approximation capability.	• It has a very simple structure where only one hidden layer exist. • It has a short training time. • It has a good approximation capability.

Drawbacks	• Possibility of being trapped at local minima of the error function. • It suffers from slow convergence as the error signal is back propagated from the network output to the input passing through the hidden layers. • Adaptation of the network structure is time consuming and problem based. • It experiences difficulties with the non-differentiable activation functions.	• It often requires too many neurons in the hidden layer to give satisfactory performance. • It is sensitive to neurons spread, as the performance is very poor with peaked or flatted neurons. • It requires a large memory which makes it unsuitable for on-line control.

7.5 SIMULATION STUDY USING MLPBP AND RBFNN

The system described in Figure 6.10 is used to further analyse the MLPBP and RBFNN learning algorithms adopted to control the UPFC free parameters. The series inverter parameters are controlled by the neural network based controller obtained in the previous sections while the shunt inverter parameters are regulated using a conventional PI controller.

The response to a step change in the power reference signal is used to test the controller performance. Figure 7.9 shows the system response to a step change in the real power while the reactive power is kept unchanged. Figure 7.10 shows the system response to a step change in the reactive power. These results show that the real power control loop gives almost identical results using either (Backpropagation) BP-controller or (Radial Basis) RB-controller. However, the BP-controller gives more robust response than the RB-controller for the reactive power flow control loop. This is because the MSE of the BP

training data (for the reactive power loop) is smaller than the corresponding RB error. Although, the RB-controller has faster response (as the error signal is not propagated backward in order to tune the network parameters), it suffers from large steady-state error which is due to poor quality training of the RBFNN.

In general, these results agree with the information given in Table 7.4. The RBFNN requires extra training data set to reduce the trained error which increases the network complexity and allocated dynamic memory of the host computer. Hence other way of updating the RBFNN parameters is suggested, as described in section 7.6.

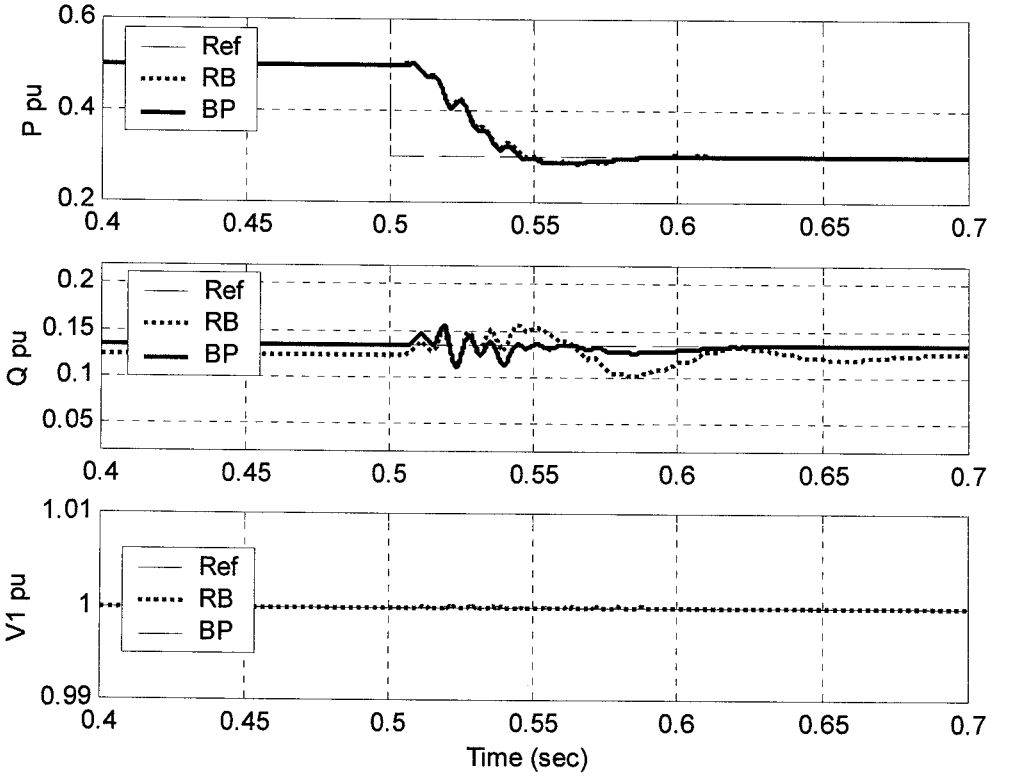

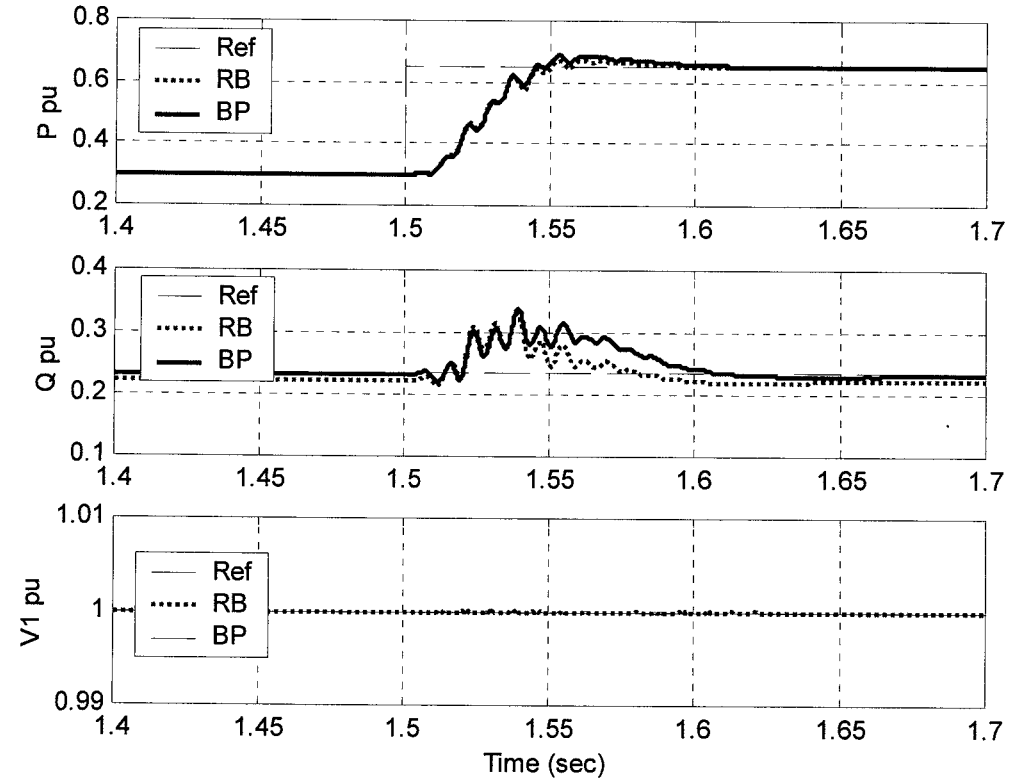

Figure 7.9 System response to a step change in real power.

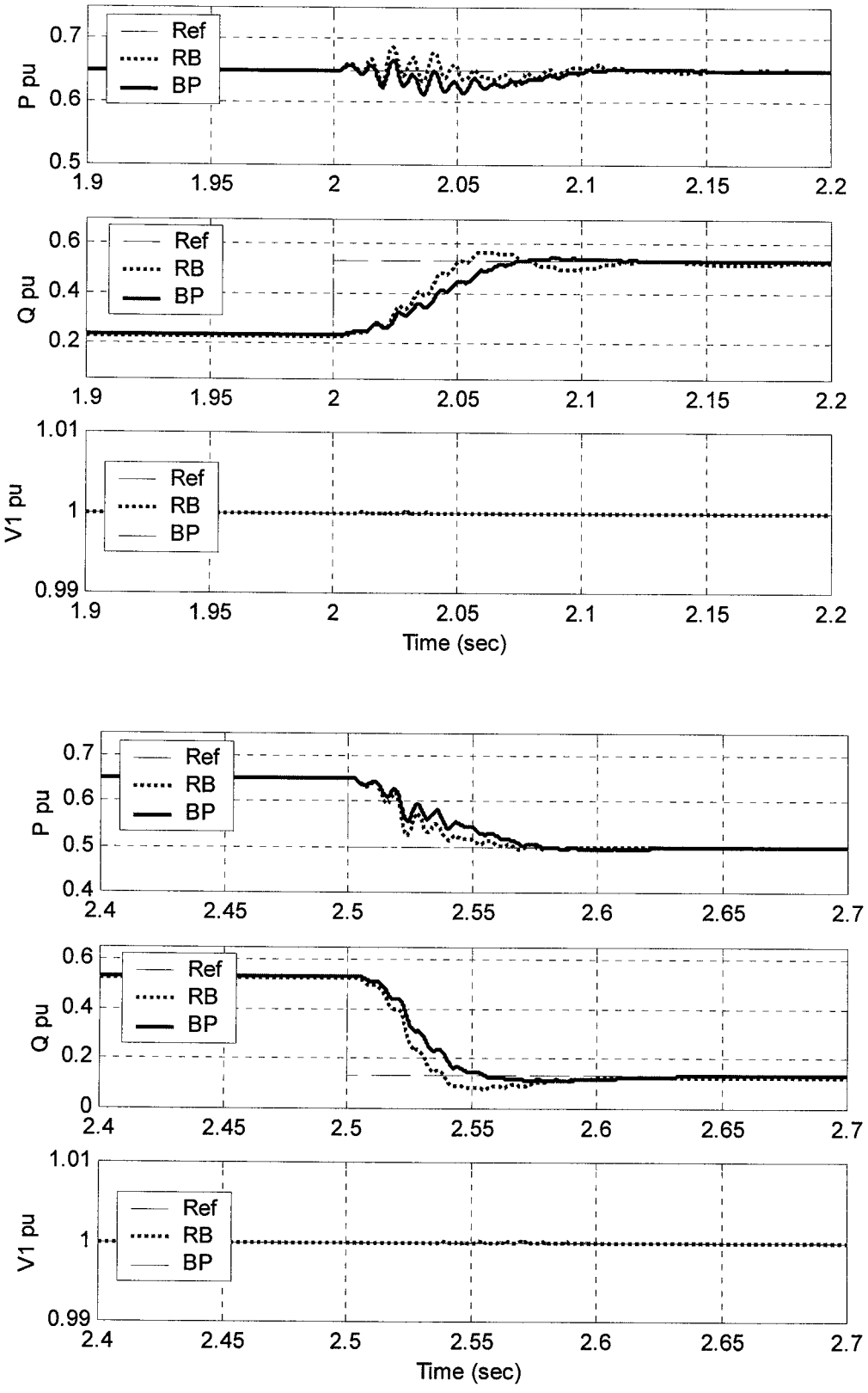

Figure 7.10 System response to a step change in reactive power.

7.6 RBFNN TRAINED BY GRADIENT DESCENT

As described in the previous section, the performance of the RBFNN depends on the number and centres of the radial basis functions in the hidden layer, their spread and the method used for learning the input-output mapping. In this section, a simple RBFNN is designed using only one neuron to control the UPFC parameters. This simple network is easy to implement in a real time control system where it needs less computation, as will be shown in the next chapter. Also, there is no need for prior training of the system data since the network parameters are readjusted at every sample step. The gradient descent learning algorithm is used to train the network parameters (W, B_2, μ and σ) by producing the incremental changes of these parameters. The error generated from the system controlled variables is used to update the network parameters. Therefore, there is no need for training data to generate the inserted voltage components of both the series and shunt inverters.

The network shown in Figure 7.11 describes the designed RBFNN controller. The network output is given as:

$$y = B_2 + W\phi(x, \mu, \sigma) \tag{7.14}$$

A Gaussian activation function, $\phi(x)$ is used in the hidden layer and is described as:

$$\phi(x, \mu, \sigma) = e^{-\left(\left|\frac{x-\mu}{\sigma}\right|^2\right)} \tag{7.15}$$

For the UPFC application, four RBFNN are essentially required to determine the system control variables, previously defined as:

γ and β are the quadrature and in-phase components of the series inserted voltage.

ξ and η are the quadrature and in-phase components of the shunt inverter output voltage.

Therefore, the network output set can be expressed as:

$$a_2 = [\gamma \quad \beta \quad \xi \quad \eta] \tag{7.16}$$

Each network input is the error signal used to derive the corresponding control variable. Referring to Equation 7.16, the network input set can be expressed as:

$$x = [\Delta P \quad \Delta Q \quad \Delta P_{tr} \quad \Delta V] \tag{7.17}$$

where,

$$\Delta P = P_{ref} - P,$$
$$\Delta Q = Q_{ref} - Q,$$
$$\Delta P_{tr} = P_{ex} - P_{sh}, and$$
$$\Delta V = V_{ref} - V.$$

In this algorithm each RBFNN is trained by minimising the error

$$E = \hat{y} - y \tag{7.18}$$

where, $\hat{y}$ is the power system output.

Substituting for y from Equation 7.14 into Equation 7.18 yields:

$$E = \hat{y} - \left(B_2 + W\phi(x, \mu, \sigma)\right) \tag{7.19}$$

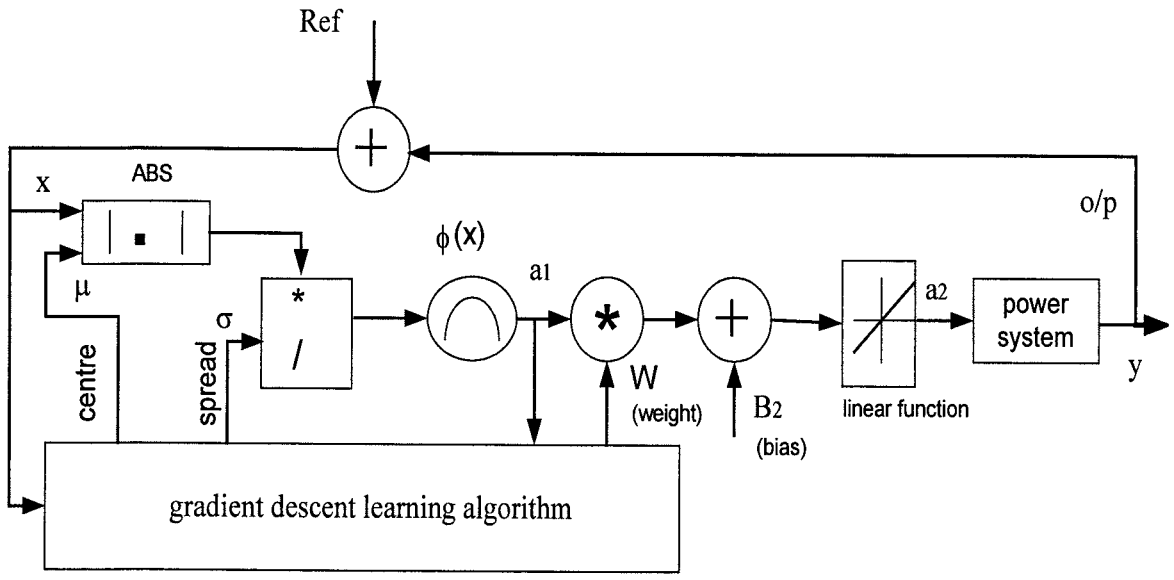

Figure 7.11 RBFNN trained by the gradient descent.

The gradient of E with respect to the neural network parameters is given as:

$$\left.\begin{aligned} \frac{\partial E^2}{\partial W} &= 2E\frac{\partial E}{\partial W} \\ \frac{\partial E^2}{\partial \mu} &= 2E\frac{\partial E}{\partial \mu} \\ \frac{\partial E^2}{\partial \sigma} &= 2E\frac{\partial E}{\partial \sigma} \end{aligned}\right\} \tag{7.20}$$

Note that the bias of the linear layer is assumed to be fixed in order to reduce the number of neural network parameters to be updated.

7.6.1 Updating the Network Weight (W)

The change of the error with respect to the network weight is given as:

$$\frac{\partial E}{\partial W} = -\phi(x,\mu,\sigma) \tag{7.21}$$

The increment in the weight can be described as:

$$\frac{\partial E^2}{\partial W} = \Delta W = -2E\phi(x,\mu,\sigma) \tag{7.22}$$

$$\Delta W = \lambda_W E\phi(x,\mu,\sigma) \tag{7.23}$$

where λ_W is the learning rate of the network weight.

The updated weight value is then given as;

$$W_k = \lambda_W E\phi_k(x,\mu,\sigma) + W_{k-1} \tag{7.24}$$

where k represents the current time step and (k-1) represents the previous time step.

7.6.2 Updating the Network Centre (μ)

The change of the error with respect to the neuron centre is described as:

$$\frac{\partial E}{\partial \mu} = -W\frac{\partial \phi(x,\mu,\sigma)}{\partial \mu} \tag{7.25}$$

$$\frac{\partial E}{\partial \mu} = -W\frac{2(x-\mu)}{\sigma^2}\phi(x,\mu,\sigma) \tag{7.26}$$

The increment in the centre may be given as:

$$\frac{\partial E^2}{\partial \mu} = \Delta\mu = -4WE\frac{(x-\mu)}{\sigma^2}\phi(x,\mu,\sigma) \tag{7.27}$$

$$\Delta\mu = \lambda_\mu WE\frac{(x-\mu)}{\sigma^2}\phi(x,\mu,\sigma) \tag{7.28}$$

Where λ_μ is the learning rate of the network centre.

The updated centre value is then given as;

$$\mu_k = \lambda_\mu WE\frac{(x-\mu)}{\sigma^2}\phi(x,\mu,\sigma) + \mu_{k-1} \tag{7.29}$$

7.6.3 Updating the Network Spread (σ)

The change of the error with respect to the neuron spread may be given as:

$$\frac{\partial E}{\partial \sigma} = -W\frac{\partial\phi(x,\mu,\sigma)}{\partial\sigma} \tag{7.30}$$

$$\frac{\partial E}{\partial \sigma} = -W\frac{2(x-\mu)^2}{\sigma^3}\phi(x,\mu,\sigma) \tag{7.31}$$

The increment in the spread can be described as:

$$\frac{\partial E^2}{\partial \sigma} = \Delta\sigma = -4WE\frac{(x-\mu)^2}{\sigma^3}\phi(x,\mu,\sigma) \tag{7.32}$$

$$\Delta\sigma = \lambda_\sigma WE\frac{(x-\mu)^2}{\sigma^3}\phi(x,\mu,\sigma) \tag{7.33}$$

Where λ_σ is the learning rate of the network spread.

The updated spread value is then given as;

$$\sigma_k = \lambda_\sigma WE\frac{(x-\mu)^2}{\sigma^3}\phi(x,\mu,\sigma) + \sigma_{k-1} \tag{7.34}$$

7.6.4 Adaptive Learning Rate

The learning rate coefficient (λ) in the gradient descent learning algorithm determines the size of the weight adjustments made at each iteration and hence influences the rate of convergence. The value of λ is important since large variations in the learning rate can result with different choice of λ. If the chosen value of λ is too large, the network response may oscillate about the steady-state value and converge more slowly. It may even diverge. On the other hand, if the chosen value of λ is too small, the descent will progress in very small steps and significantly increase the total time to convergence. The best choice of λ is a problem dependent and may require some trail and error before a good choice is found.

For best results, the learning rate value should not be kept constant throughout the learning process. In this study, a simple adaptive mechanism for choosing the best learning rate is introduced. This is accomplished by continuously monitoring the error during the training process and adjusting the value of each λ_i ($i = w, \mu, \sigma$) to best fit the local region of descent. An exponential function, shown in Figure 7.12, is used to describe the change of the learning rate with respect to the error. The function works as follows; for the network parameters which decreases the error, the learning rate is increased since the current value is too conservative for the local minima. Conversely, when the error is too big, the learning rate is reduced to avoid overshooting of the system response by a fast decay of the past parameter history.

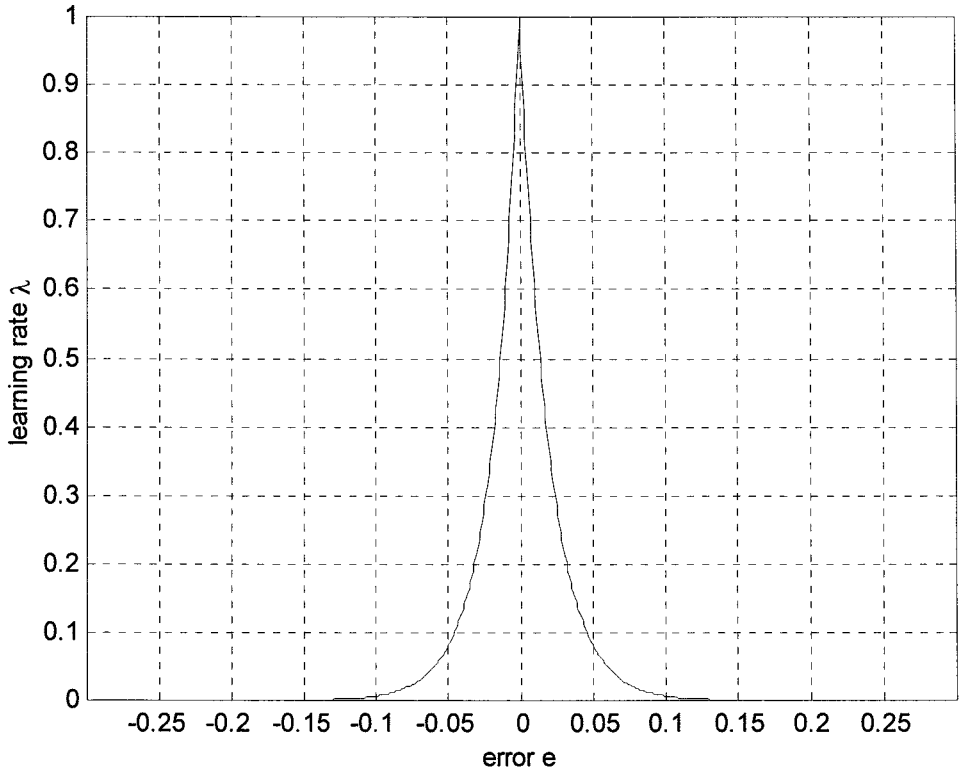

Figure 7.12 Adaptive learning rate exponential function

7.7 HYBRID NEURO-FUZZY CONTROL SYSTEM

As discussed in Chapter 6, the fuzzy logic can encode expert knowledge directly using rules with linguistic labels. It usually takes a considerable time to design and tune the membership functions which quantitatively define these linguistic labels. The concept of fuzzy logic can be incorporated into the neural network to substantially reduce the development time while improving performance. The resulting hybrid system is called Fuzzy-Neural or Neuro-Fuzzy. A neural network is used in this combination to tune the membership functions of the fuzzy system.

An Adaptive Neuro-Fuzzy Inference System (ANFIS) was introduced by Shing [111]. It combines the fuzzy qualitative approach with the adaptive capabilities of the neural network. A control system based on this can be trained without significant expert knowledge as compared with the standard fuzzy logic system. In this study, an Adaptive Neuro-Fuzzy Inference Controller (ANFIC) is designed for the UPFC. The training data is generated from the relationship between the change in the real and reactive power required in the system and the corresponding components of the series inserted voltage (similar to the data set used for training the neural networks described in the previous sections).

7.7.1 Principles of ANFIS

Fuzzy logic controllers play an important role in numerous practical applications. However, there are no standard methods for transforming human knowledge into the rule-base of the fuzzy inference system. Hence, the selection of the size, type and parameters of the input and output membership functions has often been achieved via trial and error. There is a real need for effective methods of tuning the membership functions and reducing the rule base to include only the minimum essential rules. ANFIS was proposed to alleviate these difficulties. Since it combines the fuzzy qualitative approach with the adaptive learning

capabilities of the neural network, it can be trained without a great amount of expert knowledge usually required for the design of the standard fuzzy logic system [112]. As a result, the membership functions are tuned and the rule-base can be optimised.

A typical architecture of ANFIS based on the first-order Takagi-Sugeno model is shown in Figure 7.13, where two-inputs (x, y) and one-output (f) fuzzy system is assumed. The architecture is explained as follows:

Rule ij: *if* x *is* A_i *and* y *is* B_j *then* $f_{ij} = g_{ij}x + h_{ij}y + r_{ij}$

where, A_i and B_j represent the linguistic variables of related membership function (MF),

$i = 1,2,.....,N$ is the index number for the MF of the first input,

$j = 1,2,.....,M$ is the index number for the MF of the second input and

g_{ij}, h_{ij} and r_{ij} are the parameters of the output membership functions to be determined during the training stage.

The system shown in Figure 7.13 consists of five layers, which emulate the design steps of the fuzzy control system. Each layer has either fixed nodes (that have no parameters to be tuned) represented by a circle or adaptive nodes (that have parameters to be tuned during training) represented by a square (see Figure 7.13-a).

Layer1

Every node in this layer is adaptive with an output $O_{1i} = \mu_{A_i}(x)$ or $O_{1j} = \mu_{B_j}(y)$ which represents the degree of membership of the input to the fuzzy membership function A_i or B_j. For example, if a triangular MF is used,

$$\mu_{A_i}(x) = \begin{cases} 1-(c_i - x)/a_i & for\ c_i - a_i \le x \le c_i \\ 1-(x - c_i)/b_i & for\ c_i \le x \le c_i + b_i \\ 0 & otherwise \end{cases}$$

$$\mu_{B_j}(y) = \begin{cases} 1-(c_j - x)/a_j & for\ c_j - a_j \le x \le c_j \\ 1-(x - c_j)/b_j & for\ c_j \le x \le c_j + b_j \\ 0 & otherwise \end{cases} \qquad (7.35)$$

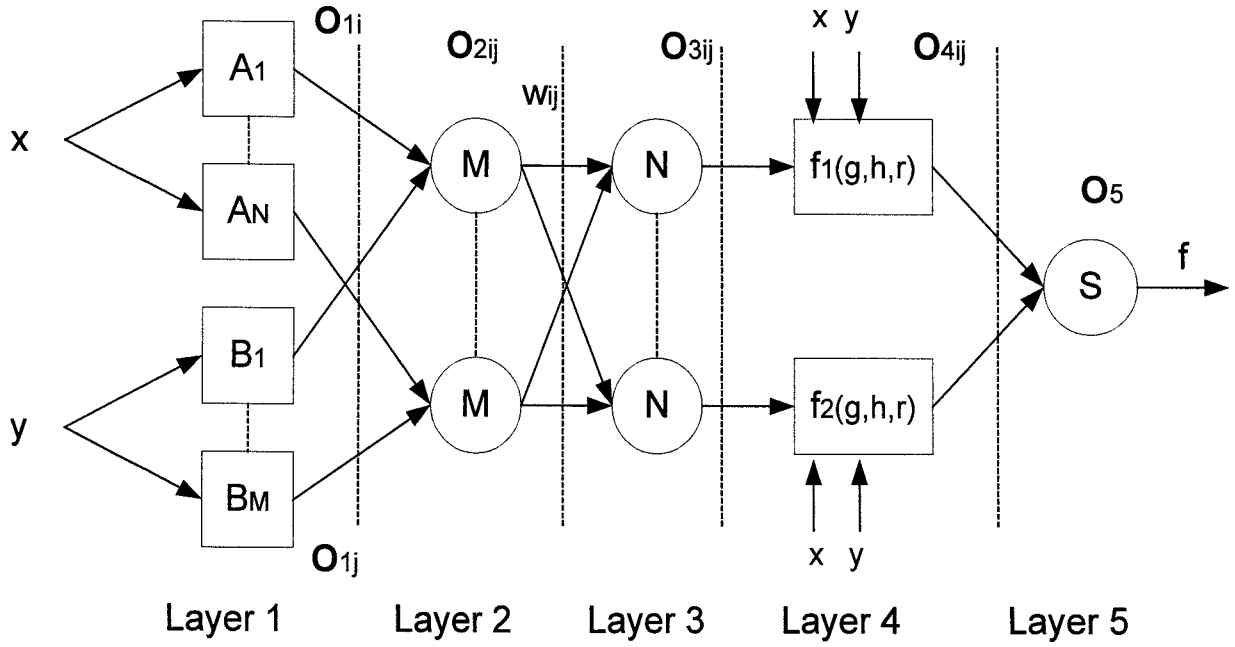

(a) ANFIS structure.

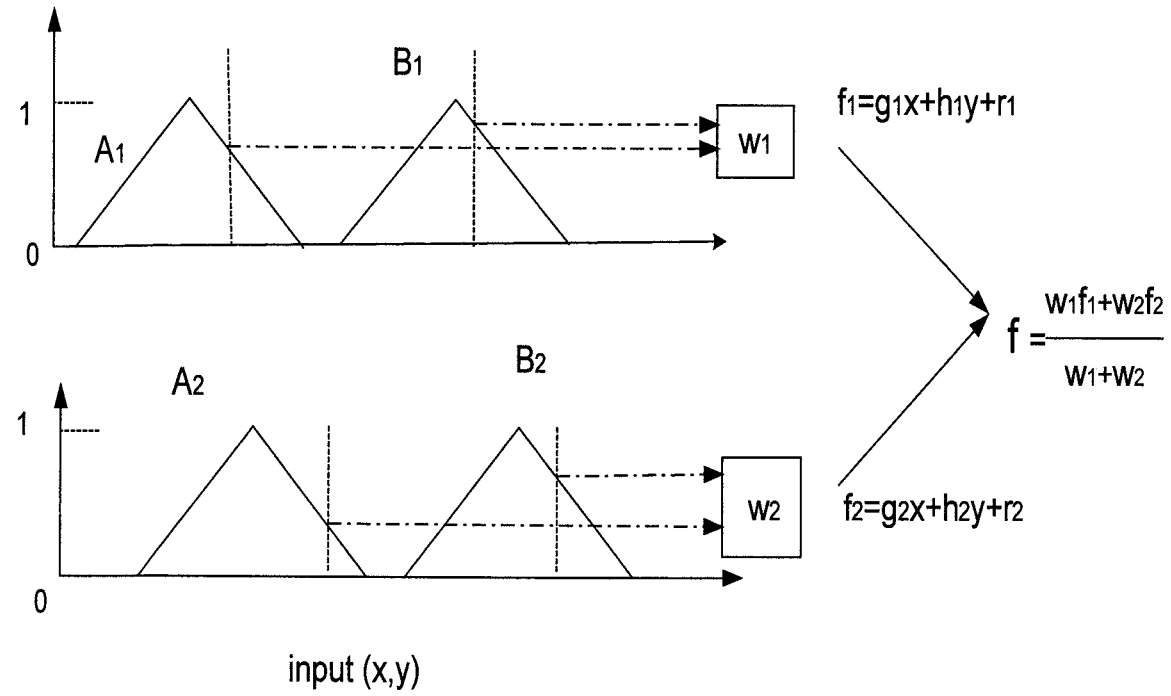

(b) Takagi-Sugeno fuzzy inference.

Figure 7.13 ANFIS model and corresponding Takagi-Sugeno fuzzy system.

where, $\{a_i, b_i, c_i\}$ and $\{a_j, b_j, c_j\}$ are the parameter sets for the premise MFs to be adjusted during the training phase.

Layer2

Nodes in this layer are fixed. They are labelled (M) to indicate that they multiply the incoming signals. The outputs of these nodes are given by:

$$O_{2ij} = w_{ij} = \mu_{A_i}(x)\mu_{B_j}(y) \quad , \quad i = 1,2,\ldots N, \quad j = 1,2,\ldots M \tag{7.36}$$

These outputs represent the firing strength of the rules.

Layer3

Nodes in this layer are also fixed. They are labelled (N) to indicate that they perform a normalisation operation on the firing strength from the previous layer. The output of each node in this layer is given by:

$$O_{3ij} = \overline{w}_{ij} = \frac{w_{ij}}{\sum_{\forall i,j} w_{ij}} \tag{7.37}$$

Layer 4

All nodes in this layer are adaptive. The output of each node in this layer is simply the product of the normalised firing strength and a first order polynomial (corresponding to the first order Takagi-Sugeno model)

$$O_{4ij} = \overline{w}_{ij} f_{ij} = \overline{w}_{ij}\left(g_{ij}x + h_{ij}y + r_{ij}\right) \quad , i = 1,2,\ldots N, \quad j = 1,2,\ldots M \tag{7.38}$$

where, $\{g_{ij}, h_{ij}, r_{ij}\}$ is the consequent parameter set.

Layer5

This layer has only one node labelled S to indicate that it performs the function of an adder. The output of this node is given by:

$$O_5 = f = \sum_{\forall i,j} \overline{w}_{ij} f_{ij} = \sum_{\forall i,j} \frac{w_{ij} f_{ij}}{\sum_{\forall i,j} w_{ij}} = \frac{\sum_{\forall i,j} w_{ij} f_{ij}}{\sum_{\forall i,j} w_{ij}} \tag{7.39}$$

In this ANFIS architecture, there are two adaptive layers (layers 1 and 4). Each node in layer 1 has three adjustable parameters $\{a,b,c\}$ representing the antecedent MF. A node in layer 4 also has three tuneable parameters $\{g_{ij},h_{ij},r_{ij}\}$ pertaining to the first order polynomial of the consequent part of the rules.

The objective of the learning algorithm is to adjust all these parameters to make the ANFIS output best match the training data. The gradient descent approach (described in section 7.6) can be applied to identify the network parameters based on minimising the sum of squared errors between the training data and what the output node produces, as given below:

$$\frac{\partial E}{\partial O_5} = -2(T - O_5) \tag{7.40}$$

where, T is the target value specified in the training data set, O_5 is the output at the final stage of the network.

The gradient descent method is generally slow and likely to become trapped in local minima. A hybrid learning strategy is used which involves the gradient method to update the antecedent parameters $\{a,b,c\}$ and Least Squares Estimate (LSE) to identify the consequent parameters $\{g_{ij},h_{ij},r_{ij}\}$ refer to [111] for more details. More specifically, the hybrid learning strategy has a forward pass in which the signals go forward up to layer 4 and the consequent parameters are identified by the LSE while the premise parameters are fixed. Then, in the backward pass the error rate defined by Equation 7.40 is propagated backward and the premise parameters are updated by the gradient descent while the consequent parameters are fixed. The cycle is repeated until convergence within a specified error.

7.7.2 Adaptive Neuro-Fuzzy Inference Control (ANFIC) for the UPFC

The ANFIC is based on the first order Takagi – Sugeno model and allows only a single output. As discussed earlier, the series part of the UPFC system has two control variables β and γ to control the real and reactive power flow in the transmission system. This requires the design of two independent neuro-fuzzy control systems, one for each control variable. These two control systems have the same inputs and the same structure.

Training data generation

The generated training data shown in Table 7.1 and Table 7.2 for β and γ, respectively with maximum inserted voltage $\Delta V_{\max} = 0.35 pu$ are organised in a vector notation to suit the training procedure. These data includes the operating points inside the system feasible region and also taking into consideration the real power priority concept for the operating points located outside the feasible region.

ANFIC training

During the training stage, the range of each input variable is initially partitioned into eleven training MFs. Therefore, for two inputs, 121 rules for each control variable are obtained. The training procedure is performed using the ANFIS file included in the MATLAB/FUZZY Logic Toolbox. The training mechanism discussed in section 7.7.1 was implemented, where the MSE (between the target values of each control variable and the trained ANFIC output) is made significantly small, as shown in Figure 7.14 for β and γ.

To validate the ANFIC learning algorithm, a test data set is presented to the trained file for each control variable. Figure 7.15 shows a sample of the resultant ANFIC output and the target of the control variables β and γ. It is clear that the training process of ANFIC is giving interpolated results very close to the target values.

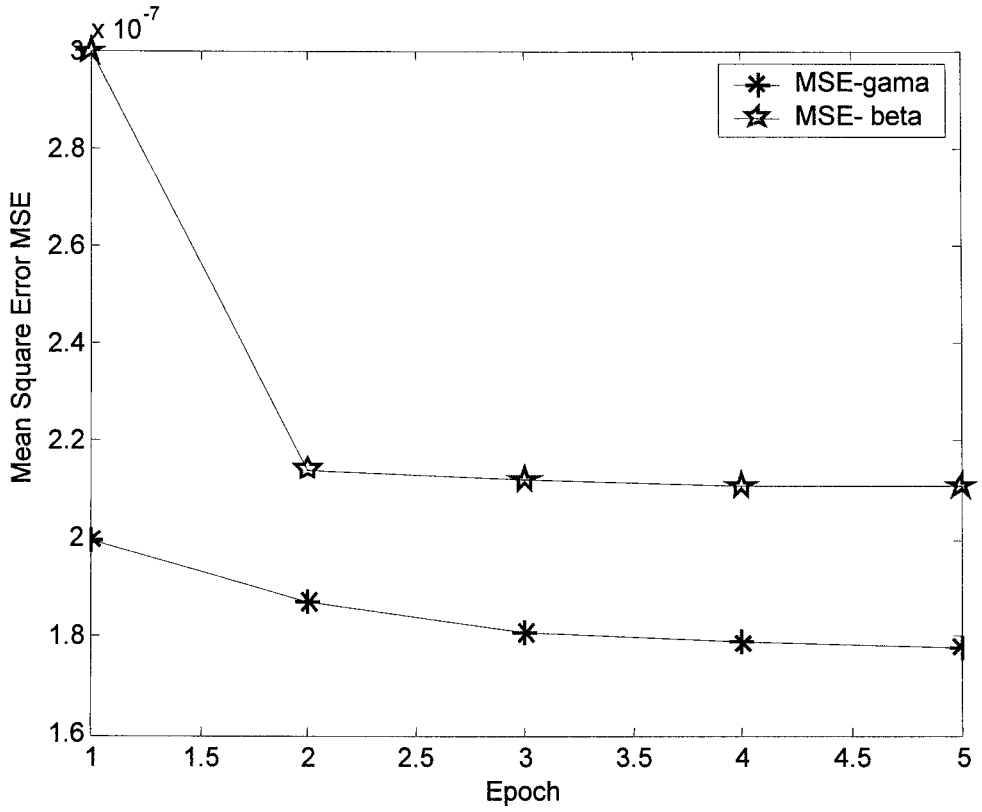

Figure 7.14 Mean Square Error (MSE) for trained control variables.

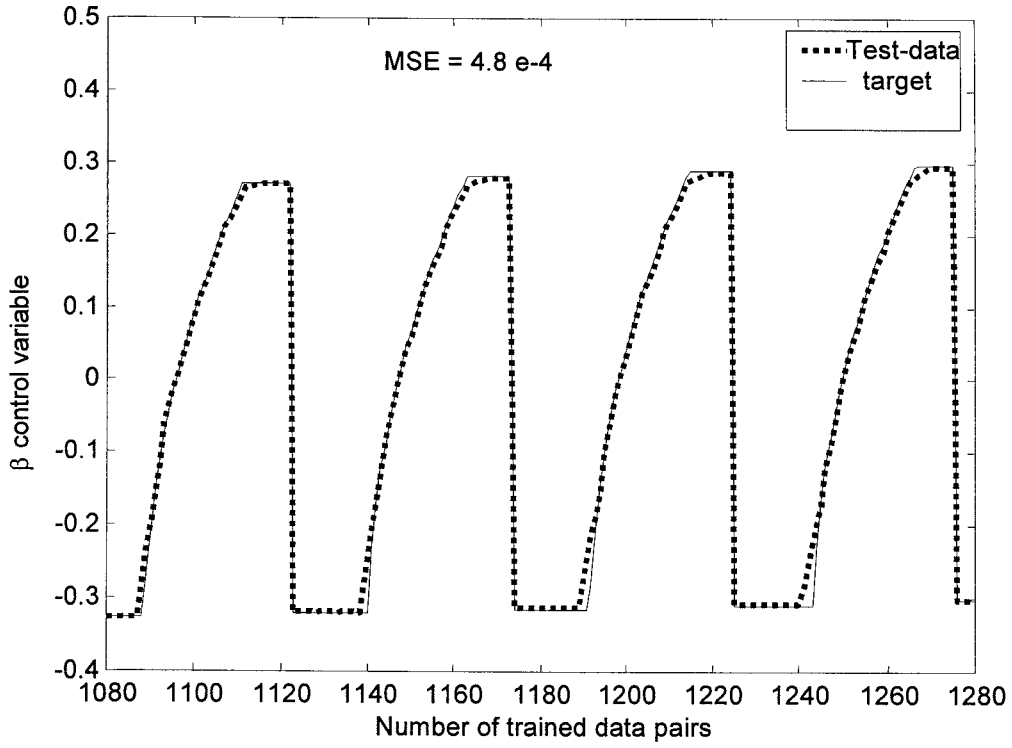

(a)

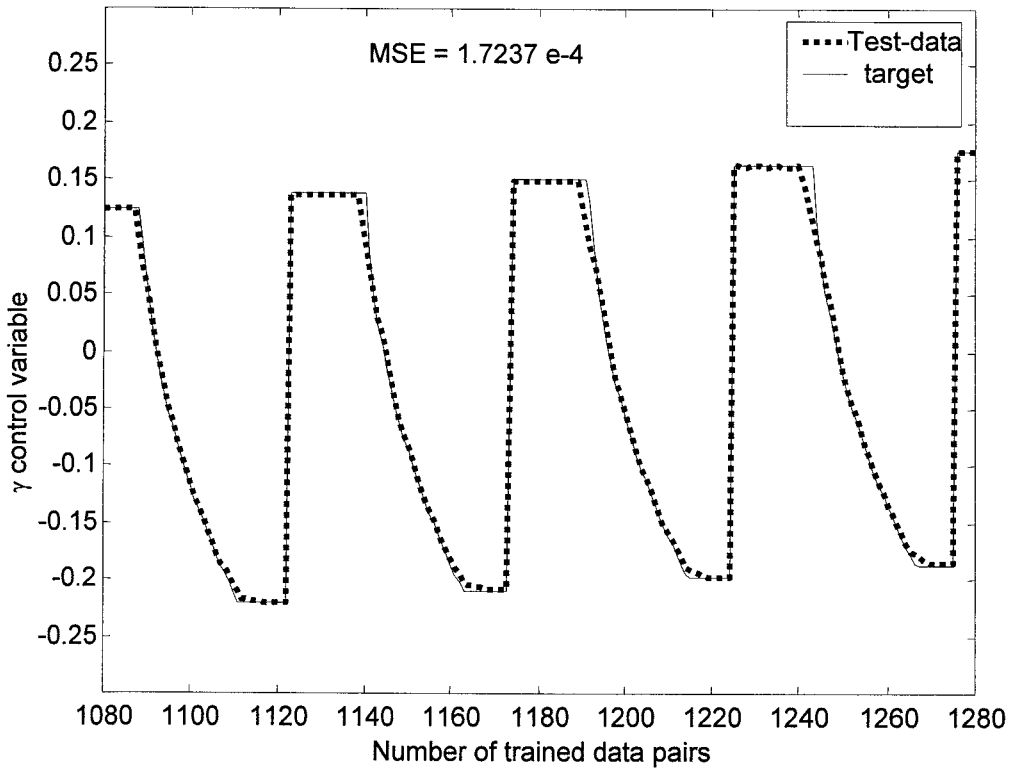

(b)

Figure 7.15 ANFIC validation test.

7.8 SIMULATION STUDY USING RBFNN AND ANFIC

The system given in Figure 6.10 is used to validate the effectiveness of the gradient descent learned controllers (ANFIC and RBFNN) in regulating the UPFC control variables. For the ANFIC controller, the neuro-fuzzy part controls the series inverter parameters while the shunt inverter parameters are regulated using a classical Fuzzy-like-PI controller. The RBFNN controller is used to control both the series and shunt inverter parameters.

Figures 7.16 and 7.17 show the results of system response to a step change in real and reactive power, respectively. These results show that the RBFNN controller has faster rise time as compared to the ANFIC controller. As clear from the results, the main advantage of the ANFIC controller is that the interaction between the real and reactive power is reduced. This is because, the controller is presented with the changes in real and reactive power in the same time, hence the right value of β and γ are deduced. However, each RBFNN controller operates to reduce the error in its control loop irrespective of the state of the other control loops.

In general, from the response point of view, it is difficult to prefer one of the controllers on the other. However, from the design procedure point of view (which includes collecting data, establishing network structure, training the network and validating the network behaviour), the RBFNN trained by on-line gradient descent algorithm is the easier to designed and test and it does not need prior data to be trained.

In this chapter, ANN and Neuro-Fuzzy based controllers have been investigated. The off-line trained controllers give an acceptable response but proved to need large computation time and memory. The on-line RBFNN controller, which have a simple structure, gives an adequate response. Its simplicity provides an attractive solution for implementation in real time as will be seen in the following chapter.

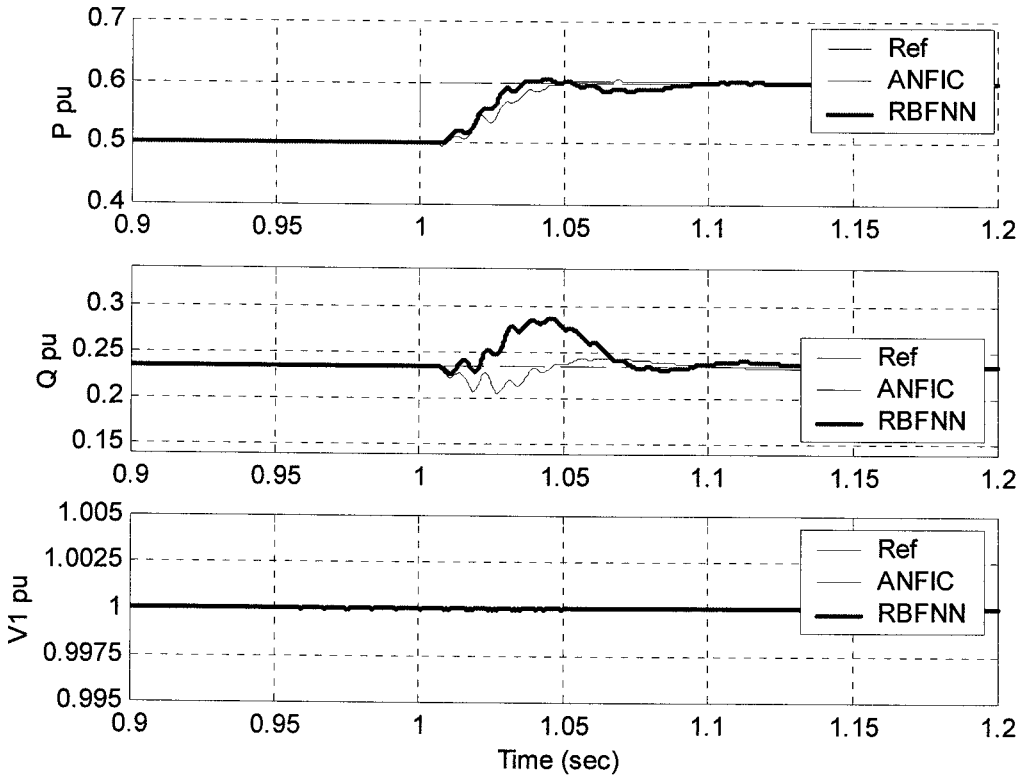

Figure 7.16 System response to a step change in real power.

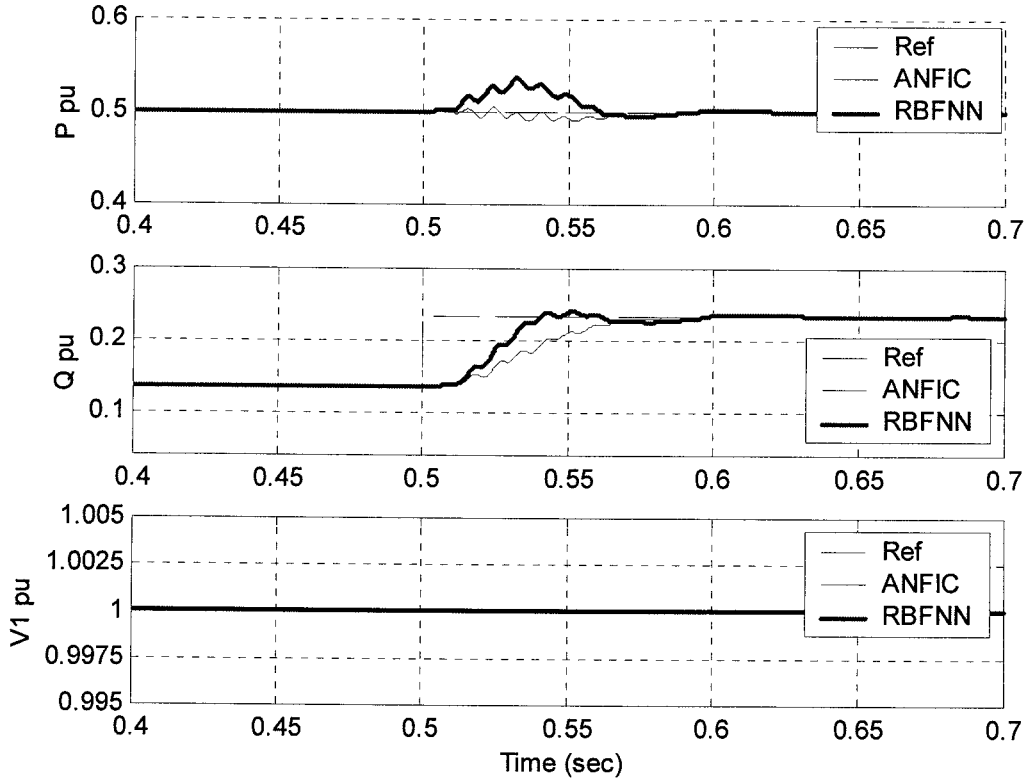

Figure 7.17 System response to a step change in reactive power.

DEVELOPMENT OF THE UPFC EXPERIMENTAL MODEL

8.1 INTRODUCTION

The experimental set-up used to verify the controller design described in Chapters 6 and 7 is shown in Figure 8.1. The set-up includes three main parts:

- The phase shifter.
- The UPFC model (two 6-pulse IGBT inverters).
- The control and data acquisition circuits.

8.2 THE PHASE SHIFTER

The phase shifting circuit consists of a three-phase Variac and a three-phase transformer. The purpose of this circuit is to introduce a phase difference between V_1 and V_2 which represent the sending-end and receiving-end voltages of the transmission line, respectively.

The Variac is connected in Star (Y) configuration while the primary side of the three-phase transformer is connected in Delta (Δ), as shown in Figure 8.2. By arranging the phases as shown in Figure 8.2-a, the shifting transformer injects a 90^o leading phase voltage with respect to the corresponding V_2 phase voltage. From the vector diagram in Figure 8.2-b, it is clear that the phase angle between V_1 and V_2 is adjusted by controlling the magnitude of the injected voltage ΔV. The waveforms of V_1, V_2 and the injected voltage ΔV are

shown in Figure 8.3. In this work, the transmission angle θ_{12} is set to 6^{o} to produce sufficient active and reactive power flow that is suitable for the experimental test.

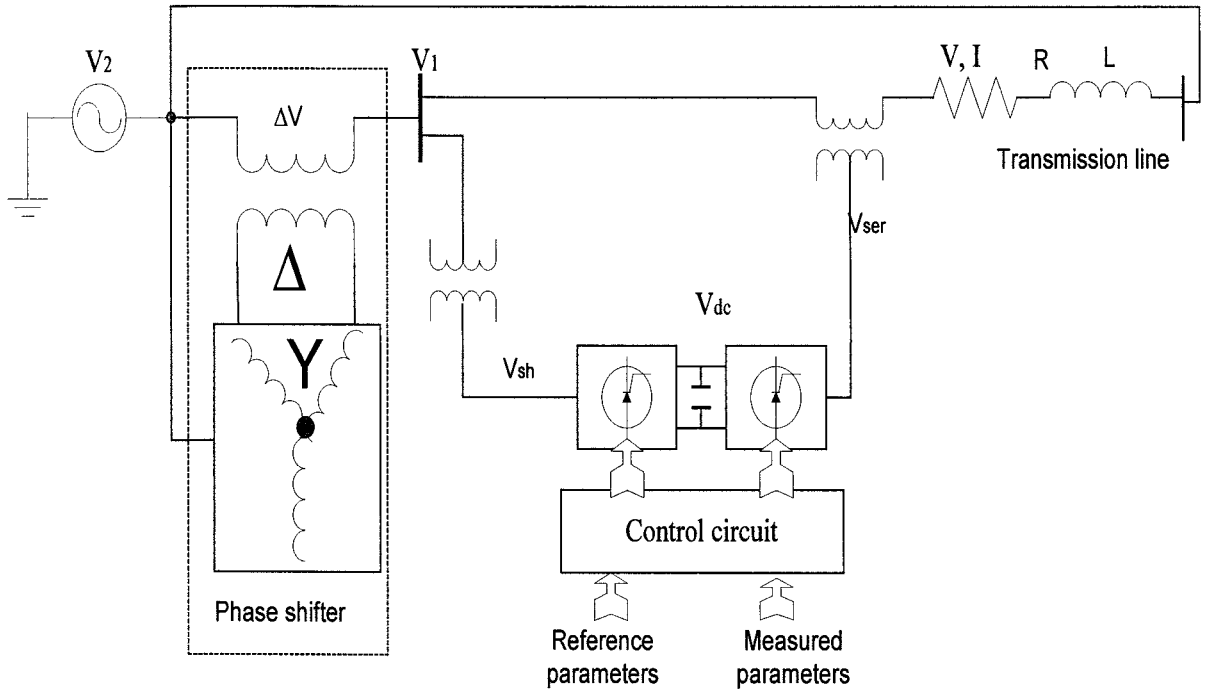

Figure 8.1 Block diagram of the experimental set-up.

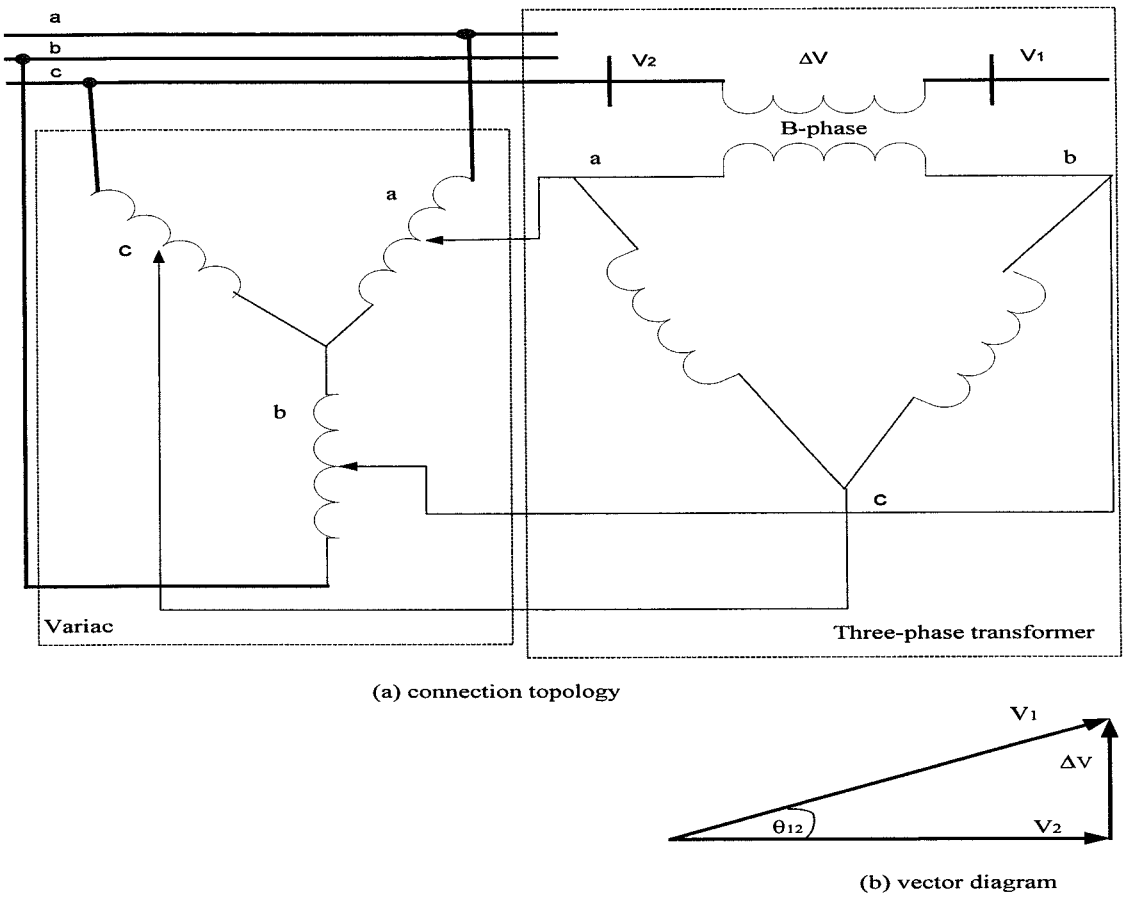

Figure 8.2 Phase shifting circuit.

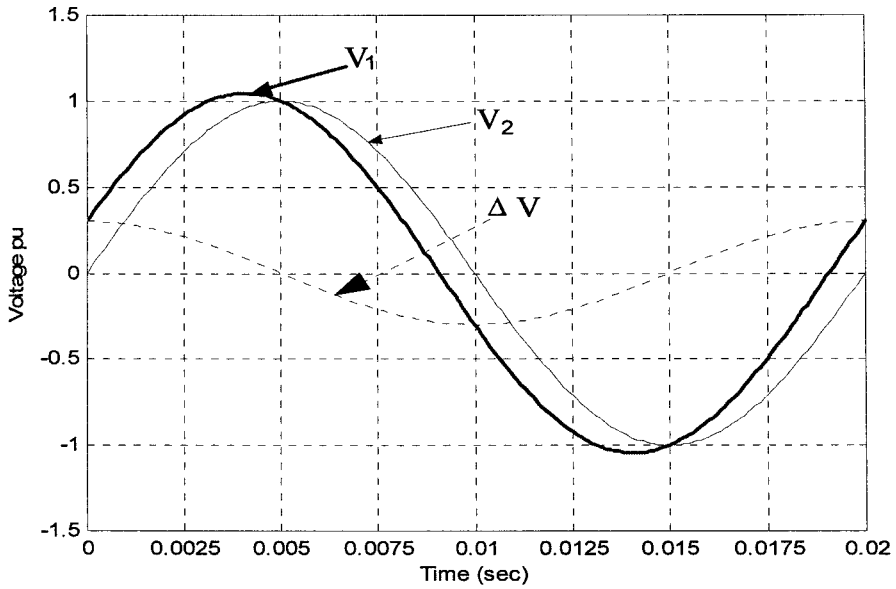

Figure 8.3 Phase-shifting waveforms.

8.3 THE UPFC INVERTERS

The UPFC model used in this investigation consists of two 6-pulse inverters. The series inverter is connected to the transmission line model through a booster transformer of 12:1 turns ratio. The a.c. side of the shunt inverter is connected to the a.c. system through an excitation transformer with a turns ratio of 1:1. The d.c. side of both series and shunt inverters are tied to a common d.c. capacitor of $C = 1000\ \mu F$. A 10 kΩ resistor is connected in parallel with the d.c. capacitor to dissipate its energy when the system is switched off.

8.3.1 Choice of Switching Devices

In the VSI based FACTS devices, in particular the UPFC, the switching devices must have a self-commutating capability. This is required so that the UPFC can absorb or generate reactive power at each inverter end and for the real power to flow between the UPFC ends independently of the reactive power. Power semiconductors with self-commutating capability include GTO thyristor, MOS Controlled Thyristor (MCT), Static Induction Thyristor (SIT) and Insulated Gate Bipolar-junction Transistor (IGBT) [113,114]. The IGBT is extensively used nowadays in the low and medium power applications because of the following technical considerations [115].

- IGBTs are available at rating up to 4.5 KV, 1200A.
- High switching frequency up to 50 kHz.
- Reverse conducting capability where an IGBT and an anti-parallel diode are available in one package.
- Low switching losses.
- Low power and simple gate drive requirements.
- Ease of paralleling.
- Square safe operating area (turn off and short circuit).

- Current controllability under fault conditions.
- Snubberless operation is possible.

Therefore, IGBTs have been chosen to build up the UPFC inverters for the laboratory model. According to the specifications of the laboratory model, it was decided to employ the discrete IRG4BC20K and discrete fast-recovery diode IR 10ETF10 [see data sheets in Appendix C]. To comply with safety regulations, the inverters used in the lab model were operated at 50 V (line–line). The circuit diagram of the 6-pulse inverter is shown in Figure 8.4.

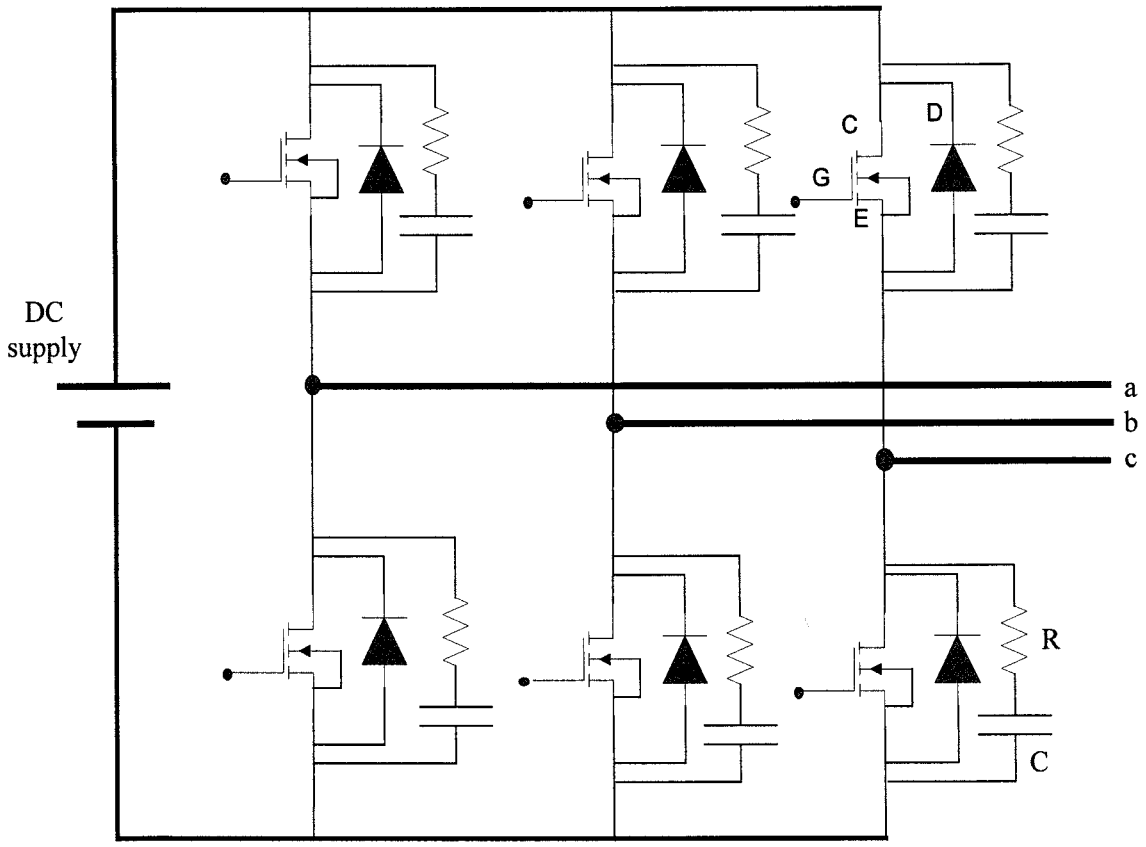

Figure 8.4 A 6-pulse inverter with anti-parallel diodes and snubber circuits.

8.3.2 Snubber Circuit

When the power device is turned off, the energy trapped in circuit stray inductance causes a voltage overshot across the device. The magnitude of this transient voltage is proportional to the stray inductance and the rate of fall of turn-off current. Similarly, when the switching device is turned-on the rapid rise in the current combined with the circuit stray inductance causes the anti-parallel diode to go through a severe recovery voltage, which may exceed the switch rating.

To reduce the electrical stresses placed on the IGBT switches during switching, a snubber R-C circuit is connected in parallel with each device. A resistance of 10 Ω and capacitance of 0.015 μF have been used for the lab model (see Reference [116] for details regarding the expressions used to calculate the snubber circuit parameters). Fuses were used at both the a.c. and d.c. sides of the inverter circuits to provide over current protection.

8.3.3 Digital Phase Locked Loop and PWM Generation

A Phase Locked Loop (PLL) is used to synchronise the inverter output voltage with the reference signal which is derived from the supply voltage. An analogue PLL is the most popular phase tracking circuitry. However, in this work, a Digital Phase Locked Loop (DPLL) is implemented using the software capabilities of the data acquisition board to achieve synchronisation.

A block diagram of the DPLL and PWM generator is shown in Figure 8.5. The three-phase reference signals are first filtered and then normalised to get a reference signal ranging between ±1 regardless of the actual signal magnitude which is suitable for the phase shifting circuit. The PWM signal has three controlled parameters which are the chopping ratio, the modulation index and the phase angle between the reference signal and the carrier [117].

The ratio of the carrier frequency and the modulating signal frequency is known as the chopping ratio (m_f) and is given as;

$$m_f = \frac{f_c}{f_m} \tag{8.1}$$

For the UPFC m_f must be maintained constant during operation. In this work, m_f has been set to 9 to eliminate the even and triplen harmonics from the inverter output voltage. The phase angle of the inverter fundamental output voltage is adjusted by changing the reference signal angle with respect to the carrier signal. A closed loop controller is used to shift the reference signal in the lead or lag direction, according to the system operation requirements. The ratio of the amplitude of the modulating signal and the carrier is called modulation index m_a and is given as;

$$m_a = \frac{V_m}{V_c} \tag{8.2}$$

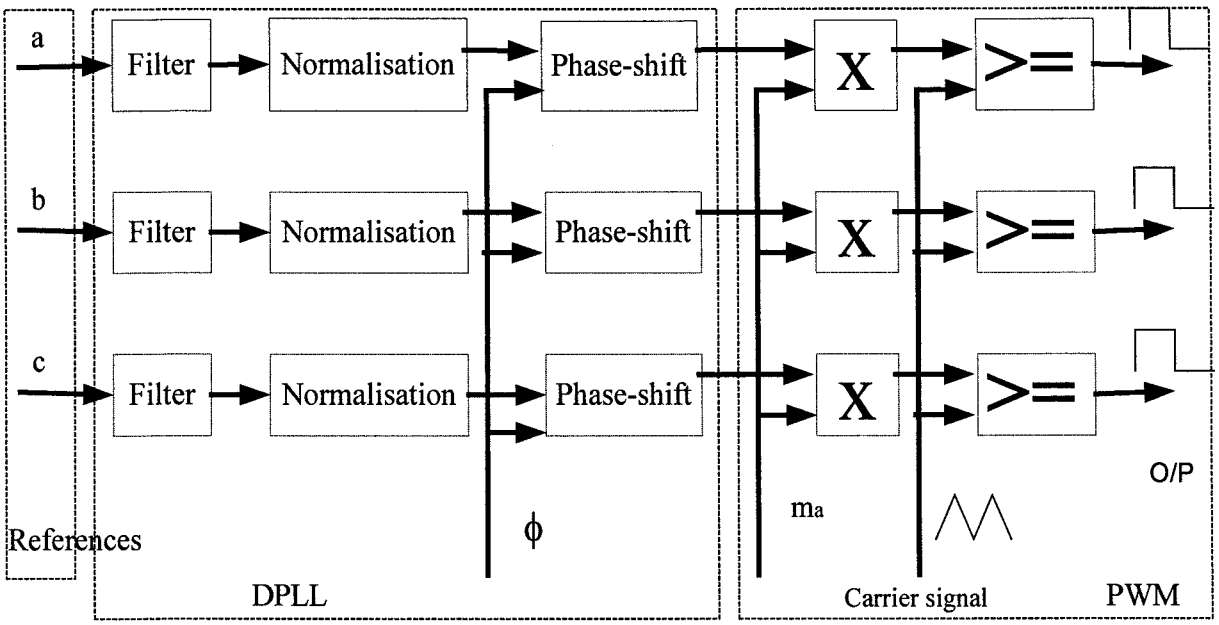

Figure 8.5 Block diagram of the DPLL and PWM.

For the UPFC, m_a is adjusted at every sample by a closed loop controller which vary the amplitude of the reference signal while keeping the amplitude of carrier signal fixed.

The modulated signal is then compared with the triangular carrier which is built using the SIMULINK blocks. Then, the three PWM lines, (output in Figure 8.5), for each inverter are sent through the digital channels of the I/O board to a signal conditioner. The SIMULINK based block diagrams of the phase shift and carrier generator are shown in Appendix D.

8.3.4 Gate Signal Conditioning

The PWM output is not strong enough to charge the input capacitance of the IGBT gate junction over the threshold value. Therefore, a signal conditioning circuit is essential to isolate and amplify the PWM output signals. Figure 8.6 shows a gate signal conditioner, which contains three main blocks, the inversion, dead-time and 5V-15V conversion.

To reduce the time used by the host computer, only three references pulses are generated inside the controller block while the firing signal for each IGBT is accomplished by an external hardware.

Short circuits across the inverter d.c. side is avoided by inhibiting two switches in the same leg from turning on at the same time. The minimum dead-time is the time necessary for the slowest IGBT to fully turned off before the subsequent IGBT in the same leg is turned on. The circuit diagram used for this purpose is shown in Appendix E where a 12 μs dead time is set according to the characteristic of the IGBT device used.

Finally, the 5V-output signal from the PWM circuit is converted to 15V which is necessary to drive the IGBTs. A block diagram of the gate driver used in this work is given in Appendix F.

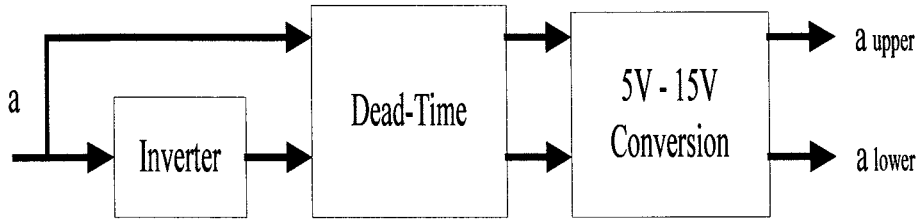

Figure 8.6 Block diagram of the gate signal conditioner

8.3.5 Operation of the IGBT Inverter

Each of the developed IGBT inverters was tested by driving the input from a d.c. power source and supplying a star-connected resistive load on the a.c. side. The reference signal, the PWM waveform generated of the phase to load neutral and the filter output voltage are shown in Figure 8.7 for different amplitude modulation (m_a) and phase angle (ϕ). The switching frequency used in this test is set to 450 Hz. It is clear that the magnitude of the reference signal has no effect on the inverter output. The output voltage magnitude is greatly affected by the modulation index. Also, the phase shift does not affect the magnitude of the inverter output voltage.

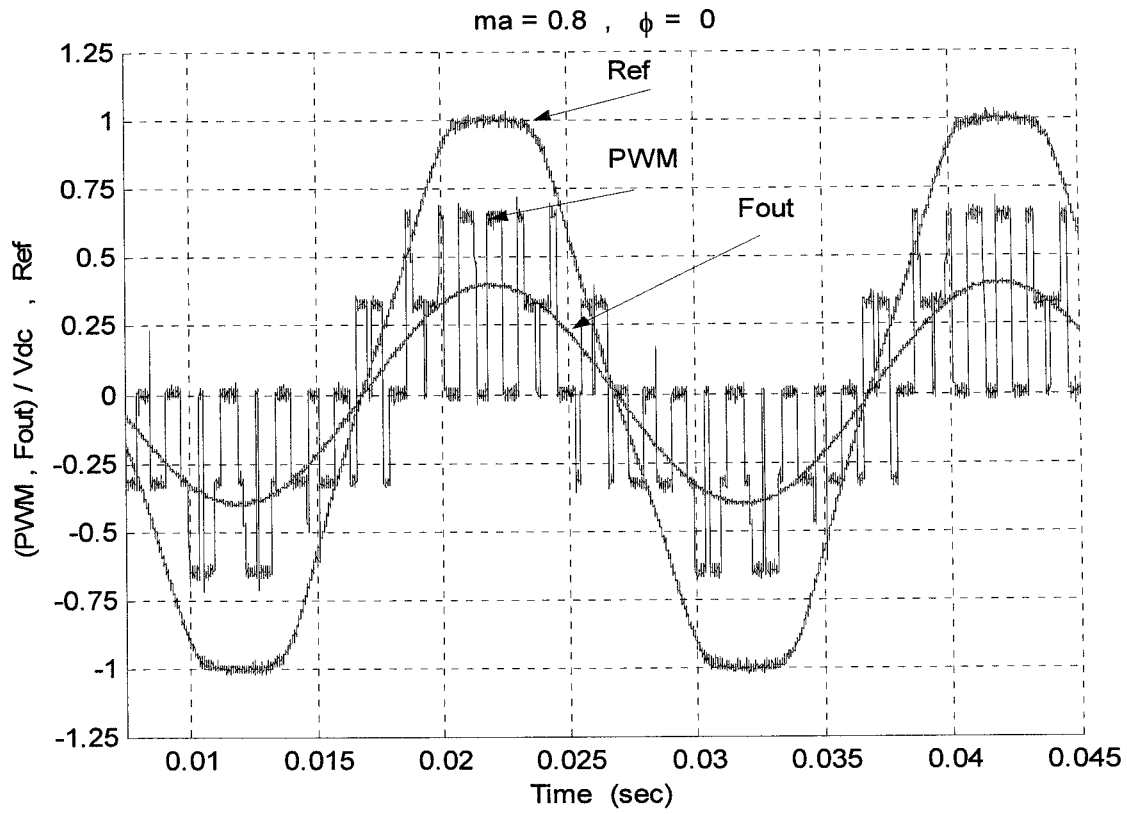

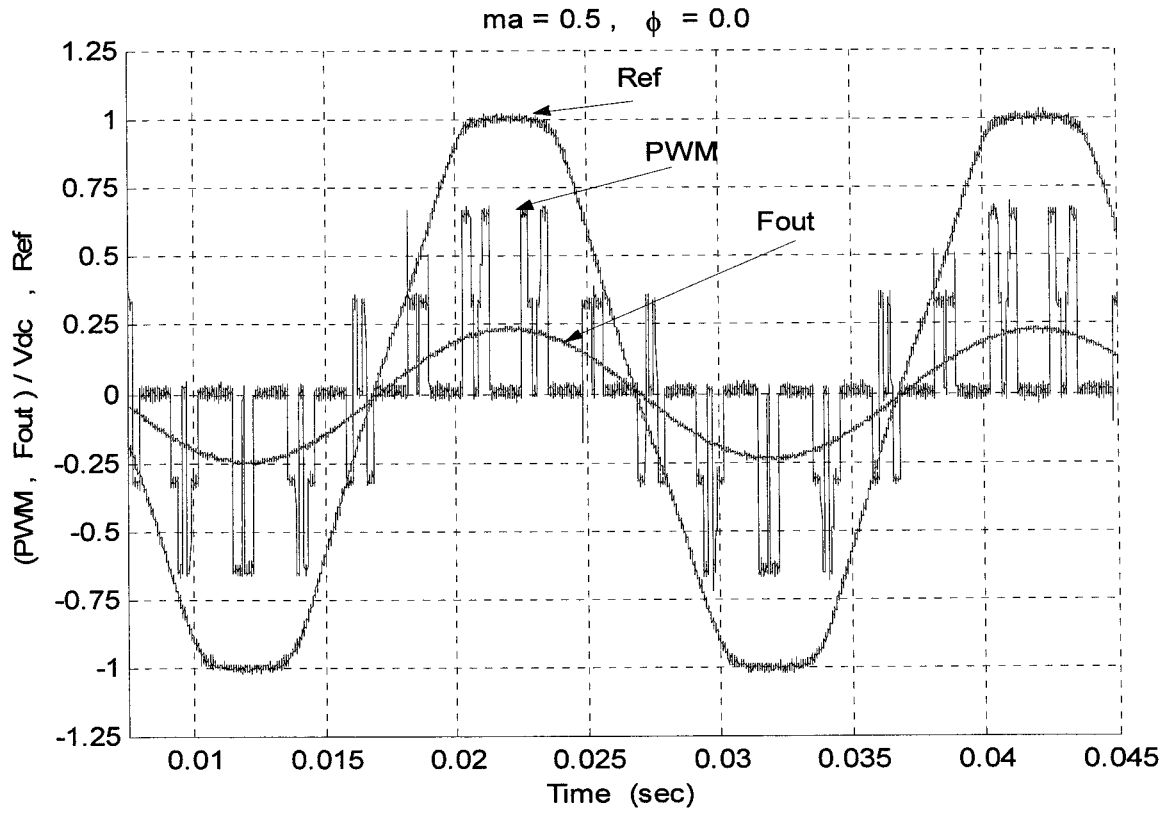

Figure 8.7 Reference signal, inverter output (PWM) and filter output (Fout).

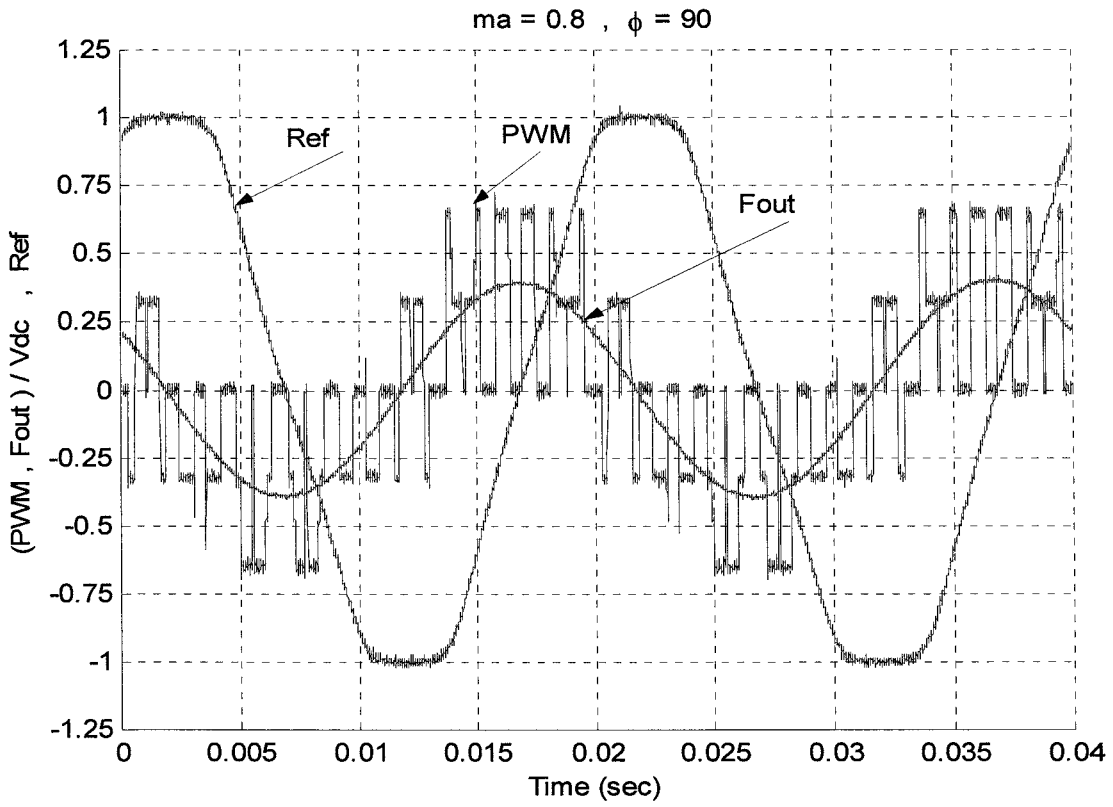

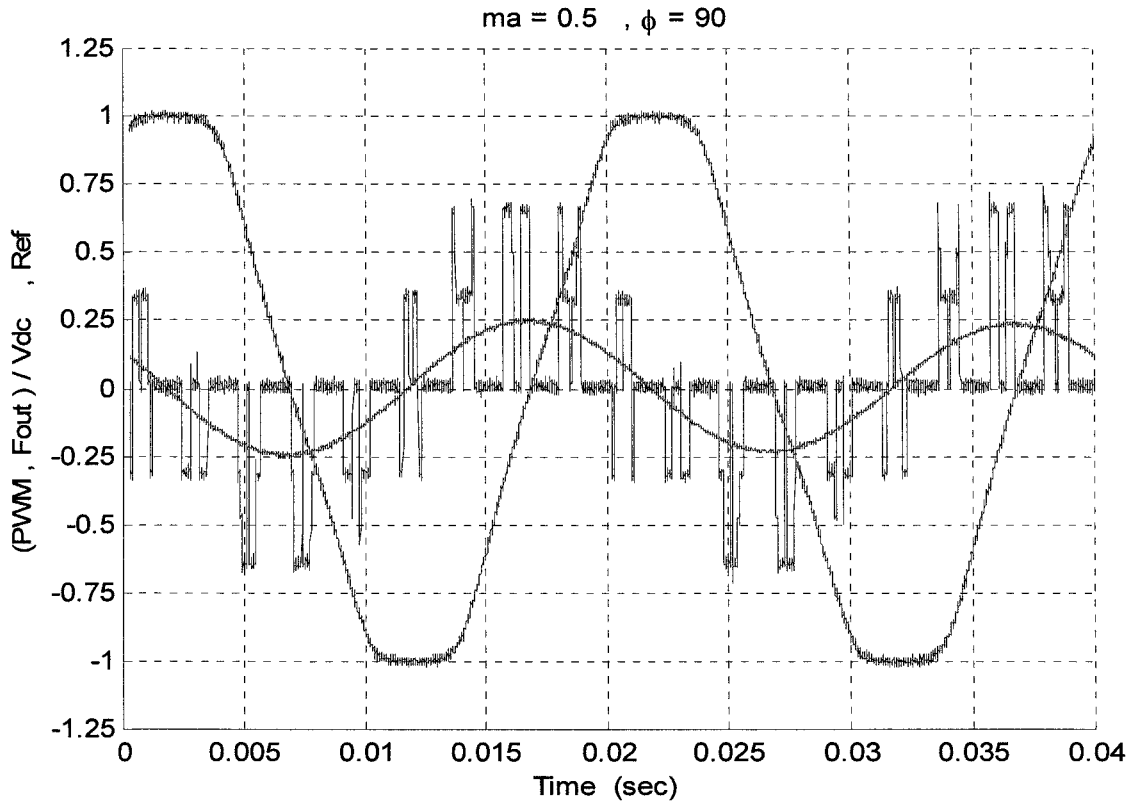

Figure 8.7 (cont.) Reference, PWM and Fout.

8.4 CONTROL AND DATA ACQUISITION

A software-based approach was adopted in the design and implementation of the UPFC controller. The main advantages of the software-based approach are better reliability, drift-free operation, easier operator-machine interface and more flexible in tuning. A software-based controller also has the ability to support extensive data acquisition and recording equipment. In addition, the control program can easily be modified to accommodate desired changes in the system under control and the controller parameters without alterations in the hardware. Moreover, the hardware is vastly reduced when the main control functions are achieved by software. In this study, software-based controllers are designed in the SIMULINK and interfaced with the hardware through the DS1103 data acquisition board.

8.4.1 The DS1103 Data Acquisition and DSP Board

The host computer was interfaced with the UPFC experimental set-up through the ControlDesk (CD) software with dSPACE DS1103 PPC controller and data acquisition board. ControlDesk, dSPACE's experiment software, provides all the functions to control, monitor and automate experiments and makes the development of controllers more effective. The DS1103 is a single board system based on the 400 MHz Motorola power PC604e processor (PPC) and has three main parts [118]. The main parts of the functional units of the DS1103 PPC controller board are shown in Figure 8.8, these are:

I/O units

This is a set of on-board peripherals frequently used in digital control systems which includes D/A channels, A/D channels, digital I/O ports (individual bits and byte) and a serial interface.

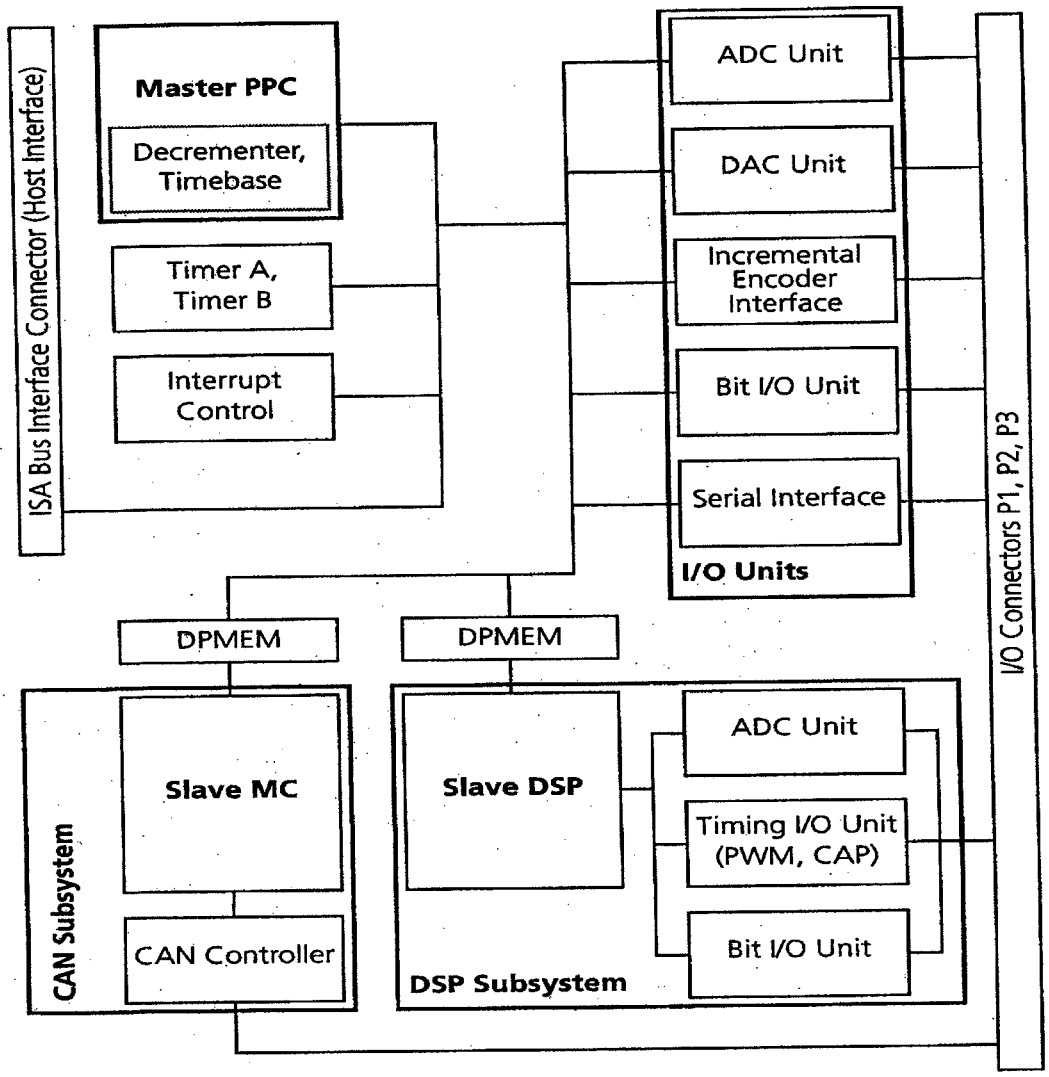

ADC	Analog/Digital Converters
MC	CAN Microcontroller 80C164
CAP	Capture
DAC	Digital/Analog Converters
DPMEM	Dual-Ported Memory
DSP	Digital Signal Processor TMS320F240
PPC	Power PC 604e Processor
PWM	Pulse Width Modulation

Figure 8.8 Functional units of the DS1103 PPC controller board.

DSP subsystem

The DSP subsystem, based on the Texas Instruments (TI) TMS320F240 DSP, has its own I/O capabilities and three-phase PWM generation which make the subsystem useful for drive application. The slave DSP can be accessed from the PPC main board or separately through its TI software.

CAN subsystem

This is used for connection to a CAN bus based on the Siemens 80C164 Micro-controller. More details of the DS1103 board and features are given in Appendix G.

8.4.2 Real-Time Controller Design

The dSPACE real-time system provides a good solution that combines all control design steps in a total development environment that can completely integrate the MATLAB development tools. With its broad range of tools for control system modelling, analysis, simulation and prototyping, MATLAB is an ideal system for developing advanced control systems.

Real-Time Interface (RTI) is the link between dSPACE's real time system and the developed model in SIMULINK. It extends the c-code generated by the MATLAB Real-Time Workshop (RTW) for the automatic implementation of the SIMULINK models on the dSPACE's real-time hardware.

The RTI can handle any kind of continuous-time, discrete-time, hybrid and multirate systems. Different channels of the DS1103 board can be used with different sample rates, and even in different subsystems. Moreover, the RTI supports non-periodic events, such as software interrupts and external hardware interrupts and also allows task prioritising for the execution of the model subsystems. Such characteristics make the dSPACE system an ideal choice to implement the control algorithms as proposed in this study.

8.4.2.1 Design steps of the real-time controller

The design of a real-time controller using the DS1103 PPC controller and data acquisition board includes the following steps:

- Design the controller and plant model using MATLAB/SIMULINK environment. Run the simulation (off-line) till the required system performance is achieved. An example of SIMULINK model is shown in Figure 8.9 which describes a power system model incorporating a UPFC control system.
- When the system is tested off-line, it has to be prepared for implementation on the real-time system. That is, the plant model (power system model) has to be exchanged for I/O components, which form the interface to the hardware model. From the dSPACE I/O library, the input/output channels blocks are connected to the controller input/output. The modified model is shown in Figure 8.10.
- The integration algorithm and the step size are then chosen from the simulation parameters dialogue.
- The RTW parameters to generate the c-code of the SIMULINK model that is required for the real-time interface are selected and identified. Once the model is successfully compiled, the RTI automatically download it on the DS1103 processor.
- When the application is running with the real-time hardware, the dSPACE system ensures a full control over each individual variable. Also, the ControlDesk graphical interface provides a virtual instrument panel that enables the operator to change the controller parameters and monitor signals on-line without regenerating the code. The ControlDesk displays time histories of any variables being used by the model, as shown in Figure 8.11.

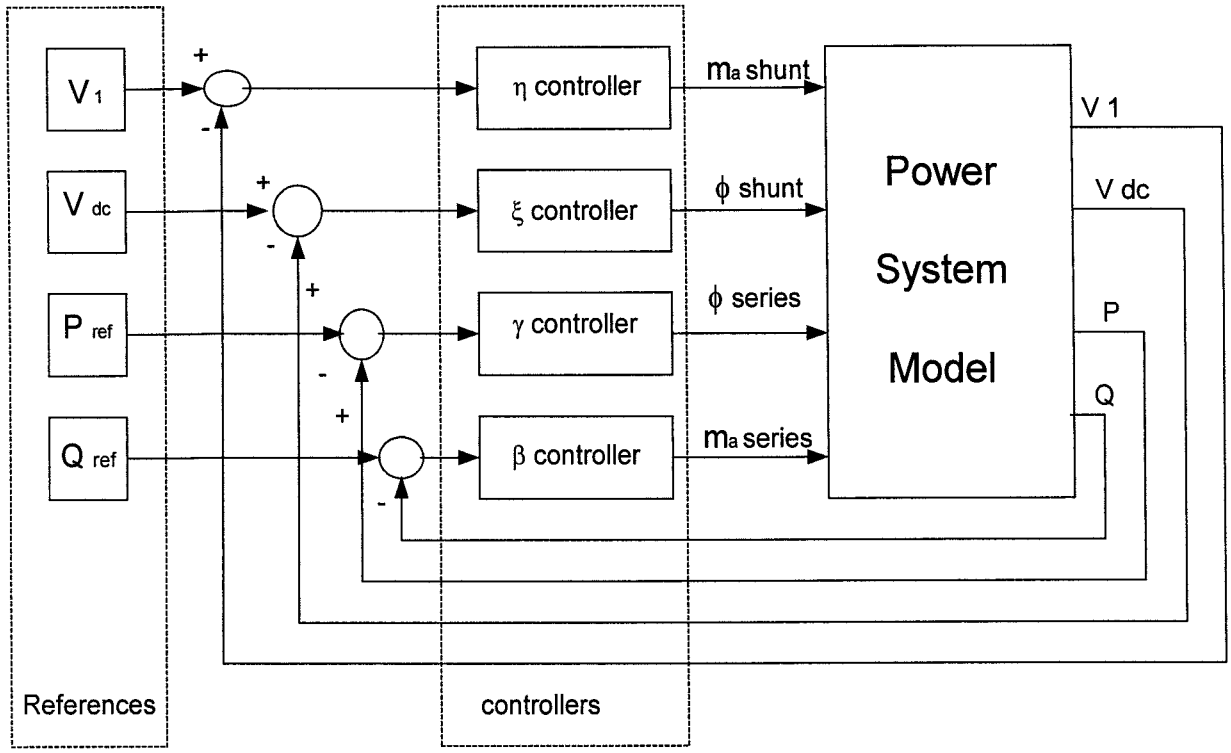

Figure 8.9 SIMULINK model of the UPFC control system.

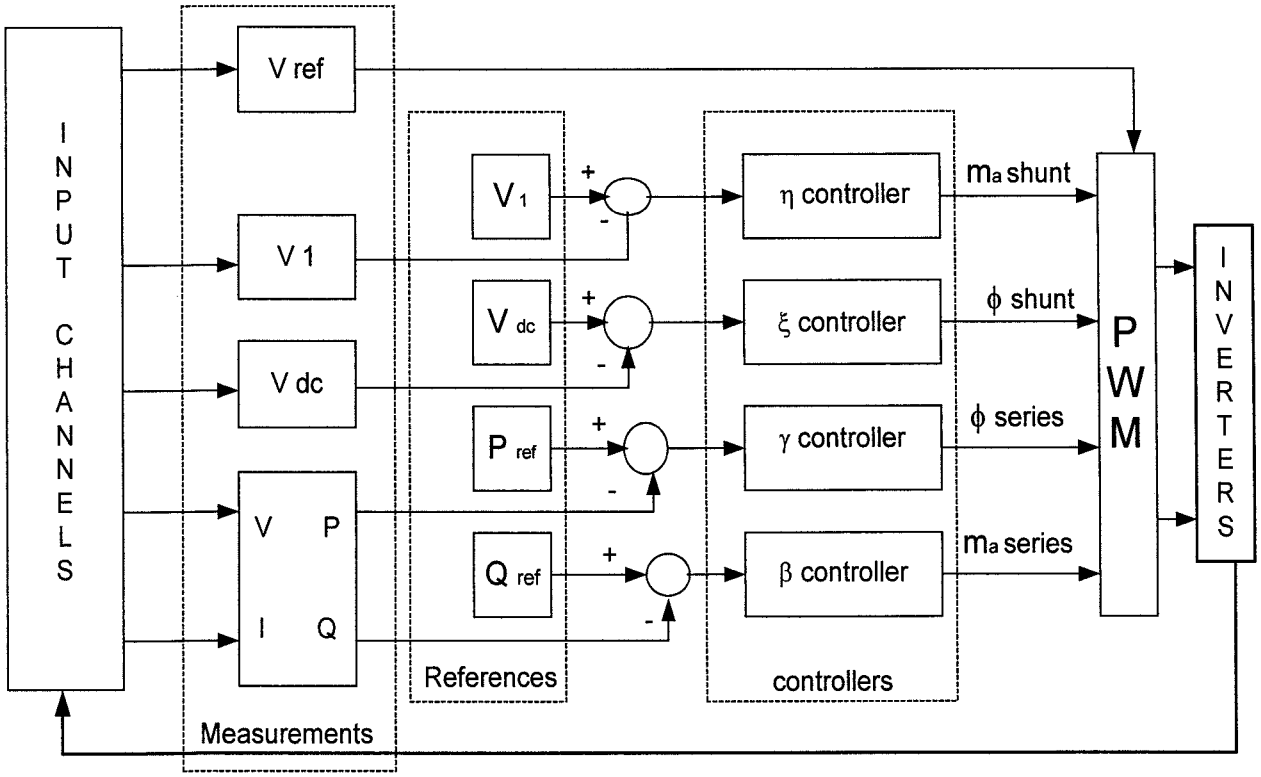

Figure 8.10 SIMULINK real-time controller model for the UPFC.

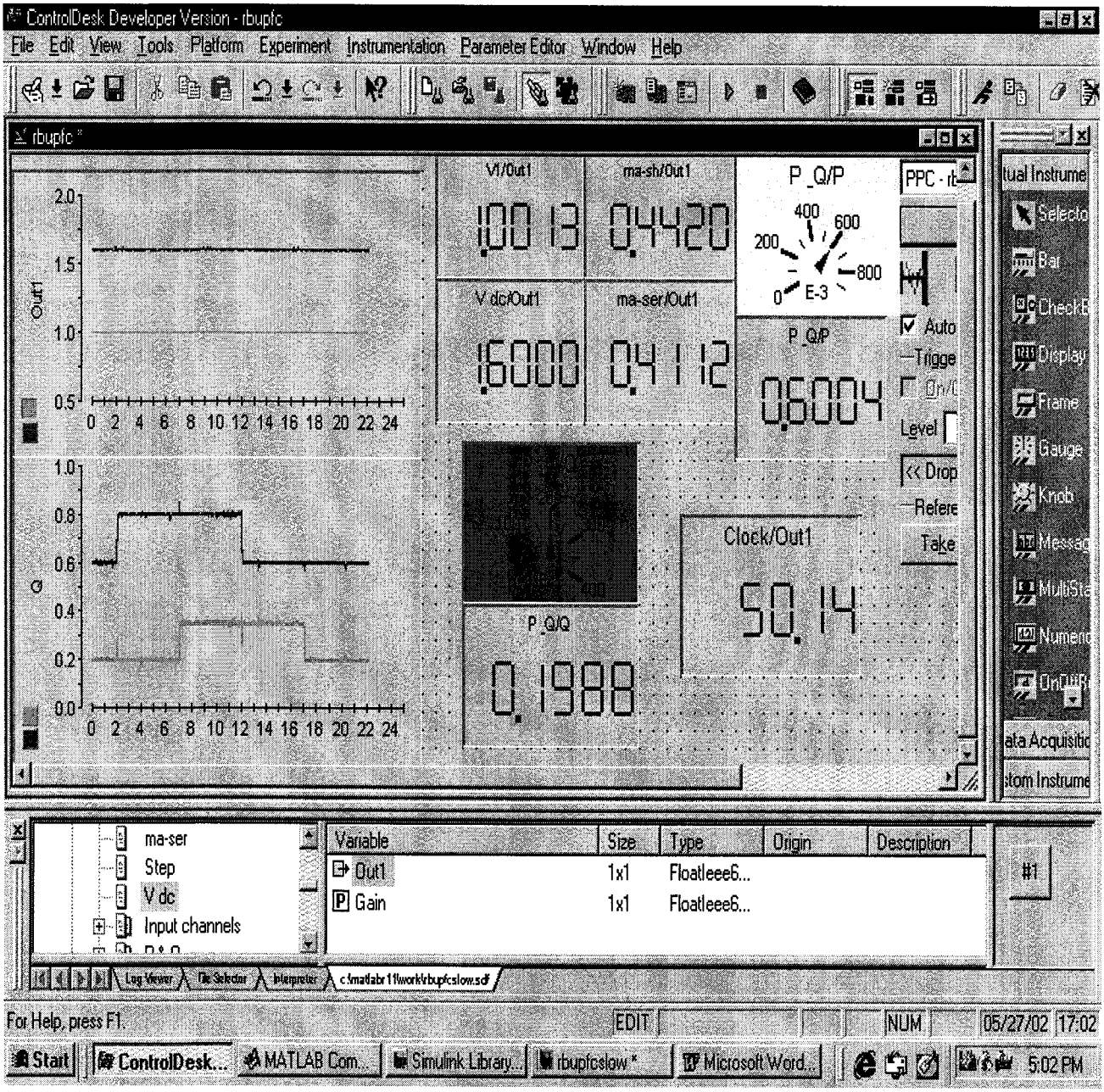

Figure 8.11 ControlDesk cockpit.

8.4.2.2 Measurements

Performing a closed loop real-time control system requires measuring feedback signals from the real-time hardware. The measured signals may contain harmonics due to the PWM technique used and need to be conditioned before they are applied to the controller. This includes the following:

- Voltage and current measurements.
- Filtering out the noise from signals.
- Sampling signals to suite the digital controller requirements.
- Scaling signals to operate in per-unit bases.
- Obtaining the d.c. equivalent signal.

Voltage and current measurements

The power system employed in this work is considered symmetrical. Therefore, signals from one phase are used to generate the appropriate control signals. In the developed lab model, five feedback signals are used to control the UPFC operation in different modes. With reference to Figure 8.1, the reference a.c. signal V_2 has been used to generate the PWM signals. The system bus voltage V_1 and the d.c. link voltage V_{dc} have been used to control the operation of the shunt inverter. The voltage V and the current flow in the transmission line (I) are measured in order to control the real (P) and reactive (Q) power flow. A high frequency current probe (Agilent N2774A) and a voltage probe (Agilent N2772A) are employed to measure the corresponding signals.

Filtering

The PWM inverters produce harmonics which influence the voltage and current signals fed-back to the controller. The switching frequency has been set to 9 times the system frequency to eliminate the even and triplen harmonics, but 5^{th}, 7^{th} and other higher harmonics are present. Therefore, filtering the measured signals is essential in this application. A simple R-C circuit has been used to get the fundamental component only of

the electrical measured quantity and to prevent aliasing. The attenuation and phase delay to the fundamental component caused by the filtering circuit are compensated.

Sampling

Continuous signals from the power system are converted into digital form by means of ADCs. The DS1103 board has 22 ADCs channels with maximum conversion time of 4μs. The minimum sampling time of these channels is inherited from the SIMULINK step-size simulation parameters. Different sampling rates can be assigned as an integer of the solver step-size. In this study, a sample rate of 72 samples per cycle is chosen which allows enough time for the UPFC controller calculations.

Scaling

The maximum a.c. input signal applied to the ADC is ±10V. Therefore, the measured signals should be scaled down to avoid over voltage problems of the interface card. The maximum output of the ADC block within the SIMULINK is ±1. Hence, a gain block is used to arrange the quantities in per unit use.

D.C. equivalent

The d.c. equivalent of the magnitudes of the bus voltage and the d.c. voltage are obtained by employing Fourier block with harmonic order 1 and 0, respectively. The d.c. equivalent of the actual real and reactive power are obtained by applying the measured V and I_{ser} to P_Q block, shown in Figure 6.5, which gives the average real and reactive power flow.

8.4.2.3 Initialising the real-time loop

The real-time control system is initialised to determine the nominal values V_{1_0}, P_0 and Q_0 in per unit with the existence of the UPFC inverters and the coupling transformers.

The series inverter PWM parameters are adjusted to be $m_{a\,ser} = 0.0$ and $\phi_{ser} = 0.0$, while the shunt inverter PWM parameters are set to $m_{a\,sh} = 0.5$ and $\phi_{sh} = 0.0$. For this test only, two d.c. power supply of 80 V are connected at the d.c. side of each inverter. The

controlled quantities are adjusted through the scaling process to be, $V_1 = 1\,pu$, $P_0 = 0.5\,pu$ and $Q_0 = 0.005pu$. The waveforms of the key quantities are shown in Figure 8.12.

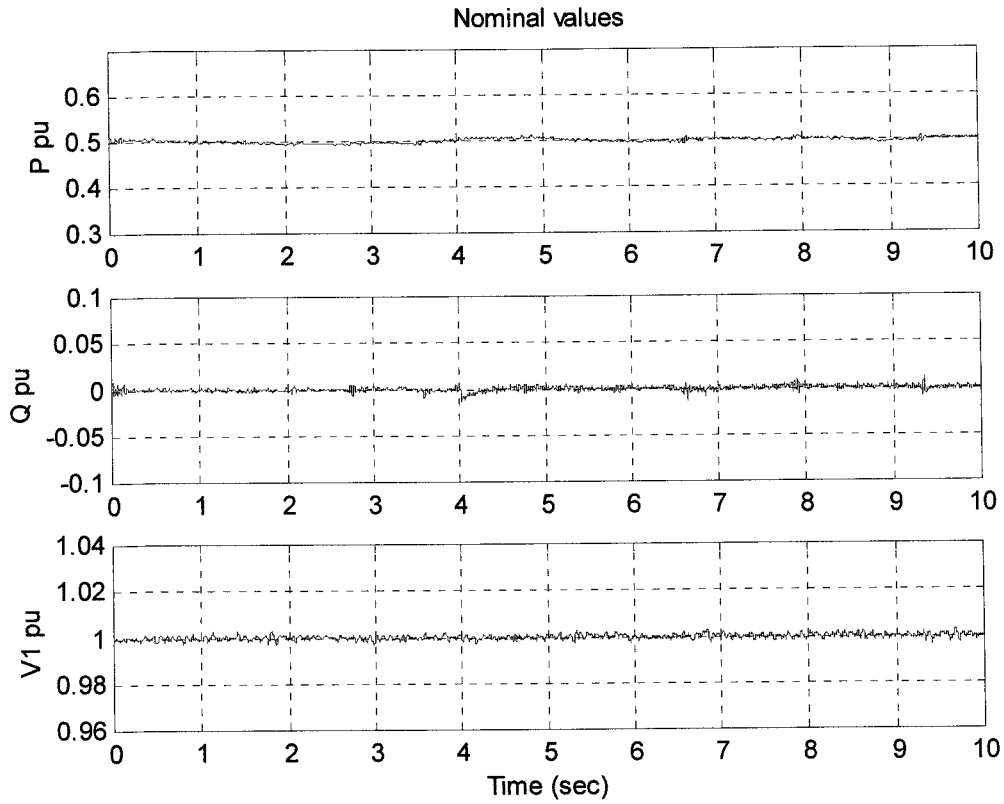

Figure 8.12 The power system initial quantities.

8.5 PERFORMANCE OF THE UPFC EXPERIMENTAL MODEL

Figure 8.13 shows the set-up for the UPFC experimental investigation. The inverters and the gate signal conditioners are shielded to reduce the system interference due to noise.

Three case studies were conducted for different system conditions. In case 1, the UPFC capabilities to independently control the real and reactive power flow in addition to supporting the system bus voltage have been tested under the influence of different control algorithms. In case 2, a system with low short circuit level was considered and the behaviour of each controller investigated. In case 3, the system short circuit level was suddenly decreased to simulate a fault occurring at the system side. The performance of the proposed controllers against changes of system parameters has been tested and verified.

8.5.1 UPFC Controllers

The UPFC has four control loops, two for each inverter to control the PWM parameters (m_a, ϕ). The following four controllers are designed and tested in real-time. The control variables of the power system incorporating the UPFC are dependent on each other e.g. controlling the reactive power influences the real power flow. Therefore, two main points are taken into consideration when a certain control loop parameters are designed. The first is to get an adequate response (fast without overshoot). The second is to minimise the effects of this control loop on the other system control loops (minimum interaction).

PI controller

It is a fixed parameters controller used for comparison purpose.

Fuzzy-like-PI controller

When implementing the Fuzzy-like-PI controller (legend as FZ-PI), Mamdani fuzzy algorithm used in the simulation phase described in Chapter 6 was found not suitable in real-time due to extensive memory and calculation time. Therefore, a Takagi-Sugeno algorithm has been used which consumes less memory locations and requires less calculation time, as compared with Mamdani algorithm.

ANFIC controller

As explained in Chapter 7, ANFIC controller is designed for the series inverter of the UPFC while the shunt inverter is controlled by employing conventional PI controller (legend as ANFIC-PI in the results) or Fuzzy-like-PI controller (legend as ANFIC-FZ).

RBFNN controller

An adaptive learning-rate RBFNN controller is designed and tested. This requires no training in advance and gave the best performance as will be shown later.

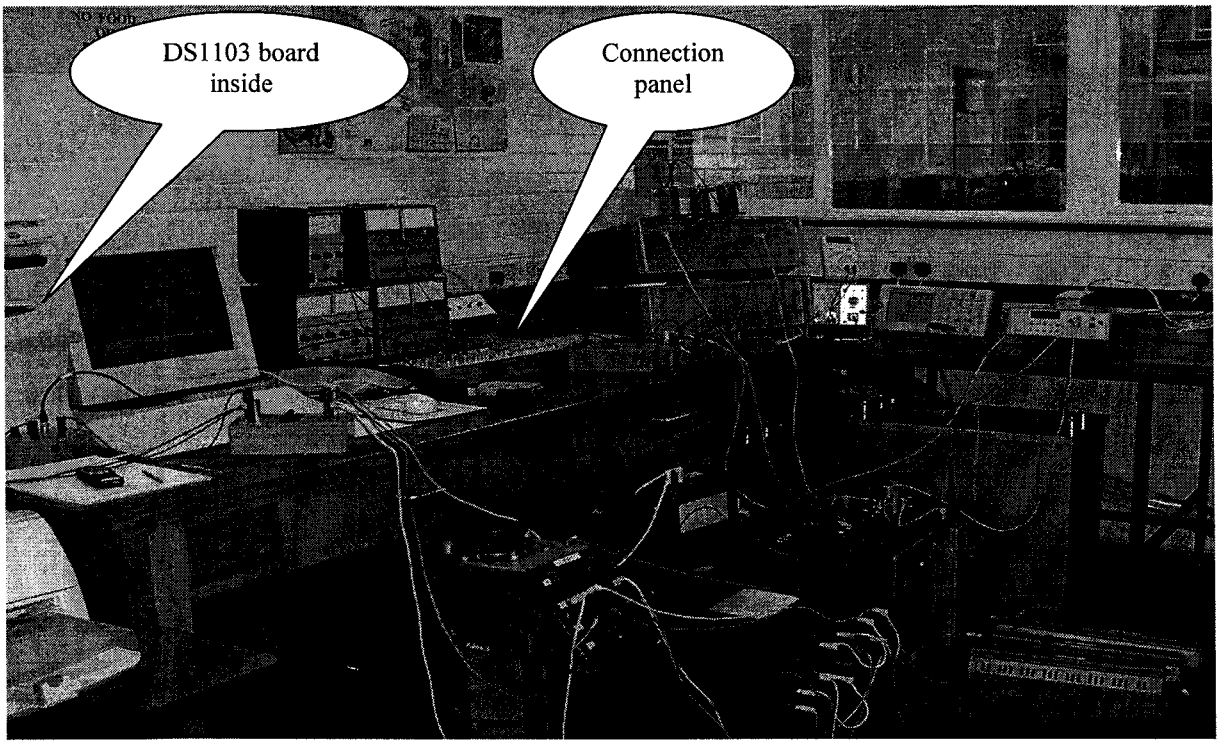

Figure 8.13-a UPFC overall experimental model.

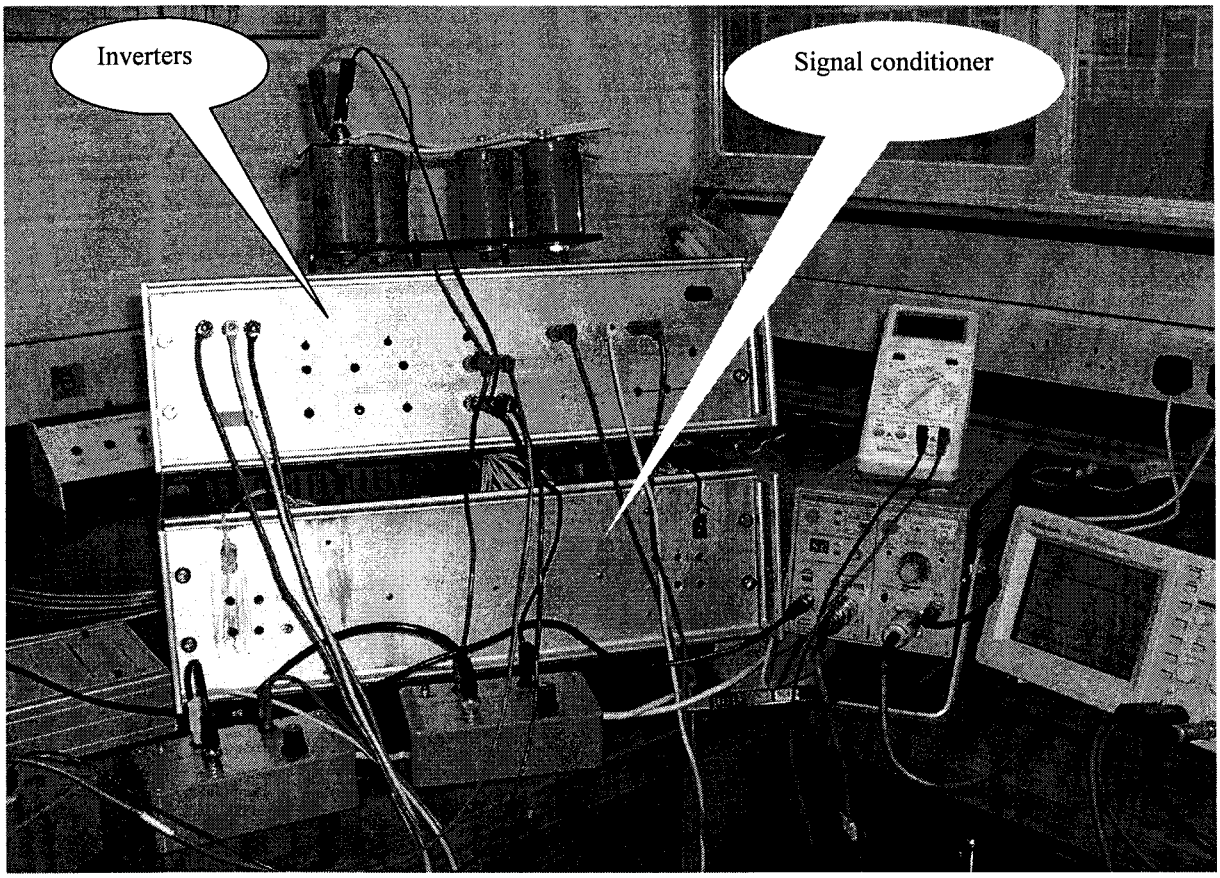

Figure 8.13-b Inverters and gate signal conditioner cabinets.

8.5.2 System Operation with High Short Circuit Level

The system is arranged to operate under high short circuit level by adjusting the inductance behind the system busbar V_1. In this case, only the leakage inductance of the phase shifting transformer (shown in Figure 8.1) is considered. A series of individual step changes in the main reference signals were applied in order to investigate the UPFC capabilities in controlling the power flow, regulating the bus voltage and adjusting the d.c. link voltage. The four controllers mentioned earlier have been applied and tested. Four scenarios of the changes in the reference signals were performed. The controlled real and reactive power (P and Q indicated in the results) are measured at the line-side terminal of the booster transformer. The system bus voltage, at which the UPFC is connected, symbolised as V_1, while V_{dc} represents the d.c. link voltage.

Scenario 1 changes in the active power:

The aim of this test is to make step change in the line active power (P) while keeping the reactive power (Q), the bus voltage (V_1) and the d.c. link voltage (V_{dc}) constant. As shown in Figure 8.14, a change of 0.2 p.u. is occurred at time 2s and the real power reference is returned to the initial state at time 12s. It is clear from the results shown in Figure 8.14 that the system controlled by PI or Fuzzy-like-PI (FZ-PI) controllers suffers from long delay time. There is no systematic way to follow in designing the parameters of the PI controller and the scaling factors of the FZ-PI controller in real time. Therefore, these parameters have been assigned by trial and error. The parameters are chosen to reduce the rise time as much as possible and at the same time minimising the influence of this control loop on the other control loops within the system.

For the ANFIC-PI and ANFIC-FZ, the UPFC series inverter parameters are controlled by off-line trained ANFIC while PI and FZ-PI are used to regulate the shunt inverter parameters, respectively. It is noticed that there is no significant difference between

the system response due to ANFIC-PI or ANFIC-FZ, as the real power is controlled by the ANFIC part of the whole controller, which is the same for both.

It is obvious from these results that the RBFNN controller trained on-line by gradient descent gives the best response, as the real power smoothly reached the desired steady-state. In the same time, RBFNN controller reduces the interactions between the real and reactive power flow as compared with the other controllers. The good response of the RBFNN controller is associated with its simple structure; one neuron with on-line tuned weight and bias.

Scenario 2 changes in the reactive power:

The objective of this test is to regulate the system bus voltage, the d.c. link voltage and keep the line real power constant while making step changes in the reactive power flow at the line sending-end. As shown in Figure 8.15, the reference of the reactive power is increased by 0.15 p.u. at time 7s and returned to the initial state at time 17s. It is clear from the results that the UPFC is capable of controlling the reactive power while maintaining the other three quantities (V_1, V_{dc}, and P) constant. As discussed in the first scenario, the superiority of the RBFNN controller over the other controller is clear from the graph. It is obvious from the results shown in Figures 8.14 and 8.15 that the series inverter parameters do not have great impact on the shunt inverter parameters.

Scenario 3 changes in the d.c. link voltage:

In this test, the capabilities of the UPFC shunt inverter to independently control the d.c. link voltage and to keep the bus voltage constant is presented. A ±10% step change in the d.c. voltage reference signal is applied. It is clear from the results shown in Figure 8.16 that the operation of the UPFC inverters can be independent. The change in the d.c. voltage affects all the UPFC parameters, hence, the other controllers persevere to maintain the pre-change state.

There is no much difference in response of the PI and FZ-PI controllers especially in terms of the settling time. However, the FZ-PI controller of the d.c. link voltage control loop has less influence on the other system parameters. This also applies to ANFIC-PI and ANFIC-FZ while the interactions between the system parameters is minimised when the system controlled by the RBFNN controller.

Scenario 4 changes in the bus voltage:

The objective of this test is to produce step change at the system busbar while maintaining the real power, reactive power and the d.c. link voltage unaltered. The voltage reference was increased by 3% at time 7s and returned to nominal value (1 p.u.) at time 12s. The results shown in Figure 8.17 demonstrate that the UPFC can successfully maintain the real and reactive power flow in the transmission line, and at the same time regulate the d.c. link voltage. The changes in the bus voltage magnitude affects mainly the d.c. link voltage and the reactive power flow.

The system with PI controller takes a long time to reach the steady-state and produces the largest interactions between the system parameters.

For the results obtained from tests in the four scenarios described earlier, it is clear that the developed UPFC system is capable to maintain or vary the real and reactive power flow in the transmission line. Also, it can regulate the bus voltage through the shunt inverter capabilities. It is obvious that the PI controller parameters need to be optimized to allow good system response at different operating conditions. The FZ-PI controller gives slightly better response than the PI controller. However, the scaling factors of the controller input and output signals must be tuned for every operating point. The ANFIC controller is working adequately for controlling the series inverter parameters, although another classical controller for the shunt inverter is always needed. The on-line trained RBFNN controller (associated with adaptive learning function) gives the best overall response.

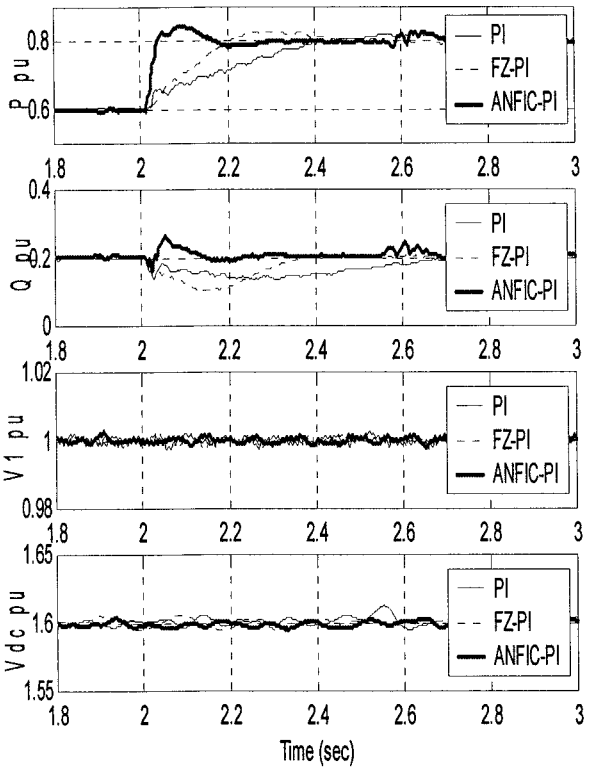

(a)

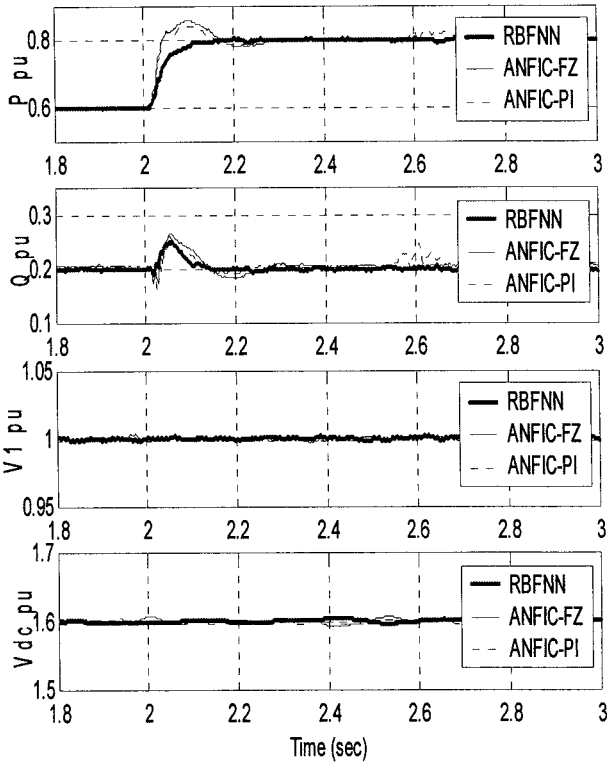

(b)

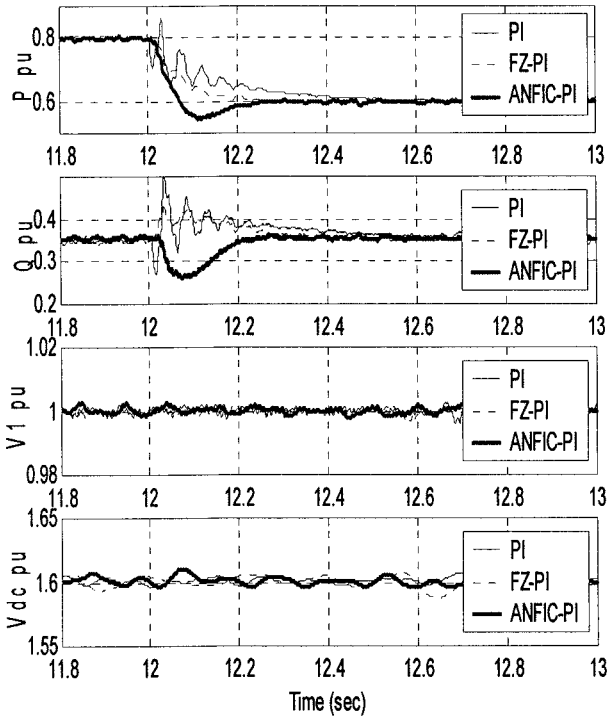

(c)

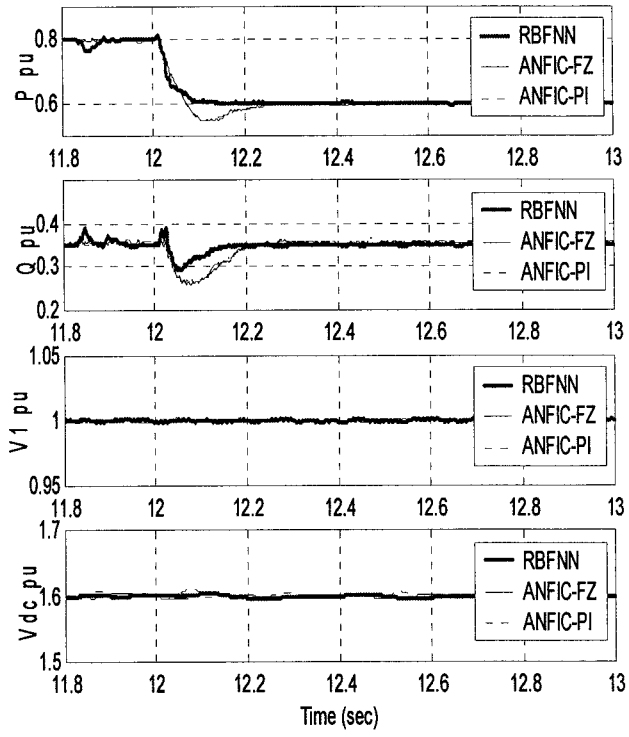

(d)

Figure 8.14 System response to step change in active power.

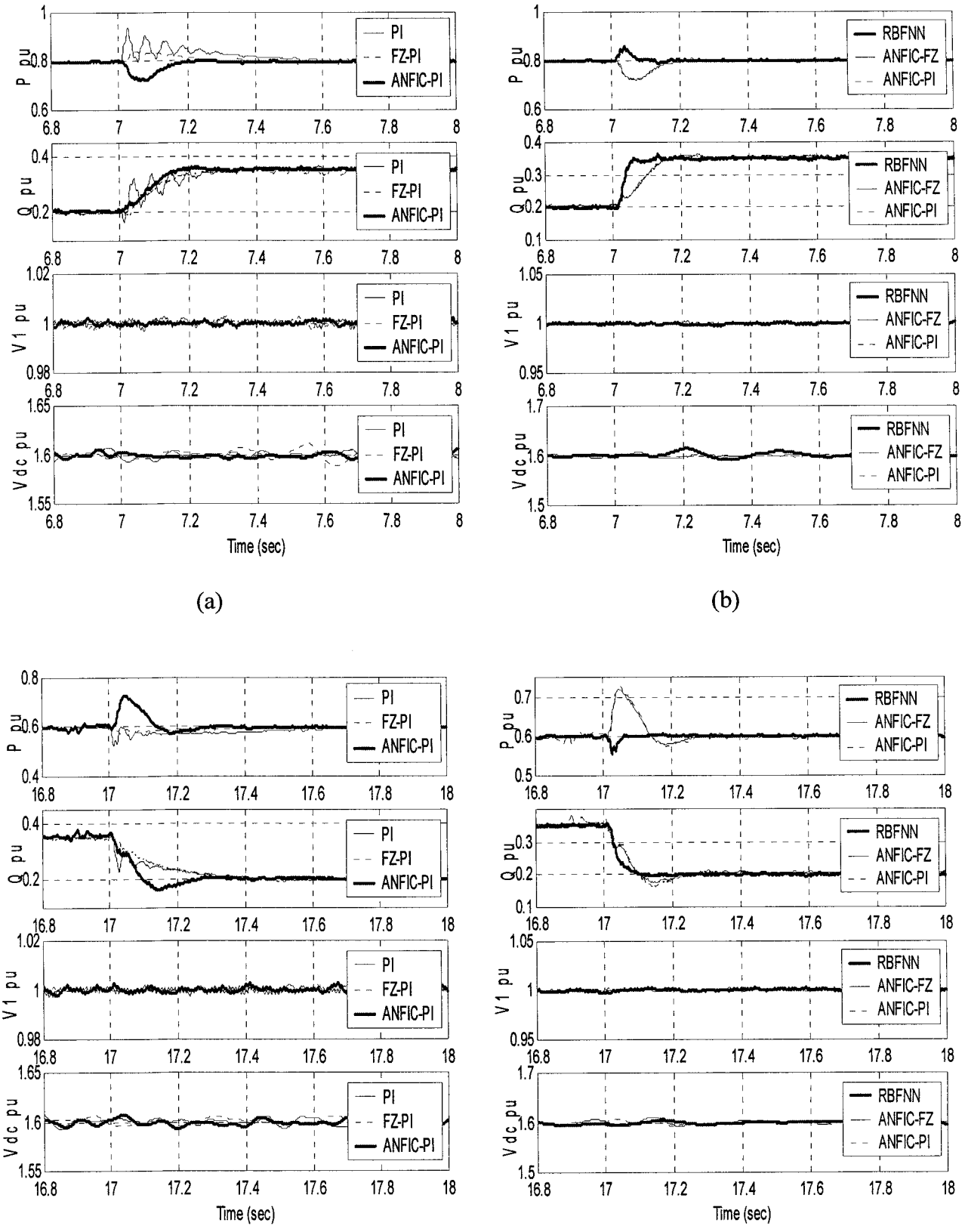

Figure 8.15 System response to step change in reactive power.

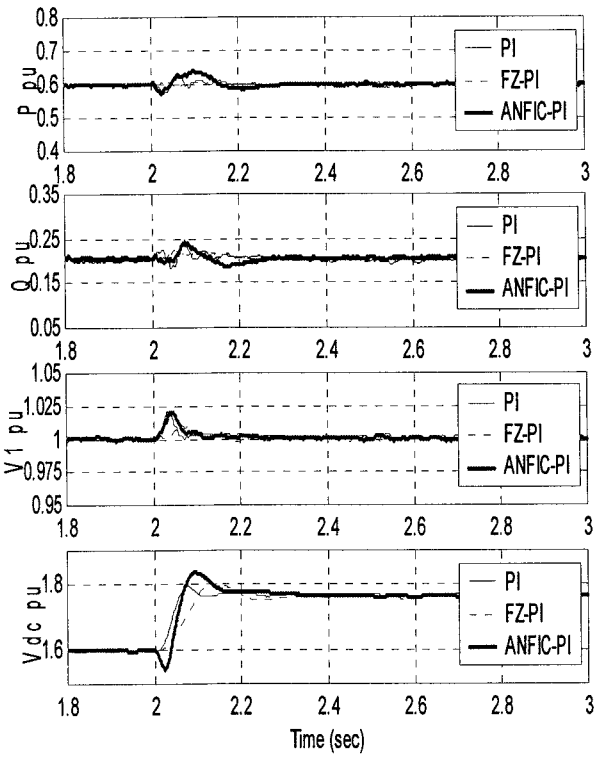

(a)

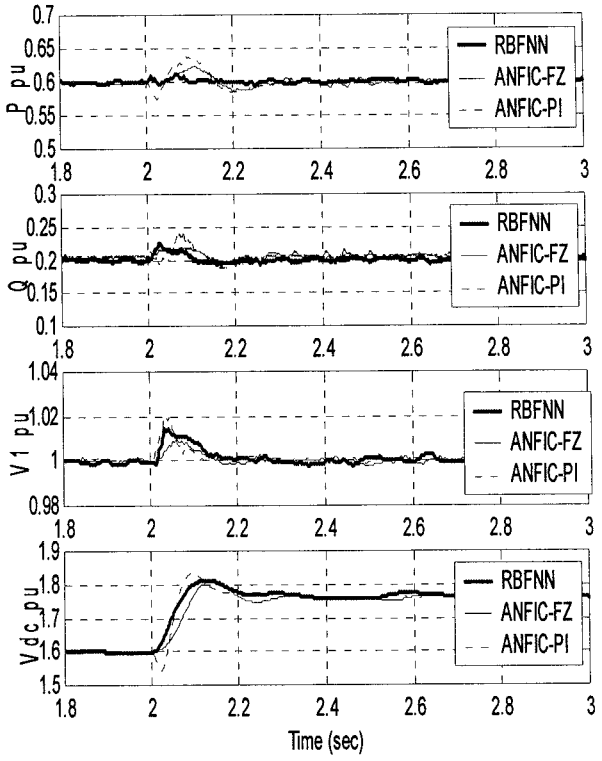

(b)

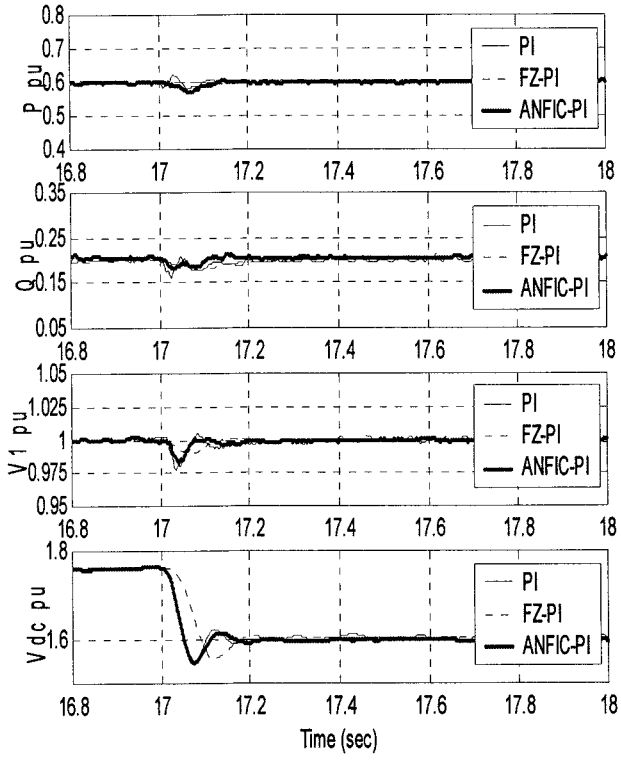

(c)

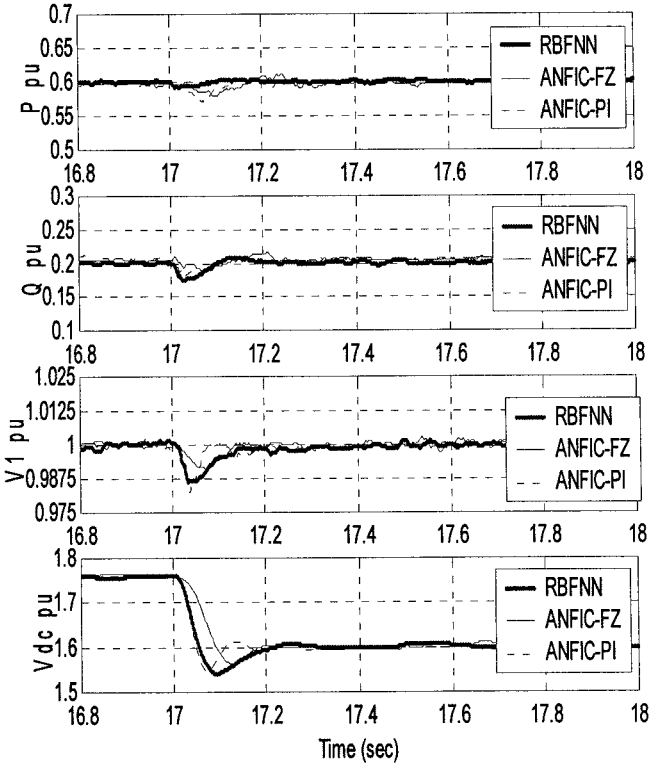

(d)

Figure 8.16 System response to step change in d.c. link voltage.

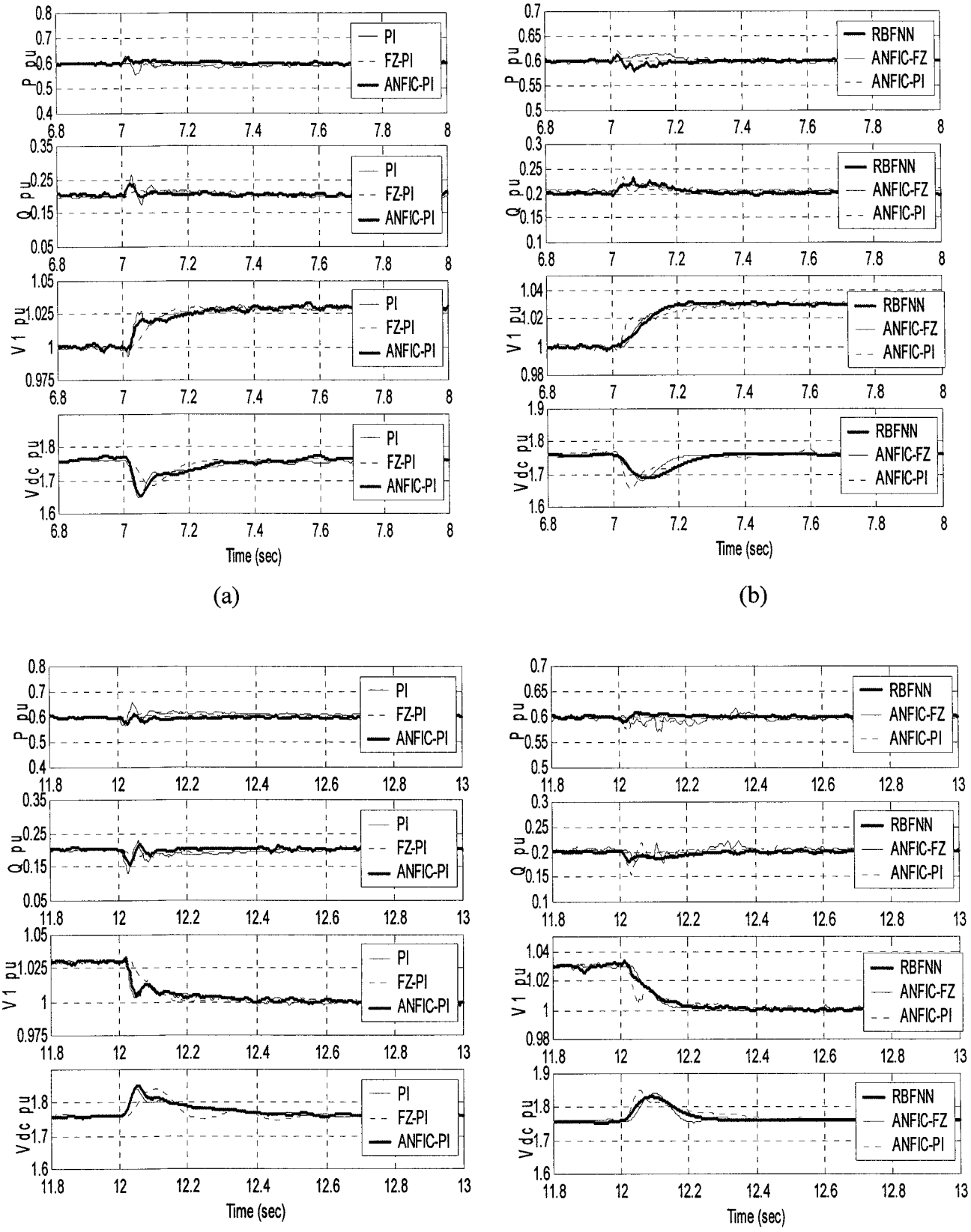

Figure 8.17 System response to step change in the test bus voltage.

8.5.3 System Operation with Low Short Circuit Level

In this case, an inductance was added to the source impedance to represent a reduction in the system short circuit level. When the four developed controllers were tested, it was found that the test bus voltage control loop is greatly affected by the new configuration. To regulate the bus voltage at 1p.u., the shunt inverter a.c. output voltage has to be increased. Hence, the shunt inverter has to work at large m_a. As discussed in Chapter 4, changing the system short circuit level affects the feasible operating area. Decreasing the SCL results in decreasing the real and reactive power flow in the transmission system. Therefore, to maintain the power flow at a certain level, the series inverter parameters (ϕ, m_a) were increased. The four developed controllers were applied to the system and step changes in the system reference signals were performed to test the robustness of the controllers.

Scenario 1 PI-controller:

The performance of the PI controller used in the previous case study (system with high short circuit level) was tested in this case. The system response to step changes in real and reactive power is shown in Figure 8.18 while the response due to changes in the bus voltage and the d.c. link voltage is shown in Figure 8.19. It was found that the PI controller was not able to generate a stable operation. Therefore, the controller parameters were modified to produce good performance. This is the main drawback of the fixed parameters controllers where they can not produce the same results at different operating conditions. It is noted from the results that the system speed of response is faster when the system becomes weaker.

Scenario 2 Fuzzy-like-PI controller:

The same changes performed in scenario 1 have been applied for the FZ-PI controller. The scaling factors of the controller input and output signals were modified to accommodate the changes in the system configurations. The system response to changes in

P and Q is shown in Figure 8.20. It is noted that, when the system becomes weak, the response is more sensitive to system changes and the interactions between different control loops become worse as shown in Figure 8.21. Therefore, designing different parameters for every operating condition is essential.

Scenario 3 ANFIC controller:

In this test, the performance of the ANFIC-PI and ANFIC-FZ controllers has been tested. As proposed in Chapter 7, the ANFIC is trained off-line to deduce the fuzzy rules which regulate the operation of the UPFC series inverter. The controller is trained for an ideal UPFC operation which assumed constant sending-end bus voltage. Hence, when the SCL is decreased the system active and reactive power operating points stay within the trained feasible region. The shunt inverter parameters are controlled using PI or FZ-PI controllers.

The system response to changes in system reference signals for the ANFIC-PI controller is shown in Figures 8.22 and 8.23 while the performance for the ANFIC-FZ controller is shown in Figures 8.24 and 8.25.

For these two controllers, the ANFIC parameters are kept unaltered and the system response is almost the same for both high and low short circuit levels (HSCL, LSCL). The shunt inverter controllers were updated in a way similar to scenario 1 for ANFIC-PI and scenario 2 for ANFIC-FZ.

Scenario 4 RBFNN controller:

The objective of this test is to examine the performance of the on-line trained RBFNN controller with different system short circuit levels. The system response to changes in power flow references is shown in Figure 8.26 while Figure 8.27 shows the system performance for step changes in the bus voltage and the d.c. link voltage. As the gradient descent learning algorithm modifies the controller parameters to suit the system changes, the controller gives an adequate response for the described two short circuit levels.

The adaptive learning rate function plays an essential role in stabilising the system performance. As discussed earlier, the system bus voltage is greatly affected by the changes in the system SCL, the shunt inverter responses (V_1, V_{dc}) oscillate for few cycles before they settle at the steady-state value. This oscillation may be eliminated by investigating different learning rate functions for the controller variables (weight, spread and centre).

Generally, the parameters of the conventional PI controller and the classical fuzzy controller need to be re-tuned when the system conditions are changed. However, the ANFIC and RBFNN controllers are giving better performance and at the same time they are less sensitive to the system changes. For ANFIC, this is because the changed system conditions can be covered in the training phase. For the RBFNN, the superior performance is attributed to its on-line training capability.

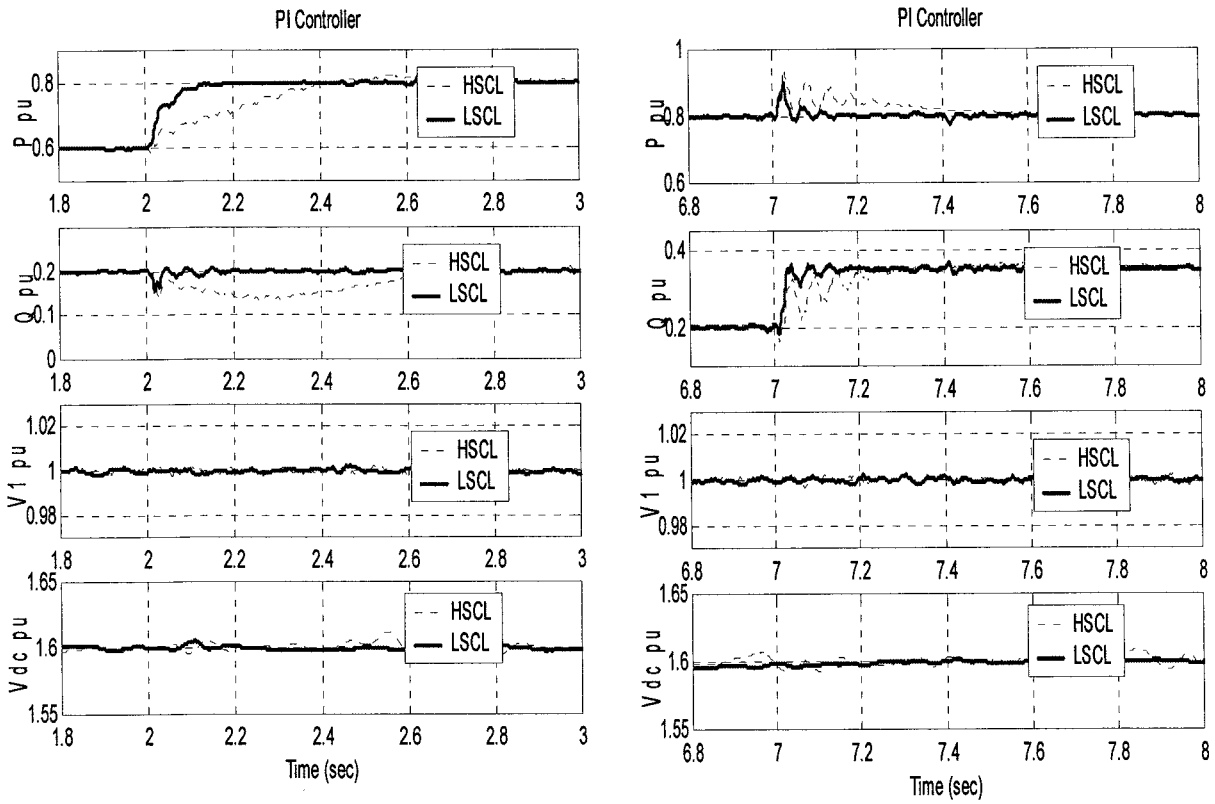

Figure 8.18 System response with PI controller to changes in P and Q.

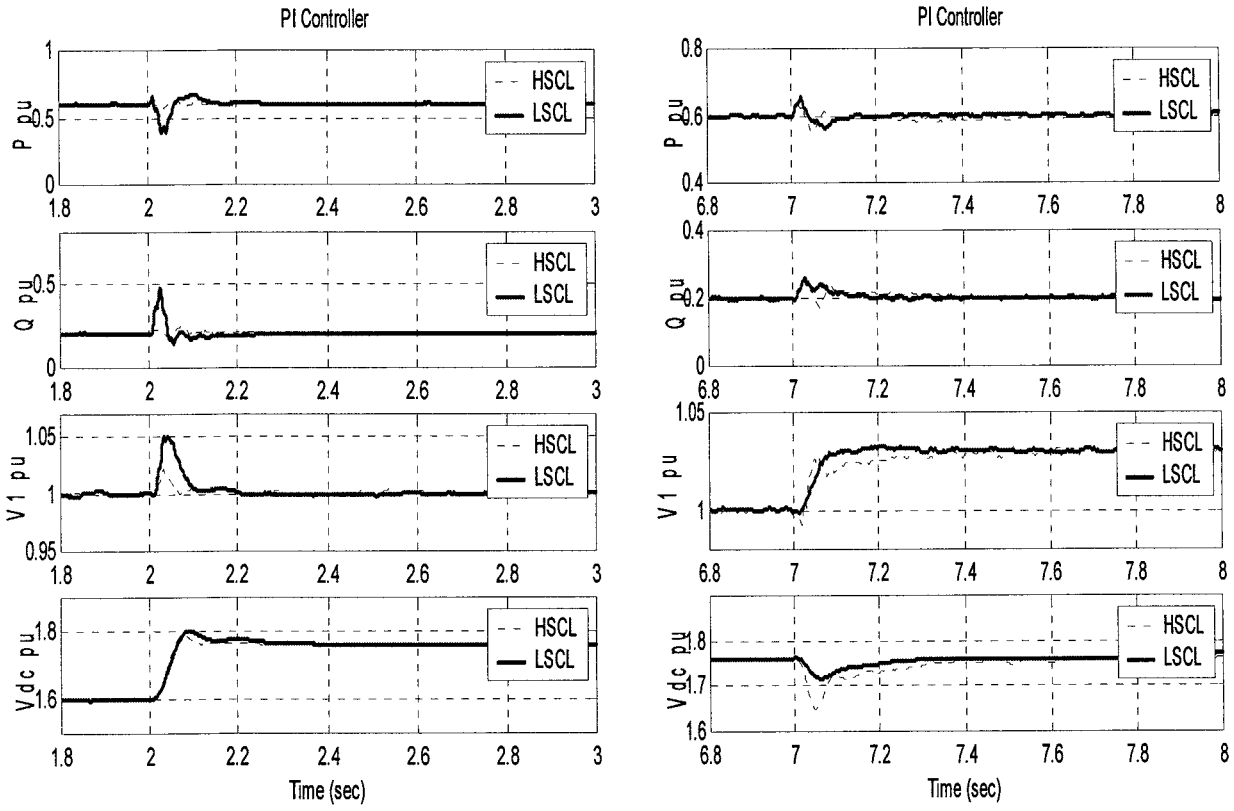

Figure 8.19 System response with PI controller to changes in V_1 and V_{dc}.

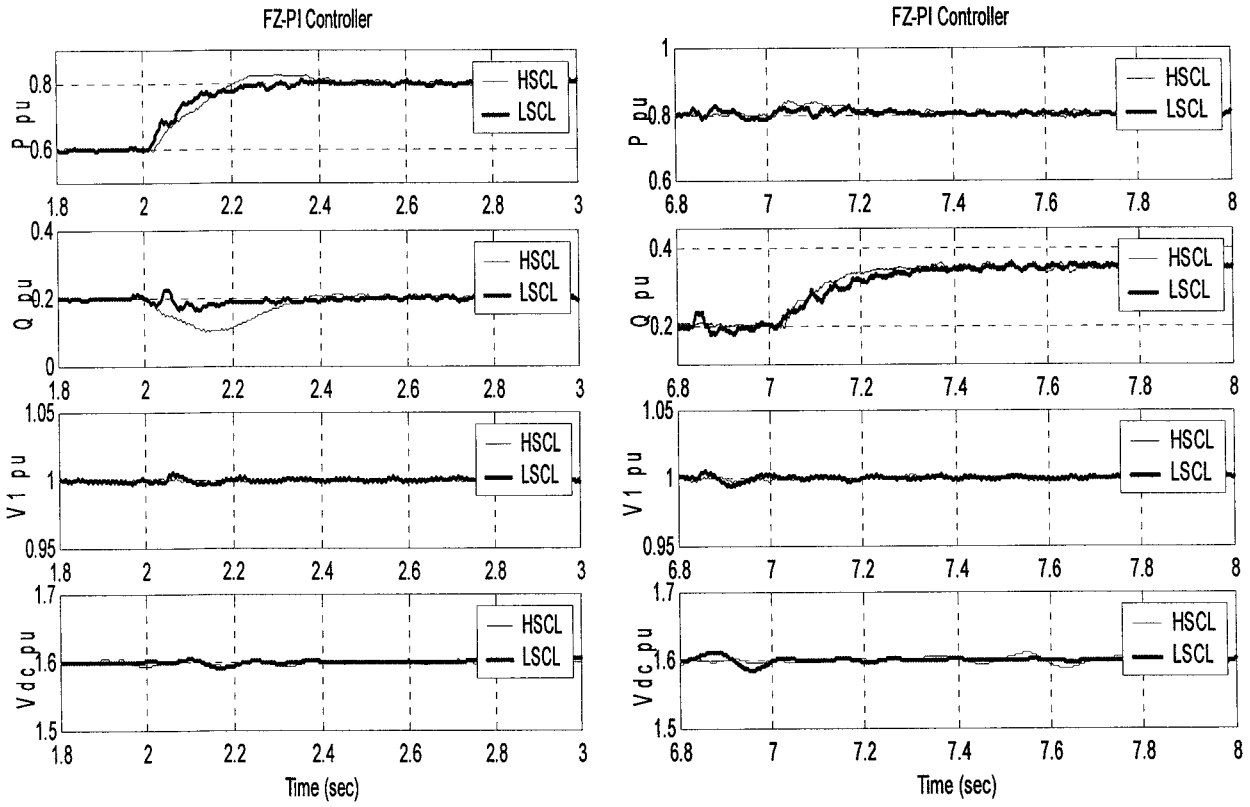

Figure 8.20 System response with FZ-PI controller to changes in P and Q.

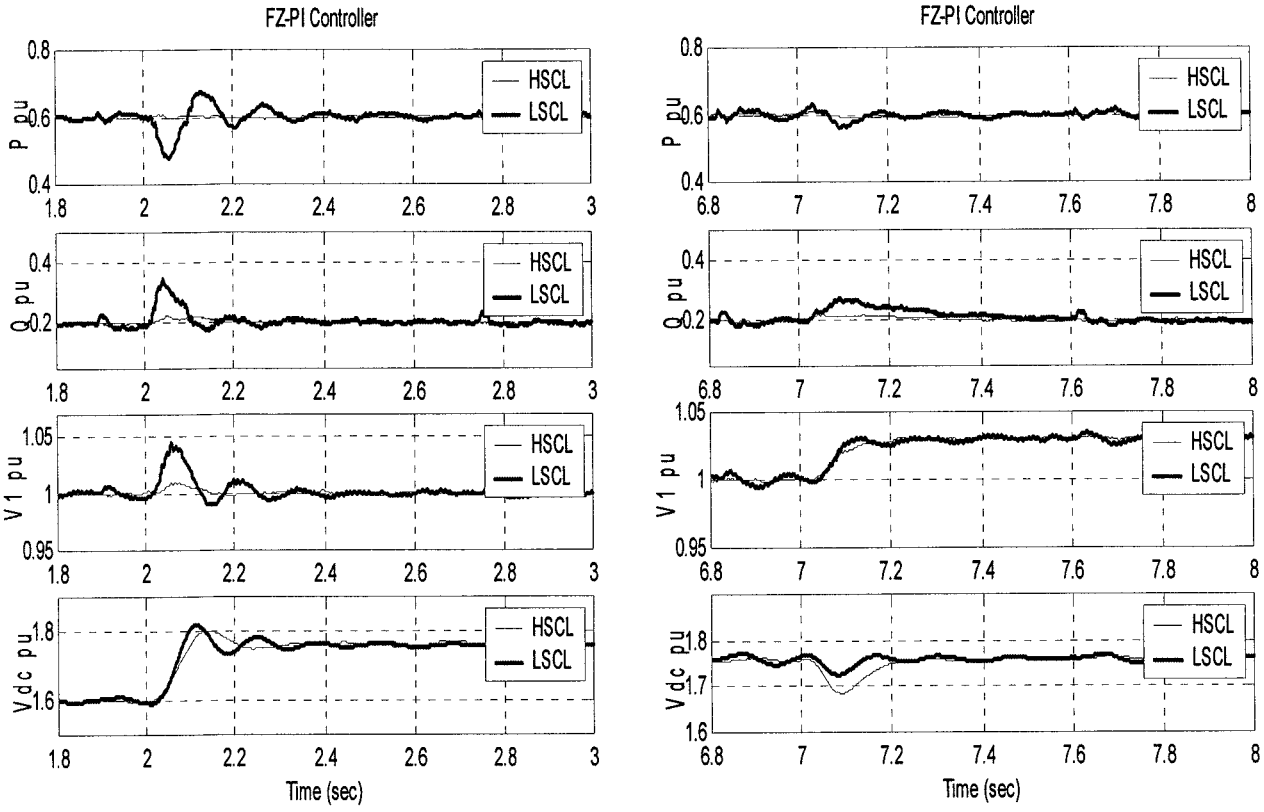

Figure 8.21 System response with FZ-PI controller to changes in V_1 and V_{dc}.

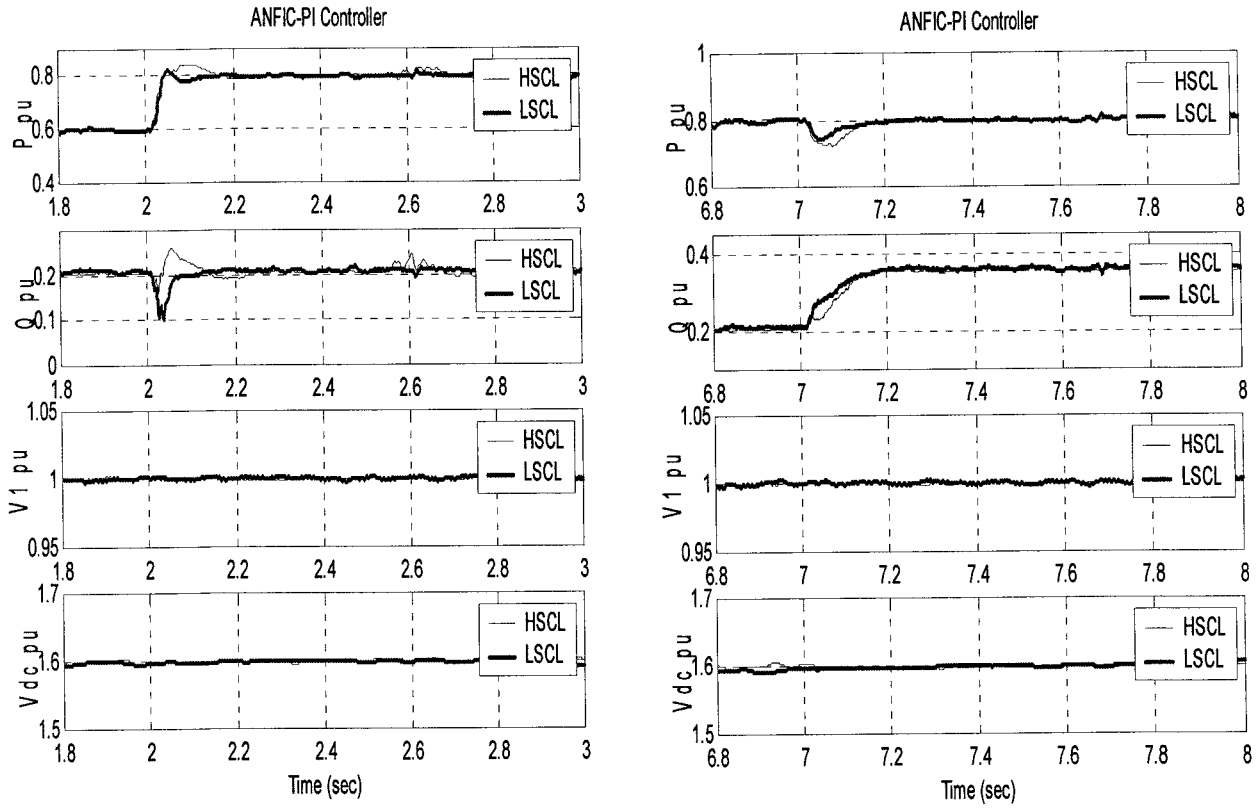

Figure 8.22 System response with ANFIC-PI controller to changes in P and Q.

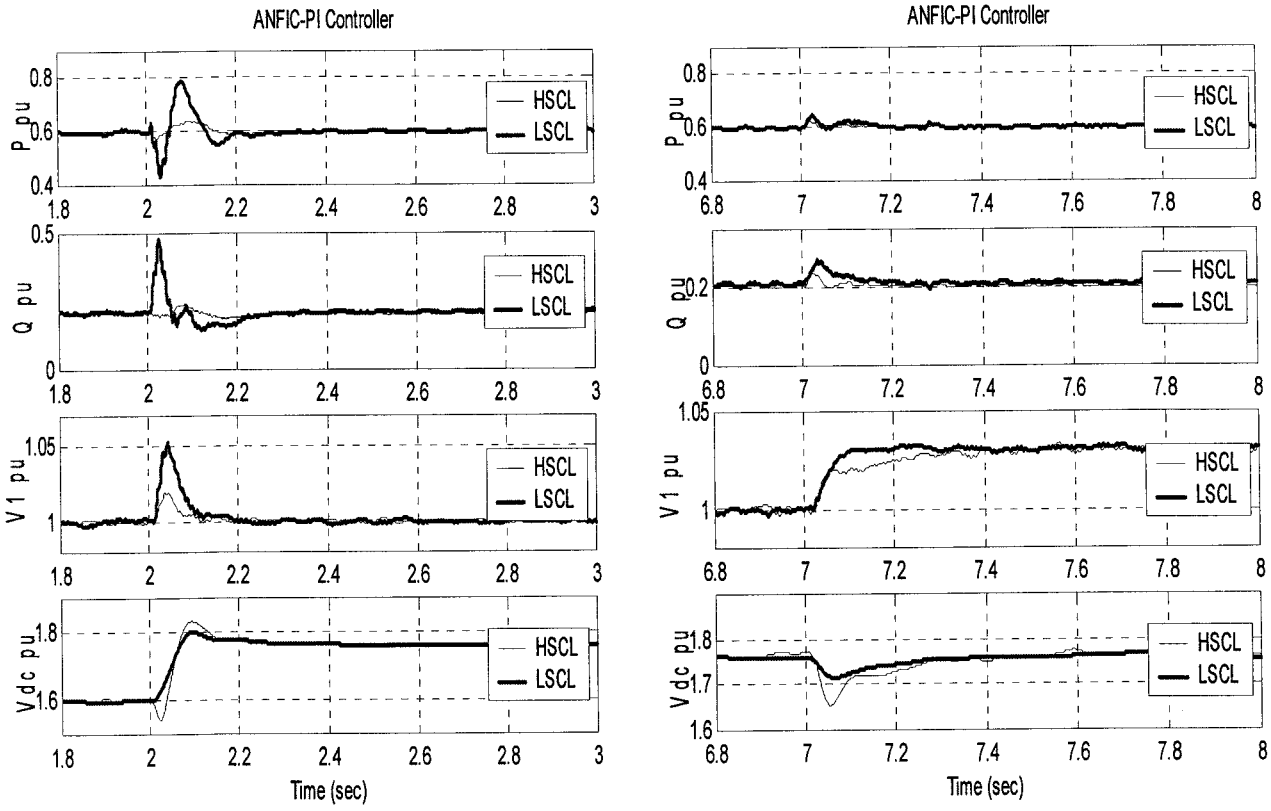

Figure 8.23 System response with ANFIC-PI controller to changes in V_1 and V_{dc}.

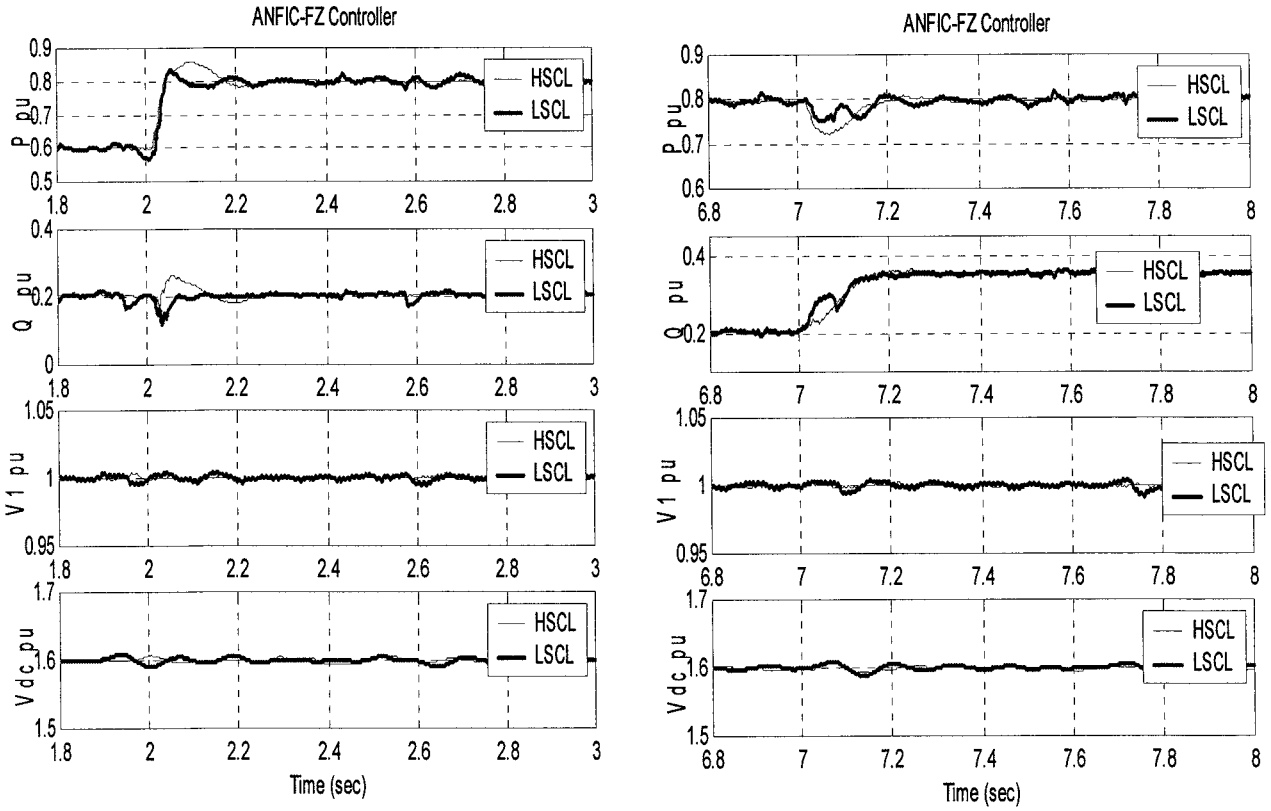

Figure 8.24 System response with ANFIC-FZ controller to changes in P and Q.

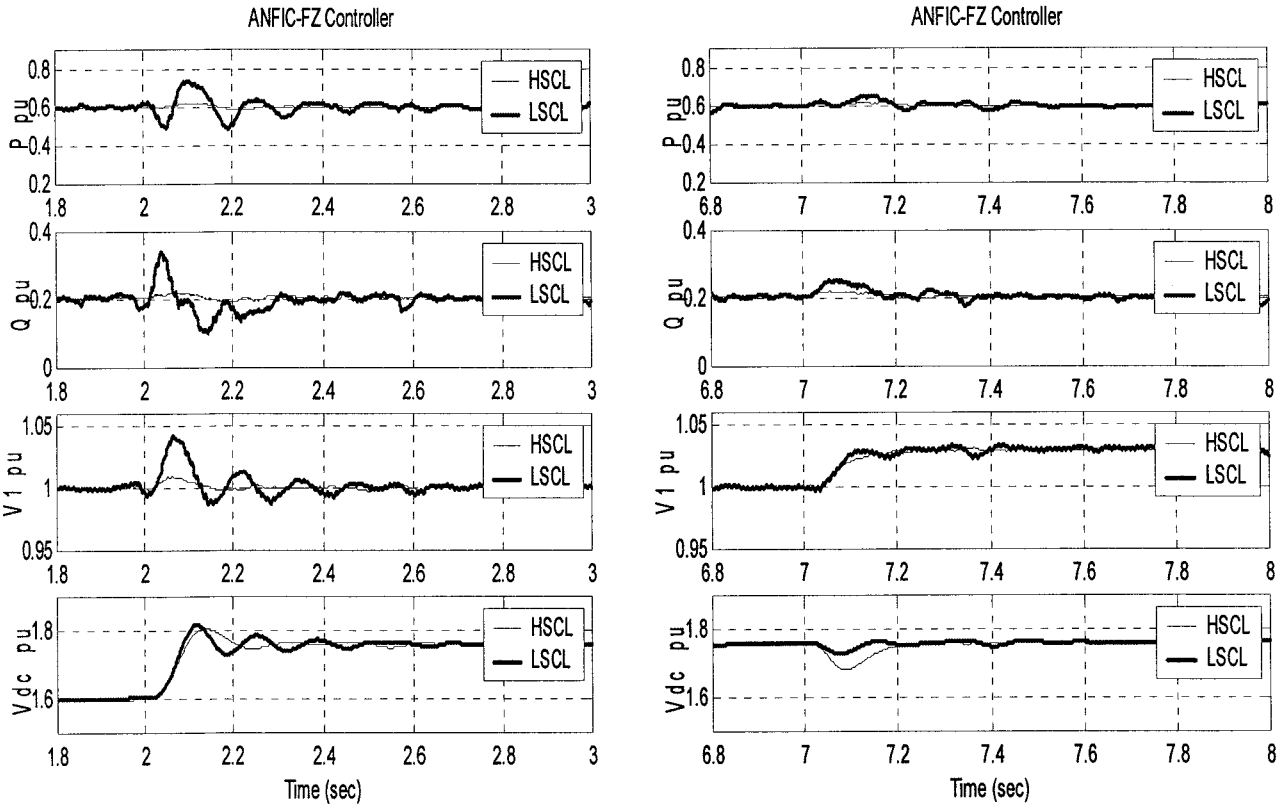

Figure 8.25 System response with ANFIC-FZ controller to changes in V_1 and V_{dc}.

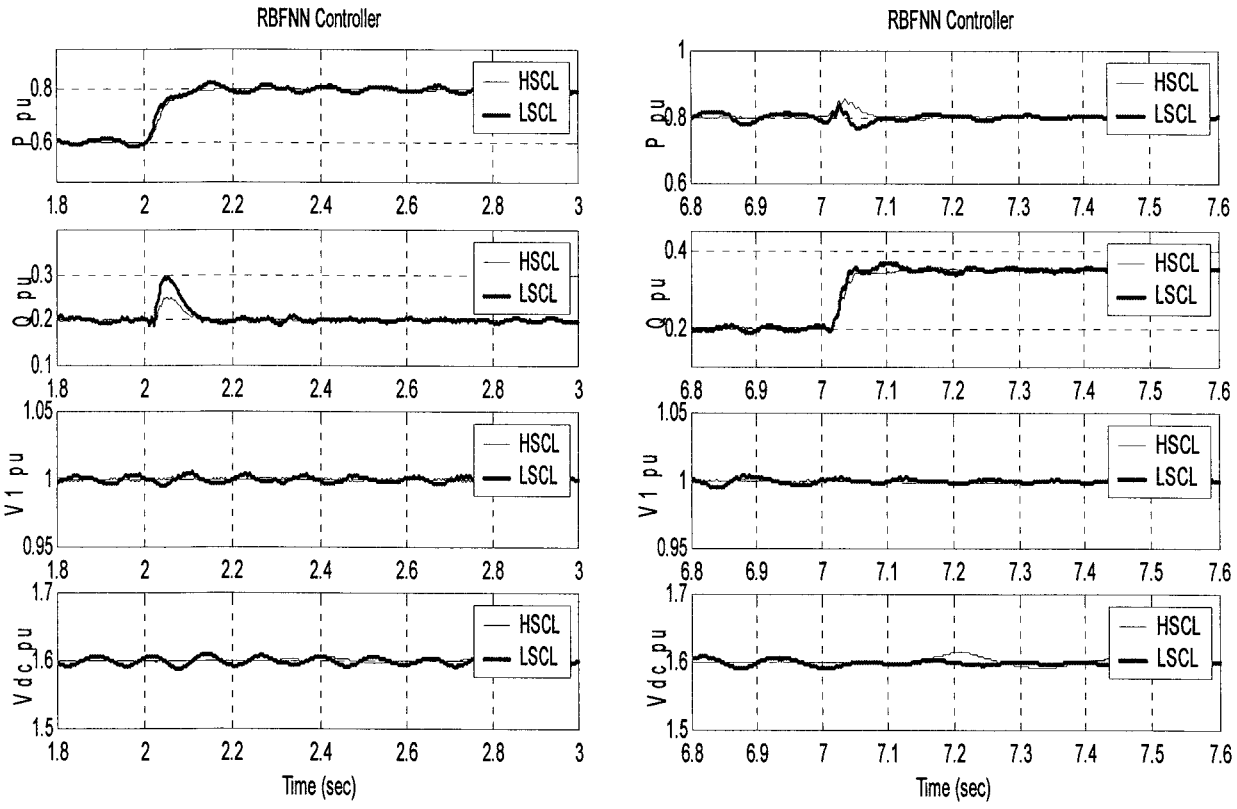

Figure 8.26 System response with RBFNN controller to changes in P and Q.

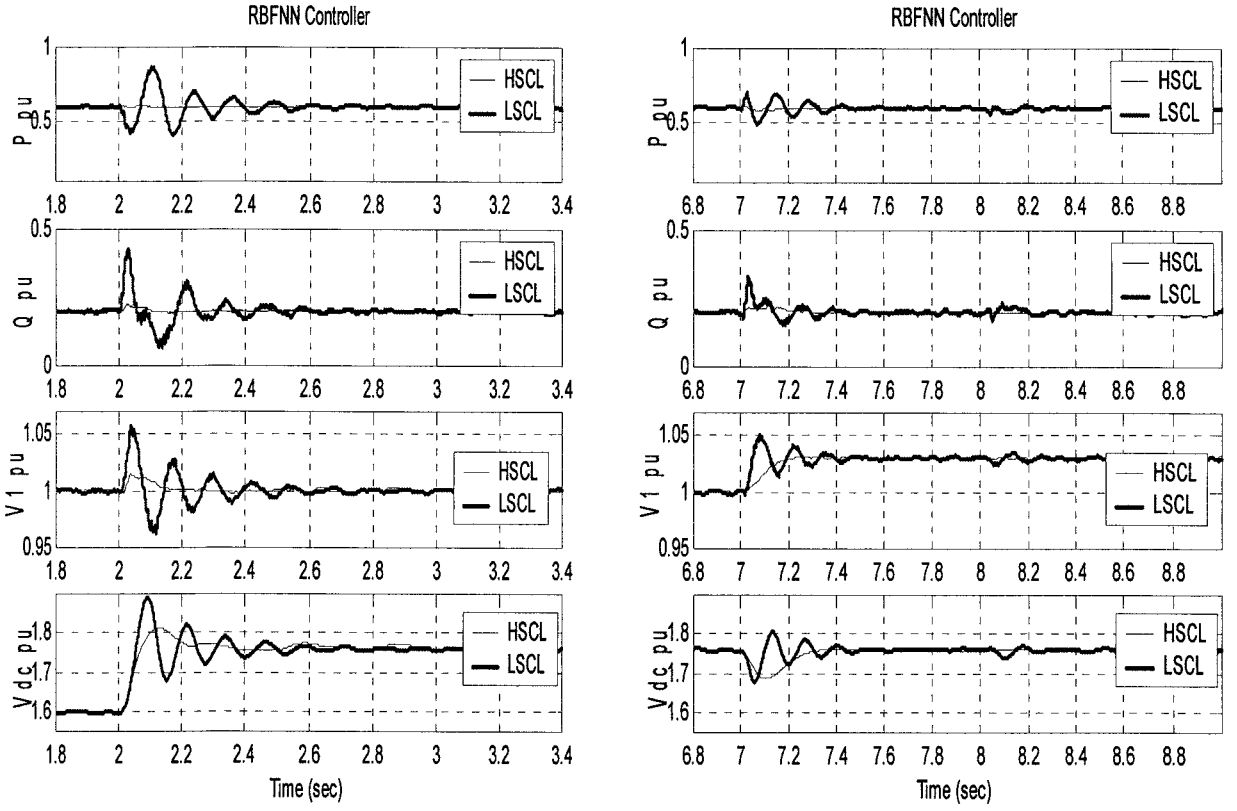

Figure 8.27 System response with RBFNN controller to changes in V_1 and V_{dc}.

8.5.4 Sudden Change of System Short Circuit Level

In this case, the source inductance is changed while the system is running to represent a sudden change in the system short circuit level. The performance of the proposed controllers was examined in this test. Initially the system was running with high short circuit level and the controller parameters are adjusted accordingly. The system was performing exactly like the first case discussed in Section 8.5.2. An inductance was switched into the circuit for a few seconds to represent fault occurred at the system side which results in reduction of the SCL and then switched out. The system responses under the effect of PI, FZ-PI and RBFNN controllers are shown in Figures 8.28-8.30, respectively. It is clear from these results that the PI and FZ-PI controllers are not able to stabilise the system performance under the changing conditions. However, as confirmed by the results given in Section 8.5.3, the RBFNN controller is capable of accommodating the system changes and generate the appropriate control signals.

In this chapter, the experimental set up of the UPFC model is developed. The various controller schemes discussed in Chapters 6 and 7 have been tested. Three case studies were conducted for different system conditions. From the results, the RBFNN controller is proved to have better response than other controllers.

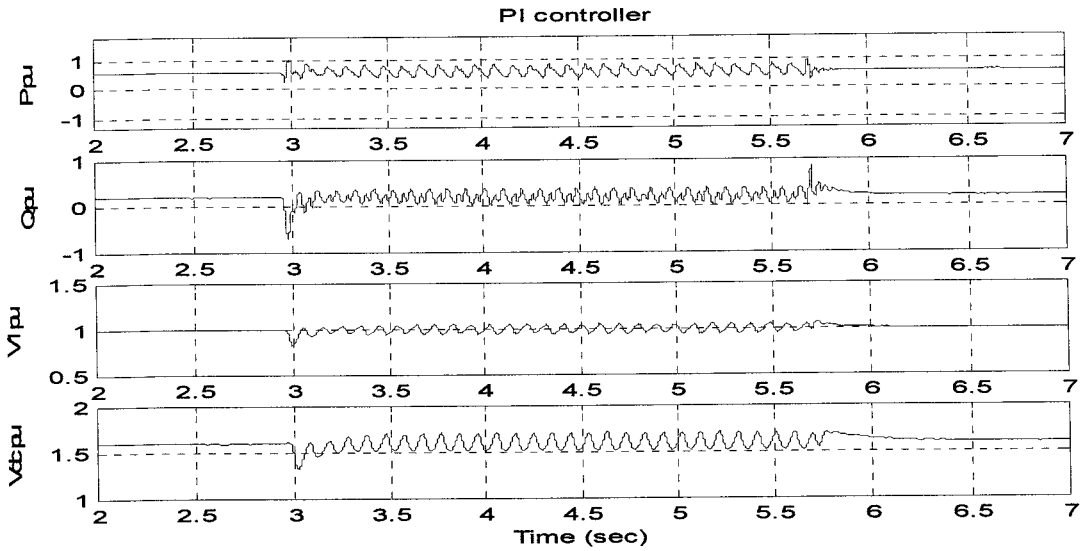

Figure 8.28 System response with PI controller to sudden change of SCL.

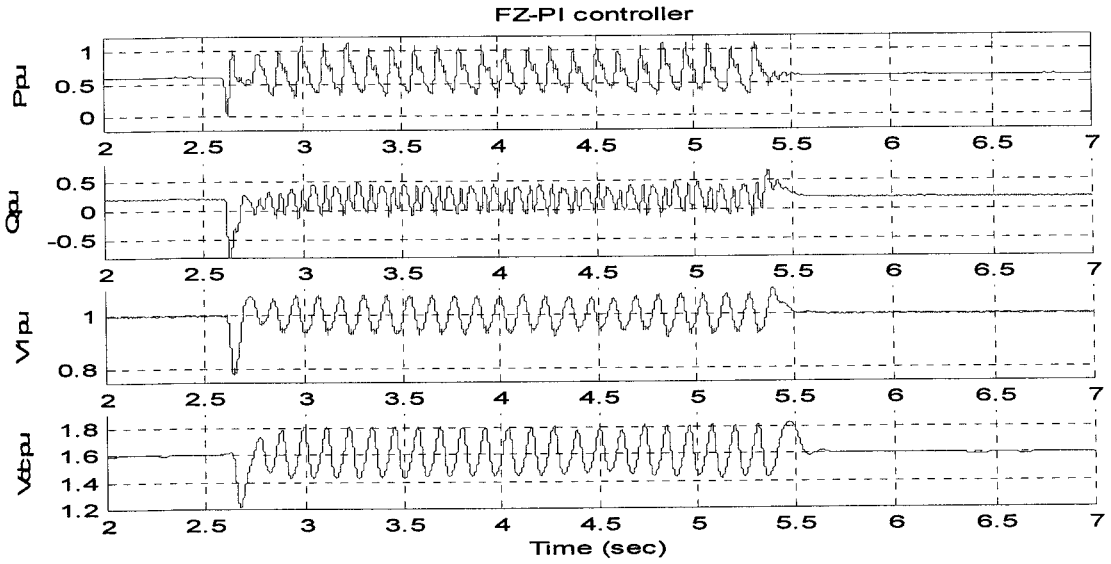

Figure 8.29 System response with FZ-PI controller to sudden change of SCL.

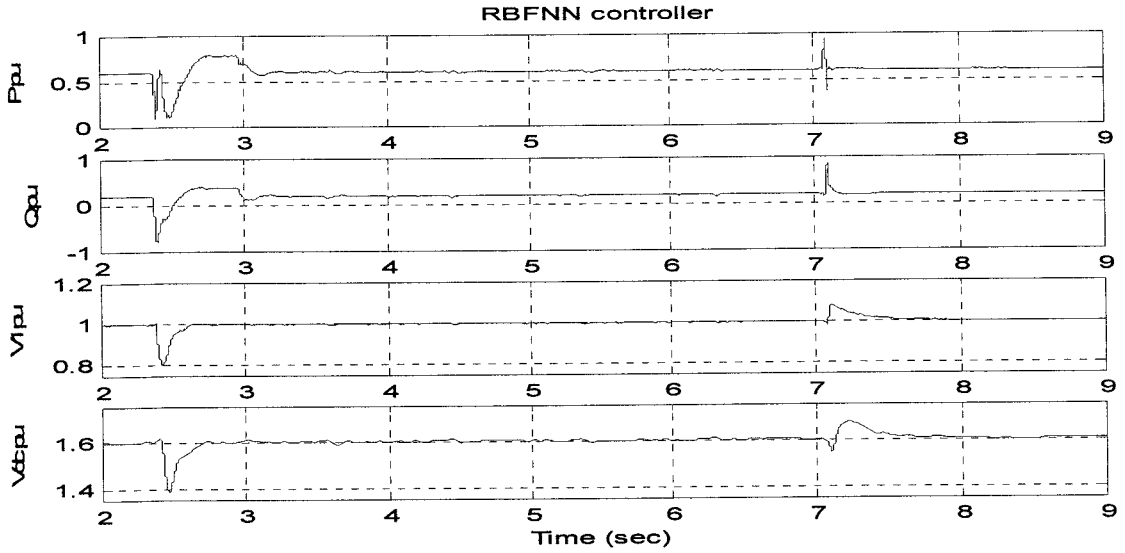

Figure 8.30 System response with RBFNN controller to sudden change of SCL.

CONCLUSIONS

In the work reported in this thesis, computer model of the UPFC incorporated in a typical transmission system has been investigated and tested. This model was used to demonstrate the capability of the UPFC to independently control the real and reactive power flow and to regulate the system bus voltage. Three modern controllers have been designed and tested. These controllers are: a fuzzy knowledge based controller, an artificial neural network based controller and a neuro-fuzzy based controller. To verify the computer simulation, an experimental laboratory model was designed and tested.

Conclusions are structured in five main sections. The first section is general conclusions for the UPFC operations and models. The second covers the system feasible operating area and the effects of change in the system short circuit level. The third considers the design of UPFC modern controllers to regulate the three power system parameters. The fourth discusses the key finding from the investigation made using the experimental model. Finally, suggestions for further work are given.

9.1 UPFC OPERATION AND MODELLING

The UPFC was identified as a promising device for multiple function and fast response compensation. Its relative advantages compared to other FACTS controllers were discussed. Different modes of UPFC operation have been investigated and the effects of the UPFC control variables on the real and reactive power flow have been analysed.

Various modelling techniques of the UPFC in transient or steady-state studies were reviewed and summarised. For the electromagnetic transient model, the relative advantages of three switching strategies; Fundamental Frequency Modulation (FFM), Selective Harmonic Elimination Modulation (SHEM) and Sinusoidal Pulse Width Modulation

(SPWM) were deemed to be suitable. The SPWM was selected as preferred choice for the work conducted in the experimental phase of this study. For the steady-state model, a computer simulation in MATLAB/SIMULINK environment was developed where each of the UPFC inverters was represented by a controlled voltage source. This model is appropriate for the control algorithms investigated in this thesis.

An "exact" power injection model of the UPFC has been proposed which is based on polar representation of its control variables (injected voltage magnitude and phase angle). The reactive power injection of the shunt inverter was taken into consideration. This model provides better representation of the UPFC in load flow analysis and study.

9.2 SYSTEM OPERATING LIMITS

The most common constraints which should be taken into account when dealing with the UPFC control capabilities are identified. These limits were summarised as the VA rating of the UPFC inverters which should be determined at the planning phase. The transmission system operating area results from installing the UPFC is defined which is a function of the system transmission angle. The analysis conducted in this work defined the system feasible operating area based on the maximum inserted voltage of the UPFC series inverter.

The analysis carried out in this work showed that the reactive compensation capability of the UPFC shunt part increases the system feasible region. The increase is dependent on the VA rating of the shunt inverter. As the real power demand of the series inverter is to be supplied by the shunt inverter, the VA rating of the latter should first be reserved to supply this demand; the surplus rating can be used to extend the feasible operating area.

The effects of changes in the system short circuit level (SCL) on the feasible area have been investigated for the series inverter. It is shown that the size of the system feasible

operating area is directly proportional to the system SCL. The area is reduced as the system becomes weaker and the UPFC output voltage has to be increased if the power flow and system busbar voltage are to be kept constant. Mathematical analysis describing the effects of the system SCL on the UPFC shunt inverter speed of response was also conducted. The results obtained show that the system speed of response increases when the SCL decreases.

9.3 UPFC CONTROLLERS

To study the closed-loop response of the UPFC in controlling the power flow and supporting the bus voltage, three modern controllers have been designed and tested in computer simulation and real time implementation.

A fuzzy-based rules controller was designed and tested in the computer simulation phase. The analysis shows that this controller has an adequate response with small interactions between the real and reactive power flow. Due to the requirement for large memory and computation time, it was not possible to implement this controller in the experimental lab model. For the same reason, this controller may not be suitable for real time implementation.

An Artificial Neural Network (ANN) based controller has also been investigated. In this sense, three network structures have been designed and tested. The first is an off-line supervised Multi Layer Perceptron Back Propagation (MLPBP) trained by back propagating the system error signal to tune the network parameters. A training algorithm was proposed which produces minimum training error for the UPFC series inverter control variables. The second network structure investigated is an off-line supervised Radial Basis Function Neural Network (RBFNN). It is recognised that complex structured network although it consumes long training time and memory allocation but it gives better response. It has been shown that for good response of the RBFNN based controller too many data need to be used for

training. Also, for the same data set, the MLPBP based controller has a better performance than the RBFNN based controller.

The third structure considered is an on-line trained (single neuron) radial basis function. It has been investigated to overcome the batch-learning difficulties. Due to its simple structure, this controller was implemented in the lab model as well as the computer simulation. The results obtained show that this controller gives an adequate system response and reduces the interactions between the real and reactive power flow.

An adaptive neuro-fuzzy controller has also been proposed to optimize the fuzzy rules and membership functions size and shape. The controller was implemented in both computer simulation and real time to control the UPFC series inverter. The controller performance proved to be acceptable for different system conditions.

9.4 EXPERIMENTAL LAB MODEL

To verify the theoretical and simulation results, an experimental laboratory model of the UPFC has been designed, constructed and tested. The UPFC was constructed using two 6-pulse inverters employing IGBTs as switching devices. The investigated controllers were implemented in SIMULINK environment and downloaded to the dSPACE DS1103 data acquisition board. The DS1103 was found very flexible in performing the control algorithms. The controller parameters can be optimized on the fly without changing the SIMULINK model. Also, the ControlDesk software associated with the board allowed monitoring the system variables and capturing long history for further analysis.

Based on the features of the DS1103, the controller SIMULINK model included the signals measurements, the system reference signals, the controller algorithm, Digital Phase Locked Loop (DPLL) and SPWM used for generating the switching pattern for the IGBTs.

The real time performance of the proposed controllers has been tested using different system conditions. Change in the system SCL was selected to evaluate the controllers' robustness. Three case studies have been conducted. In the first case, the system was operating with high short circuit level. In the second, the system was operating with low short circuit level. In the third, the system response to sudden change in the SCL was evaluated. For the first two cases, the system response to step change in the system reference signals (real power, reactive power, bus voltage and the d.c. link voltage) has been investigated. The results obtained show that the simple structure RBFNN controller perform better than other controllers.

9.5 FURTHER WORK

Based on the experience gained from this work and the results accomplished, the following aspects of UPFC operations require further investigation.

9.5.1 Improvement of the UPFC Experimental Model

- **System protection**

Further work is required to provide an adequate over current protection of the UPFC inverters. Also, some work is required to obtain better filter configuration at the inverters output coupling points.

- **Soft starting**

The d.c. link voltage may be developed using an additional charging circuit or using the free-wheeling diodes in the shunt inverter. A high inrush current is inevitable when energising a discharged capacitor and investigations are required to study the performance of the shunt inverter under starting conditions. Also, for the series inverter, the gate pattern should not be applied unless the d.c. voltage side reached its desired value. Further investigation is required to design electronic switch to synchronise the inverters' operation.

9.5.2 Improvement of UPFC Control Aspects

The following points identify possible further research that may be conducted to investigate the full potential of the proposed UPFC controllers.

- **Unbalanced system operation**

In this study, the system was considered to be symmetrical. Therefore, one phase parameters were used to control the three-phase system. Further work is required to study the performance of the UPFC under unbalanced system voltage conditions. The work may

include operation of the UPFC inverters with independent control of the three phase voltages to achieve voltage balancing and perform various control functions of the UPFC.

- **During fault operation**

The operation of the UPFC under system faults is an area of further research where a criterion is required to decide under what fault conditions the UPFC would, or would not, continue to operate and how to operate.

Another area worth considering is to use the controllers for damping power oscillations due to system disturbances.

- **Real time computation**

The Fuzzy-like-PI controller based on Mamdani definition was found to require large memory and computation time. This makes it not suitable for real time implementation. Further work is required to optimise its rules base and computation time.

- **Shunt inverter learning based controllers**

The direct relationship between the power flow and the UPFC series inverter control parameters has led to designing ANFIC and off-line trained neural network controllers. A similar relationship for the shunt inverter parameters at one side and the bus voltage and d.c. link voltage at the other side needs to be found, in order for these controllers to be applied to the shunt inverter.

- **Adaptive learning rate**

An exponential function was used to define the RBFNN learning rate which seems to give satisfactory results. Adaptive learning rate could be considered in the future to increase the controller robustness against system changes.

REFERENCES

[1] Makombe T., Jenkins N.," Investigation of a unified power flow controller," IEE Proc. Gener. Transm. Distrib., Vol. 146, No. 4, July 1999, PP. 400-408.

[2] Yu Q., et al.," Investigation of a dynamic controllers for a unified power flow controller," Proc. of IEEE 22nd International Conference on Industrial Electronics, Control and Instrumentation, IECON, Taiwan, Aug. 1996, PP. 1764-1769.

[3] Round S. D., et al.," Performance of a unified power flow controller using a d-q control system," AC and DC Power Transmission Conference, No. 423, 1996, PP. 357-362.

[4] Papič I., et al.," Basic control of unified power flow controller," IEEE Trans. On Power Systems, Vol. 12, No. 4, Nov. 1997, PP. 1734-1739.

[5] Fujita H., Watanabe Y., Akagi H.," Control and analysis of a unified power flow controller," IEEE Trans. On Power Electronics, Vol. 14, No. 6, Nov. 1999, PP. 1021-1027.

[6] Lombard X., Therond P. G.," Control of unified power flow controller: comparison methods on the basis of a detailed numerical model," IEEE Trans. On Power Systems, Vol. 12, No. 2, May 1997, PP. 824-830.

[7] Vilathgamuwa M., et al.," A synchronous reference frame based control of an unified power flow controller," Proc. on International Conference on Power Electronics and Drive Systems, Vol. 2, 1997, PP. 844-849.

[8] Vilathgamuwa M., Zhu X., Choi S. S.," A robust control method to improve the performance of a unified power flow controller," Electric Power Systems Research, Vol. 55, 2000, PP. 103-111.

[9] Kannan S., Jayaram S., Salama M. M.," Application of fuzzy logic for real and reactive power flow control using unified power flow controller," 28th North America Power Symposium, Nov. 1996, PP. 437-444.

[10] Kannan S., Jayaram S., Salama M. M.," Intelligent autonomous control of a unified power flow controller," Proc. of International Conference on Power Electronics and Drive Systems, Vol. 2, 1997, PP. 862-868.

[11] Yixin N., et al.," Fuzzy logic damping controller for FACTS devices in interconnected power systems," IEEE International Symposium, 1999, PP. 591-594.

[12] Mishra S., Dash P. K., Panda G.," TS-fuzzy controller for UPFC in a multi-machine power system," IEE Proc. Gener. Transm. Distrib., Vol. 147, No. 1, Jan. 2000, PP. 15-22.

[13] Ma T. T., Lo K. L., Tumay M.," A robust UPFC damping control scheme using PI and ANN based adaptive controllers," Int. Journal for Computation and Mathematics in Electrical and Electronic Engineering, Vol. 19, No. 3, 2000, PP. 878-902.

[14] Dash P. K., Mishra S., Panda G.," A radial basis function neural network controller for UPFC," IEEE Trans. On Power Systems, Vol. 15, No. 4, Nov. 2000, PP. 1293-1299.

[15] "Introduction to FACTS," IEEE Power Engineering Society, 'FACTS overview', CIGRE 95 TP 108, April 1995, PP. 1-1.

[16] Gyugyi L.," Converter-based FACTS controllers," IEE Colloquium on Flexible AC Transmission Systems-the FACTS, Nov. 1998, PP. 1-11.

[17] Noroozian M.," Application of shunt and series compensators for damping of electromechanical oscillations," IEE Colloquium on Power System Dynamic Stabilisation, Feb. 1998, PP. 4/1-4/3.

[18] Son K. M., Park J. K.," On the robust LQG control of TCSC for damping power system oscillations," IEEE Trans. On Power Systems, Vol. 15, No. 4, Nov. 2000, PP. 1306-1312.

[19] Fang Y. J.," Dynamic quadrature booster as an aid to system stability," IEE Colloquium on Power System Dynamic Stabilisation, Feb. 1998, PP. 11/1-11/7.

[20] Gyugyi L., et al.," Advanced static VAr compensator using Gate Turn Off thyristors for utility applications," CIGRE 23-203, 1990.

[21] Erinmez I. A., Foss A. M.," Static synchronous compensator STATCOM," Working Group, CIGRE study committee, No. 144, August 1999.

[22] Gyugyi L.," Solid state control of electric power in AC transmission systems," International Symposium on Electric Energy Conversion in Power Systems, T-IP 4, Capri, Italy, 1989.

[23] Mihalič R., Papič I.," Static synchronous series compensator- a mean for dynamic power flow control in electric systems," Electric Power Systems Research, Vol. 45, April 1998, PP. 65-72.

[24] Gyugyi L., et al.," The Interline Power Flow Controller concept: a new approach to power flow management in transmission systems," IEEE PES Summer Meeting, San Diego, July 1998.

[25] Gyugyi L.," A unified power flow control concept for flexible ac transmission systems," IEE 5th International Conference on AC and DC Power Transmission, London 1992, No. 345, PP. 19-26.

[26] Gyugyi L.," A unified power flow control concept for flexible ac transmission systems," IEE Proceeding-C- Vol. 139, No. 4, July 1992, PP. 323-331.

[27] Keri A. J. F., et al.," Unified power flow controller (UPFC): modelling and analysis," IEEE Trans. On Power Delivery, Vol. 14, No. 2, April 1999, PP. 648-654.

[28] Gyugyi L., et al.," The unified power flow controller: a new approach to power transmission control," IEEE Trans. On Power Delivery, Vol. 10, No. 2, April 1995, PP. 1085-1093.

[29] Edris A. et al.," Controlling the flow of real and reactive power," IEEE Computer Applications in Power, Jan. 1998, PP. 20-25.

[30] Nelson R. J., " Transmission planning application guidelines for the unified power flow controller (UPFC)," Proc. of the American Power Conference, IL, USA, 1997, PP. 1257-1263.

[31] Yuryevich J., Wong K. P.," MVA constraint handling method for unified power flow controller in load flow evaluation," IEE Proc. Gener. Transm. Distrib., Vol. 147, No. 3, May 2000, PP. 190-194.

[32] Liu J. Y., Song Y. H.," Determining maximum regulating capability of UPFC based on predicting feasibility limit of power systems," Electric Machines and Power Systems, Vol. 26, 1998, PP. 789-800.

[33] Cai H., Qu Z., Gan D.," Determination of the power transfer capacity of a UPFC with consideration of the system and equipment constraints and of installation locations," IEE Proc. Gener. Transm. Distrib., Vol. 149, No. 1, Jan. 2002, PP. 114-120.

[34] Ekanayake J. B.," An investigation of advanced static VAr compensator," PhD thesis, UMIST, 1995.

[35] Farrag M. E. A., Putrus G. A., Ran L.," Using PWM control to improve the speed of response of the advanced static VAr compensator (ASVC)," UPEC'01, Swansea, U.K., Sep. 2001.

[36] Farrag M. E. A., Putrus G. A., Ran L.," Real time hybrid control system for the advanced static VAr compensator," accepted for publication in UPEC'02, Staffordshire, U.K., Sep. 2002.

[37] Gyugyi L.," Dynamic compensation of AC transmission lines by solid-state synchronous voltage sources," IEEE Trans. On Power Delivery, Vol. 9, No. 2, April 1994, PP. 904-911.

[38] Ooi B. T., Kazerani M.," Unified power flow controller based on matrix converter," IEEE Annual Power Electronics Specialists Conference, Vol. 1, 1996, PP. 502-507.

[39] Liu J. Y., Song Y. H.," Digital simulation of the PWM UPFC using EMTP," IEE conference. On AC and DC Power Transmission, No. 423, 1996, PP. 351-356.

[40] Sen K.K., Stacey E. J.," UPFC – unified power flow controller: theory, modelling and applications," IEEE Trans. On Power Delivery, Vol. 13, No. 4, Oct. 1998, PP. 1453-1460.

[41] Toufan M., Annakage U. D.," Simulation of the unified power flow controller performance using PSCAD/EMTDC," Electric Power Systems Research, Vol. 46, 1998, PP. 67-75.

[42] Fujita H., Akagi H.," The unified power quality conditioner: the integration series active filters and shunt active filters," IEEE Annual Power Electronics Specialists Conference, Vol. 1, 1996, PP. 494-501.

[43] Ahmed A.," Power electronics for technology," USA, Prentice-Hall , Inc., 1999, P. 318.

[44] Enslin J. H. R., Zhao J., Spee R.," Operation of the unified power flow controller as harmonic isolator," IEEE Trans. On Power Electronics, Vol. 11, No. 6, Nov. 1996, PP. 776-784.

[45] Liu J. Y., Song Y. H.," Harmonic analysis of the unified power flow controller," UPEC'96, Vol. 2, 1996, PP. 676-679.

[46] Kamran F., Habetler T. G.," Combined deadbeat control of a series-parallel converter combination used as a universal power filter," IEEE Trans. On Power Electronics, Vol.13, No.1, Jan. 1998, PP. 160-168.

[47] Lee D. C.," Advanced nonlinear control of three-phase PWM rectifiers," IEE Proc. Electr. Power Appl. Vol. 147, No. 5, Sep. 2000, PP.361-366.

[48] Ekanayake J. B., Jenkins N., " A three-level advanced static VAr compensator," IEEE Trans. On Power Delivery, Vol. 11, No. 1, Jan. 1996, PP. 540-545.

[49] Ran L., Holdsworth L., Putrus G. A.," Dynamic selective harmonic elimination of a three-level inverter used for static VAr compensation," IEE Proc. Gener. Transm. Distrib., Vol. 149, No. 1, Jan. 2002, PP. 83-89.

[50] Nabavi-Niaki A., Irvani, M. R.," Steady-state and dynamic models of unified power flow controller (UPFC) for power system studies," IEEE Trans. On Power Systems, Vol. 11, No. 4, Nov. 1996, PP. 1937-1943.

[51] Rahman M. M., et al.," UPFC application on the AEP system: planning considerations," IEEE Trans. On Power Systems, Vol. 12, No. 4, Nov. 1997, PP. 1695-1701.

[52] Zhang X. P., Handschin E., Yao M. M.," Modelling of the generalized unified power flow controller (GUPFC) in a nonlinear interior point OPF," IEEE Trans. On Power Systems, Vol. 16, No. 3, Aug. 2001, PP. 367-373.

[53] Mihalič R., Papič I.," Power transmission control using unified power flow controller," UPEC'96, Vol. 1, 1996, PP. 285-288.

[54] Dizdarevic N., Arnborg S., Anderson G.," Possible alleviation of voltage stability problem by use of unified power flow controller," UPEC'97, Vol. 2, 1997, PP. 975-978.

[55] Verma K. S., Singh S. N., Gupta H. O.," Location of unified power flow controller for congestion management," Electric Power Systems Research, Vol. 58, 2001, PP. 89-96.

[56] Wang H. F.," Applications of modelling UPFC into multi-machine power systems," IEE Proc. Gener. Transm. Distrib., Vol. 146, No. 3, May 1999, PP. 306-312.

[57] Fuerte-Esquivel C. R., Acha E., Ambriz-Perez H.," A comprehensive Newton-Raphson UPFC model for the quadratic power flow solution of practical power networks," IEEE Trans. On Power Systems, Vol. 15, No. 1, Feb. 2000, PP. 102-109.

[58] Song Y. H., Liu J. Y., Mehta P. A.," Power injection modelling and optimal multiplier power flow algorithm for steady-state studies of unified power flow controllers," Electric Power Systems Research, Vol. 52, 1999, PP. 51-59.

[59] Kim T. H., et al.," A de-coupled unified power flow controller model for power flow considering limit resolution," IEEE Engineering Society, Winter Meeting, Vol. 2, 1999, PP. 1190-1195.

[60] Noroozian M., et al.," Use of UPFC for optimal power flow control," IEEE Trans. On Power Delivery, Vol. 12, No. 4, Oct. 1997, PP. 1629-1634.

[61] Fang W. L., Ngan H. W.," Control setting of unified power flow controllers through a robust load flow calculation," IEE Proc. Gener. Transm. Distrib., Vol. 146, No. 4, July 1999, PP. 365-369.

[62] Liu J. Y., Song Y. H., Foss A. M.," Power flow control and voltage support in a meshed power system using unified power flow controllers," Proc. UPEC'97, UMIST, UK, 1997, PP. 531-534.

[63] Lo K. L. et al.," A novel power flow control concept using ANN based multiple UPFCs scheme," IEEE International Conference on Energy Management and Power Delivery, Vol. 2, 1998, PP. 570-575.

[64] Lo K. L., Ma T. T.," UPFC damping control strategy based on transient energy," Electric Power Systems Research, Vol. 56, 2000, PP. 195-203.

[65] Ma T. T., Lo K. L.," Nonlinear power system damping control strategies for the unified power flow controller (UPFC)," International Conference on Power System Technology, Vol. 1, 2000, PP. 673-678.

[66] Noroozian M., et al.," Improving power system dynamics by series-connected FACTS devices," IEEE Trans. On Power Delivery, Vol. 12, No. 4, Oct. 1997, PP. 1635-1641.

[67] Wang H. F.," A unified model for the analysis of FACTS devices in damping power system oscillations – Part III: unified power flow controller," IEEE Trans. On Power Delivery, Vol. 15, No. 3, Oct. 2000, PP. 978-983.

[68] Wang H. F.," Damping function of unified power flow controller," IEE Proc. Gener. Transm. Distrib., Vol. 146, No. 1, Jan. 1999, PP. 81-87.

[69] Schauder C. et al.," AEP UPFC project: Installation, commissioning and operation of the ±160 MVA STATCOM phase I," IEEE Trans. On Power Delivery, Vol. 13, No. 4, Oct. 1998, PP. 1530-1535.

[70] Yu Q., et al.," A new control strategy for a unified power flow controller," Proc. of European Power Conference, Vol. 2, 1995, PP. 901,906.

[71] Padiyar K. R., Uma Rao K.," Modeling and control of unified power flow controller for transient stability," Electric Power and Energy Systems, Vol. 21, 1999, PP. 1-11.

[72] Zadeh L. A.," Fuzzy sets, " Information and Control, Vol. 8, 1965, PP. 338-353.

[73] Yager R. R., Zadeh L. A.," An introduction to fuzzy logic applications in intelligent systems," Kluwer Academic Publisher, Boston, 1992.

[74] International Electromechanical Commission (IEC)," Programmable controllers: Part 7 fuzzy control programming, " Technical Report IEC 1131, 1996.

[75] Hu B., Mann G. K. I., Gosine R. G.," New methodology for analytical and optimal design of fuzzy PID controllers," IEEE Trans. On Fuzzy Systems, Vol. 27, No. 5, Oct. 1999, PP. 521-539.

[76] Hiyamma T., Hubbi W., Ortmeyer T. H.," Fuzzy logic control scheme with variable gain for static VAr compensator to enhance power system stability," IEEE Trans. On Power Systems, Vol. 14, No. 1, Feb 1999, PP. 186-191.

[77] Maussion P., Hissel D.," Optimized fuzzy logic controller parameters for open-loop stable or evaluative electromechanical systems," Proceeding of Industrial Electronics Conference, Vol. 1,1998, PP.23-27.

[78] Park Y., Moon U., Lee K. Y.," A power system stabilization with a self organizing fuzzy logic controller,"

[79] Sugeno M., Takago T.," Fuzzy identification of systems and its applications to modelling control," IEEE Trans. System Man and Cybernetic, 1985, SMC-15, PP. 116-132.

[80] Pedrycz W.," Fuzzy control and fuzzy systems," USA, John Wiley & sons Inc., 1989.

[81] Driankov D., Hellendoorn, H., Reinfrank M.," An introduction to fuzzy control," USA, Springer-Verlag, 1993.

[82] Fararg M. E. A., Putrus G. A.," Advanced control of the unified power flow controller," UPEC'99, Vol. 1, 1999, PP. 74-77.

[83] Peiris H. J. C, Annakage U. D., Pahalawaththa N. C.," Generation of fuzzy rules to develop fuzzy logic modulation controllers for damping of power system oscillation," IEEE Trans. On Power Systems Vol. 14, No. 4, 1999, PP. 1440-1445.

[84] Limyingcharoen S., Annakage U. D., Pahalawaththa N. C.," Fuzzy logic based unified power flow controller for transient stability improvement," IEE Proceeding Gener. Transm. And Distrib., Vol. 145, No. 3, 1998, PP. 225-232.

[85] Aggarwal R., Song Y.," Artificial neural networks in power systems: part 2, types of artificial neural networks," IEE Power Engineering Journal, Vol. 12, No. 1, Feb. 1998, PP. 41-47.

[86] Aggarwal R., Song Y.," Artificial neural networks in power systems: part 3, examples of applications in power systems," IEE Power Engineering Journal, Vol. 12, No. 6, Dec. 1998, PP. 279-287.

[87] Damborg M. J., et al.," Potential of artificial neural networks in power system operation," IEEE Int. Symposium on Circuit and Systems, Vol. 4, 1990, PP. 2933-2937.

[88] Zhou Q., Davidson J., Fouad A. A.," Application of artificial neural networks in power system security and vulnerability assessment," IEEE Trans. On Power Systems, Vol. 9, No. 1, Feb. 1994, PP. 525-532.

[89] Doding G.," Applications of artificial neural networks in power system management," CURED 14th Int. Conference and Exhibition on Electricity Distribution, Vol. 4, 1997, PP. 13.1-13.5.

[90] Rukonuzzaman M., et al.," An application of neural network in power system harmonic detection," IEEE Int. Joint Conference on Neural Networks, Vol. 1, 1998, PP. 74-78.

[91] Hongesombust K., Mitani Y., Tsuji K.," An adaptive static VAr compensator using genetic algorithm and radial basis function network for enhancing power system stability," IEEE Porto Power Tech. Conference, 2001.

[92] Ma T. T., Lo K. L., Tumay M.," A robust UPFC damping control scheme using PI and ANN based adaptive controllers," Int. Journal for Computation and Mathematics in Electrical and Electronic Engineering, Vol. 19, No. 3, 2000, PP. 878-902.

[93] Dash P. K., Mishra S., Panda G.," A radial basis function neural network controller for UPFC," IEEE Trans. On Power Systems, Vol. 15, No. 4, Nov. 2000, PP. 1293-1299.

[94] Haykin S.," Neural network: a comprehensive foundation," Printice Hall, 1999.

[95] Narendra K. S., Parthasarathy K.," Identification and control of dynamic systems using neural networks," IEEE Trans. On Neural Networks, Vol. NN-1, No. 1, 1990, PP. 4-27.

[96] Cybenko G.," Approximation by superposition os a sigmoidal function," Mathematics of Control, Signal and Systems, Vol/ 2, 1989, PP. 303-314.

[97] Pineda F. J.," Generalization of backpropagation to recurrent neural network," Physical Review Letter 59, 1987, PP. 2229-2232.

[98] Fang Y., Sejnowski T. J.," Faster learning for dynamic recurrent backpropagation," Neural Computation, Vol. 2, 1990, PP.270-273.

[99] Pineda F. J.," Recurrent back propagation and the dynamical approach to adaptive neural computation," Neural Computation, Vol. 1, 1989, PP. 161-172.

[100] Funahashi K.," On the approximate realization of continuous mapping by neural networks," Neural Network, Vol. 2, PP. 183

[101] Hecht-Nielsen R.," Counter propagation networks," Proc. Of IEEE Int. Conf. On Neural Networks, Vol. 2, 1987, PP. 19-32.

[102] Hornik M., Stinchcombe M., White H.," Multilayer feedforward networks are universal approximators," Neural Networks, Vol. 2, 1989, PP. 359-366.

[103] White H.," Connectionist non-parametric regression: multilayer feedforward networks can learn arbitrary mapping," Neural Networks, Vol. 3, 1990, PP. 533-549.

[104] Grossberg S.," Competition, decision and consensus," Journal of Mathematical Analysis and Applications, Vol. 66, 1978, PP. 470-493.

[105] Kohonen T.," Self organization and associative memory," Springer-Verlag, Berlin, 1984.

[106] Parker D. B.," Optimal algorithm for adaptive networks: second order backpropagation, second order direct propagation and second order Hebbian learning," Proc. IEEE Int. Conference on Neural Networks, 1987, PP. 539-600.

[107] Werbos P.," An overview of neural networks for control," IEEE Control System Magazine, Vol. 11, No. 1, 1991, PP. 40-41.

[108] Broomhead D. S., Lowe D.," Multivariable functional interpolation and adaptive networks," Complex Systems, Vol. 22, 1988, PP. 321-355.

[109] Chen S., Billings S. A., Grant P. M.," Recursive hybrid algorithm for non-linear system identification using radial basis function networks,' Int. Journal of Control, Vol. 55, 1992, PP. 1051-1070.

[110] Park J., Sandberg I. W.," Universal approximation using radial basis function networks," Neural Computation, Vol. 3, 1991, PP. 246-257.

[111] Shing J., Jang r.," ANFIS: adaptive network-based fuzzy inference system," IEEE Trans. On System Man and Cybernetics, Vol. 23, No. 3, 1993, PP. 665-685.

[112] Bukley J. J., "Theory of fuzzy controllers," Fuzzy sets and Systems, Vol. 51, 1992, PP. 249-258.

[113] Mazda F. F.," Power electronics handbook, components, circuits and applications," Butterworth, 1993.

[114] Andersen M. A. E," A comparison of three inverters with IGBTs, GTOs and Bipolar Transistor at 600 V and 300 A," UPEC 1990.

[115] Shakweh Y.," New breed of medium voltage converters," Power Engineering Journal, Vol. 14, No. 1, Feb. 2000, PP. 12-20.

[116] Mohan N., Undeland T. M., Robbins W. P.," Power electronics: converters, applications and design," John Wiley, New York, 2nd Ed., 1995, CH. 27.

[117] Holtz J.," Pulse width modulation for electronic power conversion," Proc. Of the IEEE, Vol. 82, Aug. 1994, PP. 1194-1214.

[118] DSPACE -ds1103 controller board ' features reference' Jan. 2001.

APPENDICES

Appendix A

SERIES INVERTER FEASIBLE REGION

The inserted voltage angle as a function of the changes in active and reactive power was derived in chapter 4 and given as (Equation 4.29):

$$\begin{bmatrix} \sin\theta_{ij} & \cos\theta_{ij} \\ 2-\cos\theta_{ij} & \sin\theta_{ij} \end{bmatrix} \begin{bmatrix} \cos\phi_{ser} \\ \sin\phi_{ser} \end{bmatrix} = \begin{bmatrix} \dfrac{\Delta P}{V_{ser}} \\ \dfrac{\Delta Q}{V_{ser}} - V_{ser} \end{bmatrix} \tag{A.1}$$

The solution the ϕ_{ser} is given as:

$$\begin{bmatrix} \cos\phi_{ser} \\ \sin\phi_{ser} \end{bmatrix} = \frac{1}{1-2\cos\theta_{ij}} \begin{bmatrix} \sin\theta_{ij} & -\cos\theta_{ij} \\ -2+\cos\theta_{ij} & \sin\theta_{ij} \end{bmatrix} \begin{bmatrix} \dfrac{\Delta P}{V_{ser}} \\ \dfrac{\Delta Q}{V_{ser}} - V_{ser} \end{bmatrix} \tag{A.2}$$

$$\cos\phi_{ser} = \frac{1}{1-2\cos\theta_{ij}} \left[\frac{\Delta P}{V_{ser}} \sin\theta_{ij} - \left(\frac{\Delta Q}{V_{ser}} - V_{ser}\right)\cos\theta_{ij} \right] \tag{A.3}$$

$$\sin\phi_{ser} = \frac{1}{1-2\cos\theta_{ij}} \left[\frac{\Delta P}{V_{ser}} (-2+\cos\theta_{ij}) + \left(\frac{\Delta Q}{V_{ser}} - V_{ser}\right)\sin\theta_{ij} \right] \tag{A.4}$$

From trigonometry, it is known that

$$\cos^2\phi_{ser} + \sin^2\phi_{ser} = 1.0 \tag{A.5}$$

$$\begin{aligned} &\frac{\Delta P^2}{V_{ser}^2}\sin^2\theta_{ij} - 2\frac{\Delta P}{V_{ser}}\left(\frac{\Delta Q}{V_{ser}} - V_{ser}\right)\sin\theta_{ij}\cos\theta_{ij} + \left(\frac{\Delta Q}{V_{ser}} - V_{ser}\right)^2\cos^2\theta_{ij} + \frac{\Delta P^2}{V_{ser}^2}\left(-2+\cos\theta_{ij}\right)^2 \\ &+ 2\frac{\Delta P}{V_{ser}}\left(\frac{\Delta Q}{V_{ser}} - V_{ser}\right)\left(-2+\cos\theta_{ij}\right)\sin\theta_{ij} + \left(\frac{\Delta Q}{V_{ser}} - V_{ser}\right)^2\sin^2\theta_{ij} = \left(1-2\cos\theta_{ij}\right)^2 \end{aligned} \tag{A.6}$$

$$\begin{aligned} &\frac{\Delta P^2}{V_{ser}^2}\left[\sin^2\theta_{ij} + 4 - 4\cos\theta_{ij} + \cos^2\theta_{ij}\right] - 2\frac{\Delta P}{V_{ser}}\left(\frac{\Delta Q}{V_{ser}} - V_{ser}\right)\sin\theta_{ij}\cos\theta_{ij} \\ &+ 2\frac{\Delta P}{V_{ser}}\left(\frac{\Delta Q}{V_{ser}} - V_{ser}\right)\sin\theta_{ij}\cos\theta_{ij} - 4\frac{\Delta P}{V_{ser}}\left(\frac{\Delta Q}{V_{ser}} - V_{ser}\right)\sin\theta_{ij} + \left(\frac{\Delta Q}{V_{ser}} - V_{ser}\right)^2 = \left(1-2\cos\theta_{ij}\right)^2 \end{aligned} \tag{A.7}$$

$$\frac{\Delta P^2}{V_{ser}^2}\left[5-4\cos\theta_{ij}\right] - 4\frac{\Delta P}{V_{ser}}\left(\frac{\Delta Q}{V_{ser}} - V_{ser}\right)\sin\theta_{ij} + \left(\frac{\Delta Q}{V_{ser}} - V_{ser}\right)^2 = \left(1-2\cos\theta_{ij}\right)^2 \tag{A.8}$$

$$\Delta P^2 + \frac{4V_{ser}^2 \sin\theta_{ij}}{5-4\cos\theta_{ij}}\Delta P - \frac{4\sin\theta_{ij}}{5-4\cos\theta_{ij}}\Delta P\Delta Q + \frac{(\Delta Q - V_{ser}^2)}{5-4\cos\theta_{ij}} = \frac{V_{ser}^2\left(1-2\cos\theta_{ij}\right)^2}{5-4\cos\theta_{ij}} \quad \text{(A.9)}$$

$$\left(\Delta P + \frac{2V_{ser}^2 \sin\theta_{ij}}{5-4\cos\theta_{ij}}\right)^2 - \frac{4\sin\theta_{ij}}{5-4\cos\theta_{ij}}\Delta P\Delta Q + \frac{(\Delta Q - V_{ser})^2}{5-4\cos\theta_{ij}} = \frac{V_{ser}^2\left(1-2\cos\theta_{ij}\right)^2}{5-4\cos\theta_{ij}} - \left(\frac{2V_{ser}^2 \sin\theta_{ij}}{5-4\cos\theta_{ij}}\right)^2 \quad \text{(A.10)}$$

This can be simplified to give the following ellipse equation:

$$\left(\Delta P + \frac{B}{A}\right)^2 - C\Delta P\Delta Q + \frac{(\Delta Q - V_{ser})^2}{A} = \left(\frac{D^2 A - B^2}{A^2}\right) \quad \text{(A.11)}$$

where

$A = 5 - 4\cos\theta_{ij}$,

$B = 2V_{ser}^2 \sin\theta_{ij}$,

$C = -4\sin\theta_{ij}$ and

$D = V_{ser}^2\left(1-2\cos\theta_{ij}\right)^2$

Appendix B

MODIFIED JACOBIAN MATRIX

The linearized load flow model as given in Equation 5.26 is:

$$\begin{bmatrix}\Delta P\\ \Delta Q\end{bmatrix}=\begin{bmatrix}H & N\\ M & L\end{bmatrix}\begin{bmatrix}\Delta\theta\\ \frac{\Delta V}{V}\end{bmatrix} \tag{B1}$$

where

$$\begin{aligned}H &= H^0 + \Delta H\\ N &= N^0 + \Delta N\\ M &= M^0 + \Delta M\\ L &= L^0 + \Delta L\end{aligned} \tag{B2}$$

where, H^0, N^0, M^0 and L^0 denote the matrix parameters without the UPFC.

For the buses i and j, the change in Jacobian elements is given as:

$$\Delta H_{ii} = \frac{\partial P_i}{\partial \theta_i} = \frac{r_{ser}}{X_s} V_i V_j \cos\left(\theta_{ij} + \phi_{ser}\right) = -Q_{j_{net}} \tag{B3}$$

$$\Delta H_{ij} = \frac{\partial P_i}{\partial \theta_j} = -\frac{r_{ser}}{X_s} V_i V_j \cos\left(\theta_{ij} + \phi_{ser}\right) = Q_{j_{net}} \tag{B4}$$

$$\Delta H_{ji} = \frac{\partial P_j}{\partial \theta_i} = -\frac{r_{ser}}{X_s} V_i V_j \cos\left(\theta_{ij} + \phi_{ser}\right) = Q_{j_{net}} \tag{B5}$$

$$\Delta H_{jj} = \frac{\partial P_j}{\partial \theta_j} = \frac{r_{ser}}{X_s} V_i V_j \cos\left(\theta_{ij} + \phi_{ser}\right) = -Q_{j_{net}} \tag{B6}$$

$$\Delta N_{ii} = \frac{\partial P_i}{\partial \Delta V_i} V_i = \frac{r_{ser}}{X_s} V_i V_j \sin\left(\theta_{ij} + \phi_{ser}\right) = -P_{j_{net}} \tag{B7}$$

$$\Delta N_{ij} = \frac{\partial P_i}{\partial \Delta V_j} V_j = \frac{r_{ser}}{X_s} V_i V_j \sin\left(\theta_{ij} + \phi_{ser}\right) = -P_{j_{net}} \tag{B8}$$

$$\Delta N_{ji} = \frac{\partial P_j}{\partial \Delta V_i} V_i = -\frac{r_{ser}}{X_s} V_i V_j \sin\left(\theta_{ij} + \phi_{ser}\right) = P_{j_{net}} \tag{B9}$$

$$\Delta N_{jj} = \frac{\partial P_j}{\partial \Delta V_j} V_j = -\frac{r_{ser}}{X_s} V_i V_j \sin\left(\theta_{ij} + \phi_{ser}\right) = P_{j_{net}} \tag{B10}$$

$$\Delta M_{ii} = \frac{\partial Q_i}{\partial \theta_i} = 0 \tag{B11}$$

$$\Delta M_{ij} = \frac{\partial Q_i}{\partial \theta_j} = 0 \tag{B12}$$

$$\Delta M_{ji} = \frac{\partial Q_j}{\partial \theta_i} = \frac{r_{ser}}{X_s} V_i V_j \sin\left(\theta_{ij} + \phi_{ser}\right) = -P_{j_{net}} \tag{B13}$$

$$\Delta M_{jj} = \frac{\partial Q_j}{\partial \theta_j} = -\frac{r_{ser}}{X_s} V_i V_j \sin\left(\theta_{ij} + \phi_{ser}\right) = P_{j_{net}} \tag{B14}$$

$$\Delta L_{ii} = \frac{\partial Q_i}{\partial \Delta V_i} V_i = 2\frac{r_{ser}}{X_s} V_i^2 \cos\phi_{ser} - 2\frac{V_i^2}{X_{sh}}\left(1 - r_{sh}\cos\phi_{sh}\right) = 2Q_{i_{net}} \tag{B15}$$

$$\Delta L_{ij} = \frac{\partial Q_i}{\partial \Delta V_j} V_j = 0 \tag{B16}$$

$$\Delta L_{ji} = \frac{\partial Q_j}{\partial \Delta V_i} V_i = -\frac{r_{ser}}{X_s} V_i V_j \cos\left(\theta_{ij} + \phi_{ser}\right) = Q_{j_{net}} \tag{B17}$$

$$\Delta L_{jj} = \frac{\partial Q_j}{\partial \Delta V_j} V_j = -\frac{r_{ser}}{X_s} V_i V_j \cos\left(\theta_{ij} + \phi_{ser}\right) = Q_{j_{net}} \tag{B18}$$

Appendix C

IGBT DATA SHEET

International
IOR Rectifier

PRELIMINARY

PD - 9.1600

IRG4BC20K

Short Circuit Rated
UltraFast IGBT

INSULATED GATE BIPOLAR TRANSISTOR

Features

- High short circuit rating optimized for motor control, t_{sc} =10µs, @360V V_{CE} (start), T_J = 125°C, V_{GE} = 15V
- Combines low conduction losses with high switching speed
- Latest generation design provides tighter parameter distribution and higher efficiency than previous generations

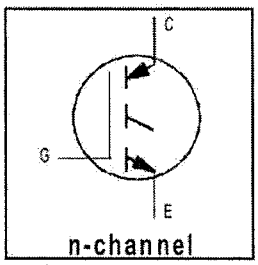

n-channel

V_{CES} = 600V

$V_{CE(on)}$ typ. = 2.27V

@V_{GE} = 15V, I_C = 9.0A

Benefits

- As a Freewheeling Diode we recommend our HEXFRED™ ultrafast, ultrasoft recovery diodes for minimum EMI / Noise and switching losses in the Diode and IGBT
- Latest generation 4 IGBT's offer highest power density motor controls possible
- This part replaces the IRGBC20K and IRGBC20M devices

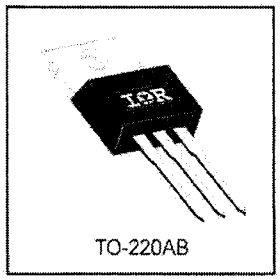

TO-220AB

Absolute Maximum Ratings

	Parameter	Max.	Units
V_{CES}	Collector-to-Emitter Voltage	600	V
I_C @ T_C = 25°C	Continuous Collector Current	16	A
I_C @ T_C = 100°C	Continuous Collector Current	9.0	
I_{CM}	Pulsed Collector Current ①	32	
I_{LM}	Clamped Inductive Load Current ②	32	
t_{sc}	Short Circuit Withstand Time	10	µs
V_{GE}	Gate-to-Emitter Voltage	±20	V
E_{ARV}	Reverse Voltage Avalanche Energy ③	29	mJ
P_D @ T_C = 25°C	Maximum Power Dissipation	60	W
P_D @ T_C = 100°C	Maximum Power Dissipation	24	
T_J T_{STG}	Operating Junction and Storage Temperature Range	-55 to +150	°C
	Soldering Temperature, for 10 sec.	300 (0.063 in. (1.6mm) from case)	
	Mounting torque, 6-32 or M3 screw.	10 lbf•in (1.1N•m)	

Thermal Resistance

	Parameter	Typ.	Max.	Units
$R_{\theta JC}$	Junction-to-Case	—	2.1	°C/W
$R_{\theta CS}$	Case-to-Sink, Flat, Greased Surface	0.5	—	
$R_{\theta JA}$	Junction-to-Ambient, typical socket mount	—	80	
Wt	Weight	2.0 (0.07)	—	g (oz)

IRG4BC20K

International
IOR Rectifier

Electrical Characteristics @ T_J = 25°C (unless otherwise specified)

	Parameter	Min.	Typ.	Max.	Units	Conditions
$V_{(BR)CES}$	Collector-to-Emitter Breakdown Voltage	600	—	—	V	V_{GE} = 0V, I_C = 250µA
$V_{(BR)ECS}$	Emitter-to-Collector Breakdown Voltage ④	18	—	—	V	V_{GE} = 0V, I_C = 1.0A
$\Delta V_{(BR)CES}/\Delta T_J$	Temperature Coeff. of Breakdown Voltage	—	0.49	—	V/°C	V_{GE} = 0V, I_C = 1.0mA
$V_{CE(ON)}$	Collector-to-Emitter Saturation Voltage	—	2.00	—	V	I_C = 6.0A
		—	2.27	2.8		I_C = 9.0A, V_{GE} = 15V
		—	3.01	—		I_C = 16A, See Fig.2, 5
		—	2.43	—		I_C = 9.0A, T_J = 150°C
$V_{GE(th)}$	Gate Threshold Voltage	3.0	—	6.0		V_{CE} = V_{GE}, I_C = 250µA
$\Delta V_{GE(th)}/\Delta T_J$	Temperature Coeff. of Threshold Voltage	—	-10	—	mV/°C	V_{CE} = V_{GE}, I_C = 250µA
g_{fe}	Forward Transconductance ⑤	2.9	4.3	—	S	V_{CE} = 100 V, I_C = 9.0A
I_{CES}	Zero Gate Voltage Collector Current	—	—	250	µA	V_{GE} = 0V, V_{CE} = 600V
		—	—	2.0		V_{GE} = 0V, V_{CE} = 10V, T_J = 25°C
		—	—	1000		V_{GE} = 0V, V_{CE} = 600V, T_J = 150°C
I_{GES}	Gate-to-Emitter Leakage Current	—	—	±100	nA	V_{GE} = ±20V

Switching Characteristics @ T_J = 25°C (unless otherwise specified)

	Parameter	Min.	Typ.	Max.	Units	Conditions
Q_g	Total Gate Charge (turn-on)	—	34	51	nC	I_C = 9.0A
Q_{ge}	Gate - Emitter Charge (turn-on)	—	4.9	7.4		V_{CC} = 400V See Fig.8
Q_{gc}	Gate - Collector Charge (turn-on)	—	14	21		V_{GE} = 15V
$t_{d(on)}$	Turn-On Delay Time	—	28	—	ns	
t_r	Rise Time	—	27	—		T_J = 25°C
$t_{d(off)}$	Turn-Off Delay Time	—	150	220		I_C = 9.0A, V_{CC} = 480V
t_f	Fall Time	—	100	150		V_{GE} = 15V, R_G = 50Ω
E_{on}	Turn-On Switching Loss	—	0.15	—	mJ	Energy losses include "tail"
E_{off}	Turn-Off Switching Loss	—	0.25	—		See Fig. 9,10,14
E_{ts}	Total Switching Loss	—	0.40	0.6		
t_{sc}	Short Circuit Withstand Time	10	—	—	µs	V_{CC} = 400V, T_J = 125°C
						V_{GE} = 15V, R_G = 50Ω , V_{CPK} < 500V
$t_{d(on)}$	Turn-On Delay Time	—	28	—	ns	T_J = 150°C,
t_r	Rise Time	—	29	—		I_C = 9.0A, V_{CC} = 480V
$t_{d(off)}$	Turn-Off Delay Time	—	190	—		V_{GE} = 15V, R_G = 50Ω
t_f	Fall Time	—	190	—		Energy losses include "tail"
E_{ts}	Total Switching Loss	—	0.68	—	mJ	See Fig. 11,14
E_{on}	Turn-On Switching Loss	—	0.07	—	mJ	T_J = 25°C, V_{GE} = 15V, R_G = 50Ω
E_{off}	Turn-Off Switching Loss	—	0.13	—		I_C = 6.0A, V_{CC} = 480V
E_{ts}	Total Switching Loss	—	0.20	—		Energy losses include "tail"
L_E	Internal Emitter Inductance	—	7.5	—	nH	Measured 5mm from package
C_{ies}	Input Capacitance	—	450	—	pF	V_{GE} = 0V
C_{oes}	Output Capacitance	—	61	—		V_{CC} = 30V See Fig. 7
C_{res}	Reverse Transfer Capacitance	—	14	—		f = 1.0MHz

ANTI-PARALLEL DIODE DATA SHEET

International
IOR Rectifier

SAFEIR Series
10ETS..

INPUT RECTIFIER DIODE

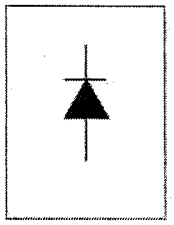

V_F < 1.1V@10A
I_{FSM} = 200A
V_{RRM} 800 to 1600V

Description/Features

The 10ETS.. rectifier *SAFEIR* series has been optimized for very low forward voltage drop, with moderate leakage. The glass passivation technology used has reliable operation up to 150°C junction temperature.
The ***High Reverse Voltage*** range available allows design of input stage primary rectification with ***Outstanding Voltage Surge*** capability.
Typical applications are in input rectification and these products are designed to be used with International Rectifier Switches and Output Rectifiers which are available in identical package outlines.

Output Current in Typical Applications

Applications	Single-phase Bridge	Three-phase Bridge	Units
Capacitive input filter T_A=55°C, T_J=125°C common heatsink of 1°C/W	12.0	16.0	A

Major Ratings and Characteristics

Characteristics	10ETS..	Units
$I_{F(AV)}$ Sinusoidal waveform	10	A
V_{RRM}	800 to 1600	V
I_{FSM}	200	A
V_F @10A, T_J=25°C	1.1	V
T_J	-40 to 150	°C

Package Outline

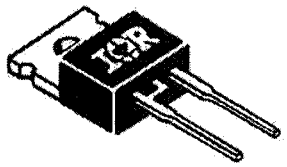

TO-220AC

Also available in D-pak (8EWS Series)

10ETS.. *SAFEIR* Series

Bulletin I2120 rev. A 07/97

International IOR Rectifier

Voltage Ratings

Part Number	V_{RRM}, maximum peak reverse voltage V	V_{RSM}, maximum non repetitive peak reverse voltage V	I_{RRM} 150°C mA
10ETS08	800	900	0.5
10ETS12	1200	1300	
10ETS16	1600	1700	

Provide terminal coating for voltages above 1200V

Absolute Maximum Ratings

	Parameters	10ETS..	Units	Conditions
$I_{F(AV)}$	Max. Average Forward Current	10	A	@ T_C = 105°C, 180° conduction half sine wave
I_{FSM}	Max. Peak One Cycle Non-Repetitive Surge Current	170	A	10ms Sine pulse, rated V_{RRM} applied
		200		10ms Sine pulse, no voltage reapplied
I^2t	Max. I^2t for fusing	130	A^2s	10ms Sine pulse, rated V_{RRM} applied
		145		10ms Sine pulse, no voltage reapplied
$I^2\sqrt{t}$	Max. $I^2\sqrt{t}$ for fusing	1450	$A^2\sqrt{s}$	t = 0.1 to 10ms, no voltage reapplied

Electrical Specifications

	Parameters	10ETS..	Units	Conditions	
V_{FM}	Max. Forward Voltage Drop	1.1	V	@ 10A, T_J = 25°C	
r_t	Forward slope resistance	20	mΩ	T_J = 150°C	
$V_{F(TO)}$	Threshold voltage	0.82	V		
I_{RM}	Max. Reverse Leakage Current	0.05	mA	T_J = 25°C	V_R = rated V_{RRM}
		0.50		T_J = 150°C	

Thermal-Mechanical Specifications

	Parameters		10ETS..	Units	Conditions
T_J	Max. Junction Temperature Range		-40 to 150	°C	
T_{stg}	Max. Storage Temperature Range		-40 to 150	°C	
R_{thJC}	Max. Thermal Resistance Junction to Case		2.5	°C/W	DC operation
R_{thJA}	Max. Thermal Resistance Junction to Ambient		62	°C/W	
R_{thCS}	Typical Thermal Resistance, Case to Heatsink		0.5	°C/W	Mounting surface, smooth and greased
wt	Approximate Weight		2(0.07)	g(oz.)	
T	Mounting Torque	Min.	6(5)	Kg-cm (lbf-in)	
		Max.	12(10)		
	Case Style		TO-220AC		

APPENDIX D

SIMULINK MODELS

PHASE HIFTER

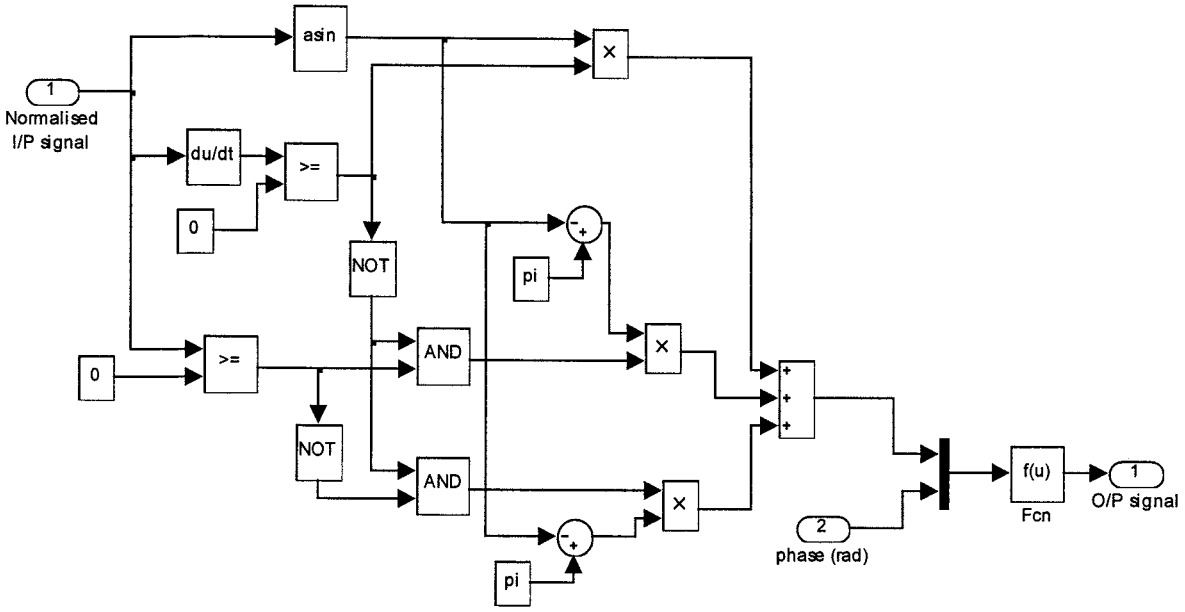

Figure D.1 Phase shifter.

TRIANGULAR SIGNAL GENERATOR

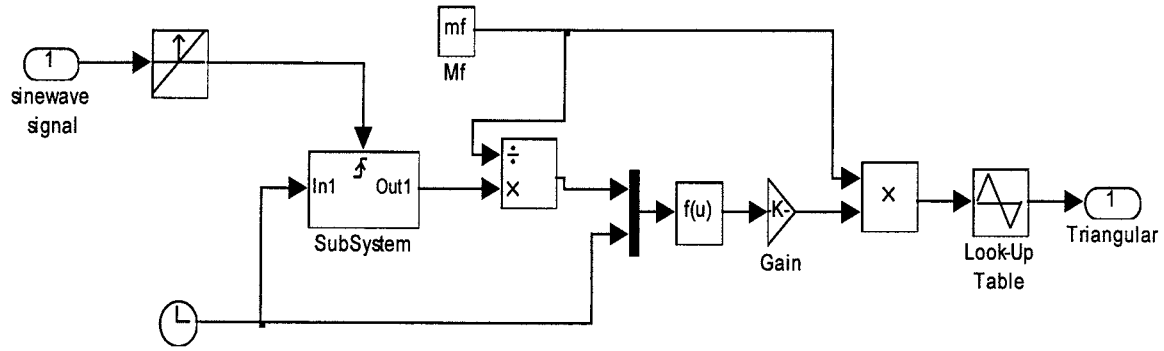

Figure D.2 Triangular signal generation.

APPENDIX E

THREE PHASE INVERSION AND DEAD TIME CIRCUIT

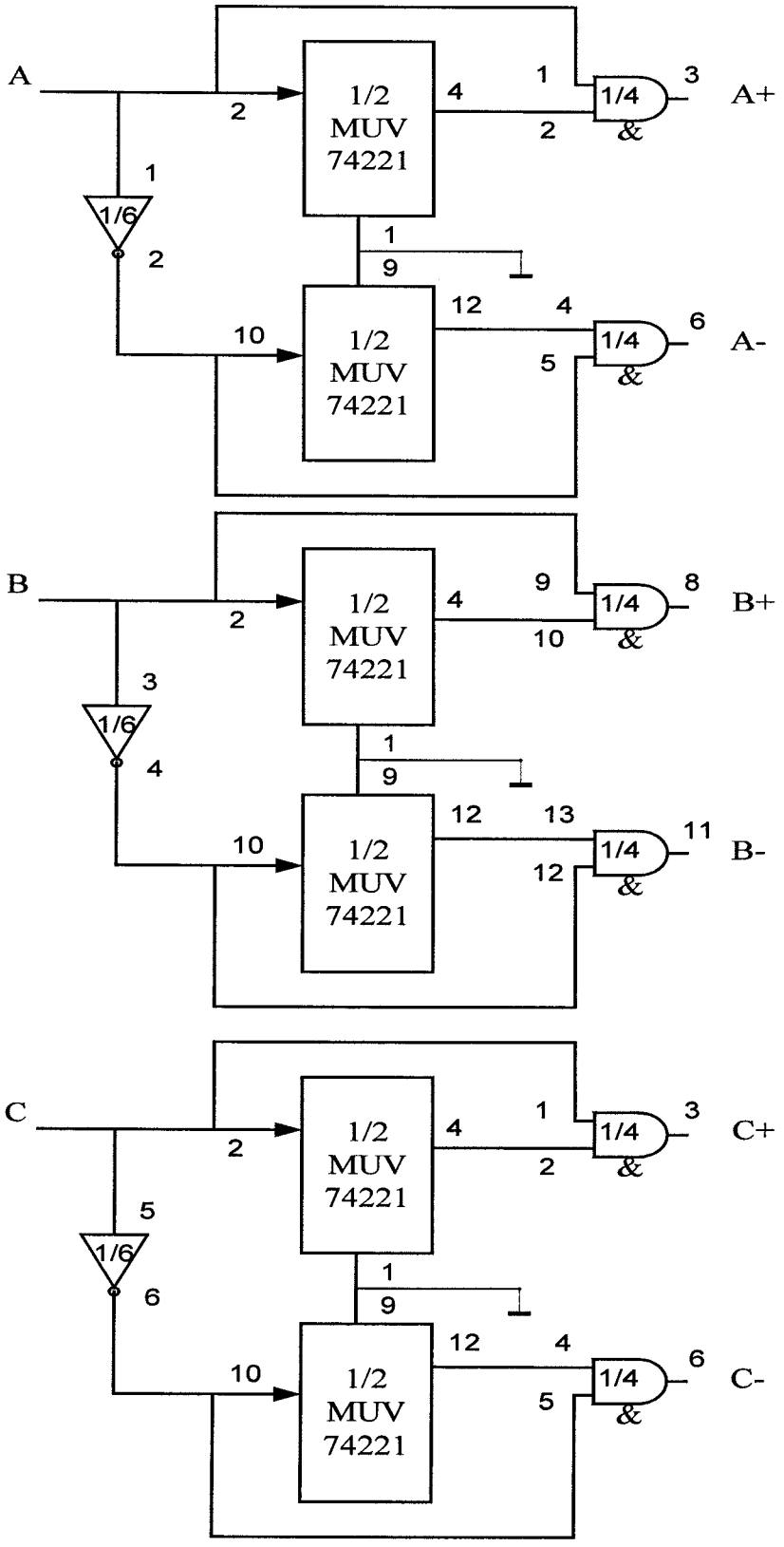

Figure E.1 Inversion and dead time circuit.

APPENDIX F

GATE DRIVE CIRCUIT

The gate drive circuit provides an isolation between the control signal and the IGBTs gate by means of two transformers. One transformer is for transmitting power from the low-side circuit and the other for transmitting the gate drive signal as shown in the block diagram below.

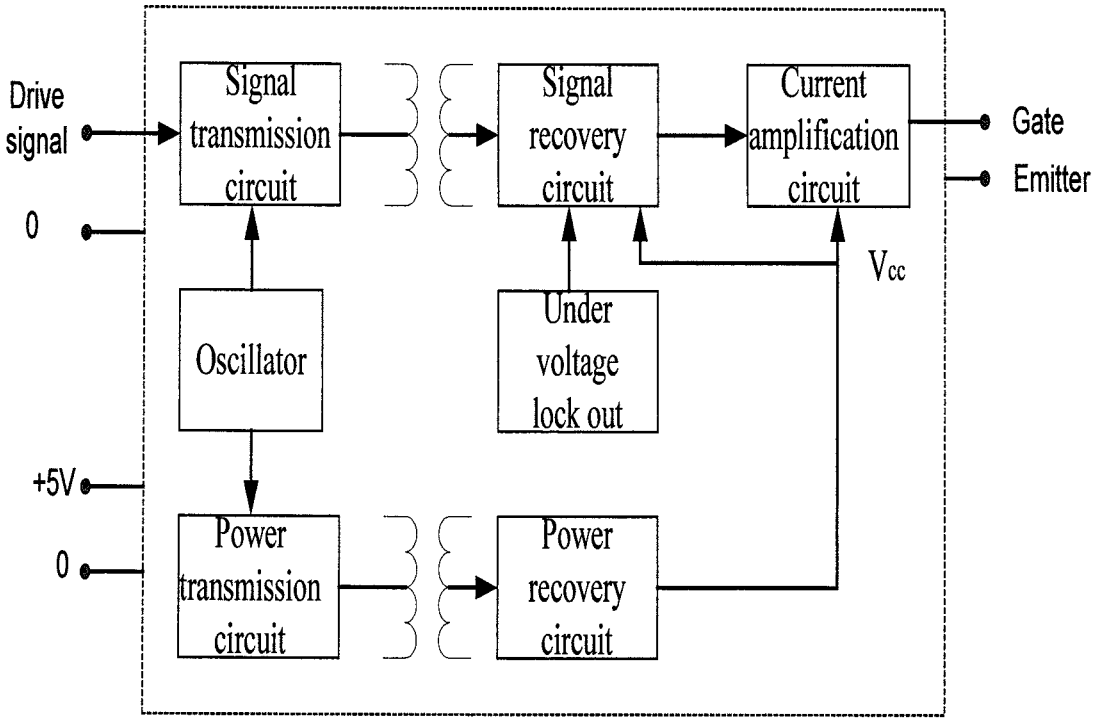

Figure F.1 Gate drive block diagram.

APPENDIX G

DS1103 PPC CONTROLLER BOARD

The DS1103 board is designed to meet the requirements of modern control prototyping. The controller board provides more power and I/O than any other single-board in the market. To avoid any development constraint, the DS1103 is equipped with a Power PC processor for fast floating-point calculation at 400MHz.

The unparalleled number of I/O interfaces makes the DS1103 PPC controller board an all rounder in rapid control prototyping. It has 50 digital I/O as well as 36 ADC channels and 8 DAC channels.

For a special I/O tasks, a DSP controller unit built around Texas Instruments' TMS320F240 is integrated as a subsystem. The DSP is perfectly suited for drive applications as it has three-phase PWM generation.

Many other comprehensive peripherals are included which have not been used in this study e.g. CAN microcontroller facility, incremental encoder. With Real Time Interface (RTI), programming is done easily via SIMULINK by Mathworks. RTI1103 was designed for the PPC controller board and supports all of the boards' I/O modules and the slave DSP I/O. The data sheet of the DS1103 board is given in the following table.

Data Sheet

The following table shows the data sheet of the DS1103:

Processor	PowerPC processor PPC604e
Memory	256Kx64-bit local memory SRAM (2 MByte) up to 16Mx64-bit global memory SDRAM (128 Mbyte)
Timer	32-bit downcounter with reload register 30 ns resolution 32-bit upcounter with compare register 60 ns resolution
Interrupt controller	interrupt controller with 22 interrupt sources 4 external interrupts
Temperature sensor	temperature sensor for the PPC
ADCs 4x16-bit ADC with mux	±10 V input range 4 µs conversion time ±5 mV offset error ±0.25% gain error 4 ppm/K offset drift 25 ppm/K gain drift >80 dB signal to noise ratio

ADCs 4x12-bit ADC	±10 V input range 800 ns conversion time ±5 mV offset error ±0.5% gain error 4 ppm/K offset drift 25 ppm/K gain drift >65 dB signal to noise ratio
DACs 8x14-bit DAC	±10 V output range 5 µs settling time (12bit) ±1 mV offset error ±0.5% gain error 3 ppm/K offset drift 25 ppm/K gain drift I_{max} = ±5mA C_{Imax} = 10nF
1 Analog Incremental Encoder	selectable 1 Vpp or 11 µApp mode resolution < 5° maximum count frequency of 2.4 MHz (fourfould line count), i.e. 600 000 encoder lines per second 32-bit loadable position counter 5 V/1 A sensor supply voltage ADC performance 6 bits, 10MSPS
6 Digital Incremental Encoder	selectable TTL or differential input fourfold pulse multiplication maximum count frequency of 6.6 MHz 24-bit loadable position counter 5 V/1 A sensor supply voltage
Digital I/O	32-bit parallel I/O each 8 bit group can be set to input or output I_{outmax} = ±8mA TTL output/input levels
CAN	Microcontroller-based CAN Subsystem with ISO 11898 integrated net-transceiver 1 Mbaud
V24	TL16C550 UART with FIFO RS232 / RS422 selectable max. 1 Mbaud

ADCs 4x12-bit ADC	±10 V input range 800 ns conversion time ±5 mV offset error ±0.5% gain error 4 ppm/K offset drift 25 ppm/K gain drift >65 dB signal to noise ratio
DACs 8x14-bit DAC	±10 V output range 5 µs settling time (12bit) ±1 mV offset error ±0.5% gain error 3 ppm/K offset drift 25 ppm/K gain drift I_{max} = ±5mA C_{Imax} = 10nF
1 Analog Incremental Encoder	selectable 1 Vpp or 11 µApp mode resolution < 5° maximum count frequency of 2.4 MHz (fourfould line count), i.e. 600 000 encoder lines per second 32-bit loadable position counter 5 V/1 A sensor supply voltage ADC performance 6 bits, 10MSPS
6 Digital Incremental Encoder	selectable TTL or differential input fourfold pulse multiplication maximum count frequency of 6.6 MHz 24-bit loadable position counter 5 V/1 A sensor supply voltage
Digital I/O	32-bit parallel I/O each 8 bit group can be set to input or output I_{outmax} = ±8mA TTL output/input levels
CAN	Microcontroller-based CAN Subsystem with ISO 11898 integrated net-transceiver 1 Mbaud
V24	TL16C550 UART with FIFO RS232 / RS422 selectable max. 1 Mbaud